2 print

NASA CR-114688
Available to the Public

DESIGN OF A FLIGHT DIRECTOR/CONFIGURATION MANAGEMENT SYSTEM FOR PILOTED STOL APPROACHES

Roger H. Hoh
Richard H. Klein
Walter A. Johnson

September 1973

STI TR 1015-3

Prepared under contract NAS2-6441 by
SYSTEMS TECHNOLOGY, INC.
13766 South Hawthorne Boulevard
Hawthorne, California 90250

for

Ames Research Center
NATIONAL AERONAUTICS AND SPACE ADMINISTRATION

FOREWORD

The research reported here was sponsored by the Ames Research Center, National Aeronautics and Space Administration. It was conducted by Systems Technology, Inc., Hawthorne, California, under Contract No. NAS2-6441 with NASA support for the simulation experiments. The NASA Project Monitors were James A. Franklin and Everett A. Palmer.

The authors would like to express their gratitude to the NASA personnel for their excellent cooperation throughout the experiments; special thanks to James Franklin and the NASA pilots who acted as subjects — Gordon H. Hardy and Robert C. Innis. Their patience, and many helpful suggestions, are greatly appreciated.

TABLE OF CONTENTS

		Page
I.	INTRODUCTION	1
	A. Background	1
	B. Organization of the Report	2
II.	CONFIGURATION MANAGEMENT	3
	A. Fundamental Characteristics	4
	B. Trim Schedule Development	7
	C. Piloting Technique	11
III.	LONGITUDINAL FLIGHT DIRECTOR SYSTEM	12
	A. Summary	12
	B. Fundamental Requirements	12
	C. Longitudinal Flight Director Design	18
IV.	LATERAL FLIGHT DIRECTOR	54
	A. Overview of Lateral Flight Director	54
	B. Functional Requirements	59
	C. Design Analysis Procedure	70
V.	RESULTS	104
	A. Task	104
	B. Configuration Management	106
	C. Longitudinal Flight Director	110
	D. Lateral Flight Director	119
	E. Composite Evaluation	133
VI.	SUMMARY	137
REFERENCES		138
APPENDIX A.	LONGITUDINAL STABILITY AUGMENTATION SYSTEMS	A-1
APPENDIX B.	SIMPLIFIED DIGITAL SIMULATION	B-1
APPENDIX C.	FEEDFORWARD GUIDANCE COMMANDS FOR LATERAL FLIGHT DIRECTOR A	C-1

Page

APPENDIX D. LONGITUDINAL CHARACTERISTICS OF AUGMENTOR WING JET STOL RESEARCH AIRCRAFT D-1

APPENDIX E. LATERAL CHARACTERISTICS OF THE AUGMENTOR WING JET STOL RESEARCH AIRCRAFT E-1

LIST OF FIGURES

		Page
1.	Schematic Block Diagram of Automatic Speed Control Curve	5
2.	Generic Survey of Speed Command Loop	6
3.	Effect of Glide Path Angle on Deceleration Capability	8
4a.	Nozzle, Flap, and Throttle Trim Functions	10
4b.	Trim Angle of Attack and Pitch Attitude	10
5.	Final Longitudinal Column Flight Director Diagram	13
6.	Final Throttle Flight Director Block Diagram	14
7.	Flight Director System Elements	15
8.	Typical Flight Director Display	16
9.	Nominal Flight Profile for Decelerating Curved Path Approach	19
10.	Approximate Column Flight Director Effective Controlled Element at 140 kt — Altitude Hold Mode	25
11.	Actual Column Flight Director Effective Controlled Element at 140 kt (With Pitch Rate Feedback) — Altitude Hold Mode	27
12.	Effective Controlled Element for Column Director at 90 kt	29
13.	Effective Controlled Element for Throttle Director at 90 kt — Altitude Hold	30
14.	Column Flight Director for Conversion Glide Slope Capture	32
15.	Throttle Flight Director for Conversion Glide Slope Capture	33
16.	Mechanization of Beam Rate Signal	35
17.	Effective Controlled Element for Glide Slope Tracking with Column at 90 kt, Speed SAS On	37
18.	Transition of Flight Directors for Frontside and Backside Operation	41
19.	Column Flight Director Block Diagram	43

Page

20. Throttle Flight Director Block Diagram 44

21. Effective Controlled Element for Column Flight Director in "STOL Mode" (M = 1) 46

22. Effective Controlled Element of Column Director with Airspeed Feedback in "STOL Mode" (M = 1) 47

23. System Survey for Glide Slope Tracking with the Throttle Flight Director at 90 kt 49

24. Effective Controlled Element for Throttle Flight Director at 90 kt and 60 kt 50

25. Effect of Increased Gains on Throttle Flight Director Effective Controlled Element at 60 kt 53

26. Block Diagram and Constants for Flight Director A 56

27. Block Diagram and Constants for Flight Director B 57

28. General Block Diagram for Lateral Flight Director A 61

29. Generic System Survey 62

30. Block Diagram of Circuit for Derived Beam Rate 73

31. Average Directional Localizer Power Spectral Density 74

32. RMS Flight Director Signals Due to Conventional Localizer Noise 75

33. Complementary Filter for Derived Beam Rate on a Curved Path 76

34. Simplified Block Diagram of Flight Director A (FD A) 78

35. System Survey for Flight Director A, $Y_p(FD/\delta_w)$ 79

36. Flight Director A Response to an Initial Condition Offset . . 81

37. Flight Director A Response to Initial Condition Offset with a 25 kt Crosswind 82

38. FD A Response to a Crosswind Shear of 2.23 ft/sec^2 84

39. Crosstrack Error Sensitivities, FD A 86

40. Effect of Bank Angle Bias on Crosstrack Error, $\varphi_{BIAS} = 50$ . . 87

Page

41. Simplified Block Diagram for Flight Director B 88

42. Generic Root Locus for Factoring $N^{\Phi}_{\delta_w}(K_p = 0)$ 89

43. Generic Root Locus for Roots of $N^{FD}_{\delta_w} = f(K_p)$ 91

44. Approximate Bode Asymptotes of G_{Φ} 91

45. System Survey for Flight Director B, $Y_p(FD/\delta_w)$ 93

46. FD B Characteristics 94

47. FD B Response to an Initial Condition Offset with a 25 kt Crosswind 96

48. FD B Response to a Crosswind Shear of 2.23 ft/sec^2 97

49. Flight Director B Curved Course Intercept, R_c = 4000 ft, V = 90 kt 98

50. Flight Director B Curved Course Intercept, R_c = 2000 ft, V = 90 kt 99

51. Geometry of Curved Path Intercept 100

52. Peak Crosstrack Deviation 102

53. Simplified Feedforward for FD B 103

54. Typical Curved Approach Used in the Simulation 106

55. Relation Between Inertial and Aerodynamic Flight Path Angles in the Presence of a Tailwind 107

56. Effect of Pitch Rate Feedback on Pilot Opinion 112

57. Curved Decelerating Approach with Zero Winds or Turbulence . . 114

58. Curved Decelerating Approach with a 20 kt Wind From the East 116

59. Curved Decelerating Approach with a 20 kt Wind From the West 117

60. Course Geometry for FSAA Simulator Study 120

61. Lateral Flight Director Computer Mechanization 121

62. Required Modification to HSI for Curved Path Status Information 123

Page

63. Curved Path Tracking with FD A; No Wind; R_c = 2000 ft 127

64. Curved Path Tracking with FD A; −20 kt East Wind; R_c = 2000 ft 128

65. Effect of Bank Angle Limit on Curved Course Tracking 129

66. Curved Path Tracking with FD B Without Washed-Out Feedforward; 25 kt East Wind; R_c = 2000 ft 130

67. Curved Path Tracking with FD B with Washed-Out Feedforward; 25 kt East Wind; R_c = 2000 ft 132

A-1. Rate Command Attitude Hold SAS Concept A-2

A-2. Attitude Responses, 60 and 140 kt Cruise A-5

A-3. Transient Response to Step q_c for 2.5 sec with RCAH SAS On (60 kt, Glide Slope) A-6

A-4. Pitch Rate Command/Attitude Hold System A-9

B-1. Block Diagram of Simulated Lateral System B-2

C-1. Generalized Block Diagram for Lateral Flight Director C-1

E-1. Lateral-Directional SAS for Augmentor Wing Jet STOL Research Aircraft (From Ref. 14) E-2

E-2. Variation of Lateral Modes and Control Effectiveness with Speed E-5

LIST OF TABLES

		Page
1.	Summary of Advantages and Disadvantages of Competing Flight Director Designs	58
2.	Pilot/Vehicle System Requirements	60
3.	Steady-State Errors	64
4.	Effect of Feedbacks on System Requirements	71
5.	Relationship Between Analytical Performance Measures and Pilot/Vehicle Requirements	77
6.	Parameter Adjustment Tradeoffs	90
7.	RMS Errors at Decision Height with and Without the Flight-Director/Configuration-Management System	133
A-1.	SAS-On RMS Response to Vertical Gusts	A-7
A-2.	Design RCAH Parameter Values	A-8
D-1.	SAS Off Longitudinal Dimensional Derivatives (Body Fixed Body Axes)	D-2
D-2.	SAS Off Transfer Functions	D-3
D-3.	Transfer Functions with Rate Command Attitude Hold SAS On	D-4
D-4.	Transfer Functions with Rate Command Altitude Hold and Speed SAS On	D-5
E-1.	SAS On Lateral Derivatives Body Axes	E-3
E-2.	SAS On Lateral Transfer Functions	E-4
E-3.	Comparison of Simulator Time Response with Transfer Functions	E-5

SYMBOLS

a_x	Longitudinal acceleration as sensed by an accelerometer
a_y	Lateral acceleration as sensed by an accelerometer
a_z	Vertical acceleration as sensed by an accelerometer
d	Deviation of aircraft center of gravity from the glide slope; measured perpendicular to the glide slope
e	Napierian base
f	Function
F_s	Column (stick) force for longitudinal control
FD_c	Longitudinal column flight director command
FD_C	Output of bank angle limiter on lateral flight director
FD_w	Lateral flight director command
FD_T	Throttle flight director command
g	Acceleration due to gravity
G_x	Transfer function in feedback loop defined by a variable, x
h	Altitude
h_{select}	Altitude hold select (cockpit control)
K_x	Gain in feedback or feedforward loop defined by a variable, x
M	Blending circuit for transfer to backside operation (see Fig. 3.1)
N	Blending circuit for transfer from Altitude Hold to Glide Slope Tracking Mode (see Fig. 3.1)
OM, MM, IM	Outer, middle, and inner marker beacons associated with ILS approach system (see Fig. 5.8)
n_z	Normal load factor, g's
N_δ^x	Numerator of x/δ transfer function
p	Roll rate
q	Pitch rate

r	Yaw rate
R	Turn radius of circular course
s	Laplace operator
t	Time
T	Time constant
T	Time gain on longitudinal column flight director (see Fig. 3.1)
T_{WO} or T_W	Washout time constant
U_o	Steady state velocity along x axis
v	Velocity along y axis
V or V_{TAS}	True airspeed
V_{GS}	Groundspeed
V_{gs}	Groundspeed at glide slope capture
V_W	Wind velocity
V_{TW}	Tail wind component
V_{cal}	Calibrated airspeed
V_{select}	Commanded airspeed (cockpit control)
V_ϵ	Airspeed error (selected minus actual)
WP	Waypoint designator (see Fig. 5.8)
X, Y, Z	Inertial coordinates
X_{DIST}	Distance from aircraft c.g. to localizer antenna; measured along the path
y	Crosstrack deviation
y_c	Command lateral position
y_ϵ	Crosstrack error, $(y_c - y)$
$\dot{y}_A$	Actual crosstrack error rate, $[d/dt(y_c - y)]$
$\dot{y}_D$	Derived crosstrack error rate
Y_p	Human operator transfer function with a gain of unity, $Y_p = (T_L j\omega + 1)e^{\tau j\omega}$

α	Angle of attack
β	Sideslip angle
γ or γ_a	Aerodynamic flight path angle
γ_I	Inertial flight path angle
δ_c	Longitudinal column deflection
δ_e	Elevator control surface deflection
δ_F	Flap deflection angle
δ_T or PLA	Cockpit throttle control angle (power lever angle)
δ_ν	Nozzle angle (0^o is full aft, 90^o is straight down)
δ_w	Lateral control wheel deflection angle
Δ	Characteristic determinant, denominator for transfer functions
ϵ_{loc}	Angle between aircraft c.g. and localizer centerline
ϵ_{GS}	Angle between aircraft c.g. and glide slope centerline
ζ	Damping ratio of second-order mode
θ	Pitch attitude
λ	Lateral flight path angle
σ	RMS value
τ	Human operator time delay
τ	Time constant in derived beam rate circuit for lateral flight directors
Φ_c	Feedforward bank angle command
Φ_{co}	Filtered bank angle command
φ	Aircraft bank angle
φ_{c_1}, φ_{c_2}	Defined in Fig. 5.9
φ_{wo}	Washed out bank angle
Ψ	Feedforward heading command
ψ	Heading angle

ω_{sp}	Undamped natural frequency of short period mode
ω_p	Undamped natural frequency of phugoid mode
ω_x	Crossover frequency corresponding to feedback loop defined by x

Subscripts

aug	Refers to augmented airplane
GS	Groundspeed
c	Command
D	Desired
SAS	Stability augmentation system
o	Initial condition
R	Roll subsidence
$(\dot{})$	d/dt

Primed variables denote that their present value has resulted from a previously closed loop. The number of primes denotes more than one loop has been closed.

SECTION I

INTRODUCTION

The inherent complexity of the basic mission of STOL aircraft gives rise to a dramatic increase in requirements for improved flight control systems, displays, and control techniques. For example, the crew of a typical STOL transport will be faced with curved path, decelerating, high angle, precision approaches down to instrument minimums followed by a short-field landing on nearly every flight. Clearly, a significant improvement in the pilot vehicle system is required to achieve this mission and still maintain a level of safety consistent with present standards. To this end, two fundamental concepts have evolved; first, a fully automatic system wherein the pilots simply act as monitors, and second, a system tailored around the pilot in such a way that the workload and task requirements for a manually controlled approach are reduced to an acceptable level. A third, and more expensive, choice is to do both, thereby allowing the pilots to take over and complete the STOL approach manually in the event of an automatic system failure. The work covered in the present report is oriented towards the pilot centered requirements, and as such, assumes the pilot will be in the loop during the entire approach.

The major areas of concentration were centered about improved flight director displays and configuration management techniques designed and combined to minimize pilot workload.

A. BACKGROUND

Some of the fundamental concepts reported here represent an extension of earlier work. In particular, the basic formulation of the configuration management scheme is reported in Ref. 1 and the initial work on the longitudinal flight director is reported in Ref. 2.

The Augmentor Wing Jet STOL Research Aircraft presently being flown at NASA Ames Research Center served as the test bed for the conceptual developments and simulations reported herein. The analysis reflects this in that the airframe characteristics and high lift devices employed on that aircraft are utilized in the design development.

B. ORGANIZATION OF THE REPORT

Each section of the report deals with the individual components of an overall system designed to reduce pilot workload to an acceptable level during curved, decelerating, descending STOL approaches.

Section II deals with refinements of the configuration management scheme with sufficient detail to give the reader a feel for the basic concepts and how they are applied to the Augmentor Wing aircraft. The basic formulation of the configuration management scheme is given in Ref. 1.

The longitudinal flight director is presented in Section III. Again, this represents an extension of previous work which is reported in Ref. 2.

Section IV contains a discussion of the development and evaluation of two competing curved path lateral flight directors.

System performance checks and piloted evaluations were accomplished on the NASA Ames Flight Simulator for Advanced Aircraft (FSAA). These results are summarized in Section V.

Section VI presents a summary of results in terms of the originally stated objectives of the program.

A rate command attitude hold pitch SAS was designed to complement the configuration management system and longitudinal flight director. This is presented in Appendix A. It represents an extension, to a wider speed range, over the Ref. 1 pitch SAS.

SECTION II

CONFIGURATION MANAGEMENT

The primary design goal of STOL transport aircraft is to achieve very low approach and landing speeds without significant sacrifice in cruise speed and payload. This implies some form of lift augmentation in the approach configuration. In many cases, this results in a redundant set of basic longitudinal controls, i.e., elevator, flaps, throttle, and thrust vector modulation. An increased complexity of the piloting task arises from the large number of control combinations which can be used to achieve a given trim state. In addition to having an extra control lever to manipulate, the pilot must also consider (and avoid) inadvertent excursions into "marginal regions" of the flight envelope. Unlike the CTOL aircraft situation where angle of attack and speed are directly related (1 g flight), the STOL pilot must consider a large variety of flight parameters to evaluate his current safety margins. The concept of the "configuration management" scheme discussed herein is to maximize the vehicle operating safety margins throughout the flight envelope from the "clean" configuration, through the conversion to STOL, and during straight and curved tracking of precision approach paths in the STOL mode. A detailed description of the method is given in Ref. 1. The following paragraphs summarize the application of the "automatic" configuration management scheme to the Augmentor Wing Jet STOL Research Aircraft for a decelerating, descending, curved approach.

Primary consideration is given to minimizing pilot workload while maximizing the operating safety margins throughout the conversion to STOL and the final approach. The desired characteristics that accompany these objectives are summarized below:

- Controls which produce "separate" changes in airplane motion perpendicular and parallel to the velocity vector (this uncouples the controls).
- Good acceleration-deceleration and climb-descent capability (without coupling) at all speeds.
- Configurations that allow unsafe flight conditions should not be possible (due to configuration management scheme).

- Small changes in pitch attitude during transition for ride comfort and to maintain acceptable safety margins.

- Minimum number of required throttle changes.

A. FUNDAMENTAL CHARACTERISTICS

As discussed in detail in Ref. 1, the pilot workload is minimized by means of a flap-nozzle interconnect so as to keep the aircraft operating within the acceptable region of its trim envelope at any speed and descent combination.* The primary considerations in design of such an interconnect are:

a) The flap and the interconnected nozzle, should be programmed as a function of speed.

b) Uncompensated flap deflections cause "ballooning". It is therefore desirable for the flap to lag rather than lead speed changes.

c) Flap actuation is slower than nozzle actuation; therefore, the flap should drive the nozzle for trim.

d) A continuous trim state is achieved by using the flap to also drive the elevator.

e) Speed regulation and command is best accomplished with the nozzle.

To summarize, a continuous trim state is achieved by driving the flap with speed and in turn driving the nozzle and elevator with flap.

A fundamental result is that the aircraft becomes neutrally stable in speed. Physically, this means that the aircraft will stay at its current airspeed until disturbed, in which case it will go to a new speed and automatically retrim for that flight condition. In terms of the characteristic modes of the aircraft, the phugoid roots are modified so that one pole is always near the origin. The resulting augmented aircraft is representative

*The Augmentor Wing Aircraft utilizes a combination of blown flaps and thrust vector control for lift augmentation. Reference to the "nozzles" in this report refers to the hot thrust vector control.

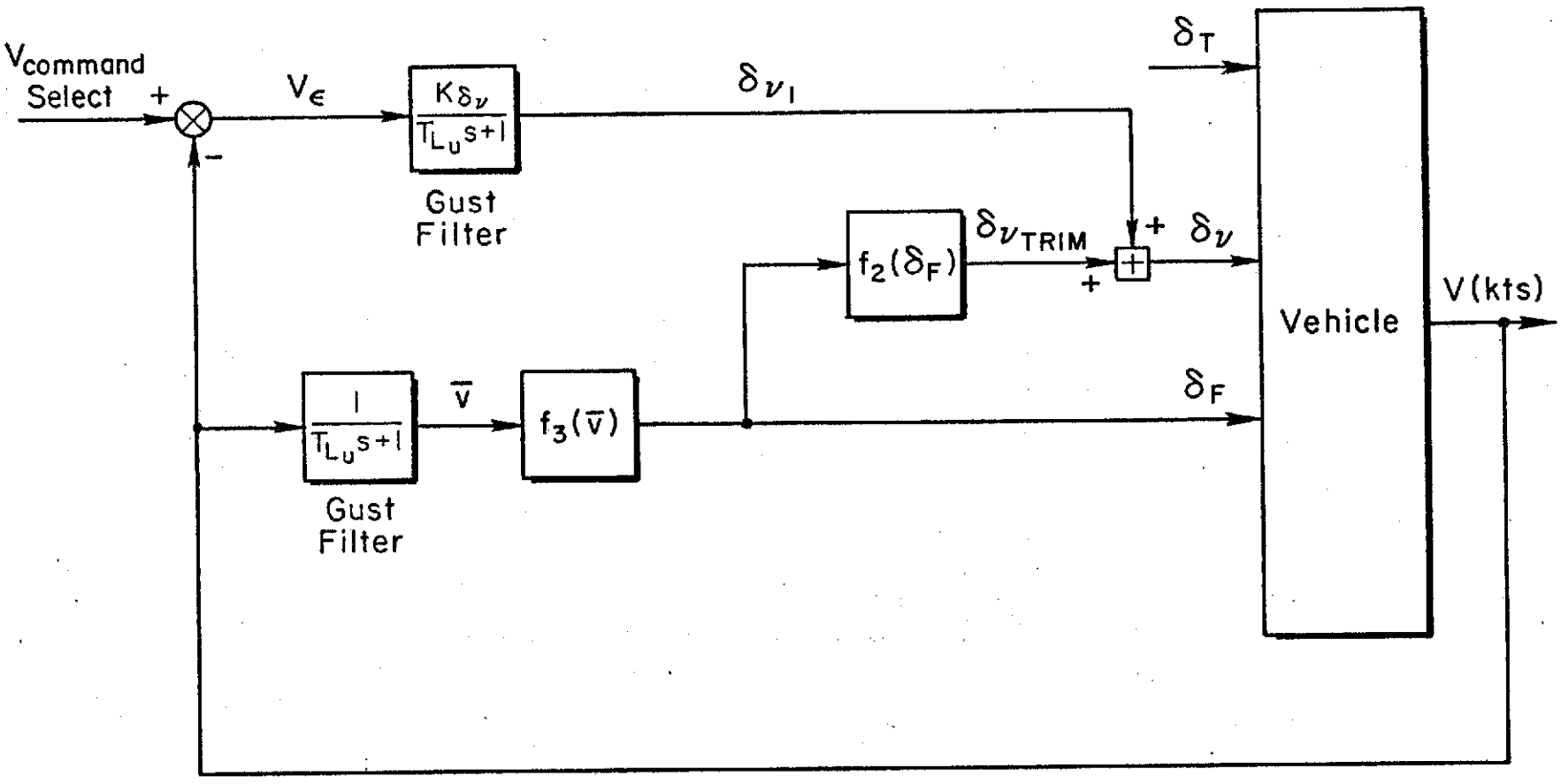

Note: f_1, f_2 and f_3 are functions derived from the trim curves in Figure 4 (for 140 > V > 60 kts)

Figure 1. Schematic Block Diagram of Automatic Speed Control System (Actuator Lags Are Not Shown)

of a type one system (looks like an integrator) at low frequency. In fact, this was a primary objective of the design in that it serves as an ideal controlled element for speed command augmentation. The speed command system (which renders the configuration management scheme "automatic") is achieved via a unity feedback of airspeed which is compared with a selectable speed command signal and fed to the nozzle (δ_ν, in the block diagram in Figure 1). The functions f_1, f_2, f_3 in Figure 1 define the previously mentioned flap nozzle and elevator interconnect required to achieve a continuous trim state. A gust filter $[1/(T_{L_u}s + 1)]$ was included to attenuate the effects of high frequency gusts on the nozzle and flap servo actuators. A generic survey of the effect of the outer speed loop is given in Figure 2. Note that the closed-loop pole at $1/T'_{u_1}$ is essentially cancelled by the zero at $1/T_{u_1}$, leaving a dominant well damped second order mode. The speed SAS gain, K_{δ_ν}, was selected to be constant for all flight conditions. The value was optimized during the FSAA simulation resulting in 10 degrees of nozzle per knot of airspeed error and a closed-loop speed mode of .69 rad/sec with a damping ratio of .72. (Ref. 1 simulations showed 10°/kt as preferable to 5°/kt — the only two values tested.)

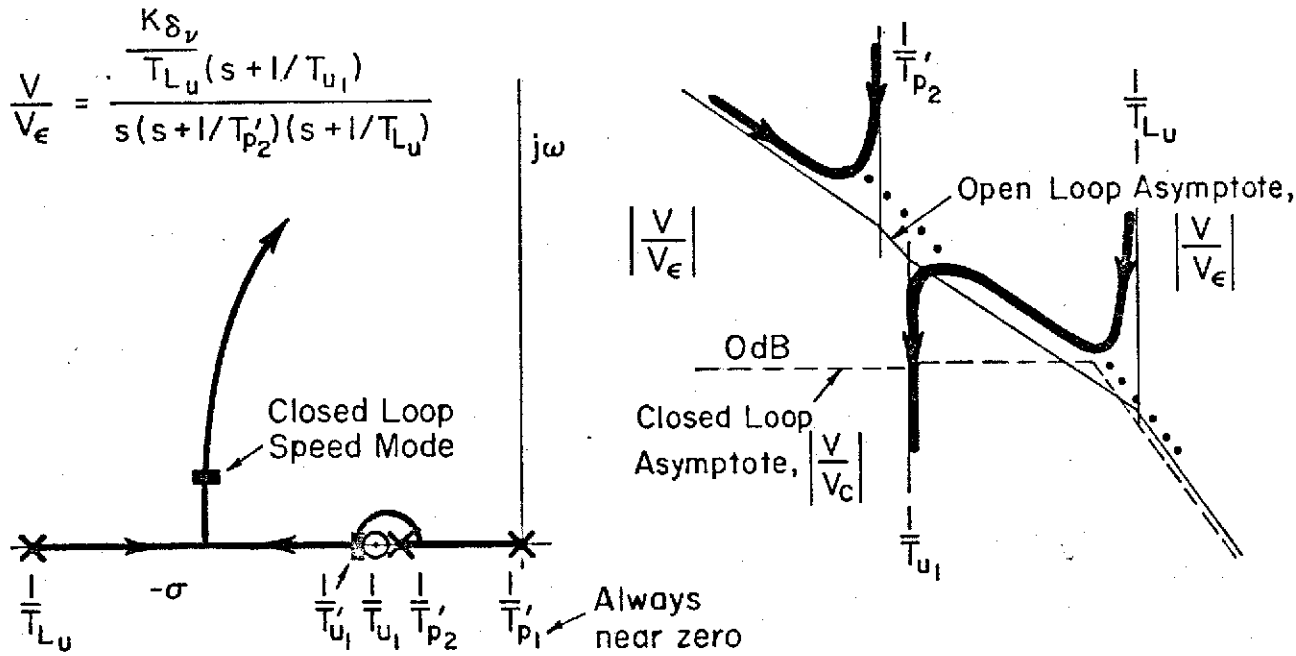

Figure 2. Generic Survey of Speed Command Loop

For speeds at and above 125 kts the nozzle is trimmed at its full aft limit of 6° leaving zero nozzle authority for closed loop speed control. The trim thrust vector angle increases to 32° at 120 kts resulting in more effective closed loop control at speeds below 120 kts.

It was initially thought that the speed command system would allow the aircraft to be operated using frontside control techniques, because a speed loop always tends to drive the low frequency h/δ_e numerator zero ($1/T'_{h_1}$) into the left half plane (see Ref. 3).* However, results obtained during the FSAA simulation revealed that if the aircraft was perturbed from the glide path, or if a large wind existed, the nozzles were driven to the limits. This effectively opens the speed control loop, thereby making frontside operation no longer possible (i.e., $1/T_{h_1}$ is no longer driven into the left half plane). Later in the program, the nozzle aft limit about trim was reduced to -20° to minimize SAS failure transient effects on lift. Backside operation was therefore clearly inevitable and was incorporated into the longitudinal flight director at speeds below 85 kts (see Section III-B).

B. TRIM SCHEDULE DEVELOPMENT

The development of the trim schedules (f_1, $_2$, $_3$) involved a number of compromises between the pilot centered and guidance and control requirements. In some cases, the desired performance was restricted by basic airplane limitations such as maximum deceleration capability, flap placards, and nozzle limits. A detailed analysis of the fundamental tradeoffs and limitations inherent in the design of the trim schedules for level flight transitions from 120 kts (CTOL configuration) to 60 kts (STOL configuration) is given in Ref. 1.

In the present work, the mission profile has been extended to include deceleration on a $-7\ 1/2^{\circ}$ glide slope. Conceptually, the method is the same (as Ref. 1), but the problem changes from one of being underconstrained (large variety of realizable turn points) to one of overconstraint (unable to achieve any acceptable trim points in some regions). The nub of the

---

*$1/T_{h_1}(\doteq -g\ d\gamma/dV) = -.1$ at 60 kts, without the speed loop closed.

matter lies in the limited capability of the aircraft to decelerate on the glide path. The total acceleration along the velocity vector, $\dot{V}$, is given as:

$$\dot{V} = a_x - g\gamma$$

where a_x can be achieved with power flap and nozzle changes. Note that in level flight, all of the deceleration capability goes directly into speed changes whereas in descending flight (negative γ) the maximum $\dot{V}$ capability is decreased by $g\gamma$. This is shown graphically in the generic sketch in Figure 3.

Figure 3 indicates that improved performance can be obtained if the pilot centered requirements are ignored. That is, increased deceleration capability can be achieved via large changes in thrust and pitch attitude. The penalty is a significant increase in pilot workload and corresponding degradation in pilot opinion. The fundamental tradeoff centers about the ability to achieve an acceptable level of deceleration capability at glide slope intercept without incurring large variations in pitch attitude and thrust; and to maximize, as much as possible under such constraints, the allowable speed for glide slope intercept, V_{gs}. The final compromise does

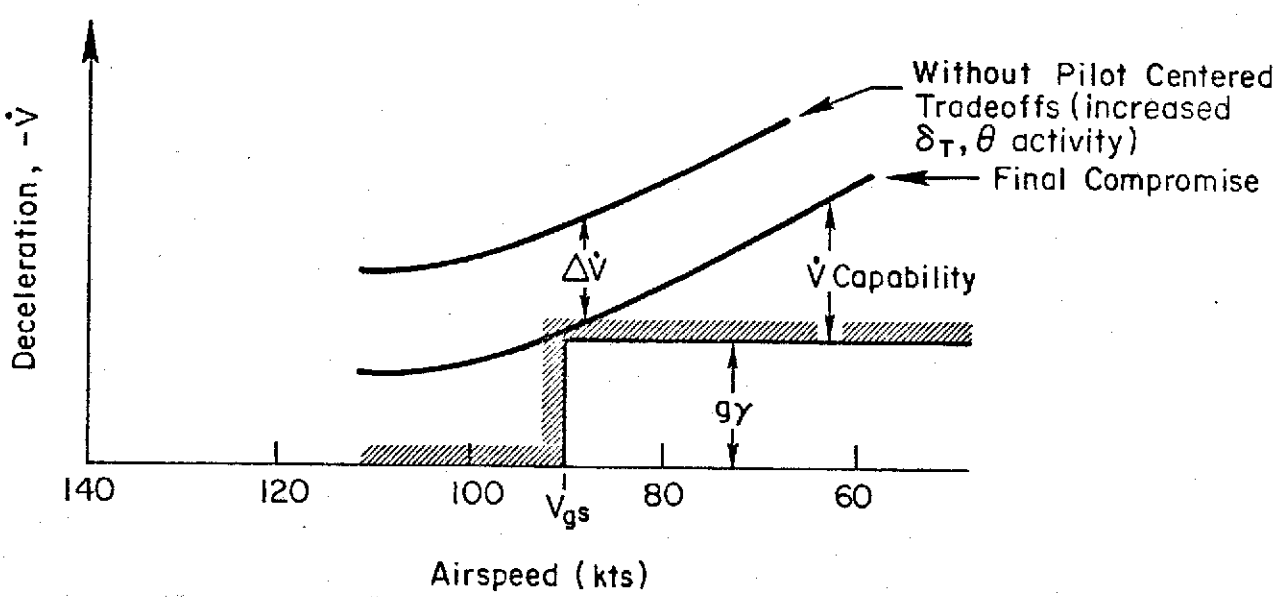

Figure 3. Effect of Glide Path Angle on Deceleration Capability

this for nominal winds (less than 25 kt). However, in the presence of a tail wind, γ is increased, and the $\dot{V}$ margin is reduced to the point where the aircraft will not decelerate below V_{gs} on the glide path. A practical solution is then to intercept the glide slope at a lower speed when this condition exists.

Attempts to maximize the deceleration characteristics via nozzle angle and thrust magnitude indicated that the resulting performance is fairly insensitive to the optimal combination. That is, going from high power settings and low nozzle angles to low power settings and high nozzle angles does not have a drastic effect on the maximum deceleration capability. Nevertheless, since the total deceleration capability is limited, some time was spent maximizing nozzle effectiveness.

In addition, the angle of attack was kept to a minimum value consistent with reasonable values of pitch attitude and power settings. This resulted in a trim angle of attack on the glide slope of 3°. The additional lift required for curved path tracking resulted in an α_{TRIM} of 5°. Abuses of the system which positioned the aircraft below the curved ILS course occasioned angles of attack as high as 8°, considered marginal but still in the acceptable range.

The nozzle, flap, and throttle trim curves which resulted from the above considerations are given in Figure 4a and the resulting trim angle of attack and pitch attitude is shown in Figure 4b. The dashed lines in Figure 4a represent the ideal nozzle trim schedule required for perfect trim at all speeds. However, since the nozzles are driven by the flap, (flap-to-nozzle crossfeed) no nozzle motion is possible when the flap rate is zero. Hence, the departure between the actual and ideal nozzle trim schedules.

The final pilot centered consideration involves frequency separation of controls. (See Ref. 4). Given a two control task, the control effects should be decoupled and separated so that responses to the primary control occur at a much higher frequency than those to the secondary control. For speeds about 85 kts, the altitude is controlled with pitch attitude and elevator is the primary control (the aircraft is inherently on the "frontside" of the thrust required curve). Accordingly, the throttle trim function

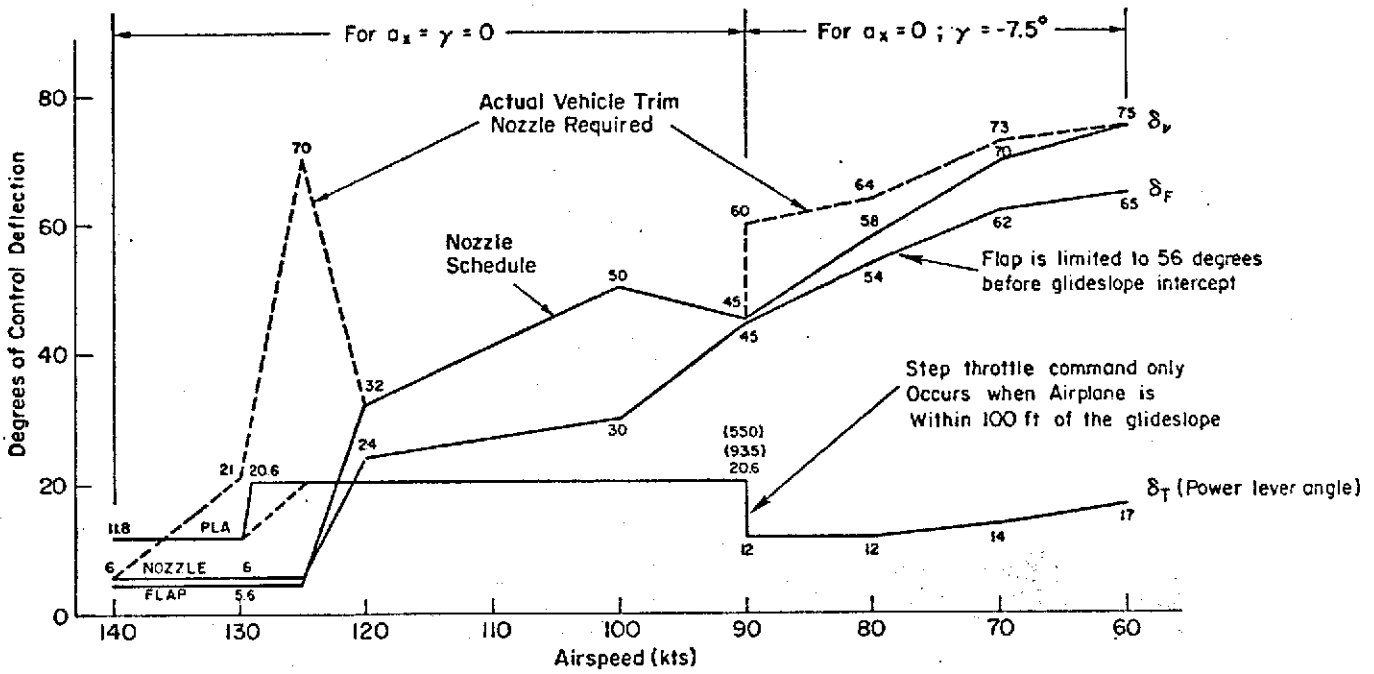

Figure 4a. Nozzle, Flap, and Throttle Trim Functions

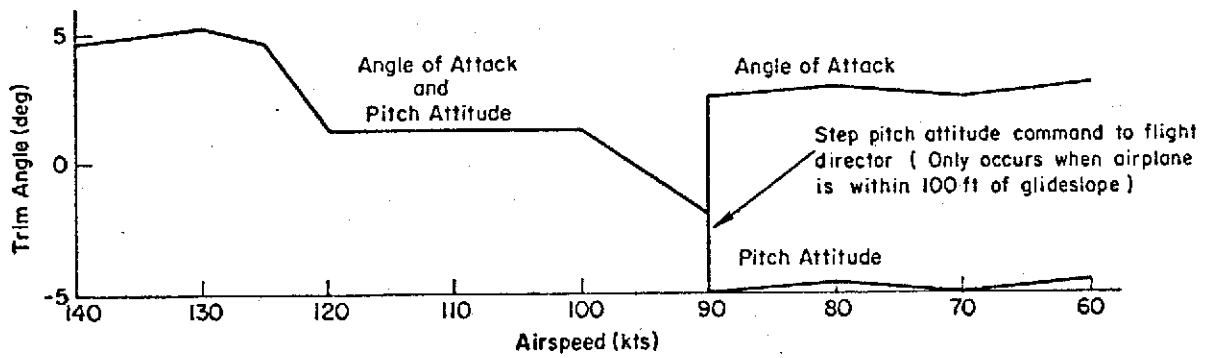

Figure 4b. Trim Angle of Attack and Pitch Attitude

was designed to be relatively inactive with only two discrete changes, one at 130 kts and the other at glide slope intercept. Below 85 kts, the control strategy is reversed and throttle becomes the primary regulatory control of altitude and/or glide slope. The trim pitch attitude is therefore a constant below 85 kts. The longitudinal flight director contains switching logic that changes the altitude/glide path feedback from the pitch bar to the throttle bug at 85 kts.

C. PILOTING TECHNIQUE

As noted above, the nozzle and flap controls are automatic when the system is engaged and therefore not used by the pilot. Speed changes are accomplished by slewing a speed command bug to the desired indicated airspeed and then keeping the pitch bar and throttle command bugs centered during the deceleration. If the aircraft is in the altitude hold mode, the pitch bar is the primary (nost active) display until the aircraft decelerates below 85 kts at which time the throttle bug becomes primary and the pitch bar simply commands a reference attitude of about -2°. The same is true in the ILS mode except the pilot must not intercept the $7\ 1/2^{\circ}$ glide slope above 90 kts to insure adequate deceleration capability on the glide slope.

SECTION III

LONGITUDINAL FLIGHT DIRECTOR SYSTEM

A. SUMMARY

This section presents a detailed formulation of the longitudinal flight director system. It is perhaps too detailed for the reader interested only in finding out what the system is and how it works. Therefore both the longitudinal and lateral flight director sections are initiated by giving a brief summary consisting of the final block diagrams, gains, limiters, mode switching logic, and a brief description of system operation.

The longitudinal flight director system consists of a column director (pitch bar) and a throttle director located on the left side of the ADI instrument. These two director commands are used by the pilot in conjunction with the speed command bug (Section II) to perform precision curved, descending, decelerating approaches.

The final column and throttle flight director block diagrams are given in Figures 5 and 6. Switching from altitude hold to glide slope tracking is blended in when glide slope deviation becomes less than 150 ft (1 - N circuit in Figure 5). As the aircraft slows to speeds below 81 kts (backside of the power required curve), the beam and beam rate functions are removed from the column flight director and blended into the throttle director via the "M" circuit in Figures 5 and 6. Speed error is simultaneously blended into the column director to support the limited authority speed SAS* during backside operation below 81 kts. The "function" blocks in each director reflect feedforward inputs from the configuration SAS trim functions in Figure 4a. Finally, protection against excessive angles of attack (greater than 8°) is obtained by feeding angle of attack to the throttle director through the threshold function in Figure 6.

B. FUNDAMENTAL REQUIREMENTS

The objective of the longitudinal flight director portion of the program was to extend the capability of the approach director system developed in

*The nozzle limit is set to -20° from trim to minimize the effect of a hardover failure.

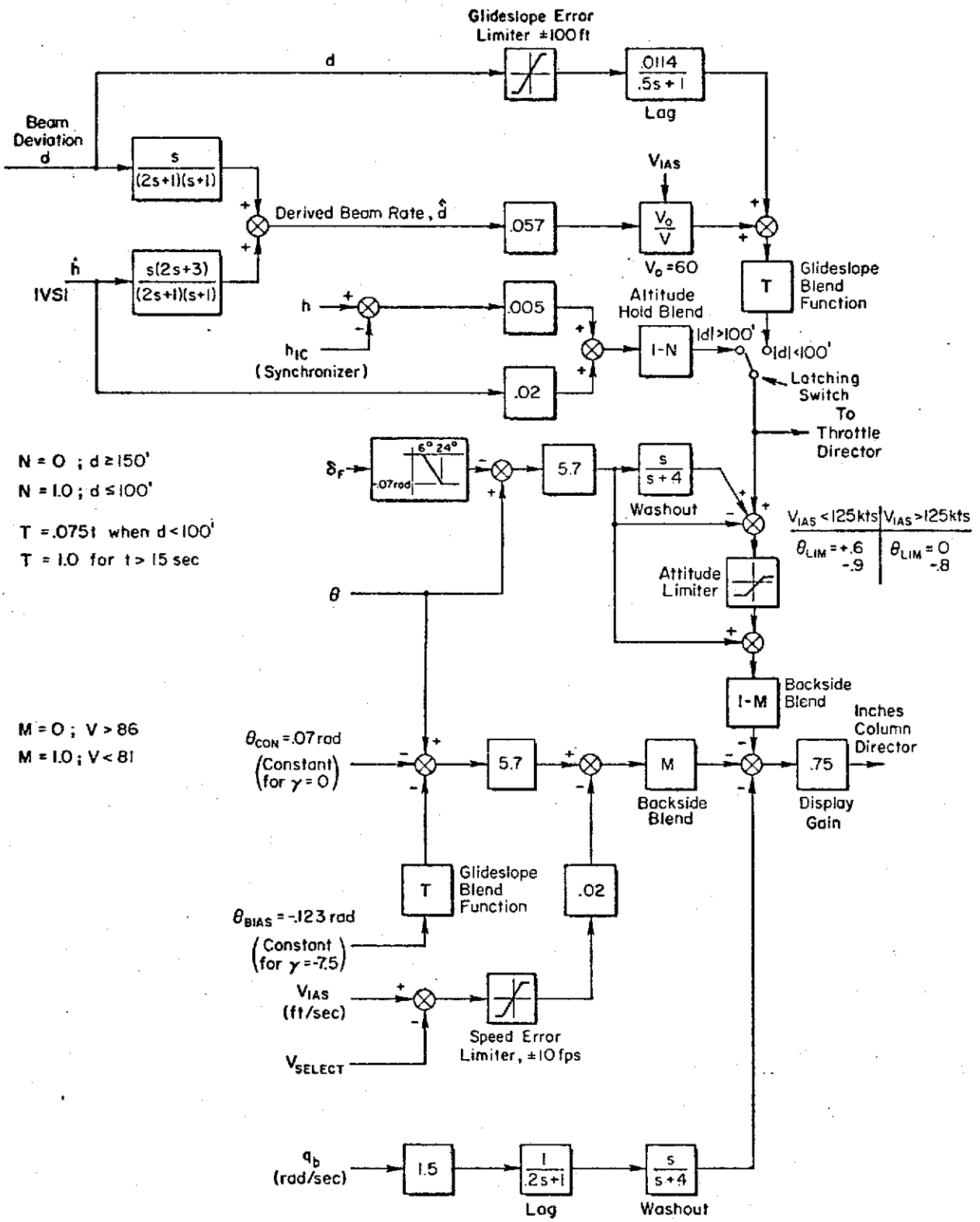

Figure 5. Final Longitudinal Column Flight Director Diagram

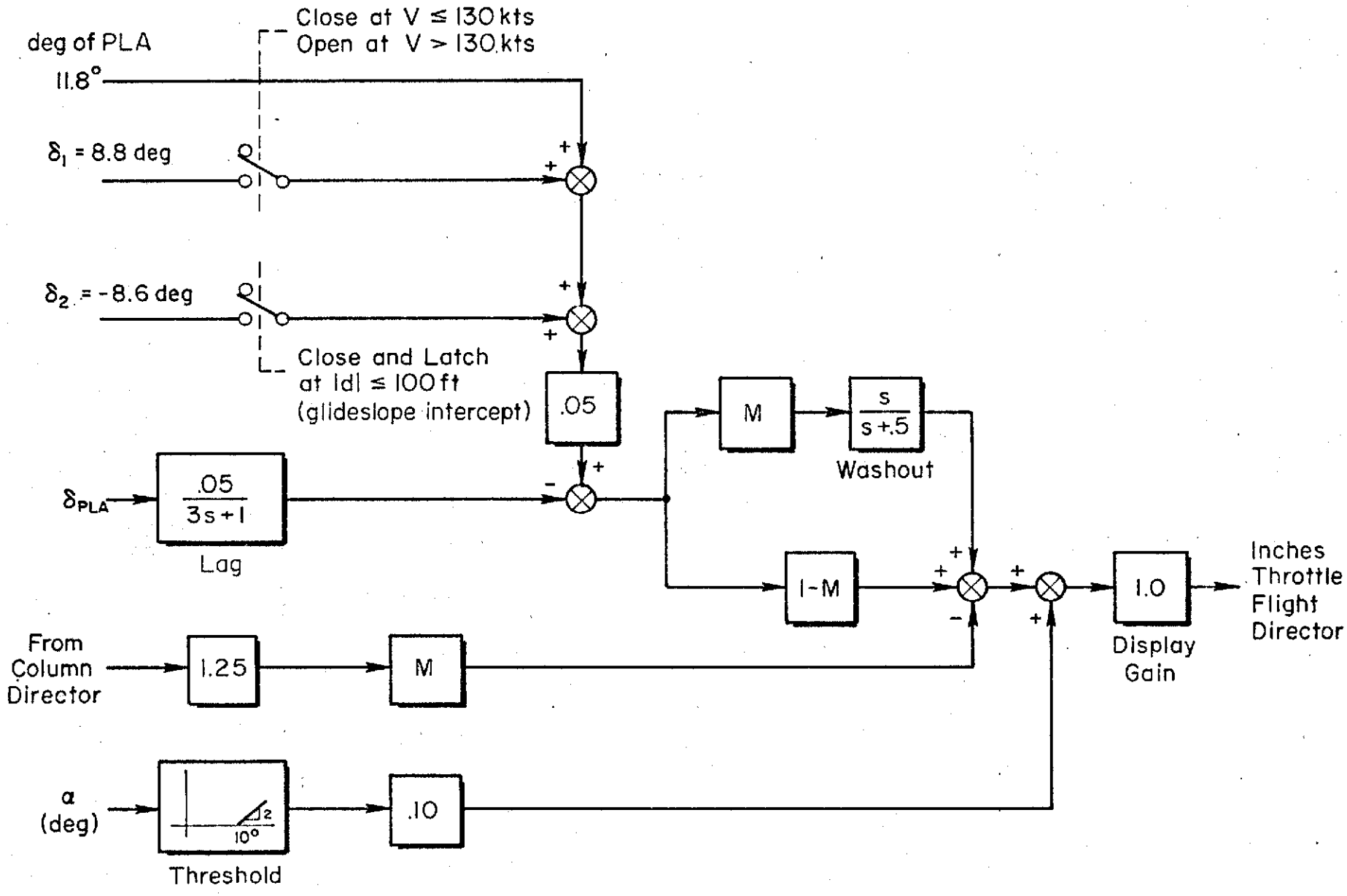

Figure 6. Final Throttle Flight Director Block Diagram

Ref. 2 (designed for constant speed [60 kt] glide slope tracking) to encompass cruise, transition to STOL, and final approach configurations. This was to be used in conjunction with a lateral flight director system for tracking curved lateral approach paths. This lateral director system is discussed in the next section.

In review, the purpose of a flight director system is to reduce the pilot workload by combining the various displayed and computation elements used by the pilot in performing a given task into one instrument, thereby forming a single-loop compensatory tracking task for each axis of control. Closed-loop analysis using existing pilot models will yield directly the vehicle motion quantities which must be displayed in order to accomplish a given task. A functional diagram depicting the elements of this closed-loop system is shown in Fig. 7.

The display portion of Fig. 7 may be represented by the typical attitude flight director indicator shown in Fig. 8. It has lateral and longitudinal command bars as well as a thrust command indication on the left side. The command elements form the basis for the pilot's control actions. In conventional aircraft there are only the two central command bars, one for column and one for wheel. For the Augmentor Wing Aircraft, however, the additional command bar is necessary since a major portion of the path control at low speeds is achieved with nozzles or thrust.

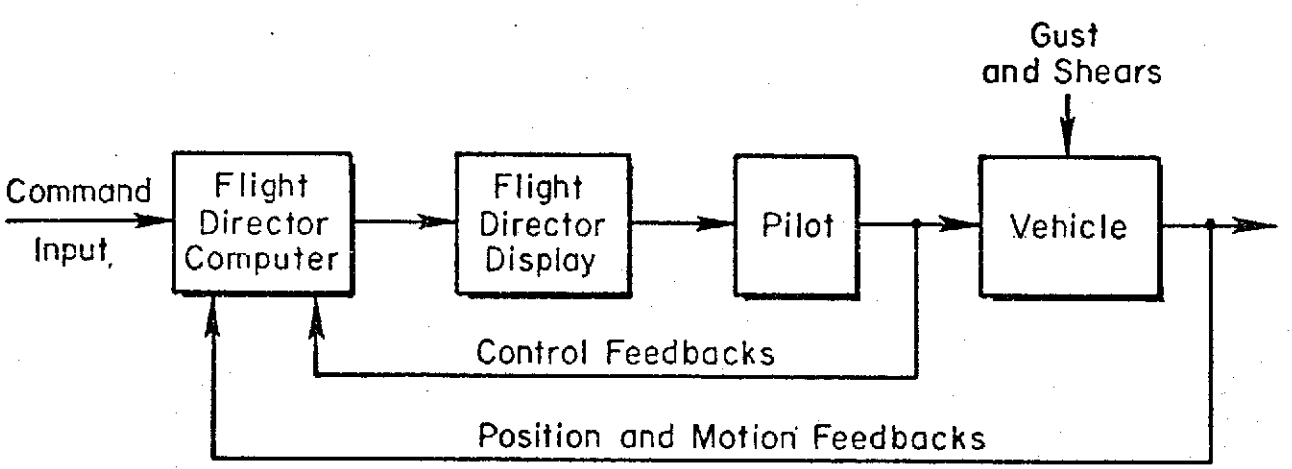

Figure 7. Flight Director System Elements

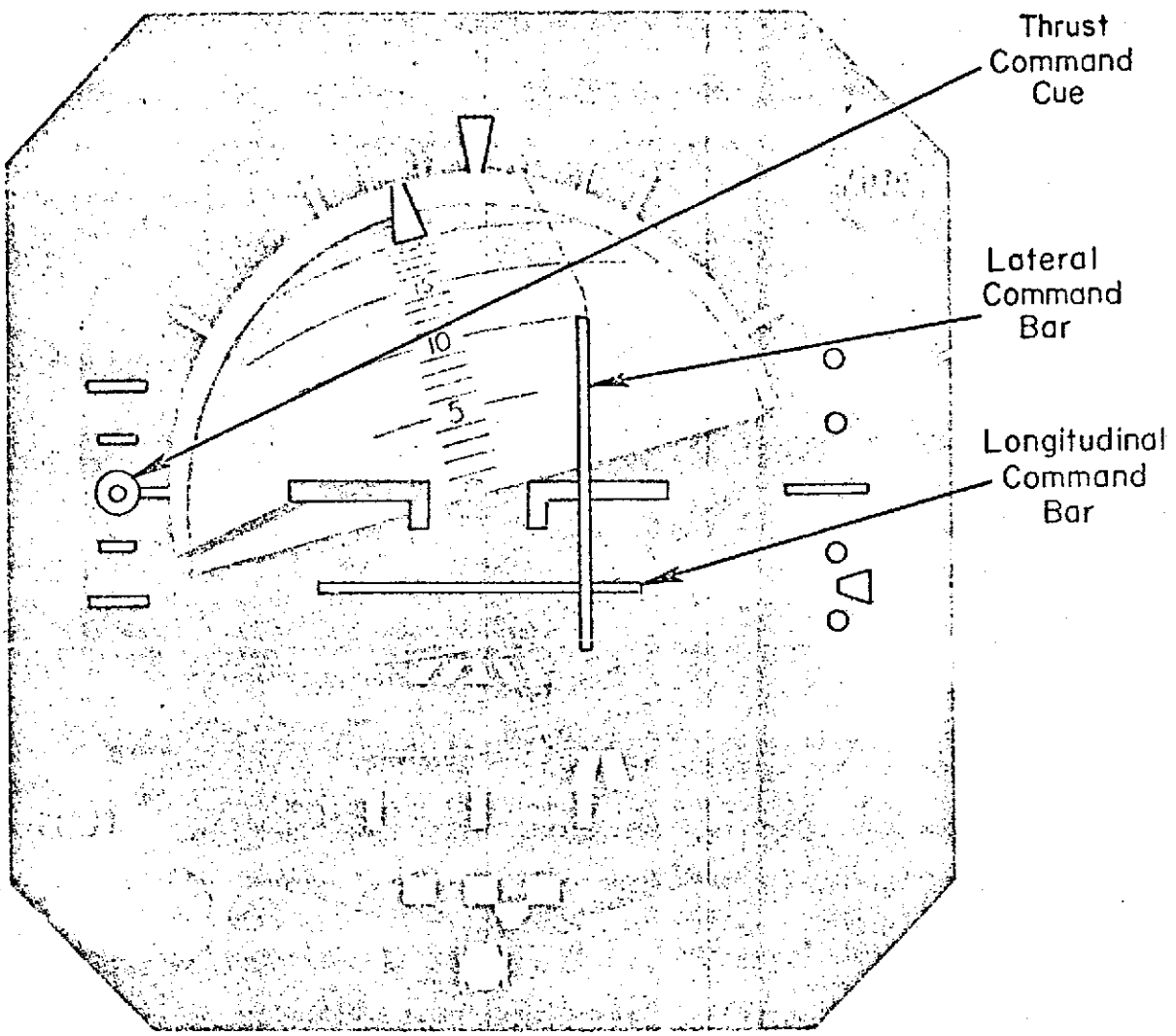

Figure 8. Typical Flight Director Display

The control laws for the command displays are derived so that when the pilot nulls the command bars the vehicle will be directed into the approach in accord with well-defined guidance and control requirements. In addition to the guidance requirements, the feedback quantities making up the "effective controlled element," i.e., the vehicle-plus-flight-director dynamics, must be weighted, filtered, and equalized in accord with a set of pilot-centered requirements so that the pilot can close the flight director system loop with ease and efficiency. The requirements for longitudinal flight director systems have been presented and discussed in detail in Ref. 1 and Ref. 5.

In summary, guidance and control requirements are independent of the type of vehicle. For an approach control system, the fundamental requirement is path control. Thus, the guidance law must provide for a stable, well-damped beam acquisition and subsequent beam following in the presence of wind disturbances and unusual initial conditions. Additional requirements related to control include attitude regulation and damping, as well as the more fundamental vehicle requirements (i.e., control power, authority, etc.). For a STOL aircraft the guidance and control requirements for the longitudinal axis may be met most effectively using two active controls. However, this increases the pilot control workload, especially when tracking a curved lateral path where status information is continuously changing. Consequently the nub of the design problem is to design a two axis director system which provides acceptable performance and workload.

Minimizing pilot workload is one of the key pilot centered requirements. As discussed in Ref. 4, pilot workload is reduced by:

- Requiring no low frequency pilot lead equalization
- Permitting pilot loop closure over a wide range of gains
- Allowing long dwell times on each instrument

This can be accomplished when the weightings of the various feedbacks in the flight director computer produce an effective controlled element, i.e., vehicle plus flight director, that approximates a pure integration, K/s, over the frequency range of pilot/director/vehicle system crossover. For this set of controlled element dynamics, the pilot response is approximately

a gain plus time delay in the frequency region of control (near crossover). This can be aided to some extent by providing stability augmentation systems on the vehicle. This satisfies the basic stability and damping requirements without having the pilot provide the compensation. However, the flight director must be such that in the event of a SAS failure the pilot can sufficiently cope with the increased task difficulty.

Workload is also reduced by minimizing the number and complexity of controls. This aspect was discussed in the previous section on the design of a flight management system. This system eliminated the need for the pilot to move the flap and/or nozzle controls.

In the following portions of this section we present the detailed rationale and design of the longitudinal flight director system taking into account both the guidance/control and pilot centered requirements for cruise, conversion, deceleration (transition to full STOL approach configuration), glide slope capture, and glide slope tracking on a curved lateral flight path.

C. LONGITUDINAL FLIGHT DIRECTOR DESIGN

The longitudinal director system provides both column and throttle commands throughout the entire approach from 140 kts level flight down to 60 kts on the glide slope. The various phases of the approach that the director must be designed for therefore include the following situations:

1. Altitude holde ($\gamma = 0$)
2. Conversion to STOL ($\gamma = 0$)
3. Glide slope capture ($\gamma = -7.5^{\circ}$)
4. Deceleration to final approach speed while maintaining glide slope ($\gamma = -7.5^{\circ}$)

These situations are depicted on an example flight planform shown in Figure 9. Note that each segment of the approach is initiated separately to minimize pilot workload. For example, conversion from 140 kt to 90 kt is nominally accomplished first during straight and level flight. Also, during wings level flight the glide slope is captured. During the descent,

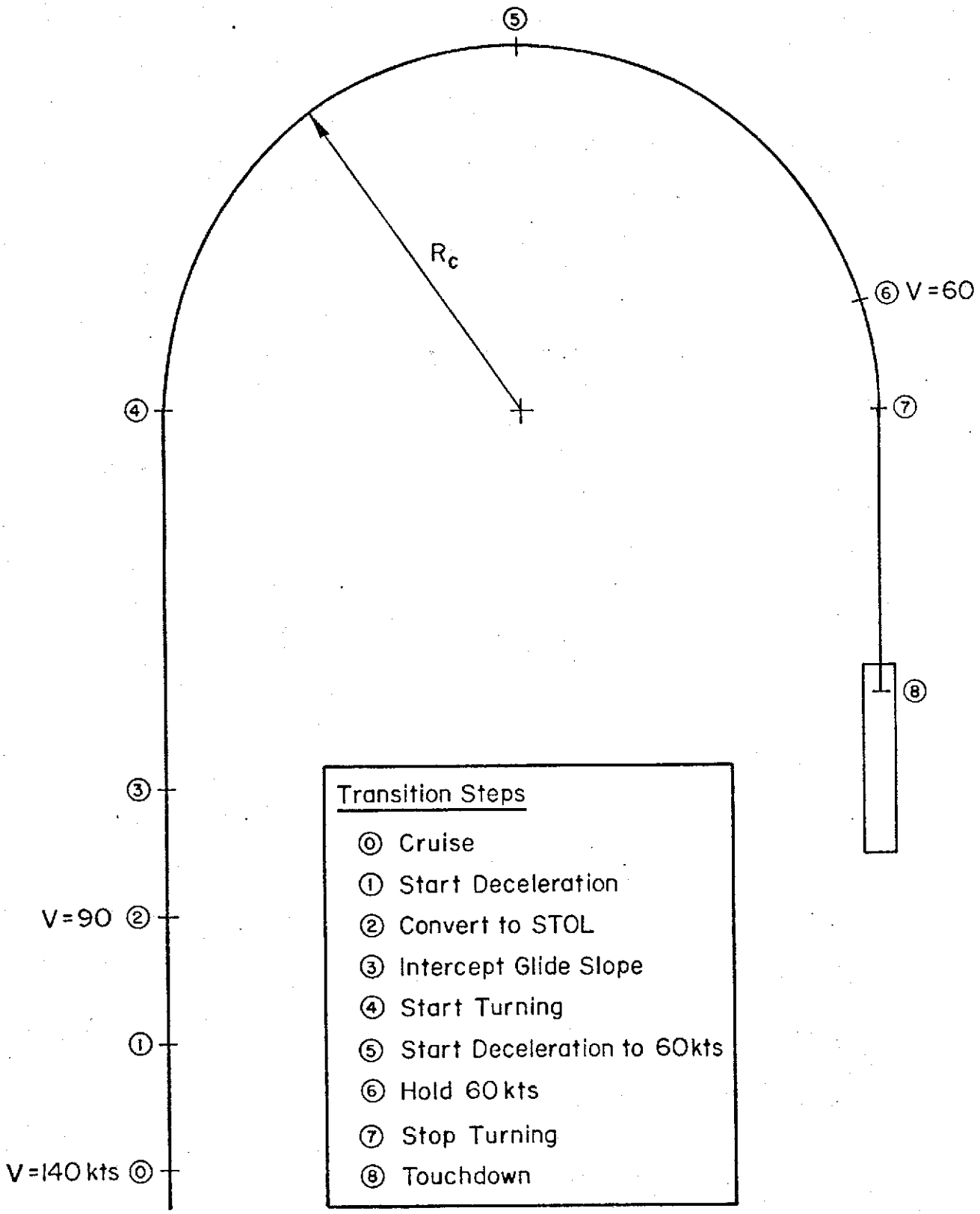

Figure 9. Nominal Flight Profile for Decelerating Curved Path Approach

the turning phase of the approach is initiated. About halfway around the turn the deceleration from 90 kt to 60 kt is initiated and is completed prior to completing the turn. The final approach is on a straight path. Deceleration and speed control is provided by the trim management systems and speed SAS.

There are several vehicle induced design requirements that should be discussed at the outset. First, glide slope capture and subsequent tracking must be at or below 94 kts. Due to flap placards, drag capability is not sufficient to decelerate the vehicle on a -7 1/2 deg glide slope in the presence of a tail wind when the speed is higher than 94 kts. This result was discussed in Section II.

A second design requirement is that the vehicle control technique be properly altered as a function of frontside/backside flight conditions. When the vehicle is on the frontside of the power required curve, i.e., $V \geq 85$ kts, the conventional control technique of flight path via elevator is preferred. Conventional flight path/attitude response times are proportional to speed and at the higher speeds, larger path mode bandwidths can be achieved with attitude (through elevator) than with thrust or nozzle. Also, at these speeds the nozzles and/or thrust do not have sufficient control power to provide an adequate DLC capability. At lower speeds where the vehicle is basically on the backside of the power curve, the STOL technique of controlling flight path with thrust and airspeed with attitude is preferred for reasons converse to those cited above for conventional control. Also, in the event of a speed SAS saturation or failure, the STOL technique avoids any flight path instability due to backsidedness. As a matter of fact, with the nozzles aligned near vertical, the only effective method of controlling speed is with attitude. A more complete discussion of control technique selection for the Augmentor Wing Aircraft was presented in Ref. 1. However, each of the above points will become more apparent from the subsequent design of the flight director system presented in this section.

A last requirement imposed on the longitudinal flight director is for glide slope interception and acquisition at any speed from 60 to 90 kts. The normal procedure to expedite the approach and keep noise levels down

is to decelerate to 90 kts while straight and level, intercept the glide slope, and slow to 60 kts when on the glide slope as was shown in Figure 3.5. However, the pilot should also be able to slow to 60 kts while straight and level and then intercept the glide slope. This situation might be necessary for approaches in a tail wind, maintaining approach spacing, etc.

The remainder of this section is devoted to the analytical design of the throttle and column directors for each phase of the approach. The analysis uses the updated transfer functions from Appendix D since they reflect the latest aerodynamic data and SAS gains anticipated for the aircraft. However, the feedback gains used in the simulation program were originally designed on the basis of original aerodynamic data and with $K_{DC} = 0$ in the pitch SAS. (See Appendix D.) The differences are generally inconsequential; however, the design values may appear somewhat non-optimum due to this data change. The analysis is supported by the simulation evaluation that is discussed in Section V.

1. Altitude Hold Phase

The first flight director task is to provide altitude hold when the vehicle is in a cruise condition prior to glide slope capture. At 140 kts the vehicle is flown as a CTOL aircraft and therefore a column flight director can be designed from the rationale presented in Ref. 2. This design basically uses path deviation, path deviation rate, and washed out pitch attitude. The use of path rate allows the attitude to be washed out without any loss of path damping.

Since the altitude holding phase of the approach will be at a speed where flight path can be controlled with attitude, the throttle director is used only to provide two discrete indications of changes in the trim thrust required (see upper left portion of Figure 6). Nevertheless, providing this information reduces workload since the pilot need monitor the throttle director only as he starts to decelerate from cruise and as glide slope intercept is approached. However, additional throttle changes may be necessary since there is no speed SAS designed for the 140 kt flight condition and the pilot must close an airspeed to throttle loop as part of

his "normal" scan pattern. In any event, throttle activity will be intermittent and minimal; and only one longitudinal (column) director will require compensatory (attentive) tracking — key factor in minimizing pilot workload.

The weighting of the feedback qualities making up the column flight director signal are determined by the guidance and control, and pilot centered requirements. Basically this implies good altitude holding performance and good effective controlled element dynamics. This is achieved by having an acceptable bandwidth, a well damped path mode that does not force the pilot to overdrive attitude, and K/s-like effective controlled element dynamics in the region of pilot-vehicle crossover. The bandwidth of the path mode specifies the altitude/attitude feedback ratio, i.e., $\omega_p = U_o K_h / K_\theta$. For example, an acceptable path mode of 0.25 rad/sec (Ref. 5) results in a K_h/K_θ ratio of .001 at 140 kts.

Since the flight director should reflect the vehicle's attitude response (command bar consistency requirement), the attitude feedback gain can next be selected. Normally the attitude indicator gain is about 10^o/inch; therefore, K_θ should be about 5.7 in./rad. Once this is selected the altitude feedback gain can be calculated. For example, a gain of .005 in./ft would produce full scale flight director displacement (1 in.) when the vehicle is 200 ft off altitude. This should provide the pilot with enough gain to hold altitude within 10-15 ft.

Path damping is achieved with altitude rate and attitude feedback. The altitude rate to attitude ratio should be approximately $1/U_o$ since, at low frequency, $\dot{h} = U_o\theta$. The altitude to altitude rate feedback ratio, $K_h/K_{\dot{h}}$ should also reflect the desired path mode frequency.

Attitude feedback must be washed out to avoid an altitude stand-off error. The washout time constant can be set at about T_{θ_2} (approximately the inverse of the airplane's heave damping, $-Z_w$) since at frequencies less than $1/T_{\theta_2}$ altitude rate is proportional to attitude, i.e., $\dot{h} = U_o\theta$. For example, at the 140 kts cruise condition $1/T_{\theta_2} = .93$ (Table B-3), therefore a washout time constant greater than 1 would be acceptable.

Attitude rate feedback must be used in the flight director if the closed loop (SAS-on) short period mode is less than 1 rad/sec. This insures that the pilot will not have to provide excessive lead equalization (at the expense of increasing his workload). Even when the short period response is between 1 and 5 rad/sec some pitch rate feedback may still be desirable. However, the feedback should be lagged at higher frequencies (i.e., >5 rad/sec) to keep the command bar response compatible with the vehicle's attitude response, thus avoiding a "busy" display. A washout should also be used on the feedback to avoid an altitude stand-off error in a steady turn when the body axis pitch rate gyro output is not zero.

With these feedbacks the flight director effective controlled element is obtained by computing the summation of feedback transfer functions shown below:

$$\frac{FD_c}{\delta_c} = K_h \frac{N^h_{\delta_c}}{\Delta} + K_{\dot{h}} \frac{N^{\dot{h}}_{\delta_c}}{\Delta} + \left[K_\theta \frac{N^\theta_{\delta_c}}{\Delta} + K_{\dot{\theta}} \frac{N^{\dot{\theta}}_{\delta_c}}{\Delta(T_{L_{\dot{\theta}}} s + 1)} \right] \frac{s}{s + 1/T_{wo}} \qquad (1)$$

In the following paragraphs this procedure is illustrated for the 140 kt flight condition.

In order to evaluate the effects of changing feedback gain ratios, the transfer functions were simplified to the primary roots that determine the response. For example, the attitude response to column (with the rate command-attitude hold SAS on) can be approximated by:

$$\frac{\theta}{\delta_c} = \frac{K_1 (2.0)}{(0)(5.)[.65;\ 3.5]}$$

which identifies a SAS lead, $1/T_E$, at 2 rad/sec, the stick filter, $1/\tau_s$, at 5 rad/sec, and the SAS-augmented short period mode at $\zeta' = .65$; $\omega'_{sp} = 3.5$ rad/sec. The high frequency gain, K_1, is dependent on the SAS. In a like manner the altitude rate/column transfer function for constant speed is given as:

$$\frac{\dot{h}}{\delta_c} = -U_o \frac{\gamma}{\theta} \frac{\theta}{\delta_c}$$

where the γ/θ transfer function may be approximated by $(1/T'_{\theta_2})/(s + 1/T'_{\theta_2})$. (See Ref. 3.) From Appendix D, $1/T'_{\theta_2}$ is given as .75 rad/sec, therefore the approximate $\dot{h}/\delta_c$ transfer function at 140 kts is:

$$\frac{\dot{h}}{\delta_c} = \frac{177\ K_1\ (2.0)}{(0)(.75)(5.)[.65;\ 3.5]}$$

The feedback gain ratios $K_h/K_{\dot{h}}$ and K_h/K_θ are checked by computing the effective controlled element, FD_c/δ_c. This is shown in Figure 3.6 for the gains previously estimated. These were:

$$K_h = 0.005 \text{ in./ft}$$

$$K_{\dot{h}} = 0.02 \text{ in./(ft/sec)}$$

$$K_\theta = 5.7 \text{ in./rad}$$

$$T_{wo} = 2.5 \text{ sec}$$

The main points to be noted from Figure 10 are that the effective controlled element has the desirable K/s-like response for nearly a decade, i.e., 0.3 to 3.0 rad/sec; the path mode, ω_h, will be at about .24 rad/sec with .6 damping when the pilot closes the loop in the region of 2 rad/sec; and the flight director response is the same as the vehicle's attitude response at high frequencies. From this it appears the selected gain ratios will provide altitude holding performance and acceptable pilot opinion.

A desirable ratio of pitch rate to pitch attitude feedback is determined by examining the resulting change in the high frequency response of Figure 10. A comparison of the Bode amplitudes showing the effect of increasing $K_{\dot{\theta}}$ from zero to 1.5 ($K_\theta/K_{\dot{\theta}} \doteq 4$) is given in the sketch at the top of page 26. The high frequency response of the approximate effective controlled element is increased by a factor of 2. This moves the pilot's lead equalization requirement from 3.5 rad/sec to 5 rad/sec which may improve pilot opinion. The low frequency response remains unchanged, therefore the altitude holding performance will not be affected by the addition of lagged pitch rate feedback.

To verify the feedback gain ratios selected using approximate vehicle transfer functions, we next compute the effective controlled element response

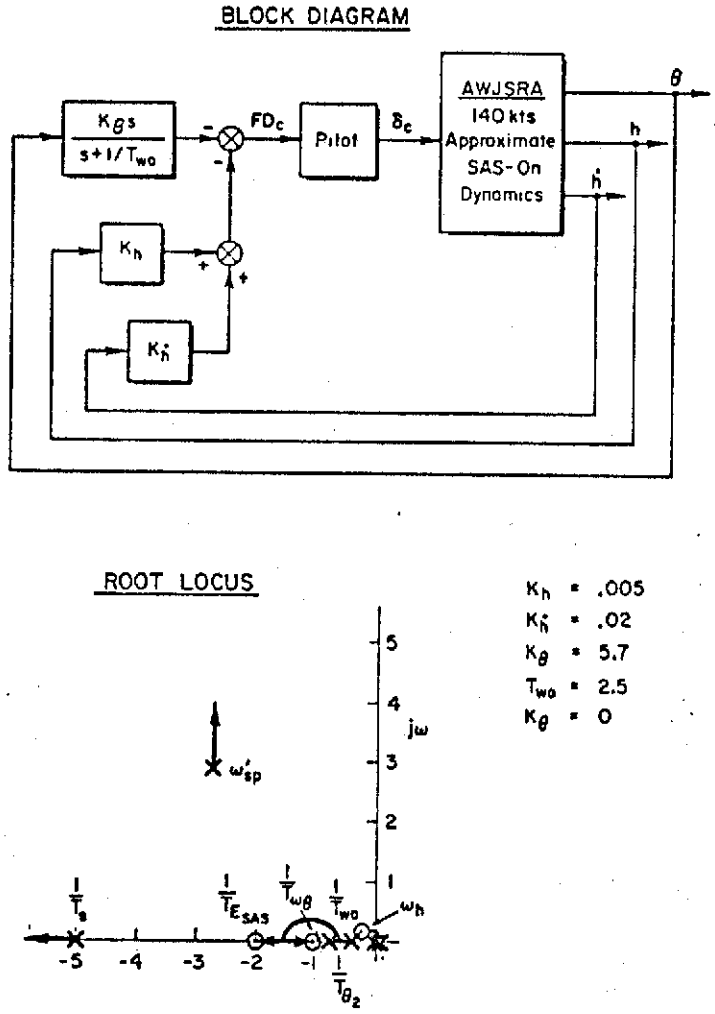

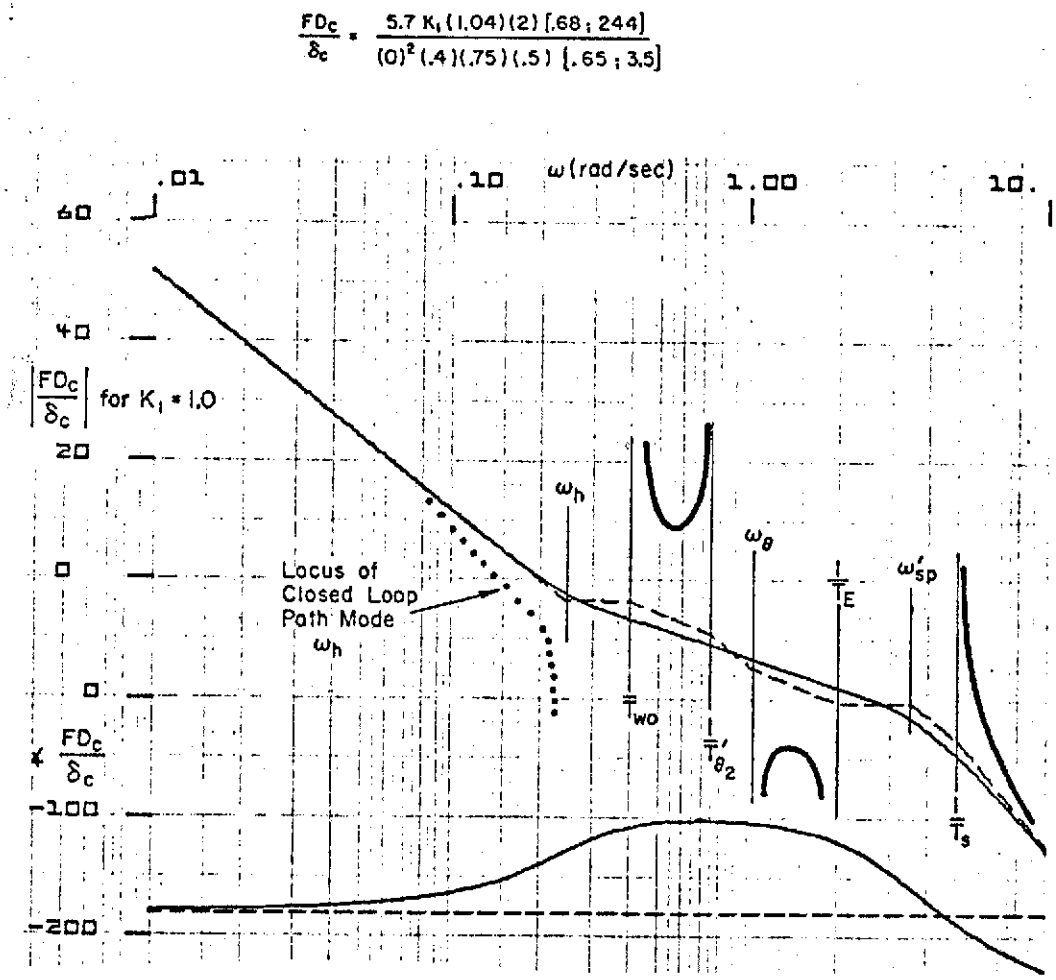

Figure 10. Approximate Column Flight Director Effective Controlled Element at 140 kt — Altitude Hold Mode

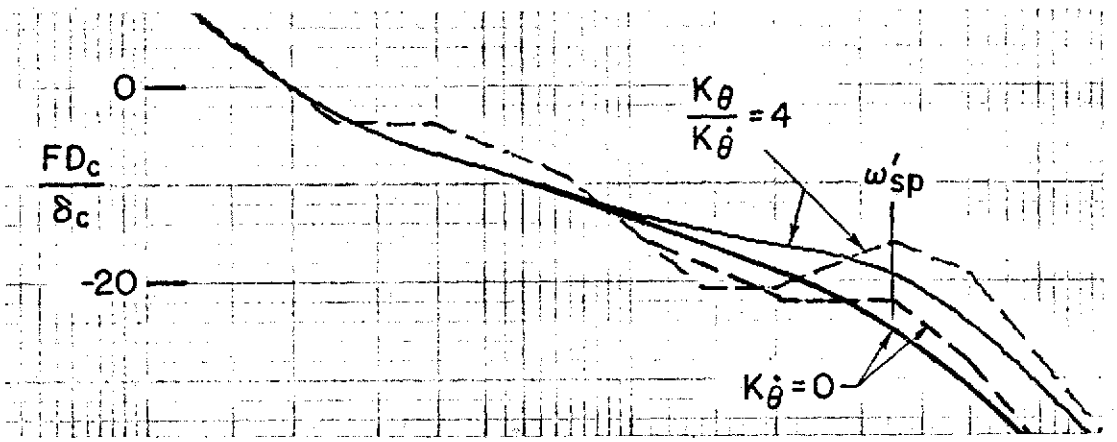

using the transfer functions presented in Appendix D. From Appendix D the SAS-on attitude and altitude rate transfer functions for the 140 kts cruise condition are:

$$\frac{N^{\theta}_{\delta_c}}{\Delta} = \frac{2.74(.065)(.93)[.84;\ 1.26]}{(0)(.085)(.67)(1.08)(5.0)[.82;\ 3.13]} \text{ rad/inch}$$

$$\frac{N^{\dot h}_{\delta_c}}{\Delta} = \frac{606.(.013)[.84;\ 1.26)}{(0)(.085)(.67)(1.08)(5.0)[.82;\ 3.13]} \text{ ft/sec/inch}$$

When combined as shown in Eq. 1, the actual effective controlled element has the frequency response shown in Figure 11. Notice that there is an extensive region of K/s-like response so that the pilot has considerable latitude in the gain he uses. For a crossover at 2.0 rad/sec, which provides maximum phase margin, the pilot gain is about 3 in. of column per inch of director displacement. The main difference between the actual and approximate flight director response is at low frequency. This occurs because the approximate transfer functions assume perfect speed control whereas the actual vehicle has no speed SAS operating at 140 kts. The difference in the high frequency response is due to the addition of the lagged pitch rate feedback. This gain was optimized on the simulator and the results are illustrated in Section V, page 112.

In the actual mechanization the altitude feedback will be limited to avoid excessive rates of climb when the system is engaged or when a large altitude deviation is encountered.

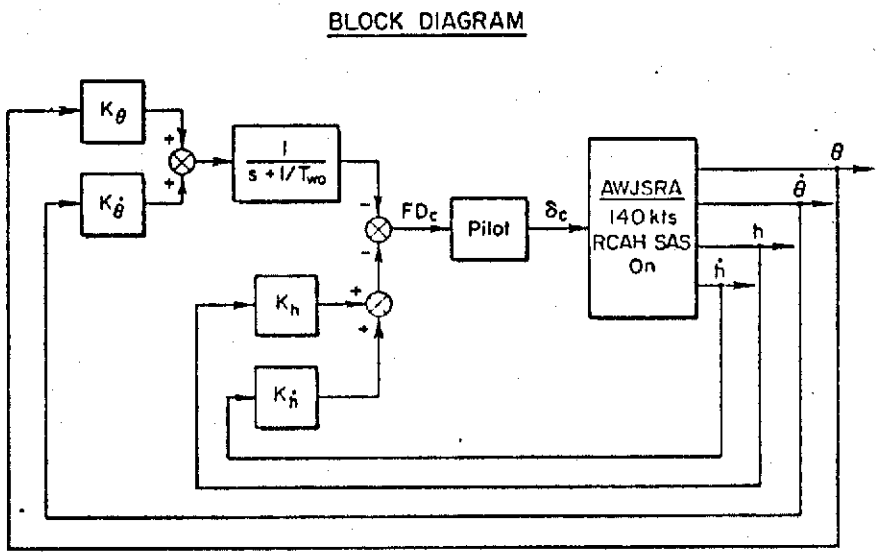

K_h = .005

$K_{\dot h}$ = .02

K_θ = 5.7

$K_{\dot\theta}$ = 1.5

T_{L_θ} = .2

T_{wo} = 2.5

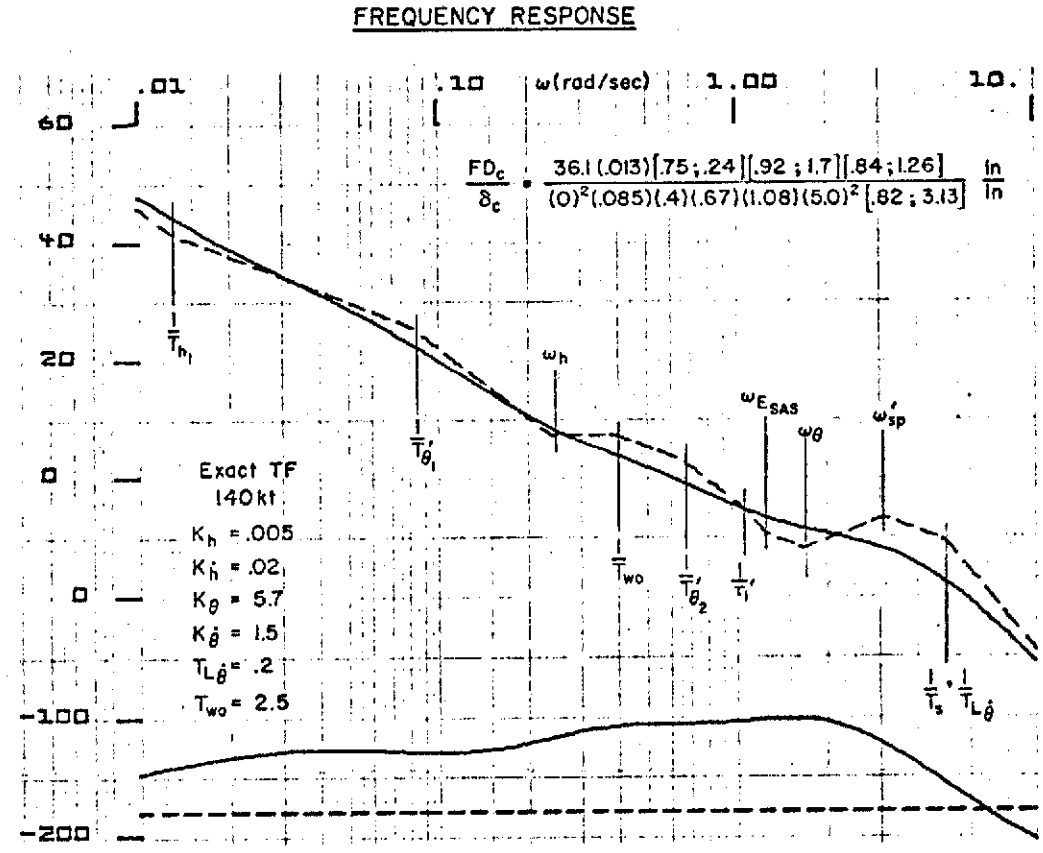

Figure 11. Actual Column Flight Director Effective Controlled Element at 140 kt (With Pitch Rate Feedback) — Altitude Hold Mode

2. Conversion to STOL

The vehicle is decelerated from 140 kt to 90 kt by the speed control, trim management system. As discussed in Section II, the pilot simply commands a new airspeed and the flaps and nozzle are automatically changed per the schedule of Fig. 4a. A change in trim throttle (from 11.8 deg to 20.6 deg) is also required during this deceleration. This change is presented on the throttle director bug, and the pilot simply moves the throttle to the commanded position to null the command. The effective throttle controlled element is therefore a pure gain which represents the easiest form of control.

The trim attitude also changes during the conversion. A plot of the trim attitude and angle of attack for the entire approach was shown in Fig. 4b. During the deceleration to 90 kts, an open-loop, nose-down attitude command as a function of flap deflection is included in the flight director pitch bar to avoid ballooning in altitude. This feedforward is washed out through the normal attitude washout. The amplitude of the feedforward is -4.5 deg at 125 kt and -3 deg at 100 kt. With this input the vehicle will assume the correct trim prior to building up an altitude error. The mechanization of the feedforward is shown later in Fig. 14 as a θ_{bias} term at the output of F_1.

When stabilized at 90 kt the flaps are at 34 deg, nozzles at 55 deg, and throttle at 20.6 deg power lever angle. The column may still be used to control flight path since the vehicle is on the frontside, i.e., $1/T_{h_1}$ is positive. The effective controlled element for the column director at 90 kt is shown in Fig. 12. The path mode, ω_h, is at 0.22 rad/sec with 0.72 damping. The K/s-like response region is similar to that for the 140 kt altitude-hold mode and therefore quite tolerant of pilot gain; however, the gain required to achieve a 2 rad/sec crossover has increased slightly to 4 rather than 3 in./in. at 140 kt.

It should be mentioned that at the 90 kt flight condition it is possible to control altitude with thrust. This can be appreciated from the $\dot{h}/\delta_T$ transfer function plotted in Fig. 13. However, modulating the thrust during level flight would produce an undesirable noise condition that would probably be unacceptable to the pilots. It would also use more fuel.

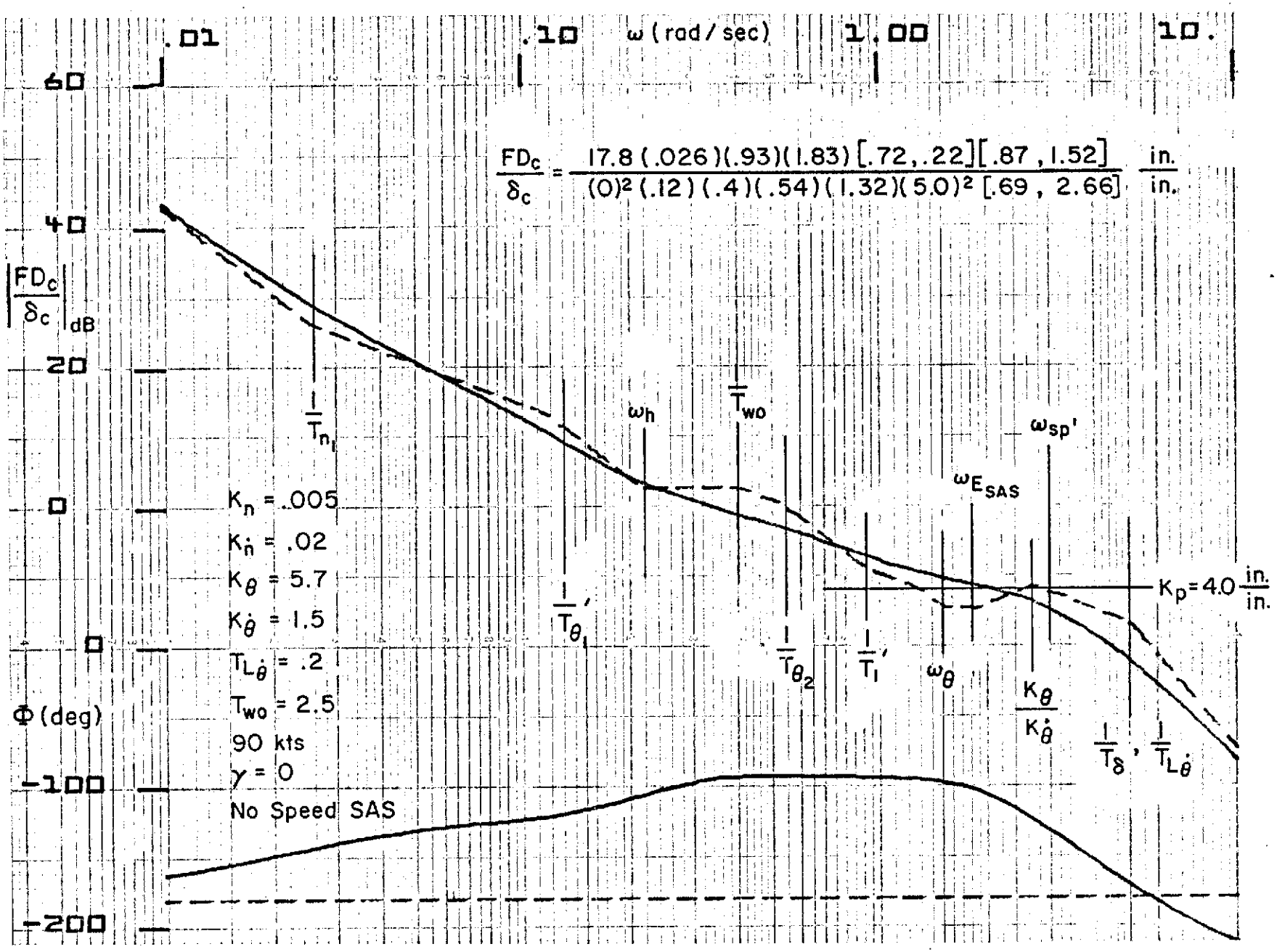

Figure 12. Effective Controlled Element for Column Director at 90 kt

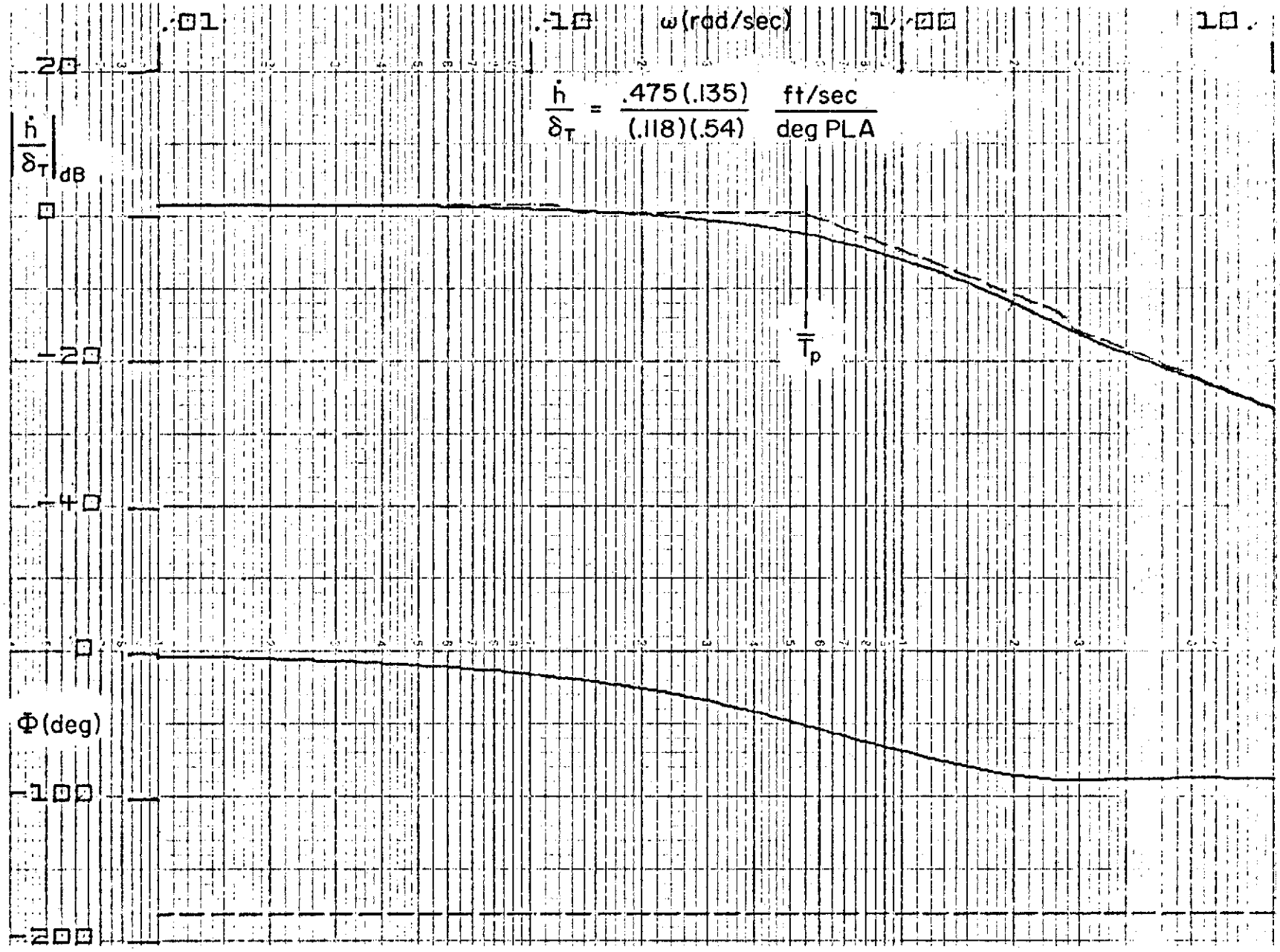

Figure 13. Effective Controlled Element for Throttle Director at 90 kt — Altitude Hold

In summary it appears that a fixed gain altitude hold system employing the CTOL control technique will provide an acceptable flight director system down to 90 kts. Speed is controlled via the speed SAS or with the throttles when the SAS limits are reached. The throttle director indicates the trim throttle position necessary to maintain the transition schedule. The advantage of this technique is that the transition is accomplished with only the pitch and roll cross bars, similar to that in a CTOL aircraft.

3. Glide Slope Capture

Normally the glide slope is captured at 90 kts although it is also possible to capture at all speeds down to 60 kts.

The column director logic designed for capture is shown in Figure 14. Altitude hold is faded out linearly as the aircraft goes from d_{II} to d_F feet from the beam. This logic is only applicable for capture from below. The glide slope deviation and rate of closure is faded in as a function of time after the altitude hold is faded out. A time function keeps the fade-in independent of approach speed. No feedforward pitch command is required for capture since the beam plus beam rate feedback times the timer gain will command a pitch over prior to intercepting the beam. The timer gain, K_t, and the fade-out distances were optimized during the simulation since the interaction of variables would require a nonlinear analysis including the throttle director.

A block diagram of the throttle director is shown in Fig. 15. The trim throttle required for cruise at 140 kt is δT_0; the thrust change required for conversion at 125 kt is δT_1; and the thrust change necessary to maintain 90 kt while on the glide glope is δT_2. From the trim thrust shown in Fig. 4a, thrust must be reduced from 20.6 deg to 12 deg for this intercept. Consequently, prior to glide slope intercept, at a distance d_I, an open-loop thrust command is presented on the throttle director. This starts the vehicle on a descending path which reduces the beam closure rate, and therefore interacts with the column director command. Hence, the selection of the distance, d_I, is again best accomplished on the simulator.

Filters are added to the feedback quantities in the throttle director to reduce any high-frequency bar motions due to gusts and/or electronic noise.

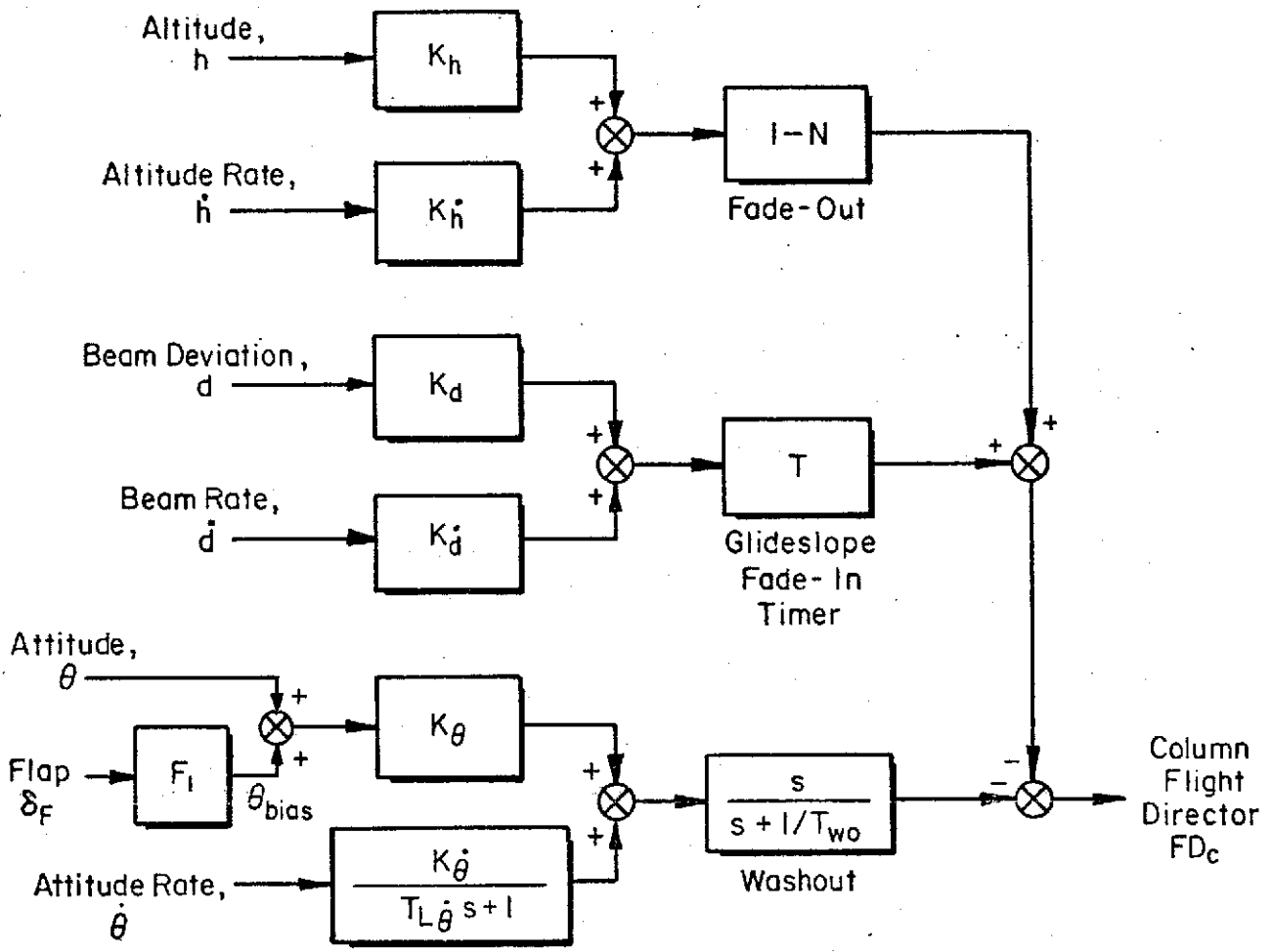

CAPTURE LOGIC

FADE-OUT

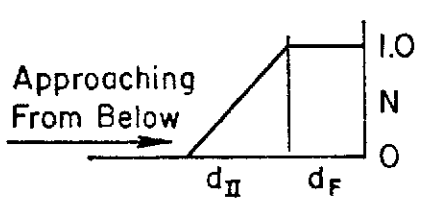

TIMER

T = 0 When $d > d_F$

T = kt When $d \leq d_F$

Limit = 1.0

Figure 14. Column Flight Director for Conversion Glide Slope Capture

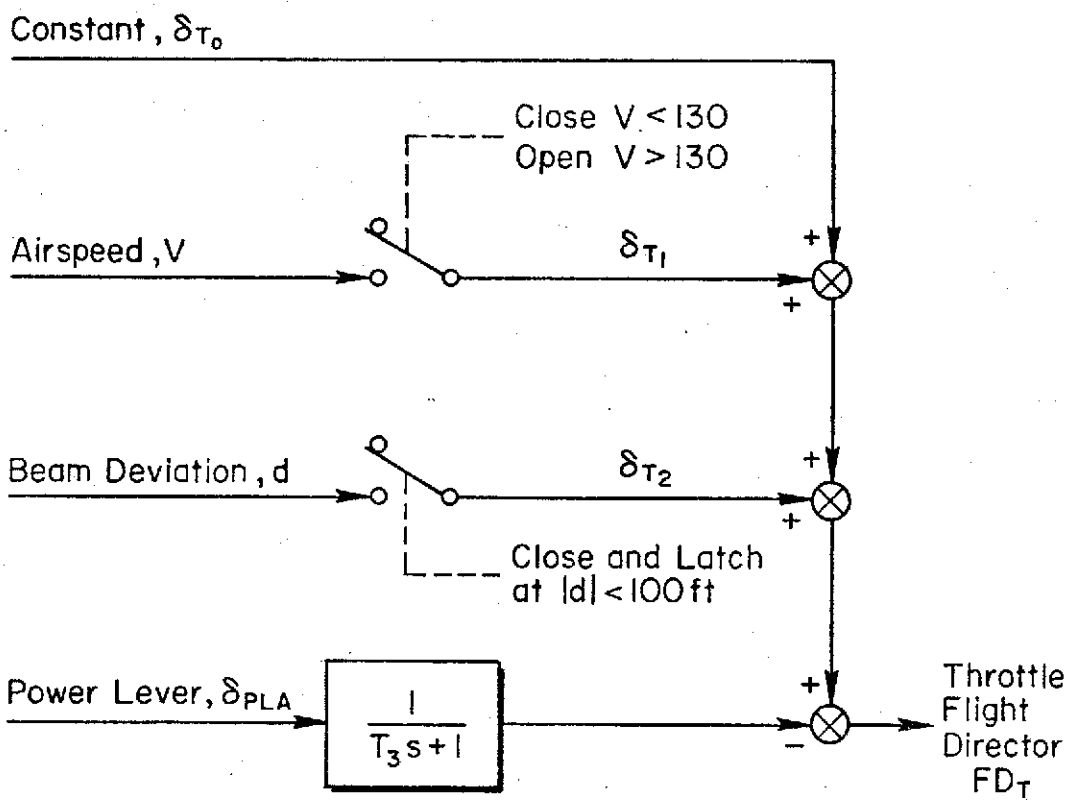

Figure 15. Throttle Flight Director for Conversion Glide Slope Capture

The filter on power lever feedback is necessary to reduce feedback of high-frequency pilot inputs, i.e., remnant. To maintain a pure gain closure of the throttle director, this lag should be at a break frequency of 3-5 rad/sec.

4. Glide Slope Tracking

a. Frontside

The first phase of glide slope tracking is accomplished at 90 kts. Since the vehicle is still on the frontside there need be no difference in the control strategy from the level flight case. In fact, a comparison of the beam deviation to column transfer function shown below shows no significant differences from the altitude hold director.

$$\left.\frac{h}{\delta_c}\right|_{\substack{90\ kt \\ \gamma=0}} = \frac{110.(.025)[.87;\ 1.52]}{(0)(.118)(.54)(1.32)(5.0)[.69;\ 2.66]}\ \frac{ft/sec}{in.}$$

$$\left.\frac{\dot{d}}{\delta_c}\right|_{\substack{90\ kt \\ \gamma=-7-1/2}} = \frac{132(.025)[.87;\ 1.52]}{(0)(.149)(.49)(1.41)(5.0)[.71;\ 2.56]}\ \frac{ft/sec}{in.}$$

There are several differences, however, in the flight director feedbacks. First, a higher path deviation gain is necessary for glide slope tracking than for altitude hold. This is especially true with a range compensated beam since the displacement sensitivity does not increase. Consequently, a constant gain system has to have a sensitivity that is acceptable for close in glide slope tracking.

To keep the path mode frequency relatively constant, the beam rate gain must be increased in proportion to the beam deviation gain. Also it is desirable to keep the $K_\theta/K_{\dot{d}}$ ratio equal to U_o as discussed in the 140 kt cruise phase. With K_θ = 5.7 in./rad this implies a beam rate gain of .038 in./(ft/sec) at 90 kt. This is nearly double the altitude rate gain used for altitude holding. Doubling the beam deviation gain in turn (to .01 in./ft) results in full scale director displacement with ±100 ft of glide slope error. The final gain selected was 0.0114 in./ft in order to slightly increase the path mode frequency from 0.25 rad/sec to 0.3 rad/sec.

Another difference is the use of beam rate feedback instead of altitude rate. Beam rate has been difficult to obtain in the past without incurring excessive noise penalties. However, this is solved with a second order complementary filter as described in Ref. 6. Basically, this derives beam rate from washed out instantaneous altitude rate (for the high frequency component), and lagged beam rate (for the low frequency component). A schematic of the mechanization is shown in Figure 16. The choice of the filter break frequencies, ω_1, ω_2, and ω_3, is based on (see Ref. 6):

- ω_1 cuts off the pseudo-differentiation of beam error; therefore, it may not be overly large. A range 0.3 to 1.0 is a likely possibility. The actual value is determined on two bases: 1) "best" total signal reconstruction in, say, an rms sense; and 2) effective bandwidth of noise, as opposed to signal.

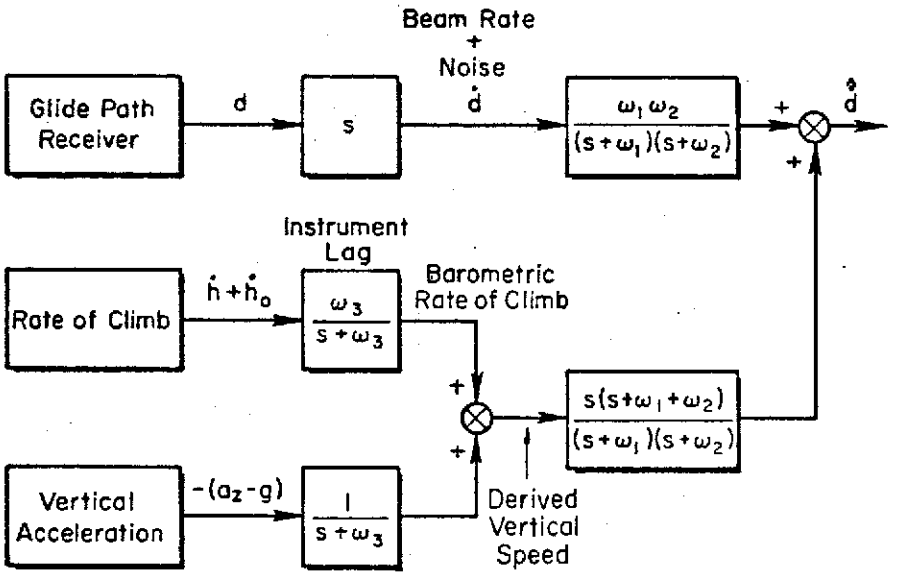

Figure 16. Mechanization of Beam Rate Signal

- ω_2 cuts off the noise on the pseudo-differentiated beam error. A good range of values is between 1.0 ω_1 and 3.0 ω_1.
- ω_3 must be chosen to approximate the barometric vertical speed lag as closely as possible.

Due to beam noise being magnified by the higher gains in the beam deviation feedback, a filter is necessary. With a path mode at 0.3 rad/sec a lag break at 1 to 2 rad/sec will not affect the performance or effective controlled element response.

Incorporating the above changes and including the speed SAS produces the controlled element for glide slope tracking at 90 kt shown in Fig. 17. The differences due to the speed SAS are the elimination of the low-frequency roots, $1/T_{h_1}$ and $1/T_{\dot{\theta}_1}$ and an increase in the flight path response mode, $1/T_{\dot{\theta}_2}$, from 0.49 to 0.63 rad/sec. This can be seen by comparing the beam deviation to column transfer functions as follows:

$$\left.\frac{\dot{d}}{\delta_c}\right|_{\substack{\text{RCAH SAS} \\ \text{90 kt, } \gamma=-7\ 1/2}} = \frac{131(.025)[.87;\ 1.52]}{(0)(.15)(.49)(1.41)(5.0)[.71;\ 2.56]}\ \frac{\text{ft/sec}}{\text{in.}}$$

$$\left.\frac{\dot{d}}{\delta_c}\right|_{\substack{\text{RCAH SAS}\\ \text{SPEED SAS}\\ \text{90 kt, } \gamma=-7\ 1/2}} = \frac{131[.87;\ 1.52]}{(0)(.63)(1.39)(5.0)[.71;\ 2.56]}\ \frac{\text{ft/sec}}{\text{in.}}$$

The primary effect of the gain change from altitude tracking to glide slope tracking is to increase the closed-loop path mode bandwidth (ω_h) from 0.22 rad/sec (Fig. 12) to 0.3 rad/sec (Fig. 17). The high-frequency portions of the two responses are identical so that the pilot should not notice any difference in the region of crossover. Note that the gain for a 2 rad/sec crossover is 4 in./in. in both cases and the phase margins are the same.

An alternative to the CTOL control technique is to control flight path with thrust. In this case the throttle director would represent the only compensatory tracking command since the column director would be used for trim attitude changes and speed regulation in the event of a speed SAS failure or saturation. A simplified analysis of the effective throttle controlled element shows the potential of this alternative. From Appendix D the simplified beam deviation rate to throttle transfer function is:

$$\left.\frac{\dot{d}}{\delta_T}\right|_{\substack{\text{RCAH SAS}\\ \text{SPEED SAS}\\ \text{90 kt, } \gamma=-7\text{-}1/2}} \doteq \frac{1.1}{s + .63}\ \frac{\text{ft/sec}}{\text{deg PLA}} \qquad (2)$$

By combining beam rate and beam deviation in a ratio such that $K_d/K_{\dot{d}} = 1/T_d = 0.63$ the effective controlled element has a pure K/s-like response, i.e.:

$$\frac{FD_T}{\delta_T} = \frac{A_d K_{\dot{d}}(s + K_d/K_{\dot{d}})}{s(s + 1/T_d)} = \frac{A_d K_{\dot{d}}}{s} \qquad (3)$$

The feedback gains should be selected for a reasonable pilot gain in the region of crossover. For example, with $K_{\dot{d}} = 0.038$ in./(ft/sec), as used in the column director, the effective controlled element would have the response sketched below. The pilot gain necessary for a 2 rad/sec crossover is 40 deg PLA/in. FD_T, which would be too high. Therefore, the display gain, or both feedback gains,

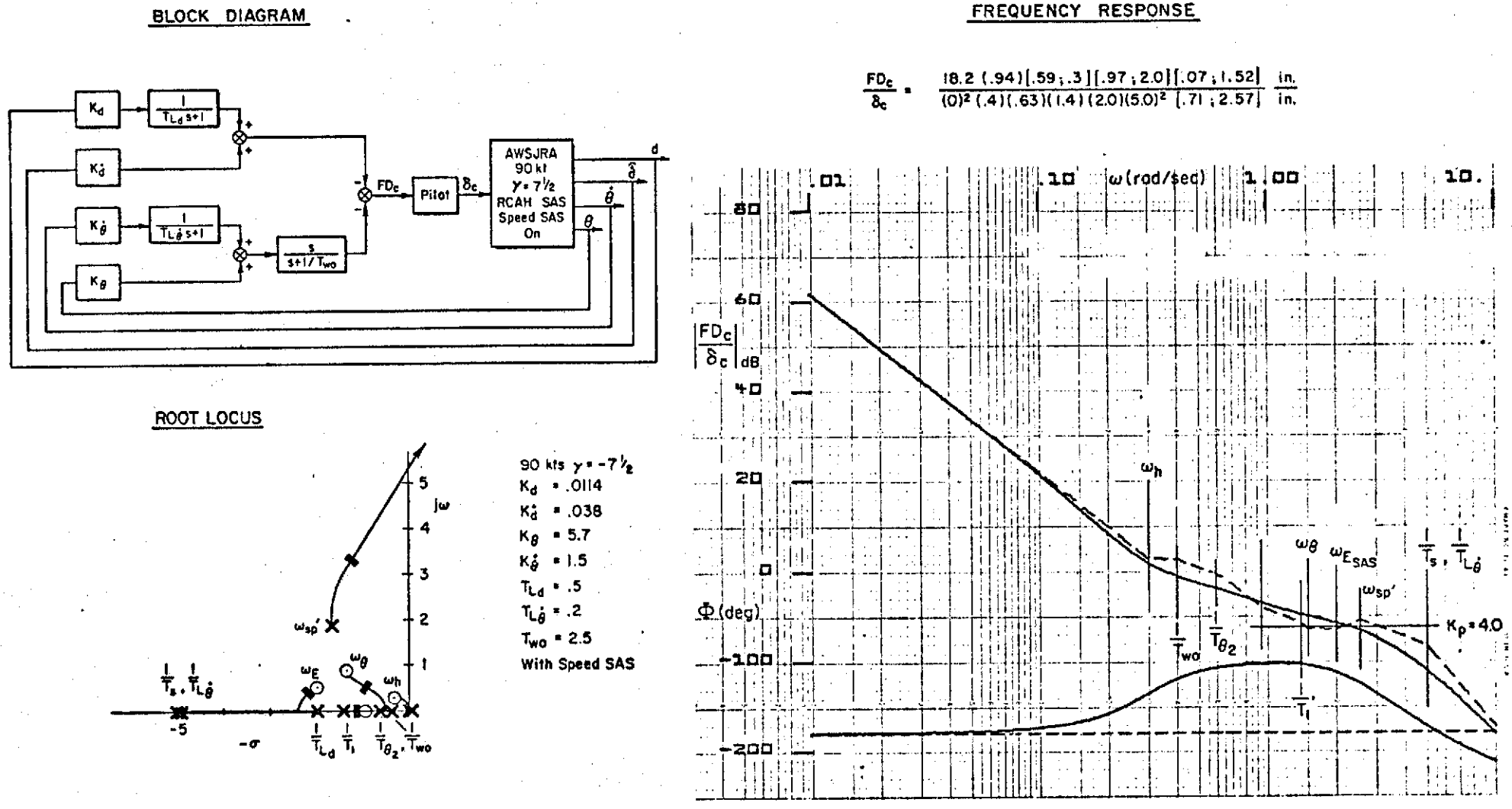

Figure 17. Effective Controlled Element for Glide Slope Tracking with Column at 90 kt, Speed SAS On

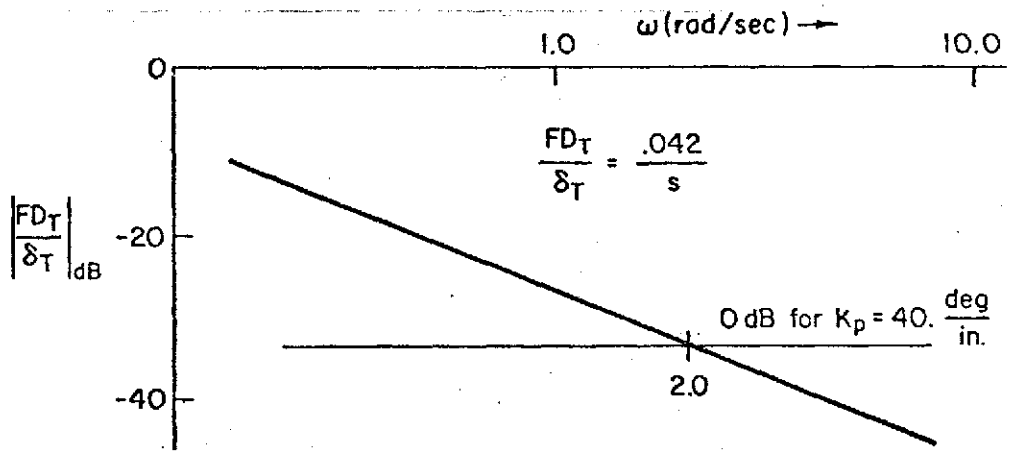

would have to be increased in order to reduce the required pilot gain to something like 20 deg/in. if the throttle director were to have a K/s-like response. However, the throttle director is more akin to a pure gain controlled element during the altitude-hold portions of the approach. Therefore, to minimize pilot readaptation in going from a pure gain director for trim to a K/s-like controlled element for tracking, it is desirable to maintain the same high-frequency response of the two systems. This can be accomplished as outlined below.

Consider first the throttle director for glide path control; it must contain beam and beam rate feedbacks in addition to throttle position feedback as shown in Eq. 4 below.

$$\left.\frac{FD_T}{\delta_T}\right|_{GS} = \frac{A_d \dot{K_d} (s + K_d/\dot{K_d})}{s (s + 1/T_d)} + \underbrace{\frac{K_{\delta_T} 1/T_{L_\delta}}{s + 1/T_{L_\delta}}}_{\text{THROTTLE POSITION}} \qquad (4)$$

where the subscript GS refers to "glide slope" control. This reduces to the form;

$$\left.\frac{FD_T}{\delta_T}\right|_{GS} = \frac{A\,(s + 1/T_p)}{s\,(s + 1/T_{L_\delta})} \qquad \text{when } \frac{K_d}{K_{\dot{d}}} = \frac{1}{T_d} \tag{5}$$

$$\text{where } A = A_d K_{\dot{d}} + K_{\delta_T}(1/T_{L_\delta})$$

$$\text{and } \frac{1}{T_p} = \frac{A_d K_{\dot{d}}}{A_d K_{\dot{d}} + K_{\delta_T}(1/T_{L_\delta})}$$

This transfer function (Eq. 5) is now equated to the throttle director transfer function applicable during altitude hold.

During frontside operation the throttle director simply combines the feedforward trim function $f_3(\bar{v})$ (Figure 1) with lagged throttle position feedback. The resulting flight director to throttle relationship is given as:

$$\left.\frac{FD_T}{\delta_T}\right|_{AH} = \frac{K_{\delta_T}(1/T_{L_\delta})}{s + 1/T_{L_\delta}} \tag{6}$$

where the subscript AH refers to the "altitude hold" portion of the approach. It can easily be verified that the high frequency characteristics of Eqs. 6 and 7 are the <u>same</u> when:

$$K_{\delta_{T_{GS}}} = K_{\delta_{T_{AH}}}(1 - 1/T_p)$$

$$A_d K_{\dot{d}_{GS}} = \frac{1}{T_p}\frac{1}{T_{L_\delta}} K_{\delta_{T_{AH}}}$$

Since a reasonable trim throttle director requires a pilot gain of about 20°/inch, and a remnant-reducing lag at about 3 rad/sec, a desirable effective controlled response is:

$$\left.\frac{FD_T}{\delta_T}\right|_{AH} = \frac{.15}{s + 3} \text{ in./deg} \tag{7}$$

A glide slope tracking director with the same high frequency gain and with a path mode at .3 rad/sec would have the effective controlled element response:

$$\left.\frac{FD_T}{\delta_T}\right|_{GS} = \frac{.15(s + .3)}{s(s + 3)} \tag{8}$$

Consequently, the pilot does not have to readapt to the throttle director if it transitions from trim system to a tracking system. The gains necessary to produce this response for the 90 kt case given in Eq. 3.1 are:

$$K_{\delta_T} = .035 \text{ in./deg}$$

$$K_{\dot{d}} = .041 \text{ in./(ft/sec)}$$

$$K_d = .025 \text{ in./ft}$$

These gains are very compatible with the gains used in the altitude hold mode; therefore very few gain changers would be required.

Finally, the throttle feedback was washed out at low frequencies to avoid a glide slope standoff error for different trim throttle settings. (See Figure 6.)

The main points that have been established in this exercise are the following:

1. Glide path control with thrust can be used effectively.
2. The throttle effective controlled element would not change dramatically in going from altitude hold to glide slope tracking.
3. The potential path mode bandwidth with thrust remains relatively constant with speed, whereas the bandwidth of path control with attitude decreases with speed.
4. For a limited authority speed SAS the STOL technique leaves the column director free to provide speed control if necessary (since the RCAH SAS holds constant attitude).

The ability to control speed with attitude may become a necessity when the vehicle decelerates below 90 kts and gets on the backside of the power curve. When this occurs flight path control with attitude is only adequate when the speed SAS is operating. However, at 90 kts on the glide slope it

takes less than 1° of steady state attitude change to saturate the speed SAS with only 20° authority (based on the open loop steady state u/θ ratio which is −3.0 kts/deg at 90 kts). Consequently, it is desirable to change control techniques when the vehicle gets below the speed for minimum drag. The throttle director design outlined above permits a comfortable interchange of flight-control techniques.

b. Transition to Backside

When the vehicle transitions to a backside condition it is desirable to track the glide slope with throttle. The advantages of this technique were just discussed. Since speed creates the backside condition, speed should be used to fade-out the beam and beam deviation feedbacks to the column director and to fade-in these feedbacks to the throttle director as shown in Figure 18. The function M changes linearly with speed, i.e.,

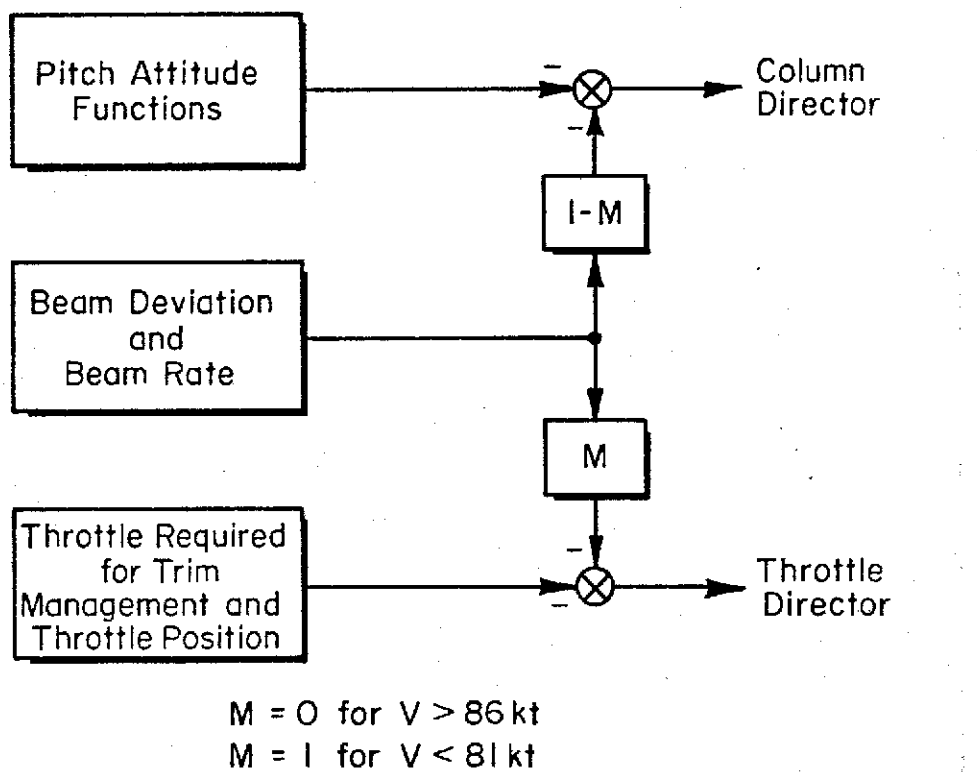

Figure 18. Transition of Flight Directors for Frontside and Backside Operation

from 0 at 86 kts to 1.0 at 81 kts. This switches the beam deviation feedback from the column director to the throttle director in about 2-3 seconds. It is not anticipated that the vehicle will be flown at an inbetween speed, but if this becomes a problem a timer could be used in place of the speed function, M.

There are several other changes that must be accomplished during the transition to the backside technique. First, the washed out attitude feedback must be replaced with true attitude deviation from the desired trim attitude on the glide path. This trim attitude will be different if the pilot flies level at speeds less than 90 kts. Second, speed error should be fed back to the column director in case the speed SAS fails or saturates. Third, the throttle position feedback must become washed out to avoid a beam deviation standoff error. And last, the angle of attack protection feedback is needed in the throttle director to insure that angle of attack is kept below some threshold, α_o, at speeds less than 90 kts. Each of these changes are incorporated in the complete column and throttle flight director block diagrams of Figures 19 and 20 respectively. These diagrams also include all the previous feedback functions required for cruise, conversion to STOL, and glide slope capture.

We will now determine the feedback gain settings required for the throttle director (at 80 kts on the glide slope) that produce good tracking performance and ideal effective controlled element response. As shown previously, it is desirable to maintain the flight director's high frequency response throughout the transition in order to reduce pilot readaptation.

Although not a requirement, it would also be desirable to retain as many feedback gains as possible in order to simplify the mechanization and improve reliability.

The column director is analyzed first. This is basically a trim director since the attitude SAS will hold the commanded attitude below 85 kts (M = 1). For changes in the commanded attitude the effective controlled element response, with speed SAS operating, is simply:

$$\frac{FD_c}{\delta_c} = \left[K_\theta + \frac{K_{\dot\theta} s^2}{(T_{L_{\dot\theta}} s + 1)(s + 1/T_{wo})}\right] \frac{\theta}{\delta_c}$$

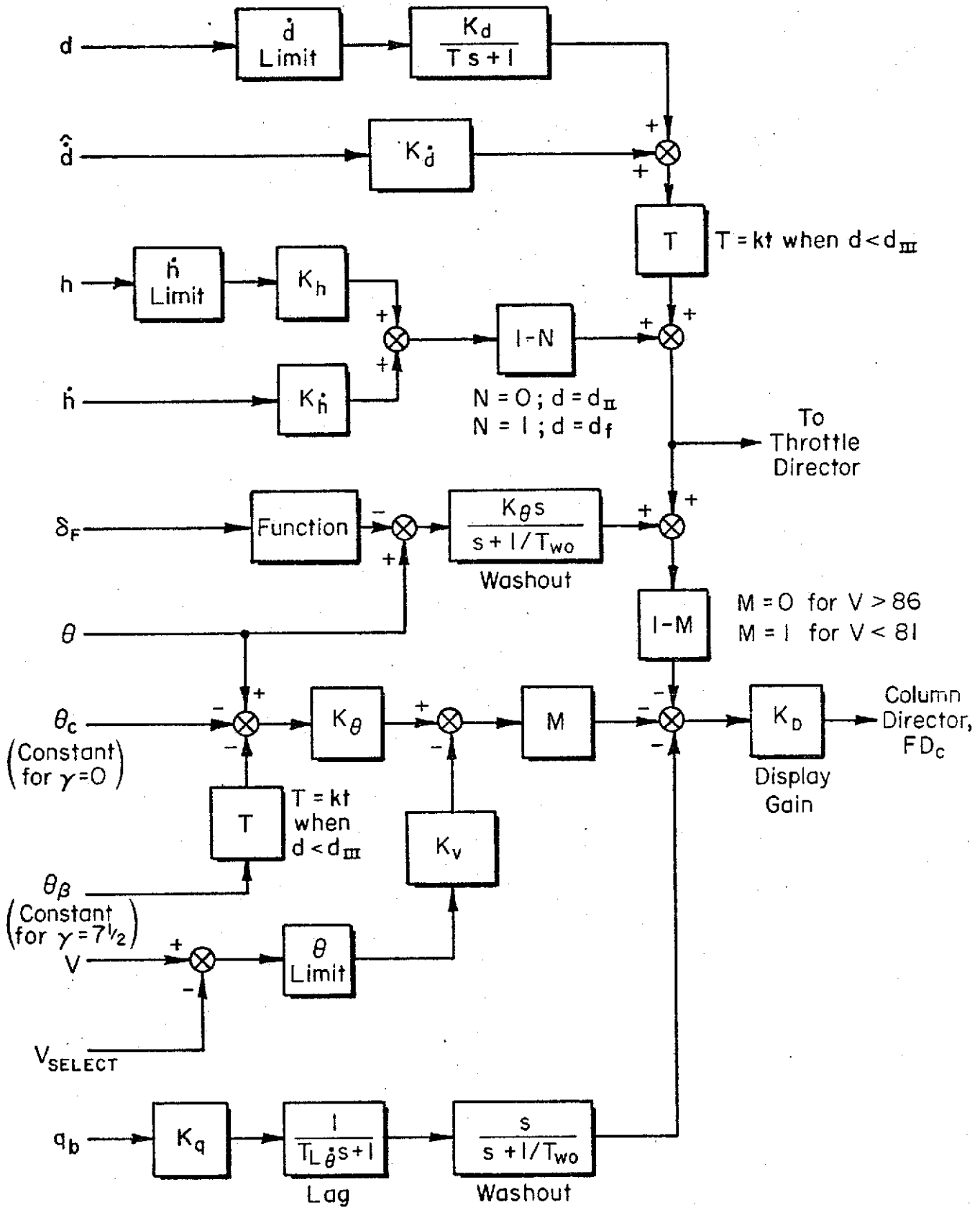

Figure 19. Column Flight Director Block Diagram

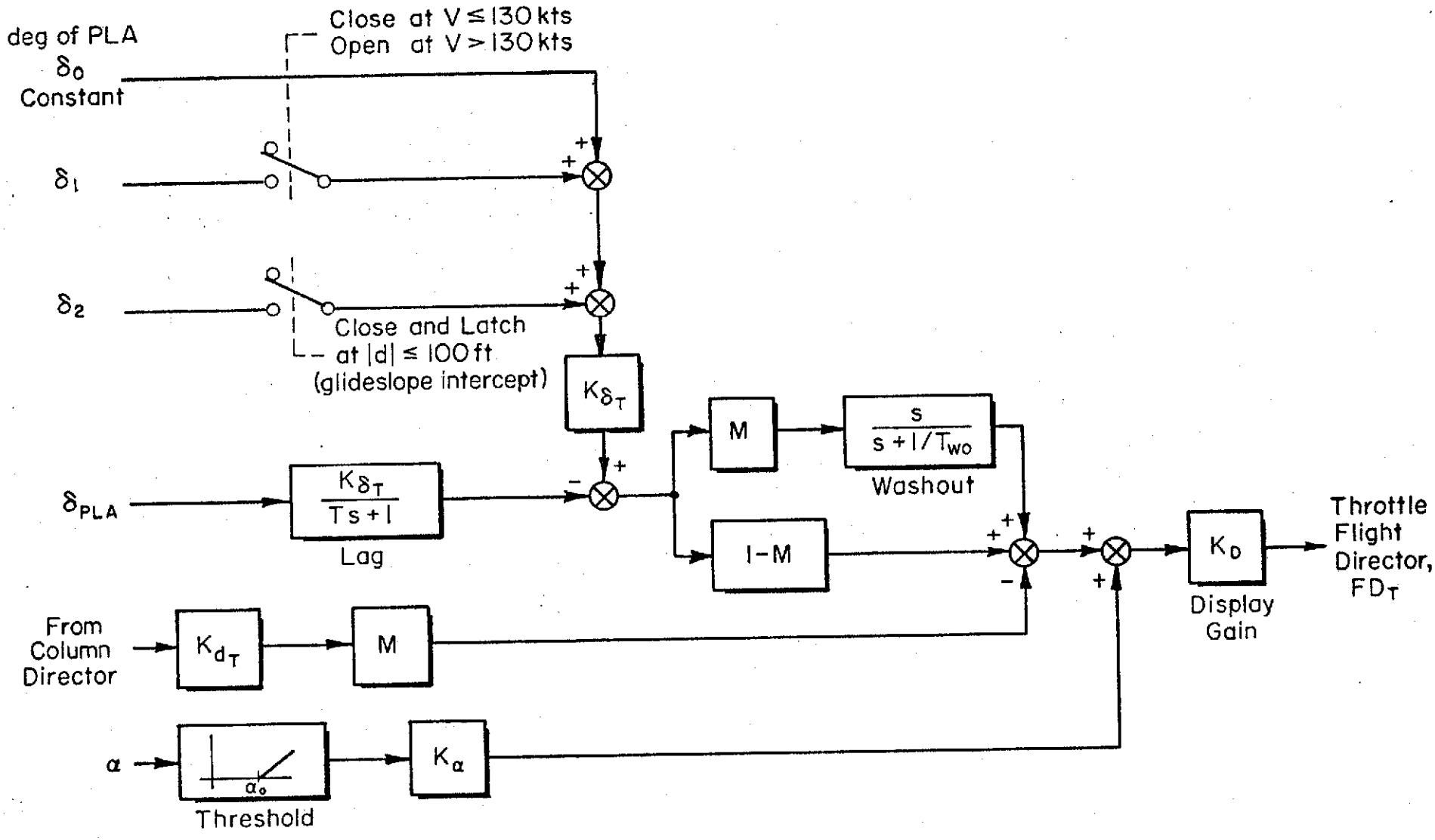

Figure 20. Throttle Flight Director Block Diagram

This response is shown in Figure 21 for the gain values previously used. These gains keep the high frequency response constant. Comparing Figure 21 to Figure 17 (for frontside operation) shows there is no difference in the responses at frequencies greater than 1 rad/sec and very little difference in low frequency response.

If the speed SAS should fail the column flight director will regulate speed with attitude. In this case the effective controlled element transfer function is given by:

$$\frac{FD_c}{\delta_c} = \left[K_\theta + \frac{K_{\dot{\theta}} s^2}{(T_{L_{\dot{\theta}}} s + 1)(s + 1/T_{wo})}\right] \frac{\theta}{\delta_c} + K_u \frac{u}{\delta_c}$$

The airspeed/attitude ratio, K_u/K_θ, can be determined from the steady state u/θ ratio given in Appendix D for 90 kts, $\gamma = -7.5$ with RCAH SAS only. This is -3 kts/deg, therefore the K_u/K_θ ratio should be $-.0035$ rad/(ft/sec). Maintaining the nominal attitude gain at 5.7 in./rad results in an airspeed feedback gain of .02 in./(ft/sec), or in reciprocal terms, 30 kts of airspeed error for full scale director displacement.

The effective controlled element response with the airspeed feedback is shown in Figure 22. The main point to be noted from this response is that the speed mode, $1/T_{\theta_1'}$, essentially moves to $1/T_u'$ when the pilot closes the loop at about 2 rad/sec. This produces an airspeed response time constant very close to that of the nozzle speed SAS. Higher airspeed feedback gains increase the response time but decrease the mid-frequency phase margin which is undesirable.

The trim attitude bias for a -7.5° glide slope should be about -4.5° (as previously shown in Figure 4b). If the vehicle is maintained in level flight during the transition to backside operation, the trim attitude bias should be $+3^\circ$. The glide slope bias is faded into the level flight bias as shown (θ_B) in Figure 19.

It should be reiterated at this point that <u>with</u> the attitude and speed SAS operating, the column director will not be moving during the backside portion of the approach. Consequently, the pilot will not be devoting any workload to the column director. His main task will be tracking the throttle director.

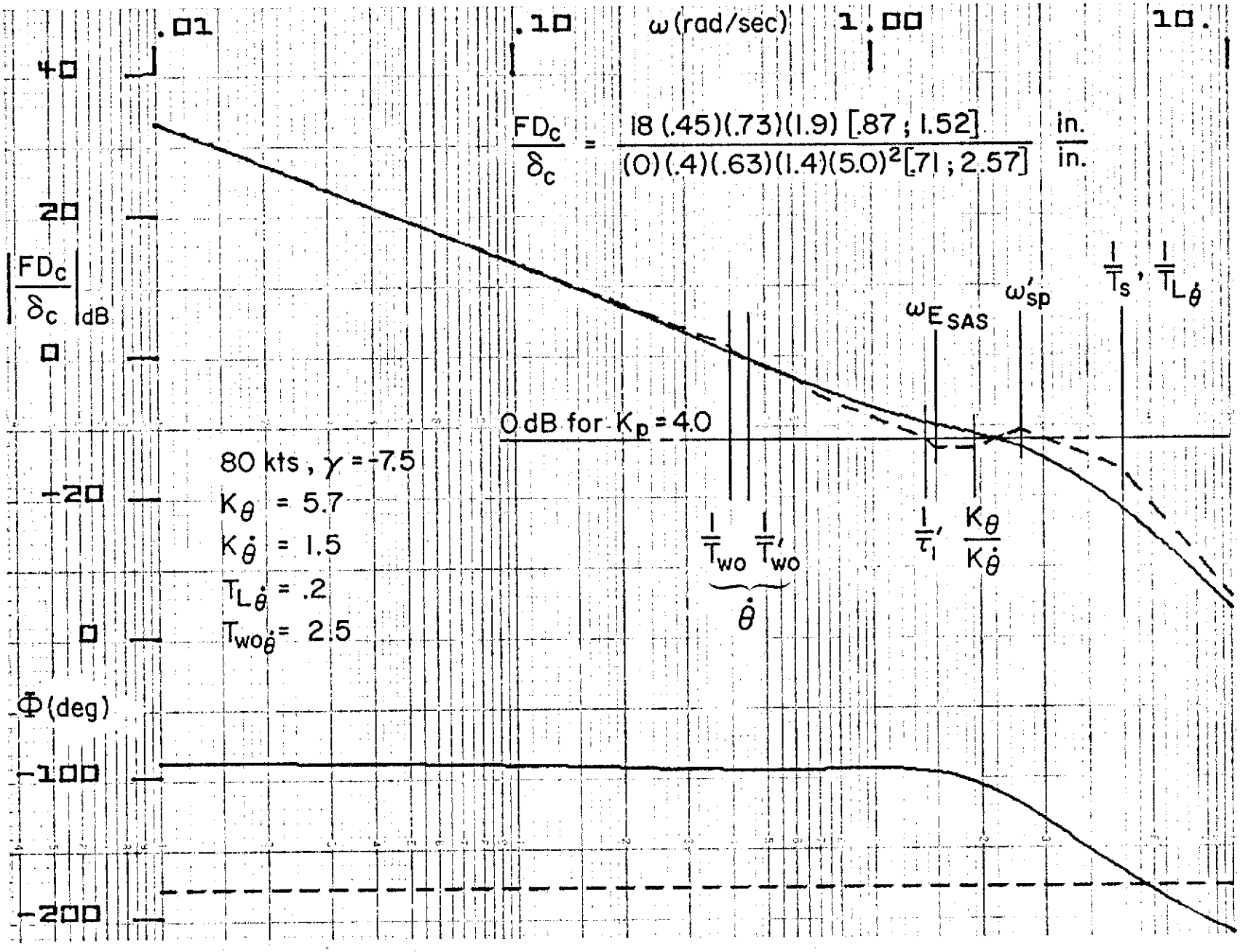

Figure 21. Effective Controlled Element for Column Flight Director in "STOL Mode" (M = 1)

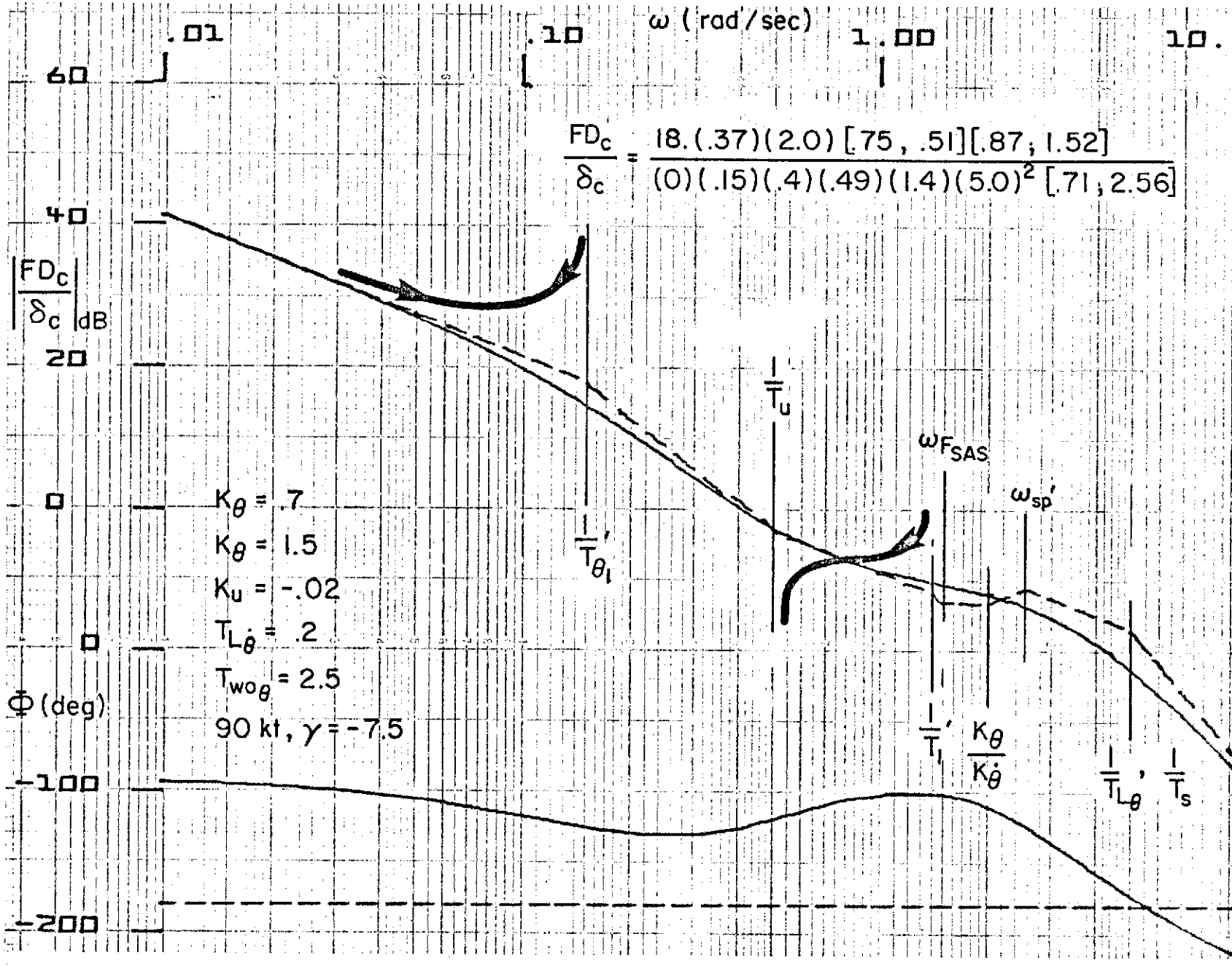

Figure 22. Effective Controlled Element of Column Director with Airspeed Feedback in "STOL Mode" (M = 1)

Glide path control with the throttle has been previously reviewed theoretically. (Eqs. 4 through 8.) However, for completeness, the exact effective controlled element response including throttle washout and lag (T_{W_O}, T_L) and beam deviation lag (T_d) is shown in Figure 23. (A speed of 90 kts is used here since it defines the approximate upper limit of backside operation.) Note that the high frequency gain is the same as the throttle director previously used from trim. The path mode, ω_d, is at higher frequency than expected due to the additional feedback compensations. The closed loop path mode, for a pilot gain of 20°/in., is at .48 rad/sec with .67 damping which will produce good glide slope tracking performance. The high frequency effective controlled element response should produce good pilot opinion.

Although the optimum feedback gains for the throttle director are slightly different from those used in the column director, the differences do not appear significant enough to warrant a gain changer when converting to the STOL mode. For comparison, the two sets of gains are:

	FRONTSIDE	BACKSIDE
$K_{\dot{d}}$	$.038 \frac{\text{in. } FD_C}{\text{ft/sec}}$	$.041 \frac{\text{in. } FD_T}{\text{ft/sec}}$
K_d	$.0114 \frac{\text{in. } FD_C}{\text{ft}}$	$.025 \frac{\text{in. } FD_T}{\text{ft}}$
K_{δ_T}	$.05 \frac{\text{in. } FD_T}{\text{deg PLA}}$	$.035 \frac{\text{in. } FD_T}{\text{deg PLA}}$

The effective controlled element using the frontside gain values is shown in Figure 24. The main difference between this response and that of Figure 23 is the lower frequency of the closed loop path mode. This is due to the reduced $K_d/K_{\dot{d}}$ ratio. However, a path mode frequency of .28 rad/sec is considered adequate and is consistent with path mode frequencies for frontside operation. The 3dB increase in the high frequency gain was not objectionable to the pilot. The effect of speed is also shown on Figure 24 and is seen to be considerable. This is discussed in detail in the following subsection.

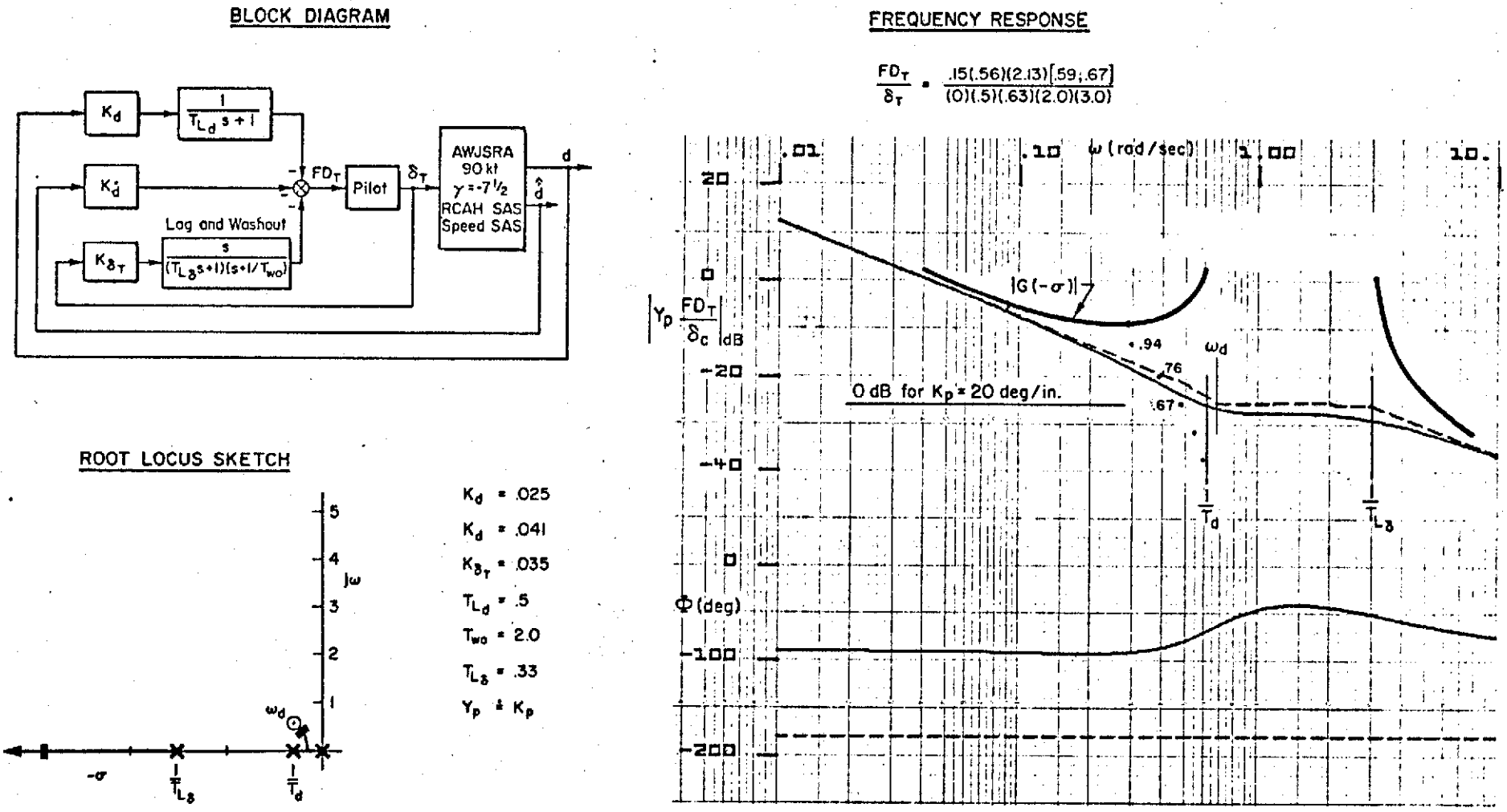

Figure 23. System Survey for Glide Slope Tracking with the Throttle Flight Director at 90 kt

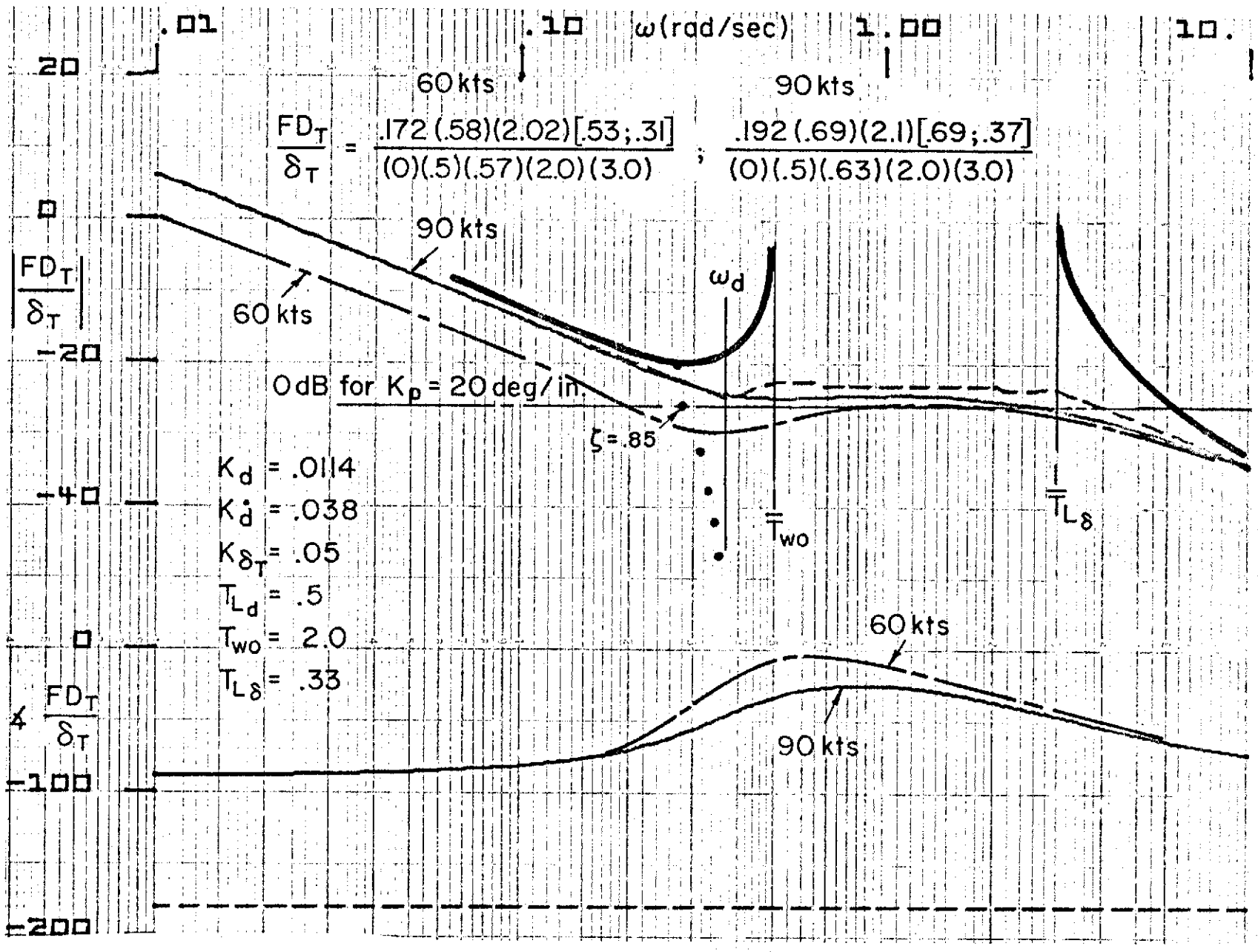

Figure 24. Effective Controlled Element for Throttle Flight Director at 90 kt and 60 kt

c. Tracking at 60 kts

The last phase of glide slope tracking is performed at 60 kts. This is very similar to the previous 90 kt example since thrust is used for path control and attitude is only used in case of a speed SAS failure or saturation.

One difference in the vehicle characteristics that influence the director design is that the beam deviation to throttle effectiveness has been reduced by about 50% at 60 kts. (6 dB reduction in Figure 24.) Comparison of beam rate to throttle characteristics at 60 and 90 kts may be obtained from the following approximations,

$$\left.\frac{\dot{d}}{\delta_T}\right|_{90\text{ kt}} \doteq \frac{1.1}{s + .63} \text{ (ft/sec)/deg PLA}$$

$$\left.\frac{\dot{d}}{\delta_T}\right|_{60\text{ kt}} \doteq \frac{.57}{s + .57} \text{ (ft/sec)/deg PLA}$$

It will be shown that this decrease in effectiveness (while maintaining the same gain ratio of $K_{\dot{d}}/K_{\delta_T}$) will result in decreased path mode frequencies. In general, it is due to the throttle position feedback overpowering the beam and beam rate feedbacks. In the limit when $\dot{d}/\delta_T = 0$ there can be no path control at all.

The decrease in path mode frequency with decreasing throttle effectiveness can be shown from an examination of the flight director effective controlled element. This expression can be derived generically since the throttle washout, T_{WO}, is picked to be close to the beam rate to throttle lag, T_d. Then the throttle director is simply approximated as:

$$\frac{FD_T}{\delta_T} = \frac{(K_{\delta_T} + A_d K_{\dot{d}})[s^2 + K_{\dot{d}} A_d / K_{\delta_T}\, s + K_d A_d / K_{\delta_T}]}{s(s + 1/T_d)(s + 1/T_{L_\delta})}$$

From this expression it can be seen that the damping ratio and frequency of the numerator quadratic will decrease with a decrease in throttle effectiveness, Ad. In terms of actual numerical values, the numerator change from ζ_d = .69; ω_d = .37, at 90 kts to ζ_d = .53, ω_d = .31 at 60 kts. When the pilot closes the loop with a gain of 20°/in. the closed loop path mode decreases from .28 rad/sec to .15 rad/sec (Figure 24). Also the mid-frequency amplitude droop apparent at 60 kts may produce undesirable director response characteristics when the pilot changes his gain.

The path mode frequency and throttle director response can be improved by increasing the beam and beam rate feedbacks to the throttle director. Accordingly, the beam and beam rate gains were increased by a factor of 1.25 in the throttle director (see Figure 10) resulting in an improved effective controlled element response as shown in Figure 25. This is nearly identical to the 90 kts case which is the desired result (keep the effective controlled element constant with speed). Since the beam rate feedback is increased by nearly a factor of 2, the gain was changed as a linear function of speed to avoid any transients in the switching.

Because the RCAH SAS maintains fairly constant attitude response throughout the speed response, the column director gains do not have to be changed from the 90 kts condition.

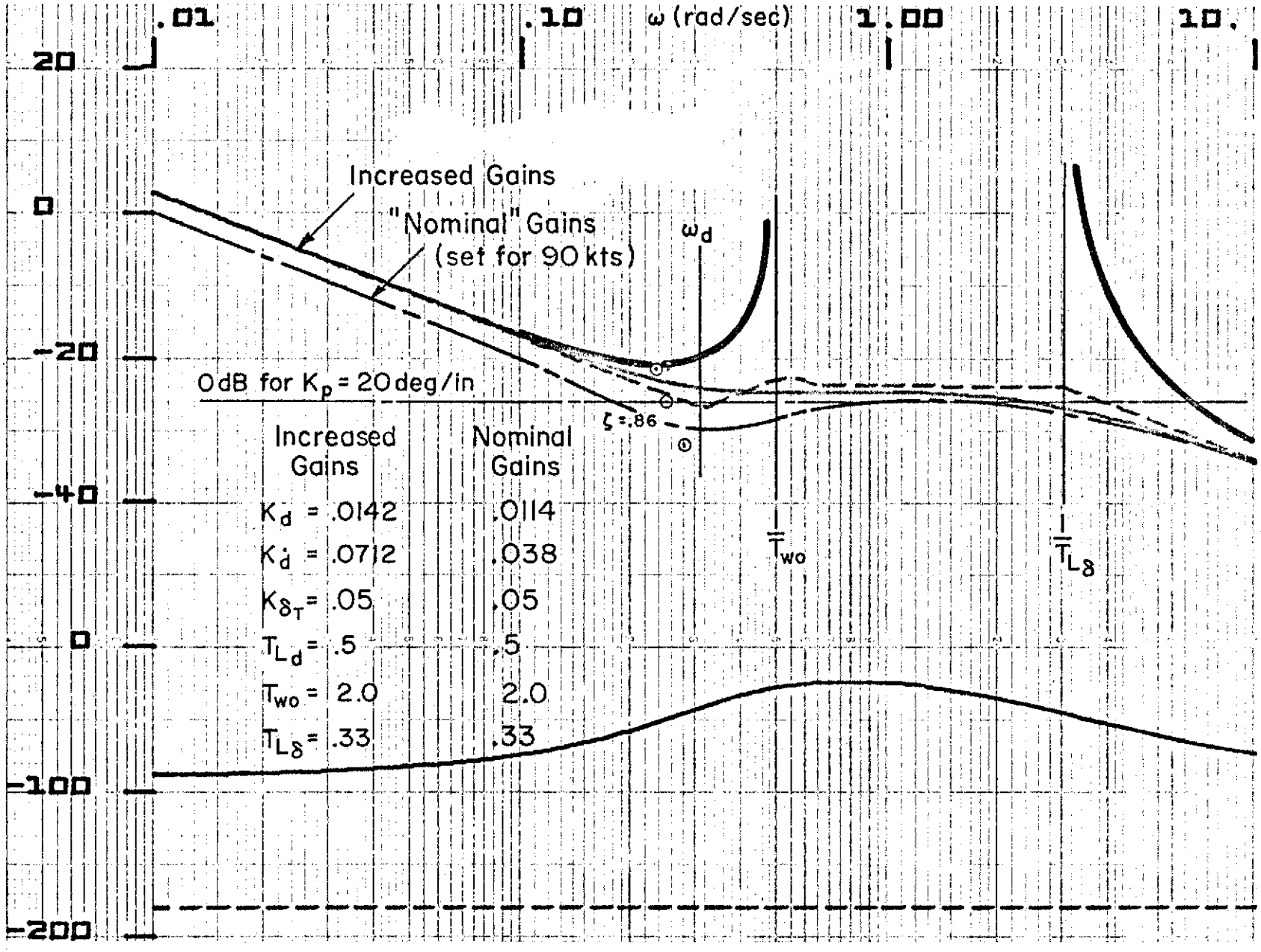

Figure 25. Effect of Increased Gains on Throttle Flight Director Effective Controlled Element at 60 kt

SECTION IV

LATERAL FLIGHT DIRECTOR

Two competing lateral flight director systems evolved from the design effort. The first part of this section contains a summary of each of these along with their advantages and disadvantages. The remainder of the section covers the details of the pilot/vehicle analysis procedures and results of simulator evaluations of the directors.

A. OVERVIEW OF LATERAL FLIGHT DIRECTOR

It is realized that many readers do not have the time, or desire, to delve into some of the more involved details of lateral flight director design covered in this section. Therefore, we have decided to present an overview of the design summarizing the final results and pointing out key figures and tables in the text.

The fundamental considerations in the design process were centered about establishing a set of "functional requirements" and then satisfying these requirements via a "design analysis procedure." A brief discussion of how this was done follows.

1. Functional Requirements

The functional requirements are classified in terms of pilot-centered and guidance and control requirements. These are summarized in Table 2 on page 60. Some requirements related to the dynamic system response are set from considerations of a generic systems survey of the lateral flight director shown in Fig. 29 (page 62). The effect of various feedbacks on the steady-state path-following and disturbance regulation characteristics are summarized in Table 3 (page 64).

2. Design Analysis

A summary of the effect of the various feedbacks on the pilot/vehicle system requirements is given in Table 4 (page 71). At the point in the

analysis, it was realized that two basic design concepts showed considerable promise. First, curved path tracking can be achieved by feeding forward certain trajectory-dependent parameters. This was dubbed Flight Director A (FD A) and represents a more conventional approach to the problem. Secondly, the functional requirements may also be satisfied by using a washed-out bank angle feedback. This concept is called Flight Director B (FD B).

The key design measures for Flight Director A and Flight Director B are summarized by pointing out the appropriate tables and figures in the text.

Flight Director A

- A system survey showing the effective controlled element characteristics is given in Fig. 35 (page 79).
- Initial condition responses and the effect of wind and wind shear is given in Figs. 36-38 (pages 81, 82, and 84).
- Errors in the feedforward bank angle command can lead to standoff errors while tracking a curved path. The resulting sensitivity coefficients are given in Eqs. 22 and 23 (page 85).

Flight Director B

- The system survey for the effective controlled element for FD B is given in Fig. 45 (page 93).
- Disturbance regulation characteristics are presented in Figs. 46-48 (pages 94, 96, and 97) and may be compared directly to Figs. 36-38 (compare FD A and FD B).
- Figures 49 and 50 show the curved path intercept characteristics of FD B (pages 98 and 99).
- Overshoot errors at curved path intercept are inherent to FD B because of the lack of an advanced bank angle command prior to curved course intercept. Fig. 52 (page 102) presents the peak crosstrack error as a function of wind and course radius.
- A simplified feedforward to eliminate curved course overshoots for low turn radius paths is given in Fig. 53 (page 103).

The final system block diagrams, gains, switching logic, and limiters for FD A and FD B are given in Figs. 26 and 27, respectively.

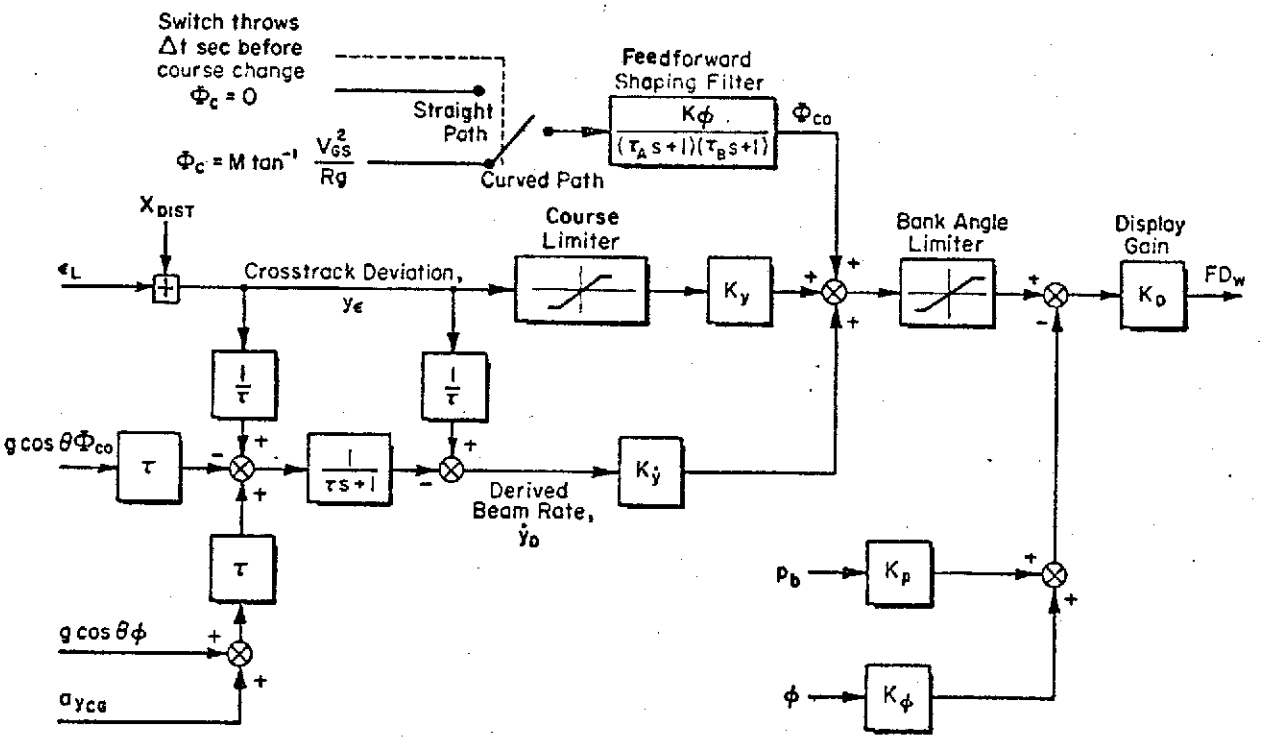

CONSTANTS	UNITS	VALUE
K_y	rad/ft	0.002
$K_{\dot{y}}$	rad/ft/sec	0.0165
K_φ	–	1.6
K_p	sec	1.3
K_D	in/rad	1.0
τ_A	sec	1.0
τ_B	sec	1.0
τ	sec	4.0
Δt	sec	3.0
M	–	+1 right turns −1 left turns
y_{LIM}	ft	2.8 V_{GS}
φ_{LIM}	rad	0.524

Figure 26. Block Diagram and Constants for Flight Director A

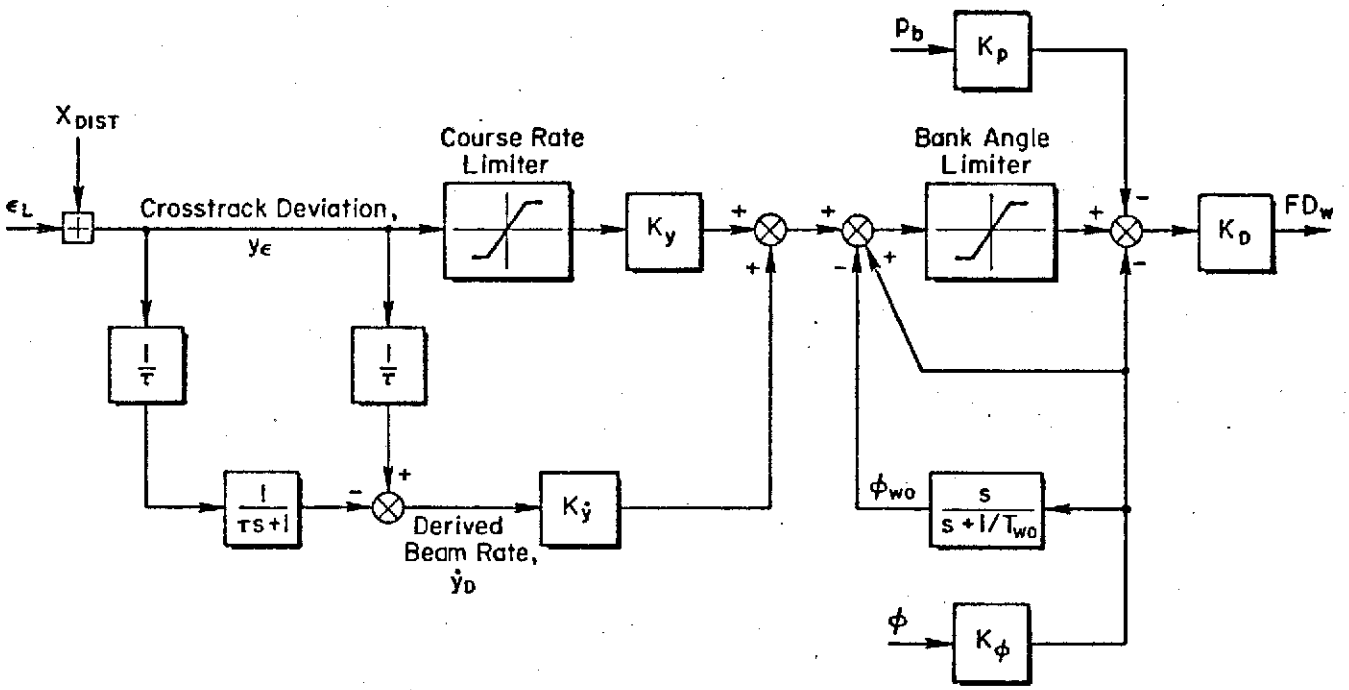

CONSTANTS	UNITS	VALUE
K_y	rad/ft	.002
$K_{\dot{y}}$	rad/ft/sec	.0165
K_φ	–	1.35
K_p	sec	.35
K_D	in./rad	1.5
T_{wo}	sec	10.0
τ	sec	0.5
y_{LIM}	ft	2.8 V_{GS}
φ_{LIM}	rad	.524

Figure 27. Block Diagram and Constants for Flight Director B

TABLE 1

SUMMARY OF ADVANTAGES AND DISADVANTAGES OF COMPETING FLIGHT DIRECTOR DESIGNS

FLIGHT DIRECTOR A (Command Feedforward System)		FLIGHT DIRECTOR B (Washed Out Bank Angle)	
Advantages	Disadvantages	Advantages	Disadvantages
Complimentary filtering to obtain derived beam rate easily accomplished	Requires sophisticated sensors for measurement of V_{GS} on curved path	Will follow any arbitrary course shape within system limits without requirement for input of trajectory parameters	Requires a relatively high quality beam to avoid the need for complimentary filtering
Has a high degree of tracking accuracy given high quality input signals	Requires accurate measurement of groundspeed to avoid standoff errors in crosstrack deviation	Is not sensitive to small errors in signal measurements (100% closed loop operation)	Tracking is not as 'tight' as with FD A. Transition to curved course results in overshoots for commanded turn radii less than 4000 ft
Has rapid well damped response to lateral offsets in the presense of crosswinds	Wind shear inputs result in a standoff	Regulates against wind shear inputs	Response to lateral offsets in a crosswind are not as rapid as FD A
	Sophisticated airborne measuring equipment and required computational capability will keep the cost high	Economical to build compared to FD A	

Finally, the advantages and disadvantages of the competing flight director design concepts are summarized in Table 1. This table indicates that the choice of Flight Director A or Flight Director B depends on factors related to signal quality, required system performance, system complexity, and cost.

B. FUNCTIONAL REQUIREMENTS

1. Compatibility with STOLAND

The lateral flight director system in its final configuration will eventually be incorporated into the STOLAND system and flight tested on the Augmentor Wing Jet STOL Research Aircraft. In its present configuration, no mode selection logic is available, and the flight director is designed to track only high-quality localizer or MLS-type beams. A tentative set of functional requirements associated with incorporation into the STOLAND system and into the flight test environment at Crow's Landing is given below.

- Make system compatible with all NAVAIDS to be used during the tests.
- Incorporate system into current mode selection logic on STOLAND.
- Insure that required signals are available with the necessary accuracy and update frequencies.

These functional requirements have not been satisfied during the phase of work covered by this report. However, they are given here to indicate the additional work necessary to mechanize the flight director on the test aircraft.

2. Fundamental Requirements

The design requirements for the flight director system may be grouped as follows:

- Guidance and Control Requirements — fundamental and independent of whether the controller is an automatic or human pilot.
- Human-Centered Requirements — relate to the fact that the controller is a man.

A summary of the requirements central to design of the flight director is given in Table 2. The satisfaction of these requirements from the basic considerations which lead to the selection, sensing, shaping, and relative weighting of appropriate feedbacks (and feedforwards) in a way which is best for manual control using the flight director. A detailed analysis of how this was accomplished for the curved path lateral flight director is presented in the following paragraphs.

TABLE 2. PILOT/VEHICLE SYSTEM REQUIREMENTS

GUIDANCE AND CONTROL
• Command Following
• Disturbance Regulation
• Stability and Damping
PILOT-CENTERED
• Minimum Pilot Compensation – Feedbacks – Equalization
• Response Quality
• Insensitivity to Pilot Response Variations
• Remnant Suppression

a. Guidance and Control Requirements

These requirements are independent of the type of controller, manual or automatic. In general, they are to establish the aircraft on a curved or straight localizer, and to reduce any path errors to zero in a stable, well-damped manner. They lead to outer loop feedbacks and command feedforwards which are required to accomplish the mission. Additional inner-loop feedbacks are needed to permit the first set of feedbacks to function. The basic system for lateral control is shown in Fig. 28. The block diagram in Fig. 28 is based on the assumptions that: 1) the beam is range compensated; 2) all turns are coordinated; and 3) localizer noise is zero.

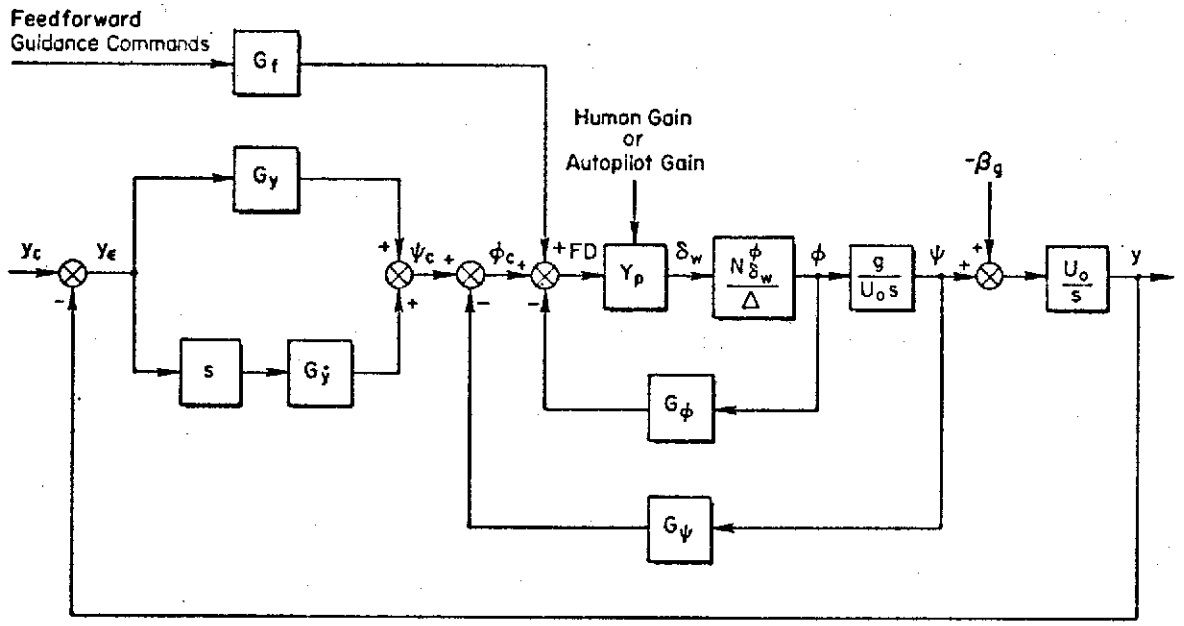

Figure 28. General Block Diagram for Lateral Flight Director A

The closed-loop system response to a course command, y_c, initial condition offset, or a wind disturbance all depend on the characteristic equation of the closed-loop system which is given as:

$$\Delta_{CL} = \Delta + Y_p N^{\varphi}_{\delta_w}\left[G_\varphi + \frac{g}{s}\left(\frac{G_\psi}{U_o} + G_{\dot{y}}\right) + \frac{g}{s^2} G_y\right] \qquad (9)$$

$$= \Delta + Y_p N^{FD}_{\delta_w}$$

Closure of the flight director loop via Y_p (human or automatic pilot) drives the system poles into the flight director zeros, $N^{FD}_{\delta_w}$. These, in turn, are defined by the selection, shaping, and relative weighting of the feedbacks and feedforwards, G_i. $N^{\varphi}_{\delta_w}$ and Δ in Eq. 9 represent the roll numerator and characteristic equation of the augmented airplane which from Appendix E has the following form:

$$\frac{N^{\varphi}_{\delta_w}}{\Delta} = \frac{L_{\delta_{w_{aug}}}}{s(s + 1/T_{R_{aug}})} \qquad (10)$$

Generically, the dominant roots of the augmented airplane consist of a roll subsidence mode and a spiral mode at the origin. It is convenient to write Eq. 9 in root locus form to evaluate the effects of closing the flight director loop on the closed-loop system characteristic equation.

$$1 + \frac{Y_p L_{\delta_{w_{aug}}} \left[s^2 G_\varphi + gs \left(\frac{G_\psi}{U_o} + G_{\dot{y}} \right) + gG_y \right]}{s^3 (s + 1/T_{R_{aug}})} = 0 \qquad (11)$$

The root locus Bode (frequency) characteristics of a typical closure are given in Fig. 29. From Eq. 9 and Fig. 29 it can be seen that the characteristic modes of the closed-loop system may be optimized by adjusting the

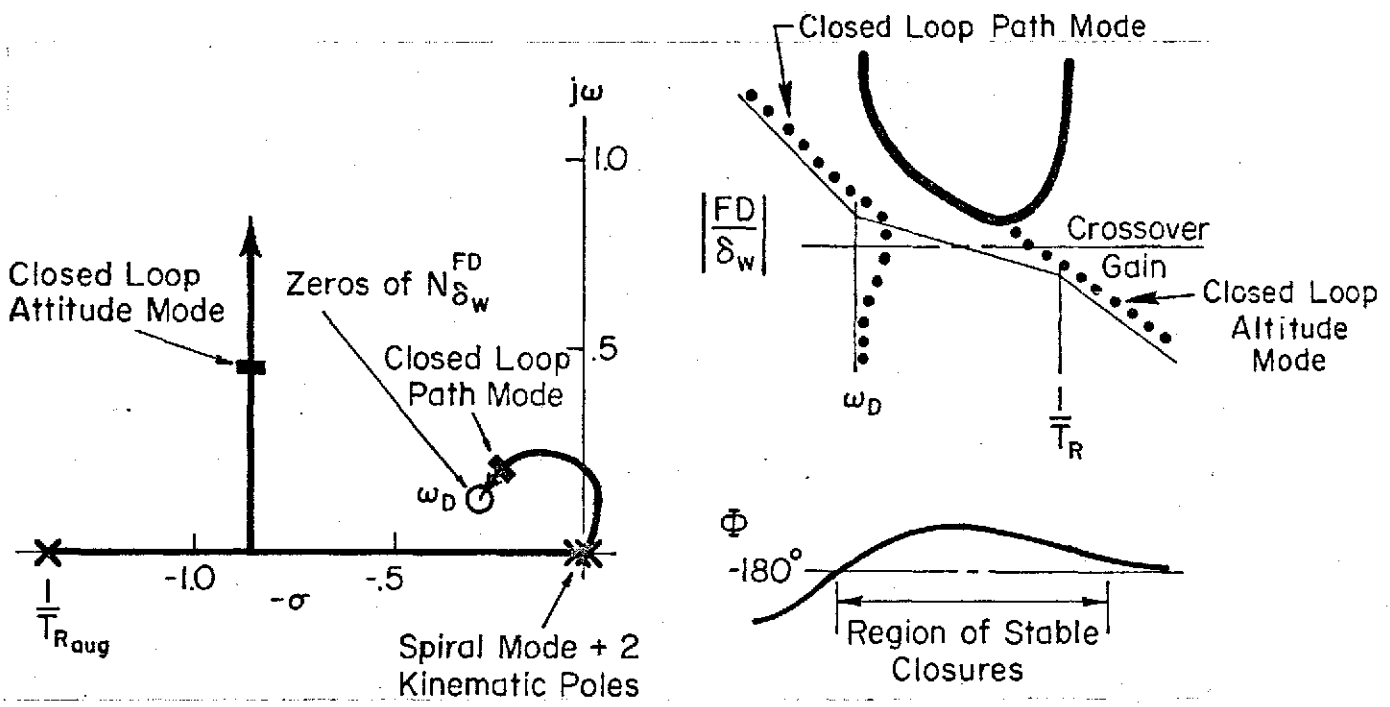

Figure 29. Generic System Survey

numerator coefficients (feedback transfer functions) in Eq. 11. The following guidance and control requirements result directly from these considerations.

1. The numerator must be at least a second order at frequencies well below the roll mode ($\omega_D << 1/T_R$) for system stability (among other things, this implies $G_\varphi \neq 0$).

2. Heading feedback, G_ψ, and/or beam rate feedback, $G_{\dot{y}}$, is necessary for system damping. Note that beam rate feedback implies differentiation of beam error, y_ϵ.

3. The zeros of the $N^{FD}_{\delta_W}$ numerator determine the maximum achievable bandwidth of the closed loop system. As such, they must be at a large enough frequency to allow good command following and disturbance regulation.

The underlined words refer to specific guidance and control requirements listed in Table 2. Note that Requirements 1 and 3, above, are in conflict and involve a fundamental tradeoff between command following/disturbance regulation and system stability.

The above analysis lends certain insights as to the necessary form of the feedbacks to obtain desirable system dynamic response. To complete the picture, we shall now consider the steady state requirements. These relate to various levels of command following (straight and curved courses) and disturbance regulation (wind and wind shear). This is accomplished by writing the differential equation for the closed loop system from the block diagram in Figure 28 in terms of the beam error y_ϵ and solving for the steady state response to y_c and v_g by use of the final value theorm. The differential equation is given in Laplace transform style as:

$$\left[s^2 + \frac{g}{G_\varphi}\left(\frac{G_\psi}{U_o} + G_{\dot{y}}\right)s + \frac{g}{G_\varphi}G_y\right]y_\epsilon = (v_g + sy_c)\left(s + \frac{g}{U_o}\frac{G_\psi}{G_\varphi}\right) \qquad (12)$$

This equation is based on the assumption that the flight director loop is closed tightly so that $\varphi/\varphi_c \doteq 1/G_\varphi$ and that the feedforward operator $G_i = 0$.

Each of the feedback transfer function blocks (G's) may assume three possible forms in order to comply with the requirements stated above. The first has a free s in the denominator, such as $G_y = K_y + (K_{\bar{y}})/s = (K_y s + K_{\bar{y}})/s$; the second has a free s in the numerator (e.g., $G_\varphi = sK_\varphi$); and the last represents just a pure gain feedback. It can be assumed that G_φ and G_ψ would not contain a denominator free s (integral equalization) since this could force a localizer standoff. Therefore, the practical guidance and control possibilities for all three flight director feedbacks are constant or washed out roll angle, constant or washed out heading, and beam error or beam error plus integrated beam error. Thus,

$$
\begin{aligned}
G_\varphi &= k_\varphi \quad \text{or} \quad sk_\varphi \\
G_\psi &= k_\psi \quad \text{or} \quad sk_\psi \\
G_y &= k_y \quad \text{or} \quad k_{\bar{y}}/s \\
G_{\dot{y}} &= k_{\dot{y}}
\end{aligned}
\tag{13}
$$

Table 3 shows the magnitude of the steady-state beam error to three orders of beam command, i.e., step, ramp, and parabola, and two wind inputs, i.e., constant crosswind and crosswind shear, as a function of various combinations of feedback equalization. For example, Line 3 shows that straight gain feedbacks of bank angle, heading, and localizer deviation would produce

TABLE 3

STEADY-STATE ERRORS

FEEDBACKS				STEADY STATE ERROR		
G_φ	G_ψ	$G_{\dot{y}}$	G_y	TO STEP BEAM	TO STEP v_g OR DUAL ANGLE BEAM	TO v_g SHEAR OR CURVED PATH
					PATH DAMPING WITH HEADING	
k_φ	sk_ψ	0	$k_y + \frac{k_{\bar{y}}}{s}$	0	0	0
k_φ	sk_ψ	0	k_y	0	0	OFFSET
k_φ	k_ψ	0	k_y	0	OFFSET	∞
k_φ	k_ψ	0	$k_y + \frac{k_{\bar{y}}}{s}$	0	0	OFFSET
					PATH DAMPING WITH BEAM RATE	
sk_φ	0	$k_{\dot{y}}$	k_y	0	0	0
sk_φ	0	$k_{\dot{y}}$	$k_y + \frac{k_{\bar{y}}}{s}$	0	0	0
k_φ	0	$k_{\dot{y}}$	k_y	0	0	OFFSET
k_φ	0	$k_{\dot{y}}$	$k_y + \frac{k_{\bar{y}}}{s}$	0	0	0

NOTE: sk_φ, sk_ψ represent washout equalization

$k_{\dot{y}}$ represents beam rate

$k_{\bar{y}}/s$ represents beam integral

No s represents a finite, non-zero gain at DC

no error to a step beam command (such as would appear for engagement), a constant error to a steady crosswind or ramp change in beam angle, and an ever-increasing error to a crosswind shear or curved path command. By washing out the heading feedback (Line 2) there is no steady-state error to a steady crosswind or ramp change in beam angle. This equalization is typically found in CTOL approach control systems.

Since wind shear and curved path approaches are much more pertinent to STOL aircraft, the more important conclusions to be drawn from Table 3 are as follows:

1. Without beam integral, beam rate ($k_{\dot{y}}$), along with washed out attitude (line 5) is the only set that has zero path error to curved paths and wind shears.

2. With beam integral it is not necessary to wash out attitude in order to assure zero error to curved paths and wind shears.

While beam integral appears attractive from a steady state analysis standpoint, the values of the integral gain, $k_{\bar{y}}$, that can be achieved without degrading the system stability results in a very long path mode response. Thus the fact that the steady-state error is mathematically zero is of little practical value. Two practical alternatives exist; one is to use washed-out bank angle and the other is to consider the addition of feedforward commands. Both alternatives were considered in the present design exercise, FD A with a feedforward and FD B with washed-out feedback.

The feedforward signals developed in Appendix C are basically guidance commands which if satisfied ideally will result in zero crosstrack error. However, once perturbed from the path, closed-loop control is necessary to develop the appropriate error signals relative to the inertially fixed geometrical course. Given the combination of closed-loop control, y_ϵ, and the appropriate guidance signal (Appendix C, Eq. C-5), the steady-state errors will, by definition, be zero.

b. Pilot-Centered Requirements

The presence of a human pilot in the control loop places additional requirements on the specification and design of the flight director. A summary of those pilot-centered requirements which have direct influence on the lateral flight director design is given in Table 2. A detailed discussion of the implications of the requirements as related to the theory of manual control is beyond the scope of this report (the reader is referred to Refs. 7-9. The following subsections treat each of the requirements in Table 2 only to the extent that they directly affect the lateral flight director design.

Minimum Pilot Compensation

The desire to minimize pilot effort while retaining maximum system performance imposes requirements on the dynamic properties of the effective controlled element consisting of the vehicle plus flight director computer. As is very well known, the human pilot adapts his characteristics to compensate for the dynamic deficiencies of the effective controlled element. As part of this adaptation, he may be forced to develop low-frequency lead(s) and/or to adjust his gain precisely. When low-frequency lead is required of the pilot, a cost in pilot dynamic capacity is incurred (Ref. 7). This is reflected in increased effective time delay and remnant. Increases in both these quantities cause a deterioration in system performance and pilot ratings.

As a result of these human pilot properties, an obvious design requirement is that the effective control element be constructed to:

- Require no low-frequency lead equalization.
- Permit pilot loop closure over a wide range of gains.

This can be achieved when the effective controlled element approximates either a pure gain, K, or a pure integration, K/s, over the frequency range

of pilot/director/vehicle system crossover. For the pure gain case, the pilot must adopt a very-low-frequency lag equalization; this corresponds to a slow trim-like operation and is not objectionable. However, the pure gain effective controlled element results in problems associated with the response quality requirements. This is further discussed in Ref. 10 where it is shown that pure-gain effective controlled elements tend to result in long tails on the response.

An effective controlled element consisting of an integrator, K/s, is nearly as good as a pure gain from the standpoint of pilot response and performance in single-loop tasks. For such dynamics the pilot response is approximately a gain plus time delay in the frequency region of control (near crossover). His time delay will be close to minimum, and the remnant can be minimized by the proper choice of controlled element gain. Pilot lead generation requirements are small, although the pilot can use a small amount of high-frequency lead to reduce his effective time delay in the loop. This lead can be minimized by making the controlled element a K/s at high frequencies, e.g., with a small amount of roll rate feedback.

In short, the key requirement is to adjust the weightings of the various motion feedbacks in the flight director computer so that the effective controlled element approximates the K/s form over a fairly broad frequency region.

Finally, the display/controlled-element dynamics should be approximately time invariant. The pilot can adjust to nonstationary situations, but it involves adaptation and learning which increases task difficulty and degrades performance. This implies that the beam error should be range compensated. The requirement for response quality must also be considered in the design of range compensation and is discussed in the following subsection.

Response Quality

Response quality refers to certain aspects of the display response and aircraft path response which directly affect the pilot's subjective opinion of the system. Those response qualities associated with the display are summarized below.

- Command Bar Consistency — Some correspondence must exist between the command signal and the vehicle or control motions in each of several frequency bands. At low frequency the command should be consistent with localizer deviation and aircraft heading. The mid-frequency response should be consistent with vehicle roll motions and at high frequency with roll rate or control displacement.

- Face Validity — The command bar motions must be consistent with the status information without discontinuities or step commands that require large sudden control inputs and/or result in bank angle overshoots.

- Response Compatibility — The command bar response should not require aggressive control activity nor should it appear "busy" to the pilot.

Response qualities associated with the resulting aircraft motions when the flight director is kept centered are given as follows.

- Modal Interactions — The closed loop system response should be rapid and well damped akin to that of a lower order system with minimum coupling between the modes of motion. This implies that the path mode and attitude mode (see Figure 29) should be well separated, i.e., piloted closure of the flight director loop should not drive the system modes into near proximity to each other.

- Path Mode Consistency — The response of the system to an initial condition offset (due to an external disturbance, pilot inattention, etc.) should not result in "long tails," localizer offsets, overshoots, or abrupt large heading changes. Large heading changes are indicative of a very "tight" system which tends to overdrive bank angle. This is not consistent with normal IFR piloting technique and results in degraded pilot opinion and passenger comfort.

Insensitivity to Pilot Response Variations

The pilot should be able to close the flight director loop over a wide range of crossover frequencies (gain) without a noticeable change in the path mode or flight director response. This implies a broad region of K/s over which the pilot can close the loop with an acceptable phase margin. Additionally, there should be no penalty for unattended operation such as would occur if beam integral were fed back to the flight director. In this case, if the pilot does not continually respond to the director commands, a

small localizer deviation will be integrated to appear as a large director command. If the pilot then centers the bar, the aircraft is driven off the localizer to a point where the integrator output is cancelled by the localizer error. The aircraft will then return to the beam with a time constant near that of the integral term.

Remnant Suppression

Remnant is the pilot's output which is uncorrelated with his perceived error signal. Three types of remnant are presently recognized (see Ref. 8). These are:

- Residual Remnant — This is the "motor" which keeps the signals throughout the loop fluctuating in the absence of any external driving source; it is wideband in character and independent of the signal variance.

- Scanning Remnant — Induced by the requirement for the pilot to scan several displays. Measurements indicate that this type remnant (using the switched gain model in Ref. 8) is so predominant compared with the other sources of remnant that the other sources cannot even be identified.

- Processing Remnant — Scales with the signal variance and derives from some signal conditioning within the pilot. Increases with the requirement for low frequency lead generation within the pilot.

Scanning remnant is decreased by reducing the number of displays required for the pilot to accomplish the desired task. This of course is the basic reason for having a flight director in the first place. The basic tradeoff here is to maximize the amount of information on the flight director while maintaining a low level of complexity on the display.

Processing remnant is minimized by eliminating the need for low-frequency lead generation. This is satisfied by making the controlled element K/s-like over a broad range of frequencies.

The residual remnant is independent of the signal variance and therefore has no impact on flight director design.

Specific details of the application of the pilot-centered and guidance and control requirements to the design of the curved path flight director are given in the following subsection.

C. DESIGN ANALYSIS PROCEDURE

The design of the two final flight director systems was accomplished using a combination of analysis procedures and pilot simulation on the FSAA simulator. Several combinations of feedbacks, feedforwards, complementary filtering and curved/straight course switching logic were considered. A review of the current state of the art was undertaken as a preliminary step in the analysis and a summary of this work is given in Ref. 11.

1. Feedbacks and Feedforwards

Table 4 summarizes the primary guidance and control and pilot-centered requirements for each of the feedbacks discussed in Subsection IV-B. Feedback selection was based on satisfying the system requirements while minimizing the number of tradeoffs between those same requirements. This procedure resulted in the final systems illustrated in Figures 26 and 27.

It was decided to use $\dot{y}$ for path damping because of the practical difficulties associated with the measurement of course angle on a curved path. It was felt that the problems associated with beam noise could be resolved using complementary filtering techniques and perhaps beam rate directly obtainable with scanning beams. This is further discussed in the following subsection.

As can be seen in Table 4, the use of p feedback results in a tradeoff between the pilot centered requirement for a long region of K/s in the effective controlled element and the guidance and control requirement for good system stability. This effect is more prominent when using washed out bank angle and is discussed in Subsection IV-B-5.

The use of bank angle feedback (FD A) results in a required feedforward guidance command for following curved paths (see Subsection IV-B). Appendix C shows that for ideal tracking the guidance command consists of a bank angle feedforward. The feedforward command signal is initiated just prior to curved course intercept and blended via a second-order lag network. This eliminates bank angle and trajectory overshoots typical of current systems when intercepting a curved trajectory from a straight line course. These overshoots are strongly related to the radius of curvature of the commanded

TABLE 4. EFFECT OF FEEDBACKS ON SYSTEM REQUIREMENTS

FEEDBACKS	GUIDANCE AND CONTROL REQUIREMENTS		PILOT CENTERED REQUIREMENTS	
	PRIMARY REQUIREMENT	COMMENTS	PRIMARY REQUIREMENT	COMMENTS
Bank Angle, φ	Stability	Requires feedforward for curved paths (See Appendix C)	Command bar consistency	Mid-frequency flight director motions should look like bank angle
Washed Out Bank Angle, φ	Stability	Washout time constant must be high enough to satisfy stability requirement yet low enough to insure good path following and disturbance regulation characteristics	Command bar consistency	Mid-frequency flight director motions should look like bank angle Washout must be high enough to maintain face validity
Roll Rate, p	None	Tends to reduce path damping	Minimum pilot compensation Remnant suppression	Provides K/s-like response at frequencies beyond the roll mode Provides good flight director response at curved path intercept point
Heading, ψ	Path Damping	Requires feedforward for curved path and for disturbance regulation on curved path — not practical	Minimum pilot compensation Path mode consistency Remnant suppression	Determines localizer capture rate
Washed Out Heading, ψ_{WO}	Path Damping	Requires feedforward for curved path and wind shear on straight path	Same as above	Same as above
Course Angle, λ	Path Damping	Requires feedforward for curved path Requires inertial navigation system or equivalent for measurement	Same as above	Same as above
Crosstrack Rate, $\dot{y}$	Path Damping	Does not require feedforward Beam noise problems due to differentiation of crosstrack deviation	Same as above	Same as above
Crosstrack Error, y_ϵ	Path Command and Disturbance Regulation		Path mode consistency	Should be compatable with localizer errors High sensitivity at long distances from touchdown are not desirable
Localizer Error, ϵ	Path Command and Disturbance Regulation	Stability problems due to constantly varying crosstrack deviation sensitivity with range	Same as above	
Beam Integral	Disturbance Regulation	Long time constant required for stability reduces regulation effectiveness	Same as above	Results in inconsistencies between command and localizer errors after periods of unattended operation

curved path. The error analysis in Subsection IV-C-4 shows that the crosstrack errors associated with curved path radii less than 4000 ft are unacceptably large when the bank angle command is not initiated prior to curved path intercept.

Bank angle feedforward is not required when the bank angle feedback is washed out (see Table 4). The resulting simplification is one of the chief advantages of this feedback and forms the basis for the FD B design concept. It also represents the key restriction to FD B in that the possibility of "leading the turn" is eliminated without some form of feedforward bank angle command. This implies that FD B will have considerably degraded performance when compared to FD A for commanded turn radii of less than 4000 ft. Evaluation of the tradeoffs between the two flight director designs includes the following considerations.

- The turn radii currently being considered by the FAA (NAFEC) are considerably greater than 4000 ft (on the order of 5000 ft).
- A simplified washed-out feedforward can be implemented into the design of FD B if small turn radii are required.

The decision to use crosstrack deviation (as opposed to localizer angle) was primarily a matter of design simplicity. Use of localizer angle would require range compensation of the flight director gains to maintain the required stability margins and to meet the pilot-centered requirements for minimum pilot compensation discussed in Subsection IV-B-2-b.

The crosstrack deviation gain was set so that a full scale flight director signal would occur at 500 ft of lateral deviation. This corresponds to full scale localizer at a range of 1.8 nm from the localizer antenna which is the point of glide slope intercept for a -7.5 deg glide slope at an altitude of 1500 ft. This sensitivity is somewhat low if the flight director is followed to touchdown and somewhat high for ranges of 5 miles or greater. However, the additional complexity of nonlinear range compensation did not seem warranted based on the current mission profile of the augmentor wing aircraft.

2. Derived Beam Rate

The practical difficulties associated with using beam rate for path damping involve considerations of beam noise. A conventional circuit for obtaining derived beam rate ($\dot{y}_D$) from the localizer error (y_ϵ) is shown in Fig. 30. The transfer function for the portion of the flight director command due to the summation of beam error and beam rate (φ_{c_1} in Fig. 30) is given as:

$$\frac{\varphi_{c_1}}{\dot{y}_\epsilon} = \frac{(K_y + \frac{1}{\tau} K_{\dot{y}})\left(s + \frac{K_y}{K_y\tau + K_{\dot{y}}}\right)}{(s + \frac{1}{\tau})} \tag{14}$$

The derived beam rate, $\dot{y}_D$, is given as:

$$\dot{y}_D = \frac{s}{\tau s + 1} y_\epsilon \tag{15}$$

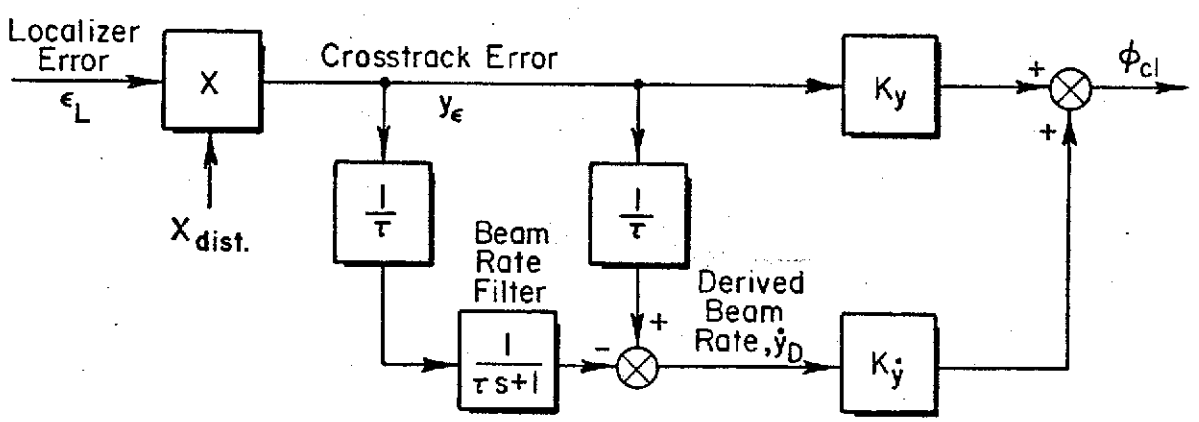

Figure 30. Block Diagram of Circuit for Derived Beam Rate

An indication of the beam noise characteristics which will be seen on the flight director can be obtained by consideration of rms values of φ_{c_1} for a given power spectral density function, $\Phi(\omega)$ of the localizer signal. A plot of the average power spectral density of nine directional localizers was

obtained in Ref. 12 and is given in Fig. 31. Using the fit shown in Fig. 31, the rms values of φ_{c_1} may be computed given an rms localizer noise:

$$\sigma^2 = 2\int_0^\infty \Phi(\omega)\, d\omega \qquad (16)$$

and adjusting the gain, K_L, appropriately. From Ref. 12 the mean-square values of localizer noise varied from 1.48μa to 6.92μa over 12 localizers. Converting μa to degress of localizer error and picking 4μa as a representative value, the rms localizer error is given as 0.066 degrees.* The

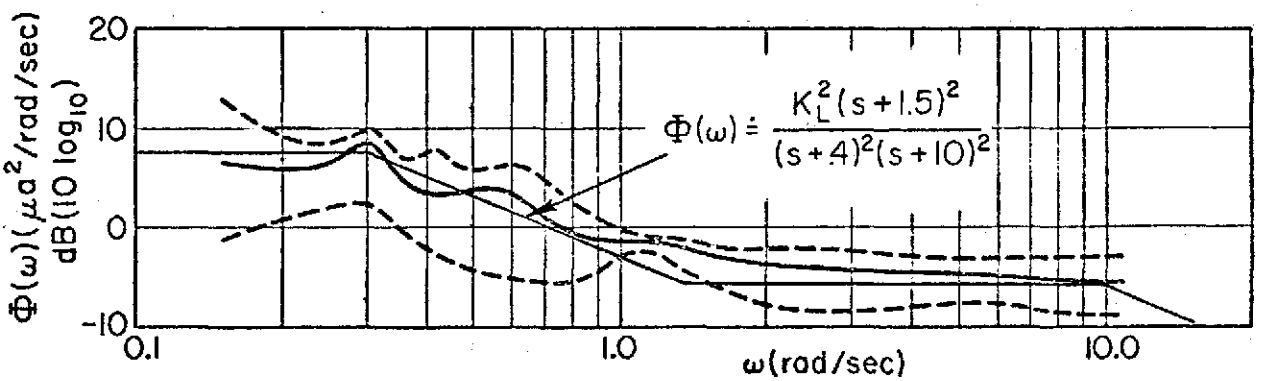

Figure 31. Average Directional Localizer Power Spectral Density

resulting rms flight director noise is given as a function of beam rate filter time constant, τ, and range from touchdown, X_{dist}, in Fig. 32.

As would be expected, increasing the beam rate filter time constant reduces the flight director noise. However, from Eq. 15 the derived beam rate is restricted to frequencies below $1/\tau$ resulting in decreased stability at the path mode frequency, ω_D, as $1/\tau$ approaches ω_D. While these results are for a conventional localizer, they are conservative in that the MLS systems are typically of a lower noise content.

The beam rate noise filter time constant was taken to be 4 sec to minimize the beam noise input to the flight director. This results in elimination of

*This assumes a standard localizer width of ±2.5 deg and ±150a full scale.

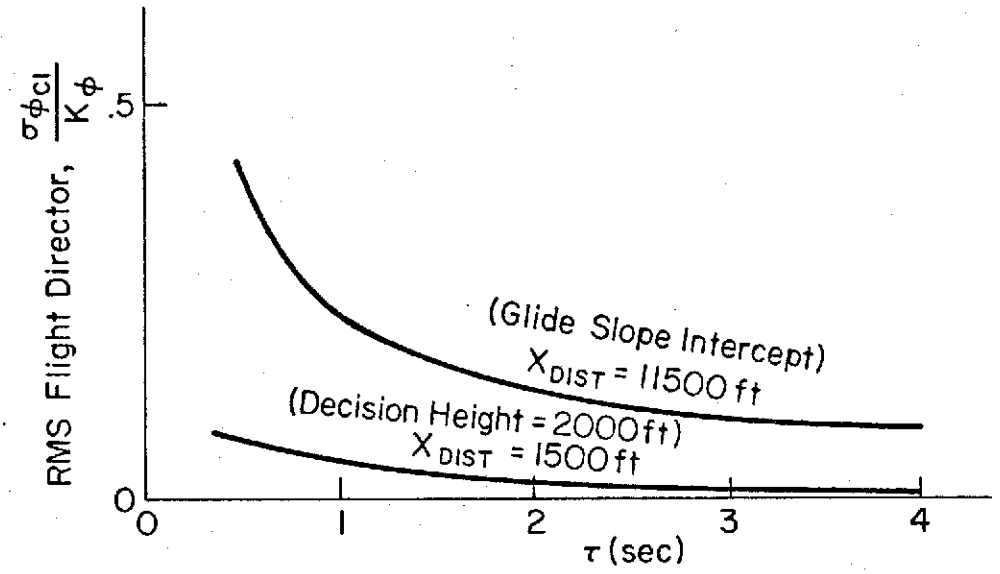

Figure 32. RMS Flight Director Signals Due to Conventional Localizer Noise

derived beam rate near the path mode frequency ($1/\tau \doteq \omega_p$) with a concomitant reduction in path mode damping to an unacceptable level ($\zeta_p = .08$). Complimentary filtering to obtain "beam rate" at frequencies greater than $1/\tau$ is accomplished by using bank angle and body fixed lateral acceleration to generate a roll stabilized lateral acceleration term which is passed through a low pass filter.

The lateral acceleration relative to a nominal curved path may be approximated by:

$$\Delta\ddot{y} = a_{y_{MEAS}} + g \cos\theta\,(\varphi - \varphi_c) \qquad (17)$$

where $\varphi_c = \tan^{-1} V_{GS}^2/Rg$ defines a commanded circular path of radius R_c (see Appendix C, Eq. C-5). This expression when passed through a first-order low pass filter with time constant, τ, gives $\Delta\dot{y}$ at frequencies greater than $1/\tau$. The final mechanization of the derived beam rate ($\dot{y}_D$) is given in Fig. 33.

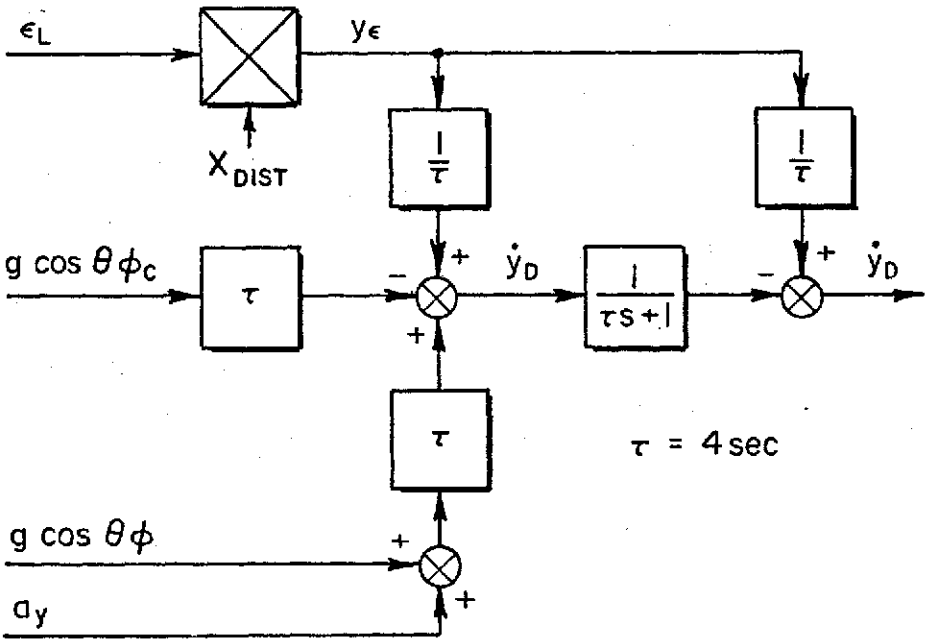

Figure 33. Complementary Filter for Derived Beam Rate on a Curved Path

3. Parameter Adjustment Analysis

The analytical design procedure utilized to set the final system gains and feedback transfer functions and limiters was formulated so that the system requirements in Table 2 could be interpreted directly in terms of certain quantitative criteria. The system requirements and corresponding analytical measures are summarized in Table 5. The remainder of this section contains a discussion of the application of these procedures to the design of FD A and FD B. As discussed in Appendix E, the lateral stability augmentation reduces the effective airplane to the following form,

$$\frac{\varphi}{\delta_w} = \frac{L_{\delta_{waug}}}{s(s + 1/T_{R_{aug}})} = \frac{0.6}{s(s + 1.6)} \qquad (18)$$

which is utilized in the following analyses. In a generic sense, the dominant modes of the augmented airplane consist of a roll subsidence mode and a spiral mode at the origin.

TABLE 5

RELATIONSHIP BETWEEN ANALYTICAL PERFORMANCE MEASURES AND PILOT/VEHICLE REQUIREMENTS

ANALYTICAL MEASURE	PILOT/VEHICLE REQUIREMENTS
Root locus of piloted closure of the effective controlled element, FD/δ_w	• Stability and damping • Response quality (modal interactions)
Frequency response (Bode plot) of FD/δ_w	• K/s near crossover for 1) Minimum pilot compensation 2) Insensitivity to pilot response variations 3) Remnant suppression • Stability and damping
Time response to initial condition offset	• Response quality (path mode consistency)
Time response to initial condition offset with crosswinds and response to wind shear	• Disturbance regulation • Response quality (face validity)
Time response to path command input (circular path)	• Command following

The time response measures in Table 5 are obtained from a simplified digital computer program (Appendix B) which includes the system nonlinearities, effects of winds, and curved paths.

a. Flight Director A

A simplified block diagram of FD A which reflects the feedback selections discussed previously is given in Fig. 34. From Eqs. 9 and 11 and Fig. 34 the flight director to wheel numerator is given as:

$$N_{\delta_w}^{FD} = \frac{K_p K_D L_{\delta_w}}{s^2}\left[s^3 + \frac{K_p}{K_p}s^2 + g\frac{K_{\dot{y}}}{K_p}s + g\frac{K_y}{K_p}\right] \qquad (19)$$

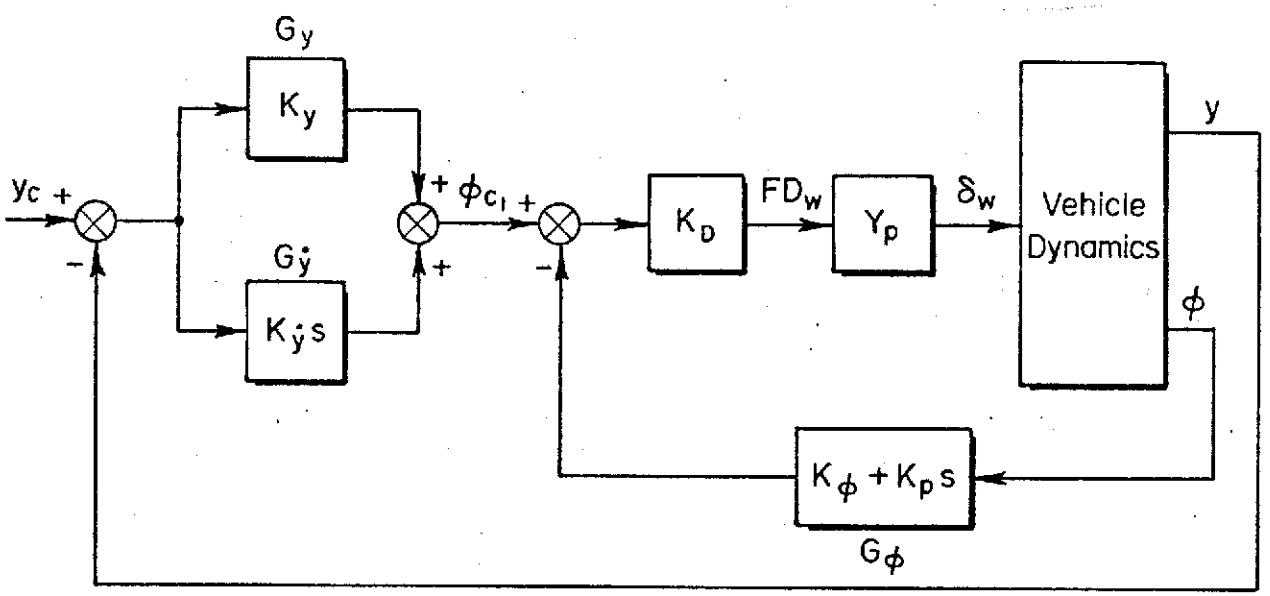

Figure 34. Simplified Block Diagram of Flight Director A (FD A)

The zeros of this numerator represent the limiting characteristics of the system closed-loop modes as the pilot increases his gain on the FD_w/δ_w closure. Comparison of Eq. 19 with Eq. 11 reveals that the addition of roll rate feedback, i.e., $G_\phi = K_\phi + K_p s$ increases the order of $N^{FD}_{\delta_w}$ from two to three making the effective controlled element, $(N^{FD}_{\delta_w}/\Delta)$ K/s-like out to infinite frequency. The coefficients of Eq. 19 were adjusted in accordance with the pilot/vehicle requirements discussed in Subsection IV-B resulting in the system survey shown in Fig. 35. The root locus in Fig. 35 indicates that the dominant system response is third order with the second-order closed-loop flight director mode, ω'_{FD}, occurring at slightly higher frequency than the first-order subsidence, $1/T'_{FD}$, in the region of crossover. The gain crossover region was estimated from the results of several simulator programs and verified on the current FSAA program resulting in the closed-loop modes shown. One of the primary goals in the design was to make the effective controlled element, FD/δ_w, K/s-like over a broad range of frequencies, and this is reflected in the Bode amplitude plot. The postulated crossover is in the K/s region and very near the frequency for maximum phase margin. Notice that deviations in pilot gain from the (assumed) nominal by, say, ±6 dB do not greatly affect the resulting closed-loop modes (see Bode).

As discussed in Appendix E, the lateral dynamics are nearly invariant with speed so that the above discussion applies for all flight conditions.

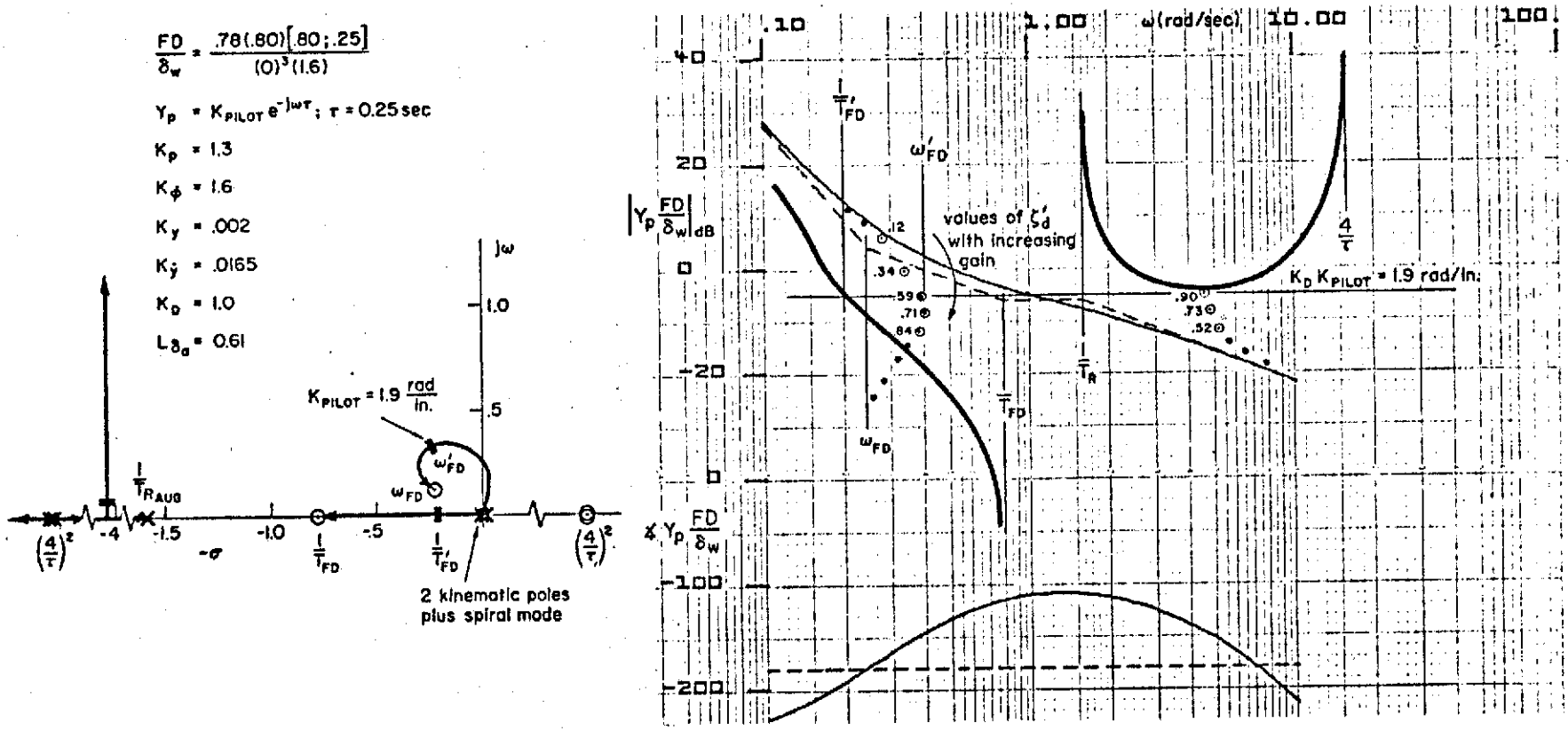

Figure 35. System Survey for Flight Director A, $Y_p(FD/\delta_W)$

Some concern was expressed initially over the unstable nature of the flight director at low frequency and the effect this might have during periods of unattended operation. However, this was not a problem, and the pilots were totally unaware of any conditional stability aspects of the flight director.

The third-order nature of the response (two modes at nearly the same frequency) required close consideration of the response qualities discussed in Subsection IV-B-2-b. Increasing the rate gain, $K_{\dot{y}}$, tends to drive $1/T'_{FD}$ towards the origin, resulting in a higher-order-type response as shown by comparison of the crosstrack deviation time histories in Figs. 36a and b.* The response with $K_{\dot{y}} = 0.0165$ meets the requirement for "path mode consistency" (Subsection IV-B-2-b), i.e., it is rapid and well damped, akin to a lower-order system. Increasing $K_{\dot{y}}$ to 0.02 results in a bimodal response, with the system initially responding like a second order at ω'_{FD} and finally like a first-order decay with time constant, T'_{FD}. This is undesirable to the pilot in that the localizer bug initially moves toward the center and then seems to stand off.

Finally, the system was checked for disturbance regulation by looking at the effect of crosswind and crosswind shear on the simplified digital simulation. The results for positive and negative crosswinds of 25 kt for an initial condition offset of 400 ft are shown in Fig. 37a and b. In both cases the disturbance regulation characteristics are seen to be quite good in that the aircraft is on course with an established crab angle within 20 sec. In the case of the left crosswind, the bank angle limiter is saturated until course convergence is established, resulting in a discontinuity in the flight director signal at about 5 seconds as the signal comes off the limiter. What this amounts to is a sudden change in the effective flight director law from $FD_W = (\varphi_{LIM} - \varphi)$ to $FD_W = f(y_\epsilon, \dot{y}_D, \varphi, p)$. While this violates the pilot-centered requirements for "face validity," it is extremely difficult to avoid since the bank angle limiter is necessary to satisfy other pilot-centered requirements. Results obtained during the piloted simulation indicated that

*These and subsequent time histories were obtained from the simplified digital simulation described in Appendix B.

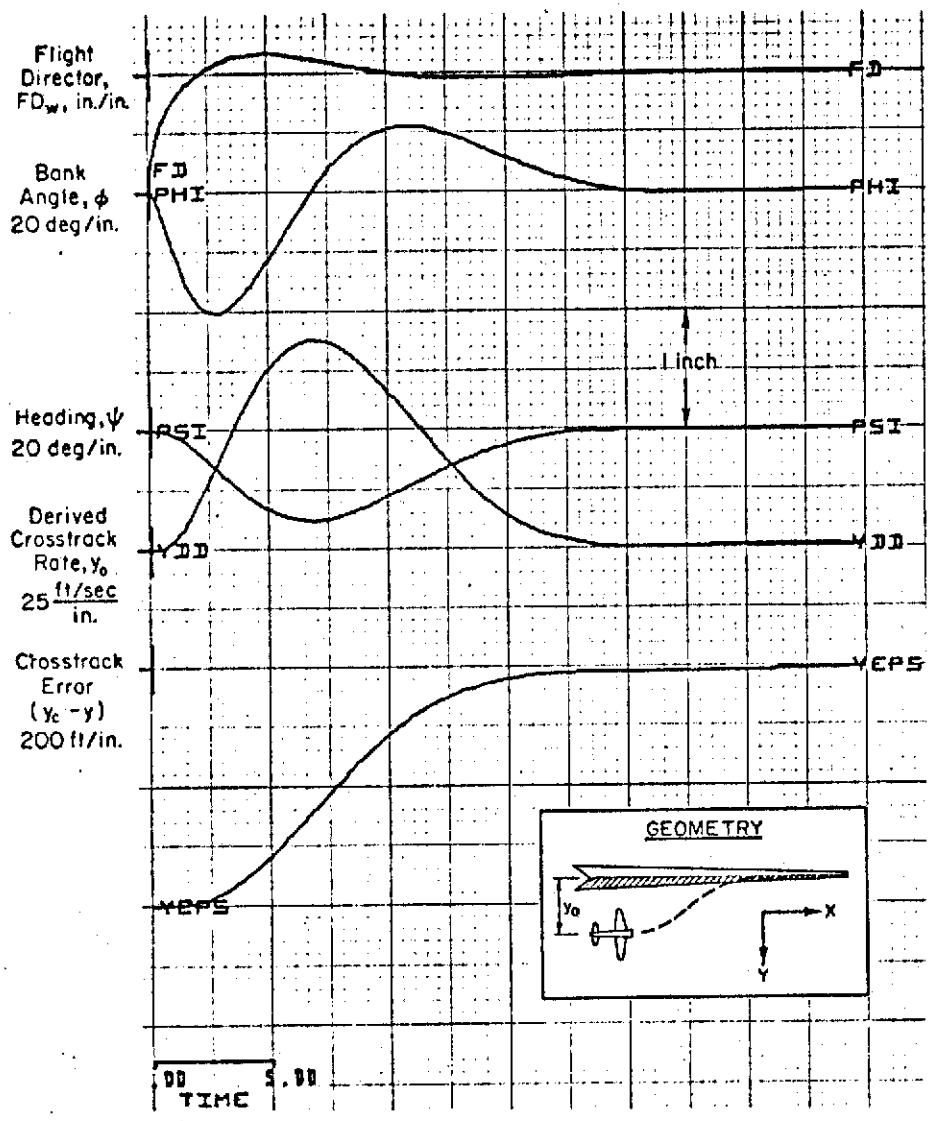

a) $K_{\dot{y}}$ = .0165 - Nominal Gain

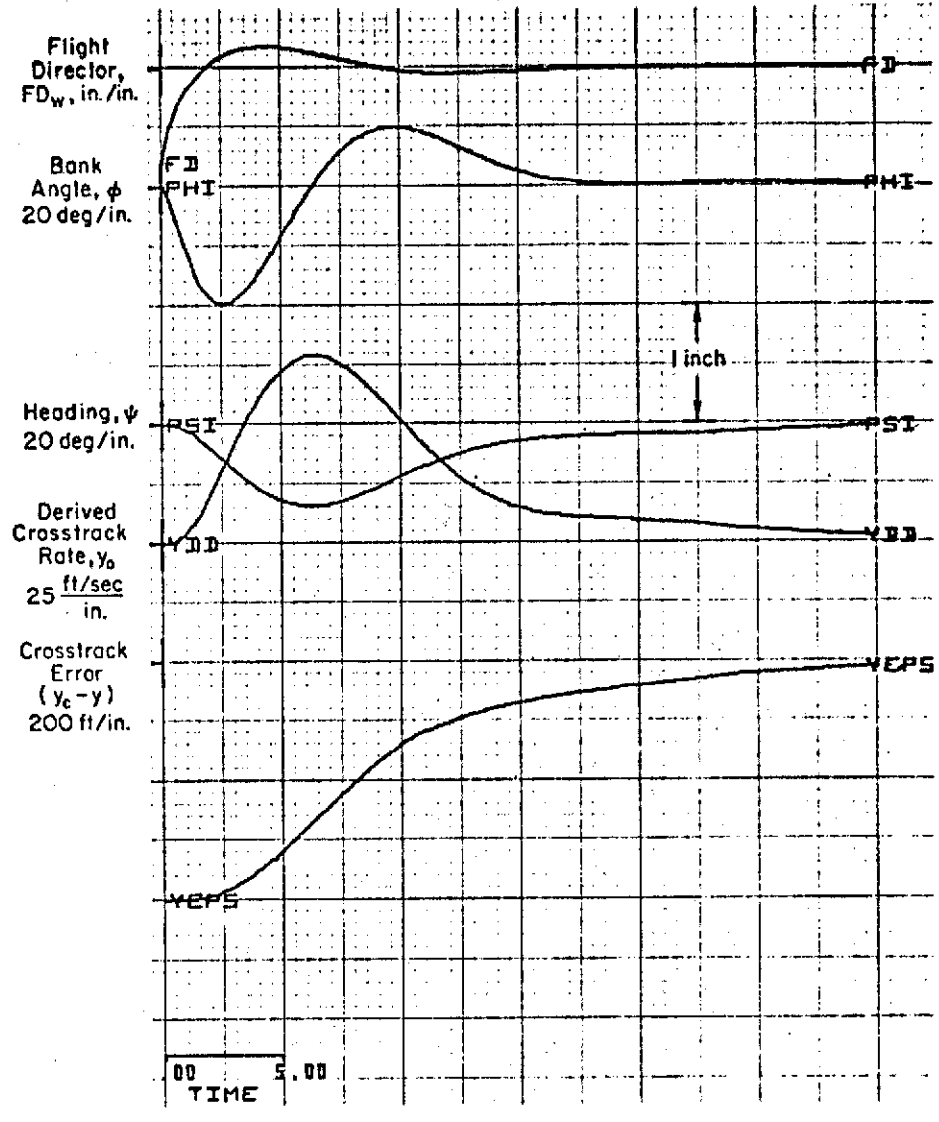

b) $K_{\dot{y}}$ = .02 - Increased Gain

Figure 36. Flight Director A Response to an Initial Condition Offset

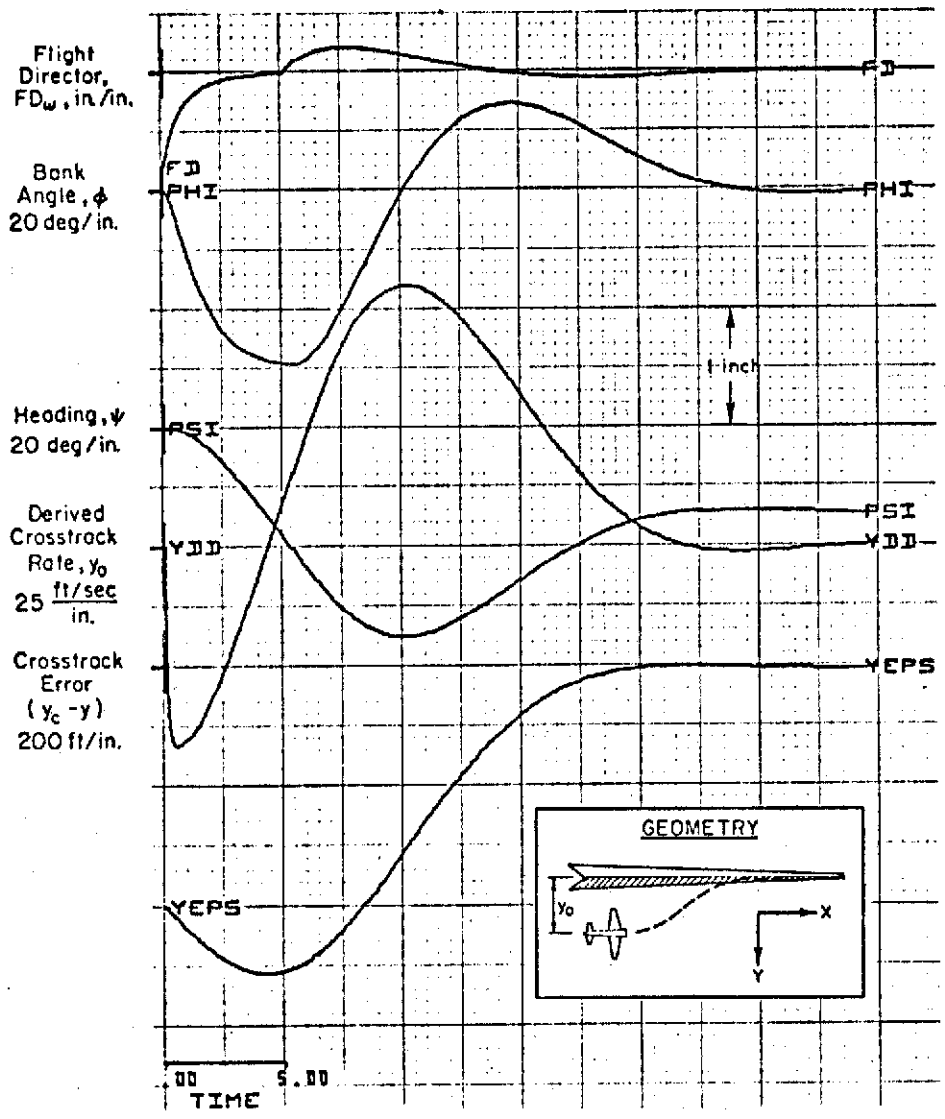

a) Crosswind From Left

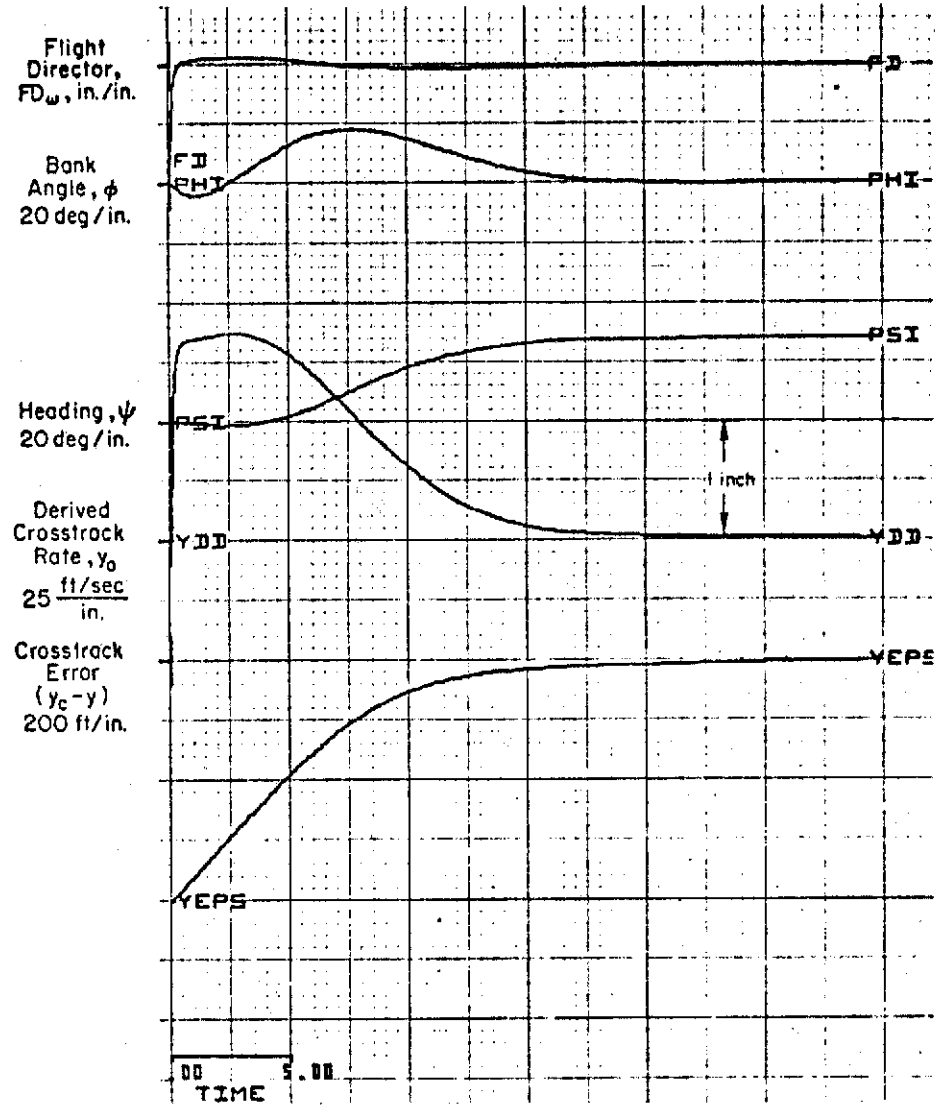

b) Crosswind From Right

Figure 37. Flight Director A Response to Initial Condition Offset with a 25 kt Crosswind

this problem only occurred after a large abuse and was not objectionable enough to downrate the system. (Note that flying a heading parallel to the localizer with a 400 ft offset in a 25 kt crosswind is a significant abuse of the system.)

From Table 3 (Line 7) we would expect to find steady-state offset to a wind shear input; more specifically, applying the final-value theorem to Eq. 12 for a gust ramp given by $\dot{v}_g/s^2$,

$$y_{\epsilon_{ss}} = \frac{\dot{v}_g K_\varphi}{g K_y} = 25\ \dot{v}_g \tag{20}$$

Wind shear is usually given as a gradient with respect to altitude. Assuming a speed of 60 kt on a −7.5 deg glide slope, 10 kt/100 ft (a strong shear) is equivalent to 2.23 ft/sec^2. The time response to this wind shear is shown in Fig. 38.

4. Error Analysis for FD A

The feedforward bank angle command and the feedback bank angle signal are subject to measurement errors which arise from errors in the measured groundspeed and vertical gyro precession in a turn. An important figure of merit of the lateral flight director system is the sensitivity of crosstrack standoffs due to these measurement errors. Ignoring the crosstrack rate and roll rate feedbacks which have no effect on trajectory standoffs, the flight director equation may be derived from Fig. 26 as follows:

$$K_y y_\epsilon + K'_\varphi(\Phi_c - \varphi_M) = FD_w \tag{21}$$

where:

$K'_\varphi = K_\varphi + g\tau K_{\dot{y}}$

$\Phi_c \doteq V^2_{GS_M}/R_c g$, commanded bank angle based on measured groundspeed, V_M

$\varphi_M = \varphi + \varphi_{BIAS}$, measured bank angle

$y_\epsilon = R - R_c$, crosstrack error or difference between the actual radius, R, and the commanded radius, R_c

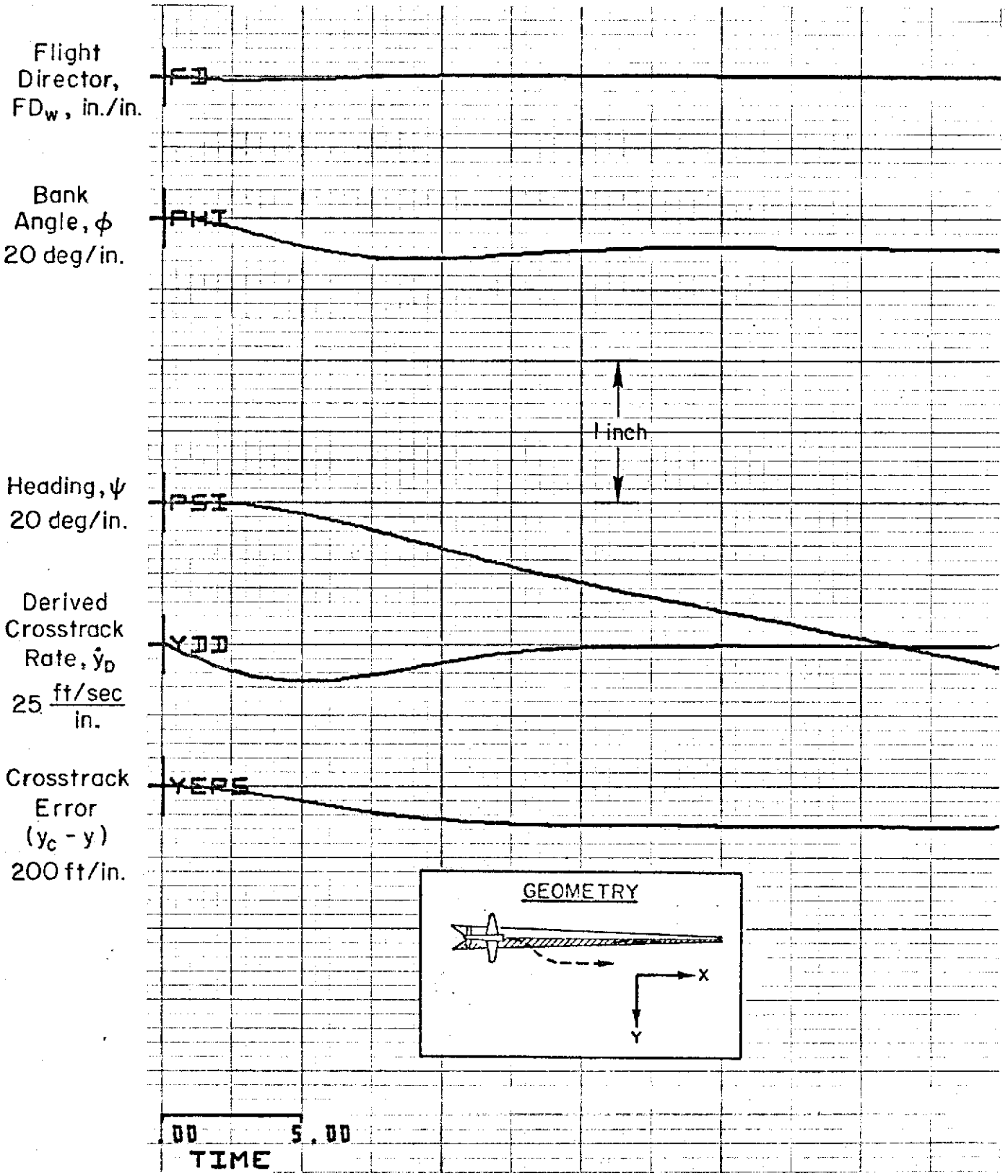

Figure 38. FD A Response to a Crosswind Shear of 2.23 ft/sec^2

Noting that $\varphi \doteq V_{GS}^2/Rg$, Eq. 21 can be rewritten in terms of the measured and actual groundspeeds and the bank angle bias as follows:

$$K_y y_\epsilon + K'_\varphi \left[\frac{V_{GS_M}^2}{R_c g} - \frac{V_{GS}^2}{(R_c + y_\epsilon)g} - \varphi_{BIAS} \right] = FD_w$$

Assuming the flight director is kept centered ($FD_w = 0$) and that $y_\epsilon << R_c$*, the sensitivity coefficients of crosstrack error to bank angle and groundspeed measurement errors are given as follows:

$$\frac{\partial y_\epsilon}{\partial \varphi_{BIAS}} = - \frac{1}{\frac{K_y}{K'_\varphi} + \frac{V_{GS}^2}{R_c g}} \tag{22}$$

$$\frac{\partial y_\epsilon}{\partial \Delta V} = - \frac{2V_{GS}}{R_c g \left(\frac{K_y}{K'_\varphi} - \frac{V_{GS}^2}{R_c g} \right)} \tag{23}$$

where ΔV represents the groundspeed measurement error ($V_{GS_M} - V_{GS}$). These sensitivities are plotted in Fig. 39 as a function of groundspeed and turn radius. The crosstrack errors for practical values of ΔV and φ_{BIAS} are seen to be quite small.

As a check on the analysis, a φ_{BIAS} of 5 deg was input on the FSAA simulator with the result shown in Fig. 40. The resulting lateral offset is shown in Channel 4 for straight ($\Phi_o = 0$) and curved ($R_o = 2000$ ft) segments at a speed between 80 and 90 kt. The computed crosstrack standoffs of 120 ft (curved path) and 162 ft (straight path) are in excellent agreement with the simulation.

*If $Y_\epsilon << R_c$, $1/(R_c + Y_\epsilon) \doteq (1/R_c)[1 - (Y_\epsilon/R_c)]$

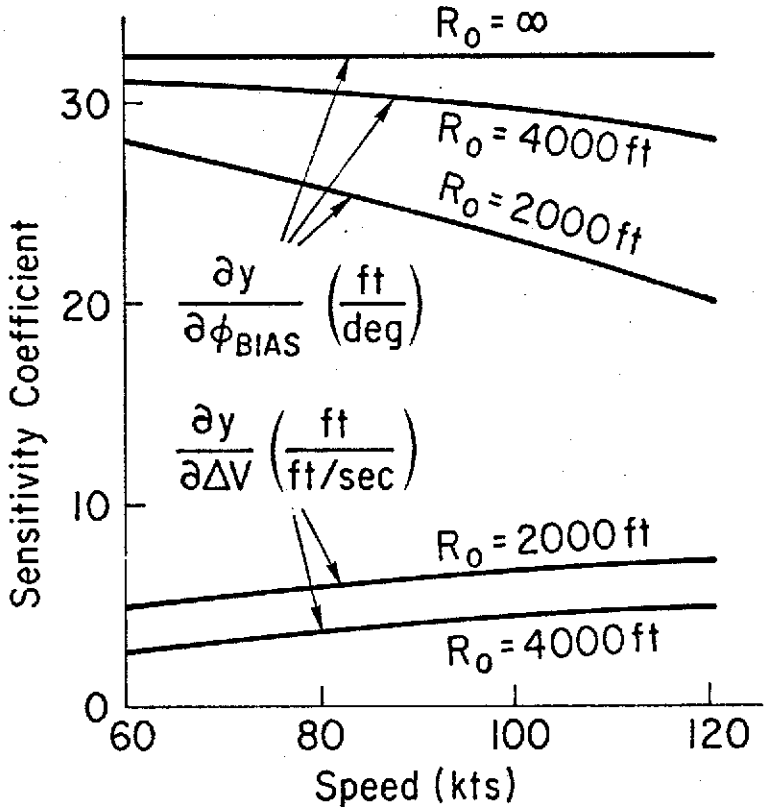

Figure 39. Crosstrack Error Sensitivities, FD A

5. Flight Director B

Flight Director B represents a somewhat more novel approach to the problem in that it does not require feedforward signals and will track any arbitrary path without external inputs. As such, the design is less straightforward than FD A, requiring additional tradeoffs and in some cases compromises in performance. As will be shown, the system limitations are of practical interest only when a small turn radius is required ($R_c < 4000$ ft). For cases where $R_c < 4000$ ft, a washed out step bank angle command must be added to allow the aircraft to "blend in" to the curved path prior to reaching the point of tangency. A simplified block diagram of FD B which reflects the basic feedback structure is given in Fig. 41.

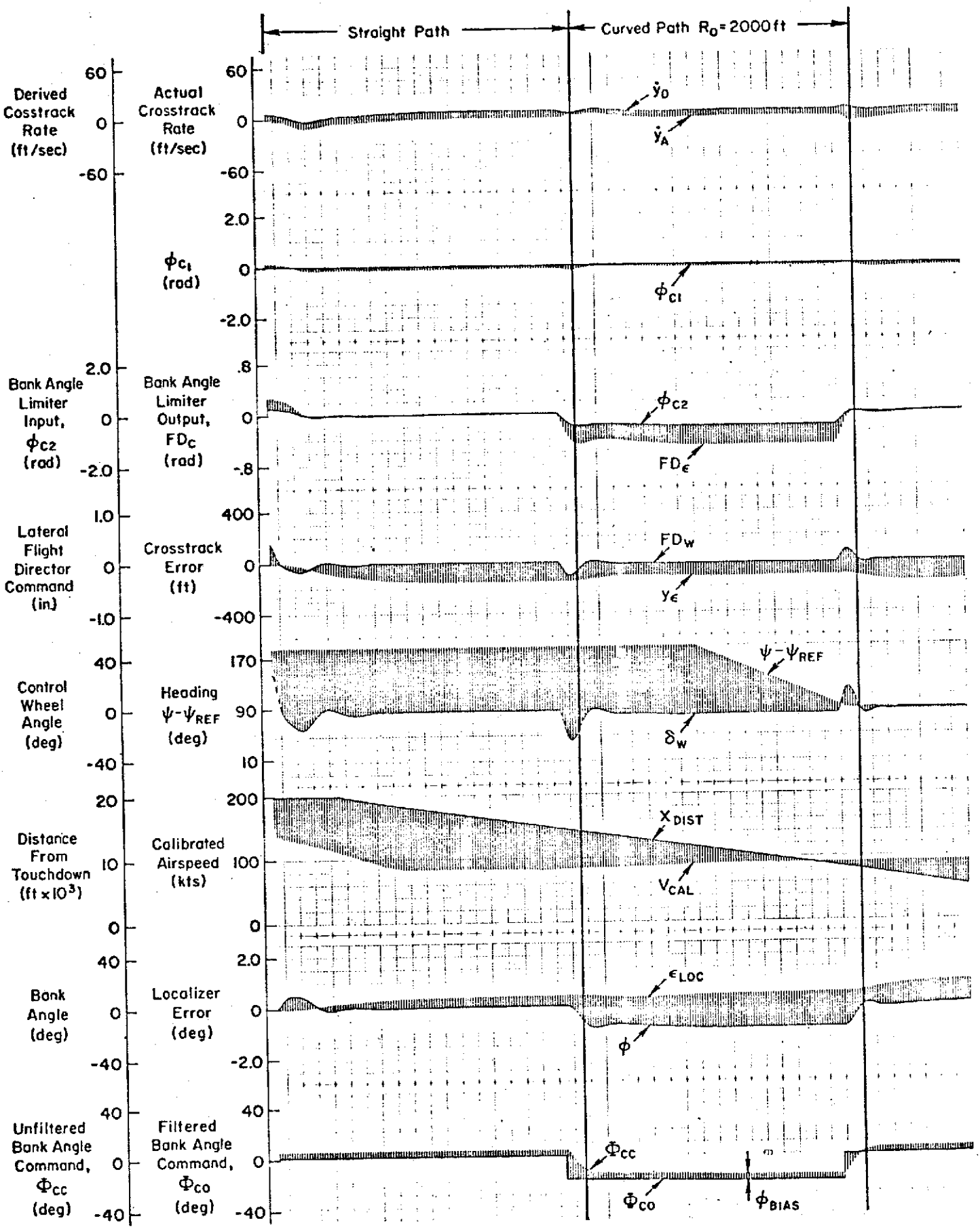

Figure 40. Effect of Bank Angle Bias on Crosstrack Error, $\Phi_{BIAS} = 5^0$

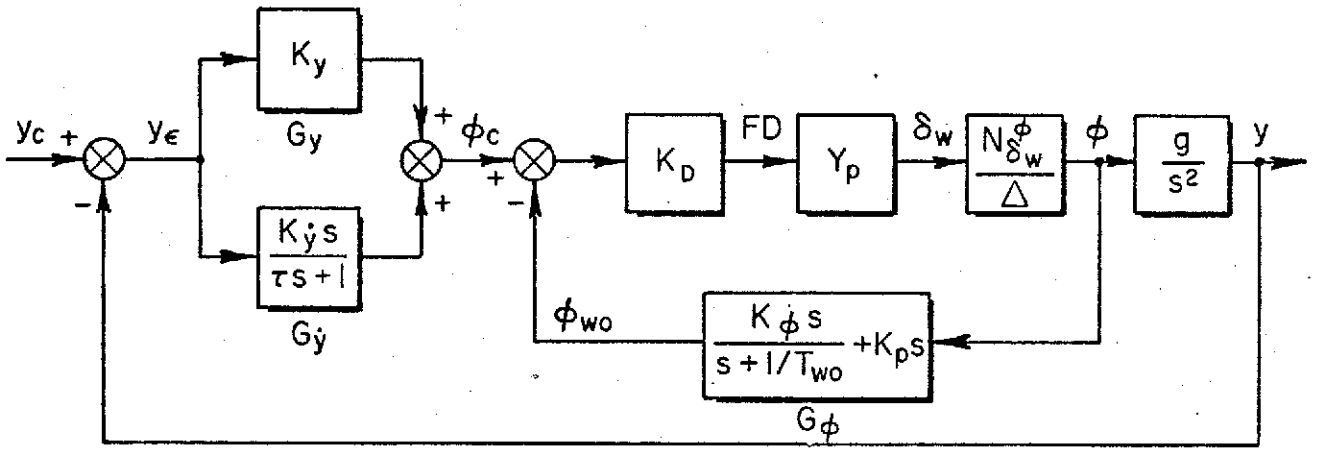

Figure 41. Simplified Block Diagram for Flight Director B

From Eqs. 9 and 11 and Fig. 41 the flight director to wheel numerator is given as:

$$N^{FD}_{\delta_w} = \frac{K_D L_{\delta_w}}{s\left(s+\frac{1}{T_{wo}}\right)\left(s+\frac{1}{\tau}\right)}\left\{K_p s^5 + \left[K_p\left(\frac{1}{T_{wo}}+\frac{1}{\tau}\right)+K_\phi\right]s^4 + \left(\frac{K_\phi}{\tau}+\frac{K_p}{T_{wo}\tau}\right)s^3 + g\left(\frac{K_{\dot{y}}}{\tau}+K_y\right)s^2 + g\left[\frac{K_{\dot{y}}}{\tau T_{wo}}+K_y\left(\frac{1}{T_{wo}}+\frac{1}{\tau}\right)\right]s + \frac{gK_y}{T_{wo}\tau}\right\} \quad (24)$$

The increase from a third order numerator (FD A) to a fifth order numerator is due to the bank angle washout circuit, and the lag in $G_{\dot{y}}$ required to filter beam noise. This lag is effectively eliminated in Flight Director A by complementary filtering (see Subsection IV-C-2). The design of Flight Director B is predicated on being able to follow any beam shape (within system limits) without prior knowledge of the beam geometry. Complementary filtering schemes require knowledge of the beam geometry and are therefore "not allowed" in the design of FD B. A key design tradeoff is to maximize the beam rate filter time constant, τ, to reduce system noise while maintaining the required stability characteristics.

Preliminary adjustments of the system parameters were accomplished using root locus factoring techniques to determine the effects of the system parameters on the zeros of $N^{FD}_{\delta_w}$. The first step in this process was to set $K_p = 0$

and to factor Eq. 24 in terms of K_φ. Noting that for all practical cases $1/T_{wo} << 1/\tau$ and $K_y << K_{\dot{y}}/\tau$, the resulting equation takes on a relatively simple form as follows:

$$1 + \frac{g}{\tau}\,\frac{K_{\dot{y}}}{K_\varphi}\,\frac{\left(s + \frac{K_y}{K_{\dot{y}}}\right)\left(s + \frac{1}{T_{wo}}\right)}{s^3\left(s + \frac{1}{\tau}\right)} = 0 \qquad (25)$$

A generic sketch of the locus of the roots of $N^{FD}_{\delta_w}$ as a function of the roll gain, K_φ, is given in Fig. 42. The "desirable locus" (solid lines) reflects the need for a low-frequency, well-damped, second order (ω_{FD}) to maximize the K/s region in the effective controlled element. Consideration of the factors required to obtain the desirable locus give rise to the observations and system tradeoffs shown in Table 6.

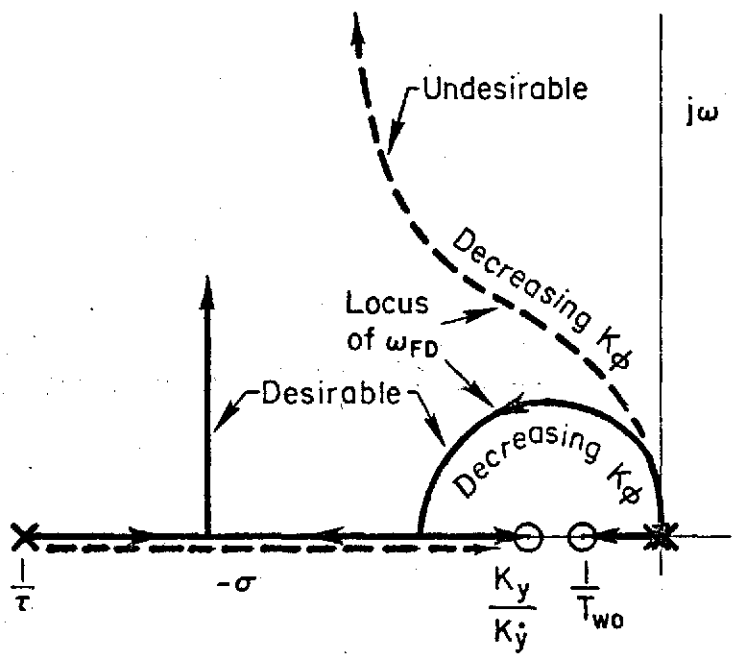

Figure 42. Generic Root Locus for Factoring $N^{\varphi}_{\delta_w}(K_p = 0)$

The upshot of all this is that the price we must pay to eliminate the need for feedforward commands is an increased number of tradeoffs and system compromises between the pilot/vehicle requirements (Table 2). From Table 6 it is clear that the parameters $K_y/K_{\dot{y}}$, $1/T_{wo}$, and τ must be minimized only

TABLE 6. PARAMETER ADJUSTMENT TRADEOFFS

REQUIRED FOR "DESIRABLE LOCUS"	OTHER SYSTEM CONSIDERATIONS
Minimize $K_y/K_{\dot{y}}$	Very low values of $K_y/K_{\dot{y}}$ result in poor response quality due to "long tails" during capture. (The dominant mode in low frequency occurs at $s = -K_y/K_{\dot{y}}$.)
Maximize T_{wo}	Bank angle must wash out faster than the dominant path mode (ω_{FD}) to minimize residual feedback which will result in standoffs with y_ϵ.
Minimize τ	The break frequency of the beam rate filter is $1/\tau$, and as such, requires τ be kept large enough for adequate noise rejection.

to the extent that a "desirable locus" is attained and in such a way that the system conflicts are resolved in an acceptable way. To this extent several combinations of these parameters were picked and tested via the quantitative measures in Table 5.

The final parameter adjustment involved setting the roll rate feedback, K_p, to maximize the region of K/s in the effective controlled element. Again root locus factoring was used to gain an appreciation of the effect of varying K_p on the FD_w/δ_w numerator. A generic sketch of the root locus factoring of Eq. 24 with "optimum values" of $K_y/K_{\dot{y}}$, T_{wo}, and τ is given in Fig. 43.

This sketch indicates that increasing p feedback has a deleterious effect on the dominant path mode zero, i.e., tends to increase ω_{FD} and decrease ζ_{FD}. This was somewhat surprising since roll rate is not normally associated with the path mode response. The following explanation is offered to give the reader a physical appreciation for the problem.

Assuming the crosscoupling between r and p to be small ($\dot{\varphi} >> r \tan \theta_o$), the relationship between bank angle, φ, and the actual feedback quantity, φ_{wo} (see Fig. 41) is given by the approximate Bode asymptotes of G_φ (for $1/T_{wo} << K_\varphi/K_p$) in Fig. 44. These asymptotes indicate that pure bank angle

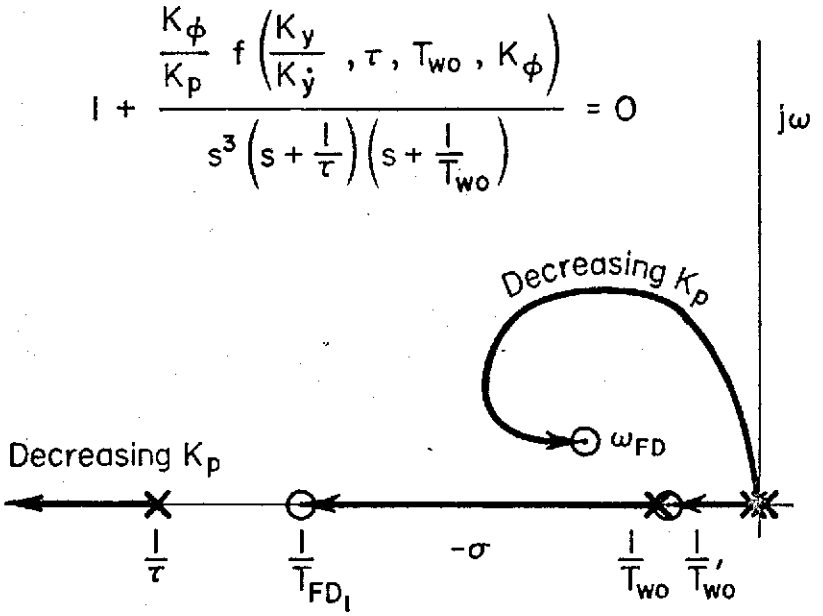

Figure 43. Generic Root Locus for Roots of $N^{FD}_{\delta_w} = f(K_p)$

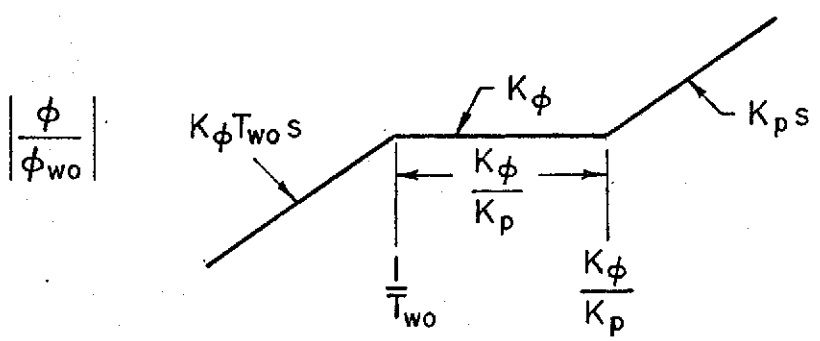

Figure 44. Approximate Bode Asymptotes of G_φ

feedback ($K_\varphi\varphi$) exists over a frequency region bounded by $1/T_{wo}$ and K_φ/K_p and that the feedback is essentially roll rate at all other frequencies. Thus, as K_p is increased, the effective feedback becomes the derivative of cross-track acceleration, $\ddot{y}(\ddot{y} \doteq g\varphi)$ with the corresponding effect on the path mode shown in Fig. 43. While this effect exists on more conventional systems (FD A), it is more pronounced when the bank angle is washed out. As a result,

it is necessary to strike a compromise between the pilot-centered requirement for K/s at high frequencies and path mode stability.

With the above considerations in mind, the system parameters were adjusted to give the controlled element characteristics shown in Fig. 45. The crossover frequency shown was estimated from the FSAA simulator time responses. (Notice, again, that it corresponds to near-maximum phase margin.) The compromise involved in setting the p feedback gain is evident from the region of K/s^2 between $1/\tau$ and $1/T_{FD_2}$ in the Bode asymptotes, and the resulting slight increase in the slope of the magnitude curve (greater than K/s) at frequencies beyond $1/T_R$ (1.6 rad/sec).

Comparison of the Bode amplitudes between FD A and FD B indicates that FD B is down by a factor of 1.5 in the region of crossover. Piloted simulator experiments indicated that this was too low and the display gain was therefore set to 1.5.

As in FD A, the low-frequency instability was found to have no effect on pilot opinion.

The initial condition response characteristics are given in terms of the time and frequency characteristics in Fig. 46. Focusing first on the closed-loop frequency response (Fig. 46b), the midfrequency response is seen to be primarily second order at ω'_{FD}. The effect of the bank angle washout shows up at a low-frequency droop in the frequency response. We would therefore expect that all but a small part of any lateral offset will be eliminated at frequency ω'_{FD} (0.41 rad/sec), and the remainder as a first-order decay with time constant $1/T'_S$ (closed-loop spiral mode). This is borne out in Fig. 46b where it is seen that all but 5% of the lateral offset is removed in 12 seconds and that the last 5% (20 ft) seems to stand off but, in fact, goes to zero in $3T'_S$ of 43 sec. This effect is inherent to the washed-out system and is attributable to the residual output of the washout circuit which causes an effective stand-off with y_ϵ (compare φ and φ_{WO} in Fig. 46b). The low-frequency droop is minimized by driving the spiral mode directly into the washout zero as in Fig. 42. Note that this implies $K_y/K_{\dot{y}}$ should be set equal to or greater than $1/T_{WO}$, which in effect sets an upper limit on $1/T_{WO}$. The residual lateral offset in Fig. 46b was found to be negligible during the simulator evaluations of FD B.

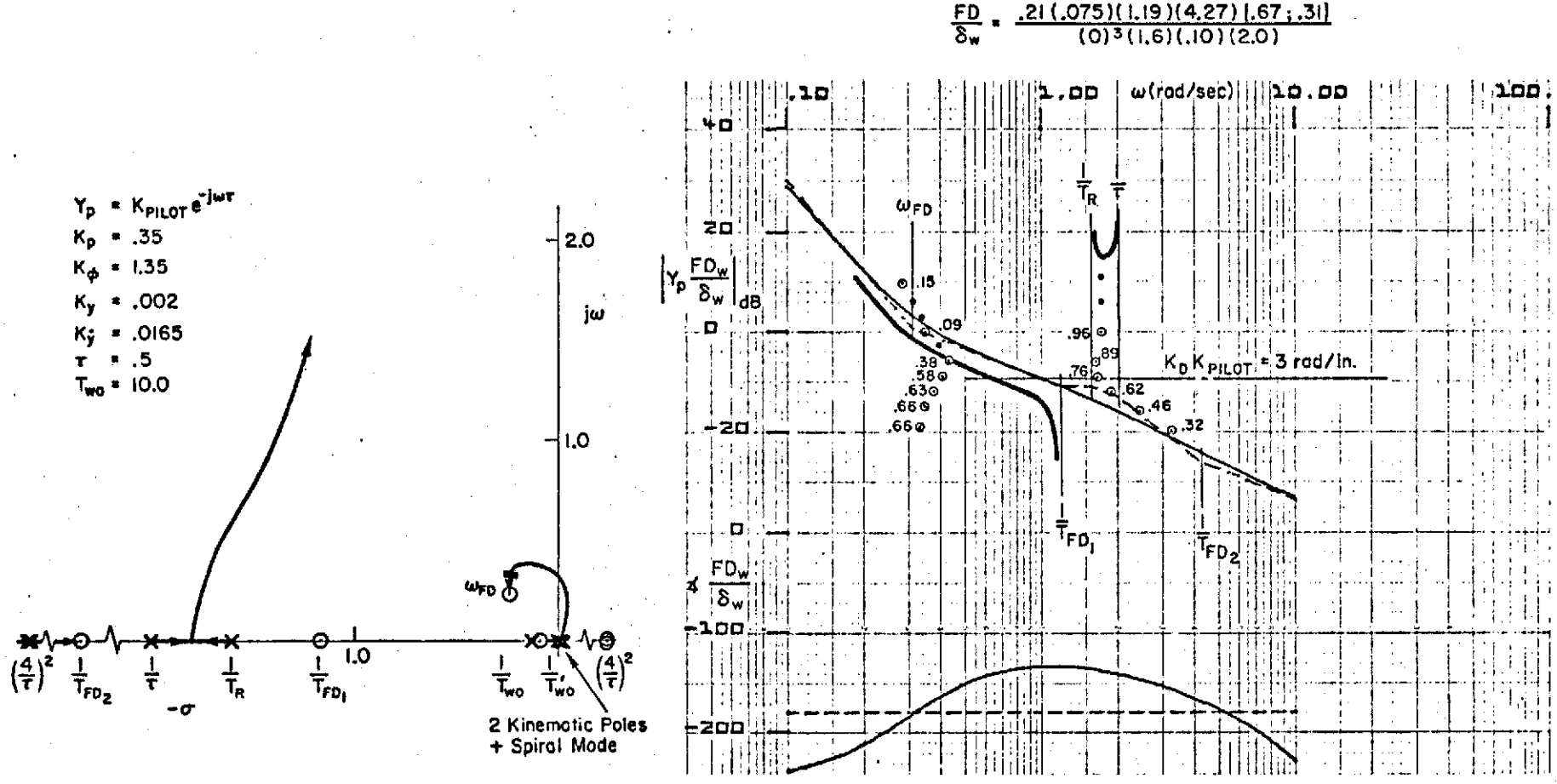

Figure 45. System Survey for Flight Director B, $Y_p(FD/\delta_w)$

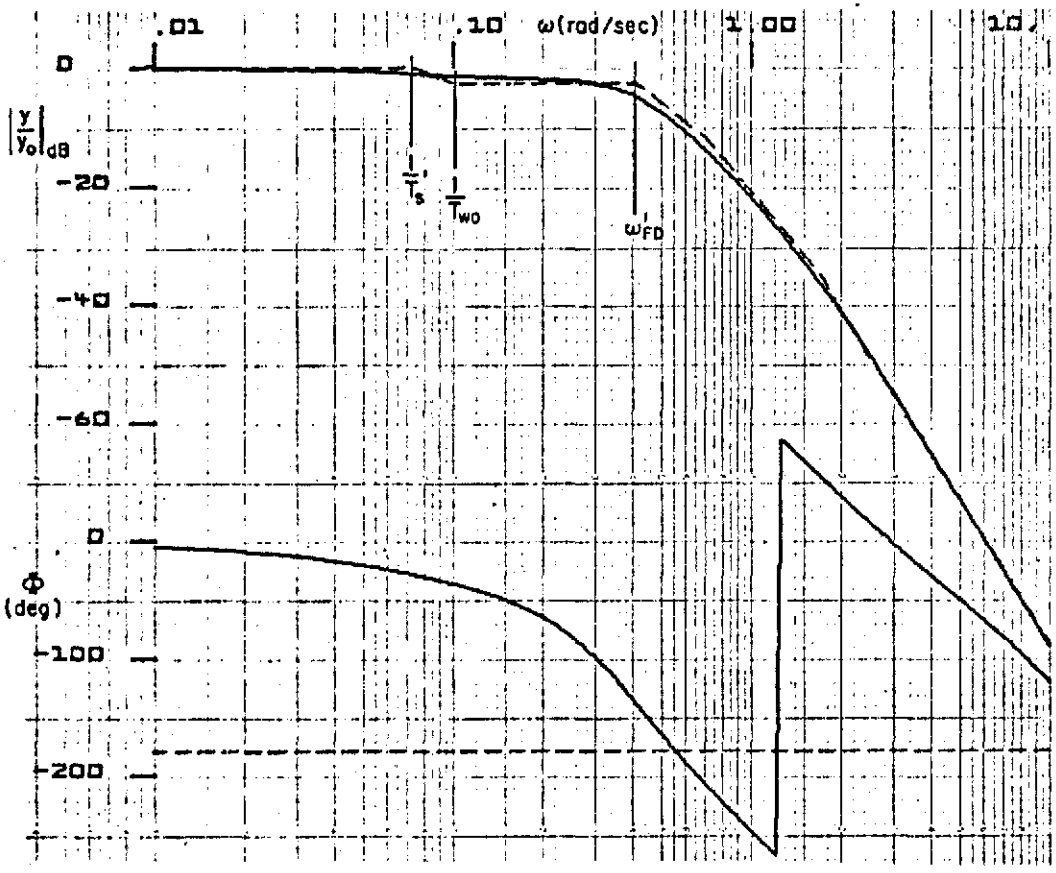

a) Closed-Loop Frequency Response of Crosstrack Error to an Initial Condition (FD B)

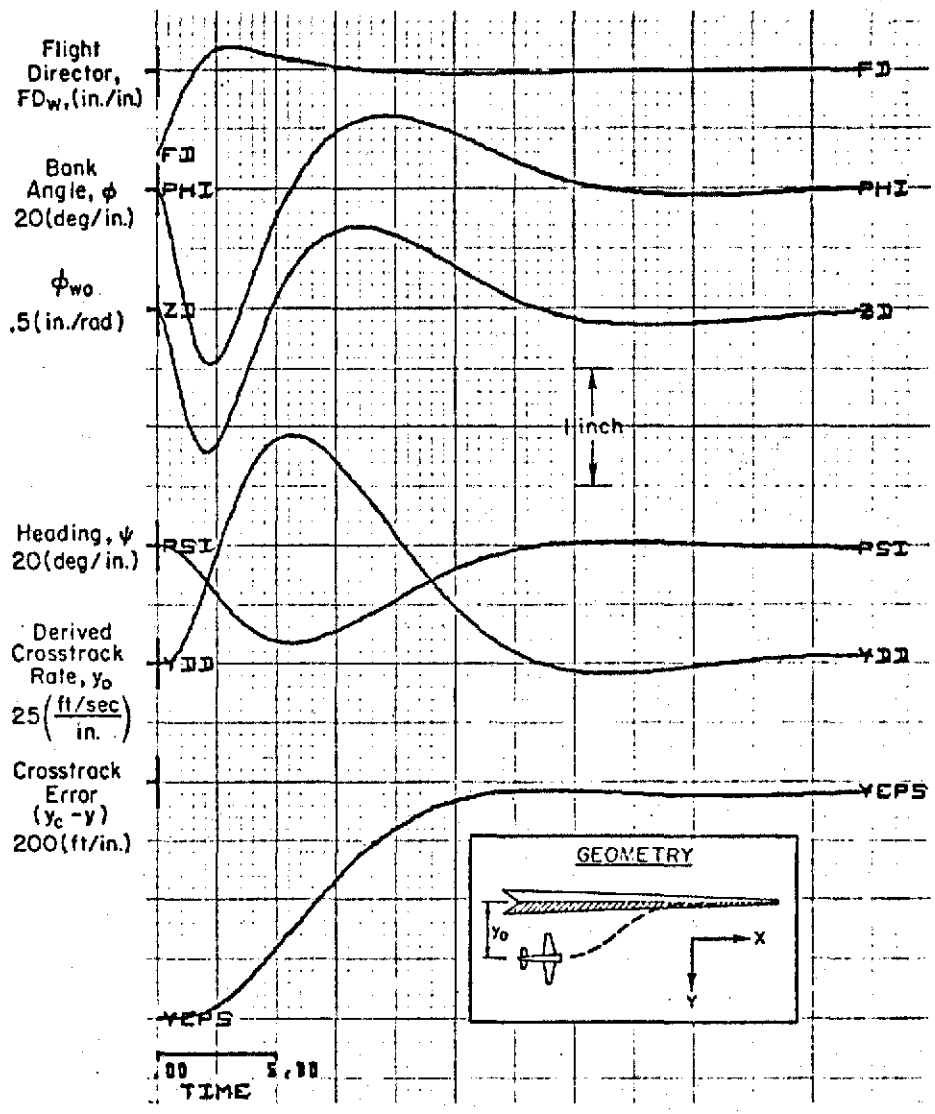

b) Initial Condition Response for FD B

Figure 46. FD B Characteristics

The disturbance regulation characteristics to crosswind and crosswind shear are shown in Figs. 47 and 48. Comparisons with FD A (Figs. 37 and 38) indicate that regulation against crosswind shear is considerably improved. However, this is compromised by a somewhat degraded response when correcting for a lateral offset in the presence of a negative crosswind (wind which tends to blow the aircraft towards the course as in Fig. 47b). From a practical standpoint, it is more likely that the aircraft will encounter a crosswind shear while tracking the localizer than correcting for large offsets in the presence of a steady wind. This is especially true when the aircraft is near touchdown (or decision height) and time to reintercept the localizer is a critical factor in the approach. It is therefore felt that the slower response time in a right crosswind (Fig. 47b) is not a significant drawback when compared to the improved response to wind shear shown in Fig. 48 (compare with Fig. 38).

The fundamental advantage of the washed-out bank angle director lies in its ability to track an arbitrary course (within design limits) without the benefit of external guidance inputs in the form of feedforward commands. The time response characteristics of a curved course intercept from a straight course are shown in Fig. 49 in calm air and with a 25 kt tailwind. These results are for a 4000 ft turn radius and a true airspeed of 90 kt. Course transients at the intercept point are inherent due to the lack of an advanced bank angle command and are sensitive to the commanded turn radius, true airspeed, and wind. Decreasing the turn radius to 2000 ft results in the response shown in Fig. 50. Note that in this case the aircraft goes to the bank angle limit of 30 deg and that the peak lateral deviation occurs shortly thereafter. This is a fundamental limitation of the pilot/vehicle system in that the bank angle limit defines the minimum radius achievable for a given true airspeed and wind. An analysis of the sensitivity of path overshoot as a function of course radius and wind is given in the following subsection.

6. Sensitivity Analysis for FD B

The dominant tracking errors are seen to occur at curved path intercept. These errors are induced by the fact that the required bank angle is not achieved until several seconds after the intercept point. This "effective time delay" is a function of the maximum roll rate and pilot reaction time.

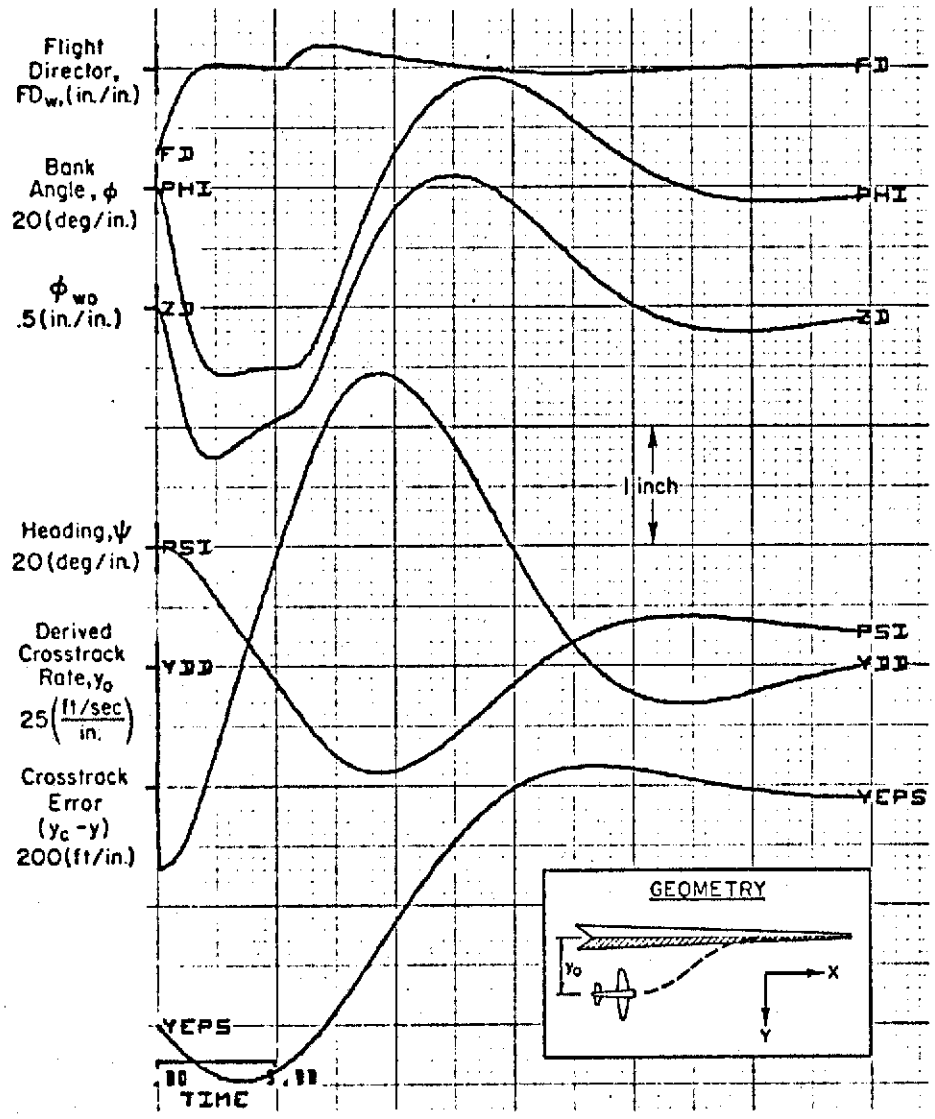

a) Crosswind From Left

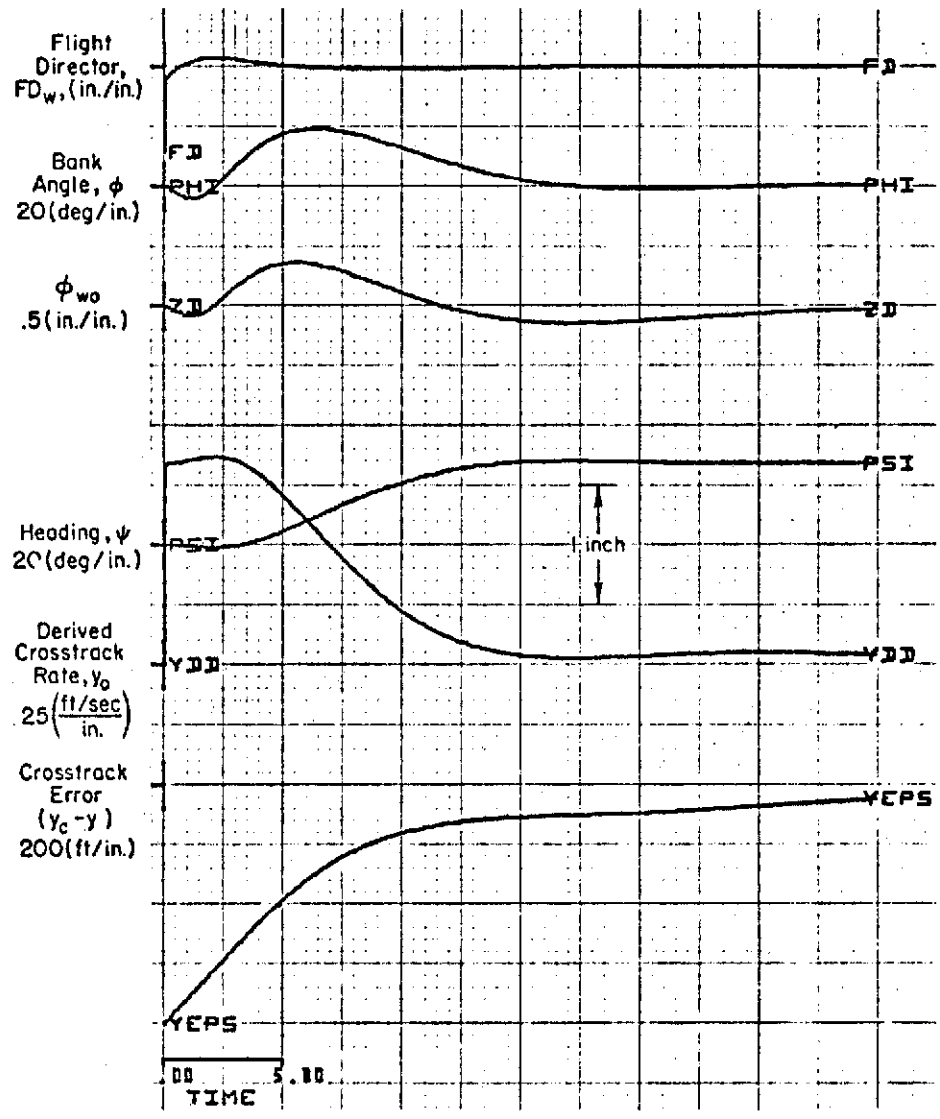

b) Crosswind From Right

Figure 47. FD B Response to an Initial Condition Offset with a 25 kt Crosswind

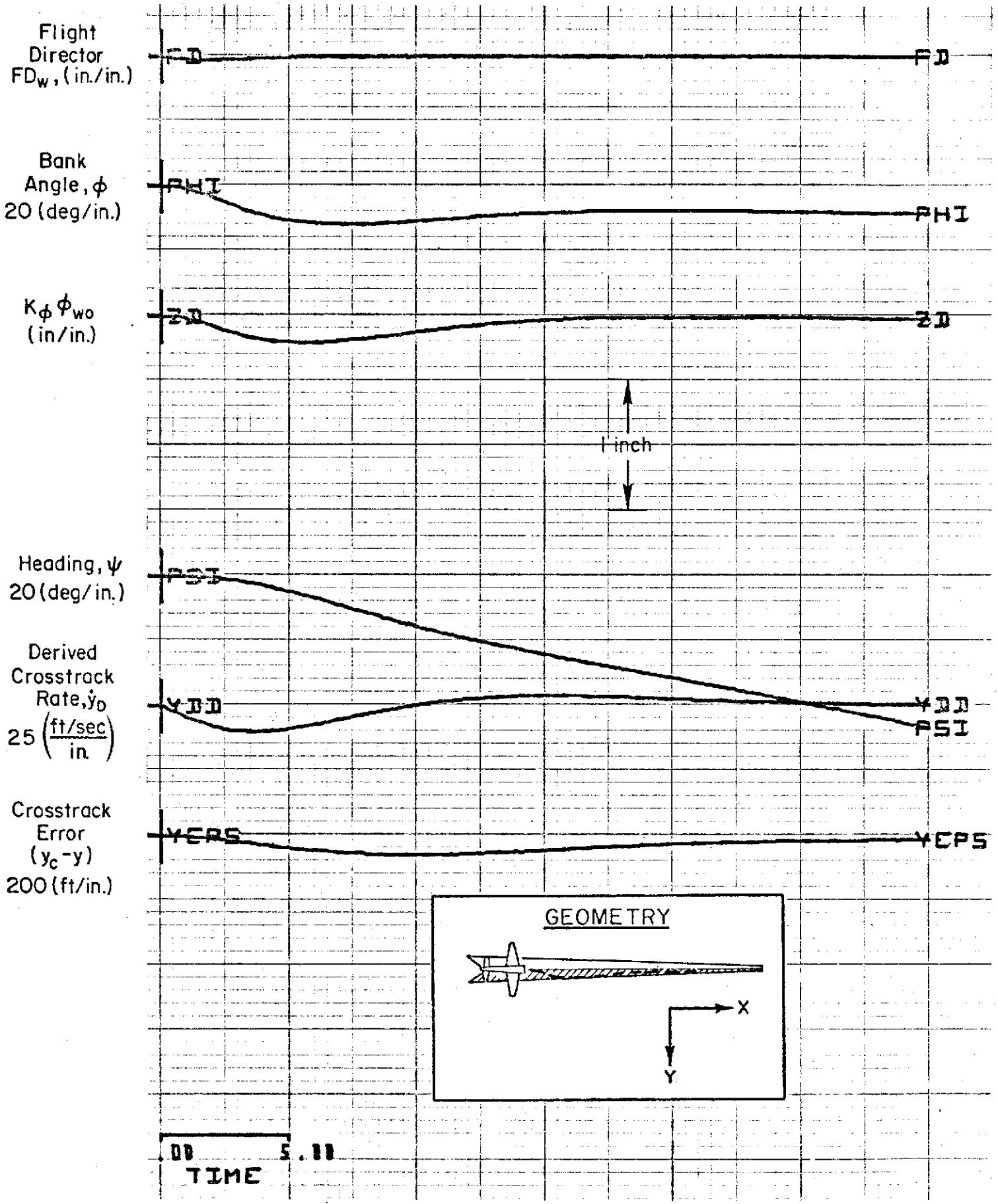

Figure 48. FD B Response to a Crosswind Shear of 2.23 ft/sec^2

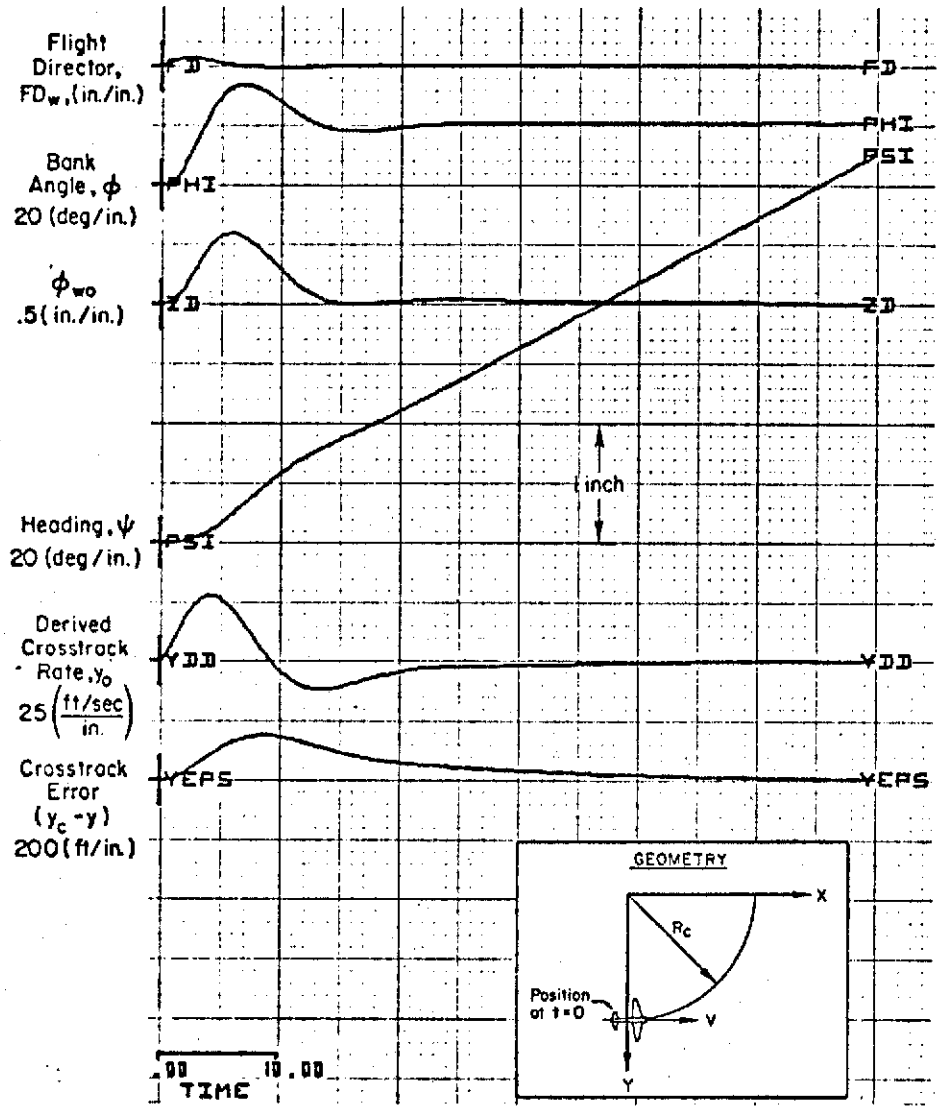

a) No Wind

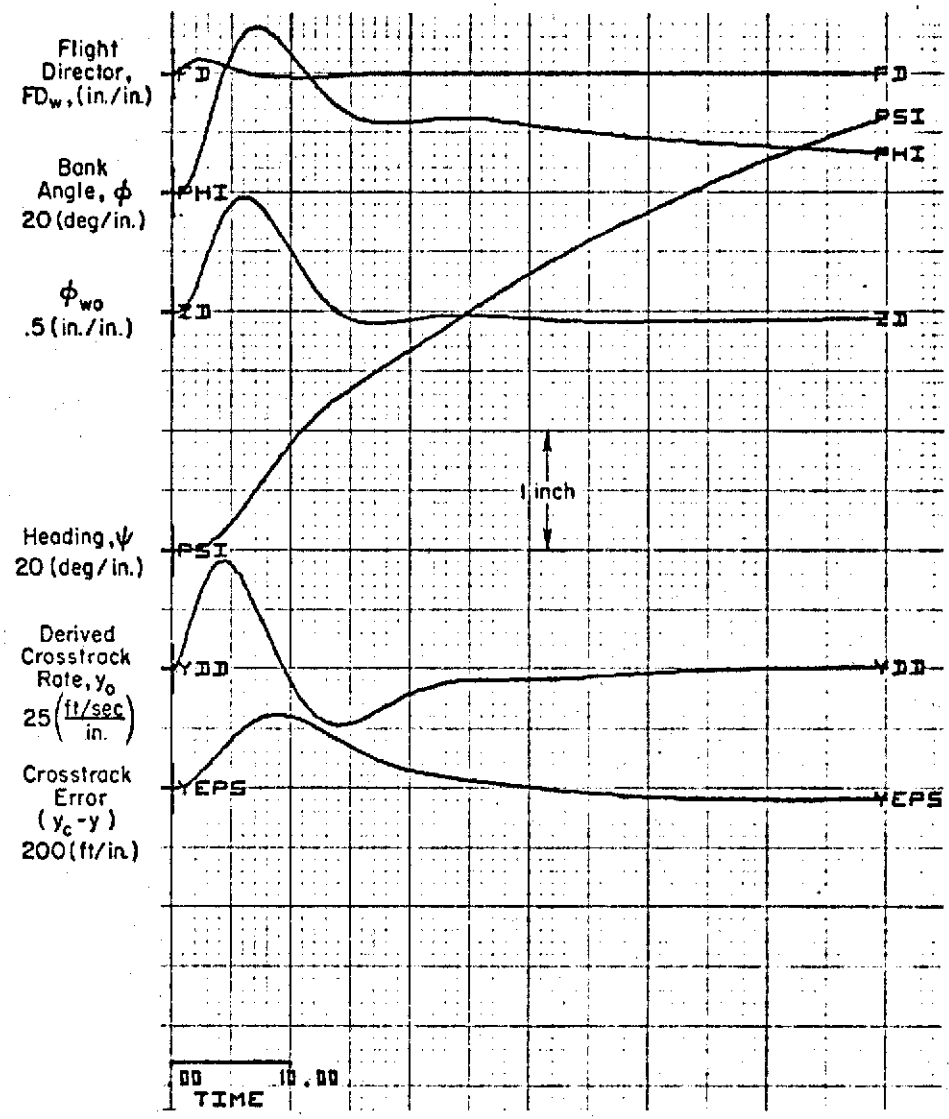

b) 25 kt Tailwind

Figure 49. Flight Director B Curved Course Intercept,
R_c = 4000 ft, V = 90 kt

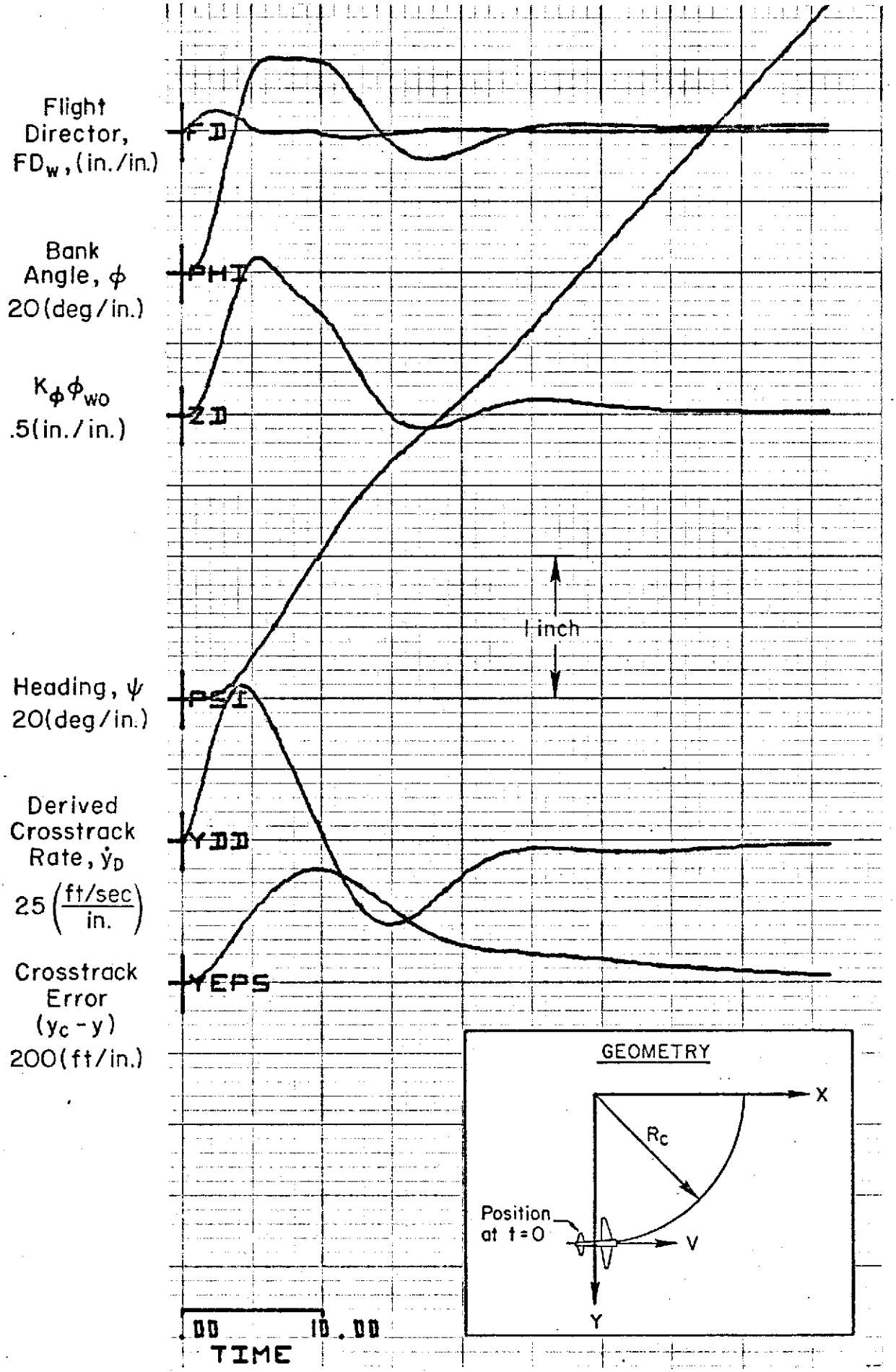

Figure 50. Flight Director B Curved Course Intercept, R_c = 2000 ft, V = 90 kt

If we simplify the bank angle response to a constant step of magnitude Φ, occurring ΔT sec after the curved course intercept, the path geometry may be represented as shown in Fig. 51.

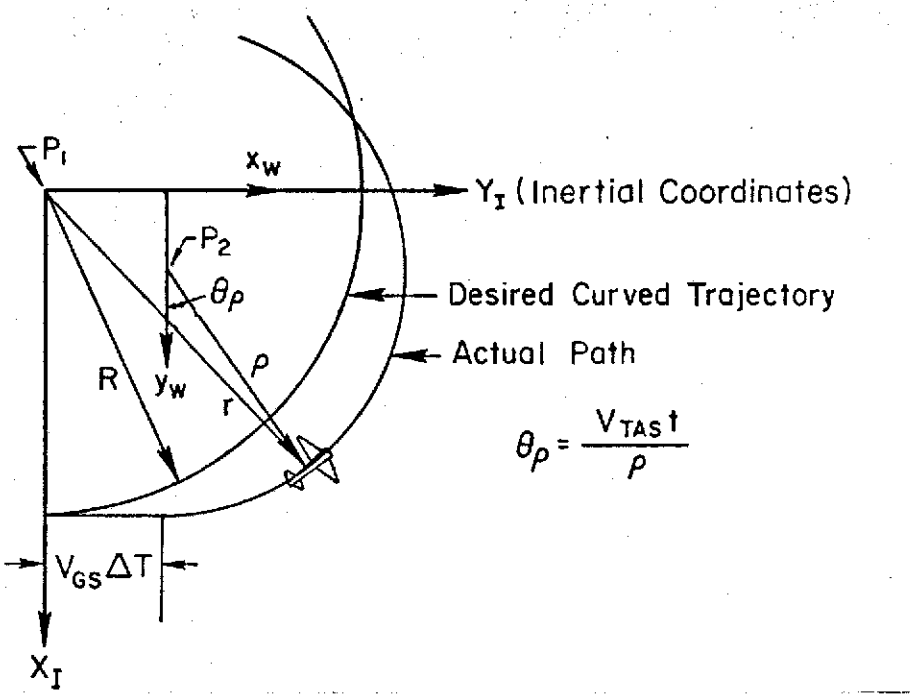

Figure 51. Geometry of Curved Path Intercept

The following definitions apply to Fig. 51:

P_1 = Center of the desired circular trajectory, fixed inertially

P_2 = Center of the osculating circle* which defines the actual path; moves with $x_w y_w$ frame

R = Radius of the commanded path

ρ = Inverse radius of curvature defined by the aircraft bank angle and speed as follows:

$$\rho \doteq V_{TAS}^2/\Phi g$$

r = Vector defining the aircraft position in the inertial frame

x_w, y_w = Coordinates fixed in the air mass

*An osculating circle is simply a circle defined by the radius of curvature at any point in an arbitrary curve (in this case the aircraft trajectory).

The maximum course overshoots occur with a tailwind at course intercept. In this case the $x_W y_W$ coordinate frame translates to the right at the wind speed, V_W, along the inertial x axis. The position of the aircraft in each of the coordinate systems is given as follows:

$$\begin{aligned} x_W &= R - \rho(1 - \cos \theta_\rho) \\ y_W &= \rho \sin \theta_\rho \\ X_I &= x_W \\ Y_I &= V_W t + \rho \sin \theta_\rho + V_{GS}\Delta T \end{aligned} \tag{26}$$

The crosstrack error is given as:

$$\begin{aligned} y &= r - R \\ &= (X_I^2 + Y_I^2)^{1/2} - R \end{aligned} \tag{27}$$

Since R is constant, the problem becomes one of finding the maximum value of r. Taking the derivative of r^2 and setting the resulting expression to zero results in an equation for t_{MAX}, the time when peak r occurs.

$$[V_{TAS}(R-\rho) - \rho V_W] \sin \frac{V_{TAS} t_{MAX}}{\rho} = (V_W t_{MAX} + V_{GS}\Delta T)\left(V_W + V_{TAS} \cos \frac{V_{TAS} t_{MAX}}{\rho}\right) \tag{28}$$

Values of t_{MAX} are solved from Eq. 28 using Newton Raphson iteration. The resulting t_{MAX} is used to compute y_{MAX}, the peak crosstrack error. Solutions for the peak crosstrack error were obtained by solving Eq. 28 for t_{MAX} (graphically) and using the resulting values in Eq. 27. These results are shown in Fig. 52 for effective time delays of 3 and 6 sec, a true airspeed of 90 kt, and steady tailwinds of 0, 10, and 25 kt. Additionally, the aircraft was assumed to roll to the bank angle limit, i.e., Φ = 30 deg. The major conclusions to be drawn are:

a) Commanded radii of less than 4000 ft are not practical without an advanced bank angle command.

b) The sensitivity to tail wind magnitude increases rapidly as the commanded radius is decreased.

c) Peak crosstrack errors are quite sensitive to the time required to reach the required bank angle, i.e., to ΔT. (ΔT = 3 sec is consistent with measurements from piloted simulation.)

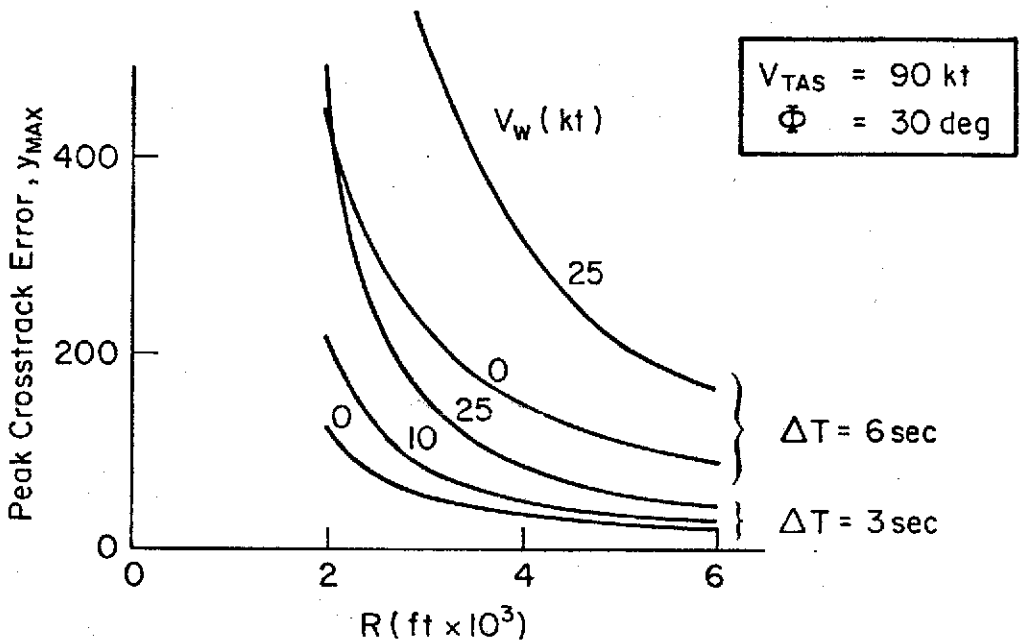

Figure 52. Peak Crosstrack Deviation

Note that when the peak crosstrack errors are small, the bank angle limit may not be reached (i.e., $\Phi \neq 30$ deg) resulting in a slightly larger error than predicted in Fig. 52.

7. System Modification for R_c < 4000 ft

As shown in the above analysis, the crosstrack errors become unacceptably large at curved course intercept when the commanded radius, R_c, is less than 4000 ft. This problem is alleviated by adding a constant washed-out

step bank angle command to be initiated at the appropriate time (approximately 3 sec) prior to course transition. As in FD A, the command signal magnitude is $\tan^{-1} V_{GS}^2/Rg$ and is passed through a second-order lag for smoothing (see Fig. 53). The simplification arises from the fact that the input is a constant and, because of the washout, is not sensitive to errors in computed

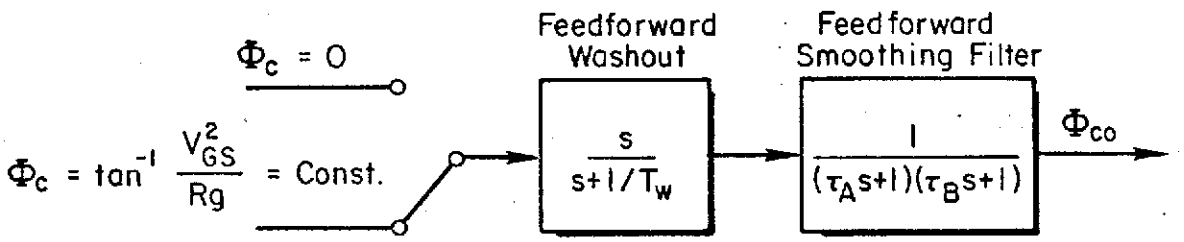

Figure 53. Simplified Feedforward for FD B

ground speed. The feedforward in Fig. 53 is required only for turn radii less than 4000 ft. Since the overall objective of FD B is to maintain design simplicity, and since turn radii of less than 4000 ft are unlikely in practice, the feedforward is not considered a basic part of the FD B design. It is given here as a possible "fix" in the event that low turn radii are required.

SECTION V

RESULTS

A four-week simulation was conducted on the NASA Ames Flight Simulator for Advanced Aircraft (FSAA). The objectives of the simulation were to:

- Validate the analytical results discussed in Sections II through IV.
- Optimize system parameters and make necessary design changes based on initial pilot commentary and performance.
- Obtain pilot commentary on Final Systems.
- Evaluate system performance in terms of gust regulation and sensitivity to pilot abuses.
- Determine limits of performance and safety margins.

The simulation results are presented in terms of system performance and piloted evaluations and are categorized with respect to the longitudinal and lateral systems. The pilot commentary and performance results were very favorable in that the system allows a significant reduction in pilot workload while minimizing tracking errors in the presence of wind and wind shear. Certain limitations were noted during the simulation, and these are detailed in the following paragraphs. In addition, design changes that resulted from initial pilot commentary and performance characteristics are discussed.

Finally, the composite system was evaluated from an operational standpoint. This occurred when the system was used as part of a joint FAA/STI program to formulate preliminary STOL certification criteria. The subject for this experiment was an FAA pilot who had never seen the system before and had been flying the basic Augmentor Wing simulation without flight directors or configuration management. Thus, he was in an excellent position to evaluate the benefits of the flight-director/configuration-management system.

A. TASK

The task was to fly a downwind leg (while decelerating from 140 to 90 kt), intercept the glide slope, turn on a constant radius circle onto final (while decelerating from 90 to 60 kt) and breakout at 200 ft for a visual landing.

A typical flight profile for this task is shown in Fig. 54. The initial conditions at Step 0 are 140 kt airspeed, 2000 ft altitude, and 90 deg heading. The pilot then commands 90 kt with the V select knob on the center console. The vehicle automatically slows to 90 kt at a rate of about 2 kt/sec. When the glide slope is about 1 dot high, the throttle director commands a power reduction and the column director commands a pitchover to intercept the −7.5 deg glide slope. During the descent the lateral director commands an initial 20 deg bank in order to stay on the 2000 ft radius approach circle. When the heading passes 180 deg, the pilot selects 60 kt from the speed control system. As the vehicle decelerates onto the backside, the glide slope tracking switches from an attitude modulation task to a throttle modulation task. When the turn is completed, the lateral director commands wings level, and a normal straight-in ILS approach at 60 kt is made. Total time for the approach is about 2-1/2 minutes from the time the pilot initiates the transition.

B. CONFIGURATION MANAGEMENT

1. Design Aspects of Simulation

Several competing trim schedules were tried on the simulator to determine the optimum tradeoff between maximizing the safety margins and minimizing the required thrust based on noise and fuel consumption considerations. In cases where a basic conflict existed, the design philosophy was to weight the safety margin aspects as having the highest priority.

It is felt that little additional insight is to be gained from presenting all of the competing trim schedules, since the basic factors that went into the final system selection are covered in Section 2 and in the following discussion on system performance.

2. Performance

The configuration management scheme finally selected for the moving-base experiments was the result of considerable analysis along with a limited amount of fixed-base simulation. The performance was quite good in that desirable configurations were obtained at all speeds; and, in general, the commanded speed changes were accomplished at an acceptable rate, and then maintained

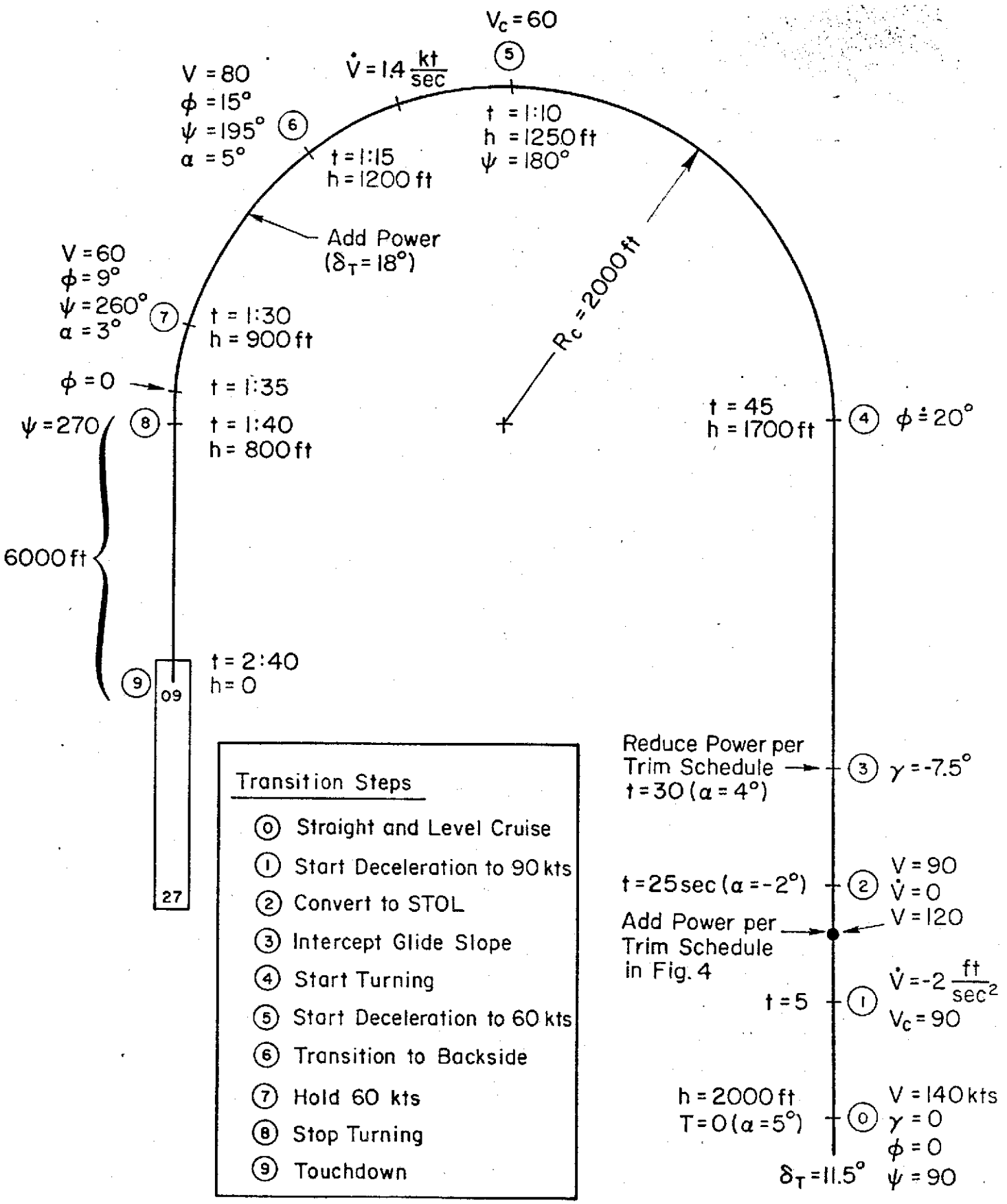

Figure 54. Typical Curved Approach Used in the Simulation

very accurately (even in the presence of 20 kt head and tail winds, shears, random gusts, and "abuse" situations). Further, no "ballooning" nor speed overshoots occur.

Within the context of a very successful system design there are two particular performance aspects that, although acceptable, are less than ideal due to certain basic airplane characteristics and the resulting necessary system tradeoffs that were made. These characteristics involve the deceleration capability while descending at −7.5 deg in the presence of a tailwind, and the larger than desirable angle of attack obtained during two specific flight situations (one again being descending in a tailwind). They are mentioned here to point out areas where specific improvements would result in relatively high payoffs. Other areas of improvement are also indicated and discussed in the following summary list. (A few of the items in this list are merely pertinent performance items, and are not areas to be improved. They are presented here because this seems like the logical place to include them.)

- Descent in the presence of a tailwind produces an "aerodynamic" flight path angle that is steeper than the inertial flight path angle (as seen in Fig. 55). To fly at the steeper aerodynamic flight path angle requires a different trim condition which may be beyond the physical limitations of the aircraft. The result is that tailwinds restrict airplane performance quite severely. Simulation has shown that a −7.5 deg glide slope is near the maximum capability of the vehicle (for steady flight).

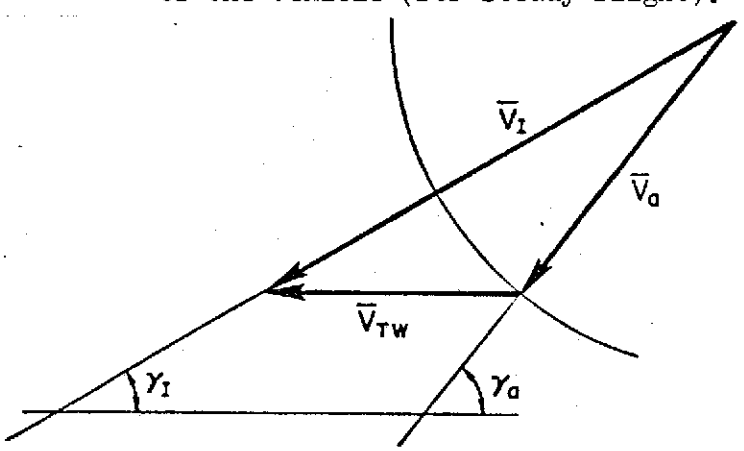

For Small Angles:

$$\gamma_a \doteq \left(1 + \frac{V_{TW}}{V_a}\right) \gamma_I$$

Figure 55. Relation Between Inertial and Aerodynamic Flight Path Angles in the Presence of a Tailwind

- Because $a_x + g\gamma$ is constant at any given flight condition, $\Delta\gamma = (1/g)a_x$ can be used to determine the tradeoff between flight path angle capability and acceleration (deceleration) capability. Thus, a 1 kt per sec deceleration capability is equivalent to 3 deg of flight path angle change capability (down). The significance of this is that the maximum deceleration is less than 1 kt/sec for flight conditions that are within 3 deg of the maximum (descending) flight path angle capability. Such a situation is typical of the AWJSRA on a −7.5 deg flight path. Therefore, very low decelerations will have to be tolerated — especially in the presence of tailwinds!

- For speeds above about 94 kt, a 20 kt tailwind on a −7.5 deg glide slope results in no deceleration capability (with the configuration management schedule used). That is, a stable situation exists at 94 kt with the nozzle at its forward limit (with a 20 kt tailwind on a −7.5 deg glide slope). Based on this information it would seem reasonable to require decelerating to below 85 kt prior to descending on a −7.5 deg glide slope when tailwinds are present.

- Low acceleration capabilities occur at those flight conditions where the throttle setting is small. The resulting nozzle effectiveness is also small and the −20 deg limit on nozzle travel (from trim) further degrades the total acceleration capability. To alleviate this situation a limited pitch command is fed to the column director below about 85 kt. ($\Delta\theta_c/V_\epsilon$ = −0.3 deg/(ft/sec) up to a maximum of 3 deg).

- A speed standoff error of 6 kt exists at a speed of 126 kt when 120 kt is commanded. This is due to the large trim nozzle required (70 deg), which can only be obtained by a speed error. (No nozzle trim can be obtained from the flap function prior to lowering any flap; and the flap placard prohibits flap extension at a speed greater than 125 kt.) In order to slow down below 126 kt it is necessary to command about 117 kt (or less) so that an additional 30 deg (or so) of nozzle can be obtained. This is not a serious drawback, but it is an imperfection in the system.

- Below about 85 kt a speed error (fast) will result in a pitch command (up), which, in turn, will result in an increased angle of attack. When this increment (3 deg) is added to the nominal angle of attack in turning flight (about 4 deg), the result could be a larger than desired angle of attack in the presence of turbulence or pilot abuses.

- In a tailwind situation below 85 kt (and on the glide slope) the power must be reduced to track the beam. This decrease in power causes an increase in angle of attack (to compensate for the loss of the thrust contribution to the lift). Further, the decrease in thrust causes a decrease in the effectiveness of the nozzles.

- To alleviate these larger than desired angles of attack, it is recommended that a slightly modified trim schedule be used (to lower the trim angle of attack). Thus, a pitch attitude of about -6 deg might be more appropriate than the current -4.5 deg.

- Off-nominal conditions, such as a hot day, will merely result in a small shift in the trim nozzle required. This will lead to an even smaller speed shift [due to the 10 deg/(ft/sec) gain]. The main point here is that all off-nominal conditions end up as small shifts in trim nozzle required.

- Descent in a headwind situation results in higher than desired throttle and nozzle settings (due to the trim schedule that maintains constant pitch attitude for all wind conditions). A more desirable situation would probably be to accept a slightly higher pitch attitude (and angle of attack) to gain slightly smaller throttle and nozzle settings.

- Fuel consumption, noise, and engine wear arguments which restrict the vehicle configurations to those with low power settings result in reduced operating margins. The STOL capability of the vehicle is not being fully utilized at relatively low power settings.

3. Pilot Evaluation

It was not possible to completely separate pilot commentary related to configuration management from those related to the flight director. This, of course, is due to the fact that the systems were designed to work together. (For example, the trim thrust states are achieved via the throttle flight director.) The following pilot commentary reflects the decreased workload which, in part, results from the trim schedules selected.

- With the full system turned on, "workload goes way down. Worth a couple points of POR on a straight path, and more on a curved path."

- "Looks pretty good to me. All I had to do was center the needles and it came right back." (Reference to recovery from an intentional abuse situation. The large margins designed into the trim management schedule result in simple recoveries from off-nominal conditions.)

- "I like this director because it keeps me out of trouble." (Reference to successful use of trim management schedule to constrain vehicle states in a way that allows only "good" configurations to be achieved.)

Additional commentary is presented in the following subsections on the longitudinal and lateral flight directors. As noted, the majority of comments were quite favorable. Criticisms of the system centered about occasional angle-of-attack excursions about 10 deg, the inability to decelerate on the glide slope above 94 kt, and somewhat higher than desired power settings when tracking the glide slope in a strong headwind.

C. LONGITUDINAL FLIGHT DIRECTOR

1. Design Aspects of Simulation

Several of the longitudinal flight director parameters were adjusted based on initial simulation results. A brief discussion of the considerations involved is summarized in the following paragraphs.

a. Glide Slope Capture — Glide slope capture mechanizations using exponential intercept logics did not produce repeatable results. Different initial conditions arising from turbulence or steady winds made each capture different, consequently a timed fade-in was used.

b. Column-to-Throttle Director Conversion for Glide Slope Tracking on the Backside — Both pilots felt that flight path control with attitude was unacceptable when the vehicle was flown below 80-85 kt. This occurred because the speed SAS did not have sufficient authority to keep the vehicle on the frontside of the power curve. Consequently, the flight director utilizing conventional control technique produced an unstable situation. The blended director system operated as anticipated and, regardless of wind conditions and intentional pilot abuses, kept the vehicle in a stable tracking condition (see Section III).

c. Addition of Speed Error to the Column Director During Backside Glide Slope Tracking — A speed error signal was fed to the column director to protect against speed excursions while tracking the glide slope. The use of attitude for speed control produced a desirable relationship between glide slope error and speed error. This was noted particularly if the vehicle was low and slow (beyond the speed SAS capability). In this case the column director commands a pitchover to pick up the speed and the throttle director commands more power to get back to the glide slope. This was deemed a desirable sequence by the one pilot who experienced this condition.

d. Attitude Rate Feedback to Column Director — The use of some attitude rate feedback in the column director was preferred by both pilots. The final attitude rate feedback selected was 1.5 in./(deg/sec) plus a 0.2 sec lag. The difference between too little and too much attitude rate feedback is shown in Fig. 56. Although this appears as only a slight amplification of the high-frequency portion of the response, the pilots were quite sensitive to this difference.

e. Pitch Attitude Limiter — An attitude limiter should be provided when tracking glide slope with attitude. With washed-out attitude feedback it was possible to develop large pitch attitudes in an attempt to recover the glide slope from an off-nominal condition when flying above the backside transition speed (see page 34 for an example).

f. Angle-of-Attack Protection — The angle-of-attack protection used in the throttle director resulted in some unfavorable pilot commentary. One pilot felt it was too easy to exceed the angle-of-attack threshold. This altered the controlled element response and sometimes produced oscillatory throttle motions. While undesirable from a pilot-centered standpoint, the angle-of-attack protection circuit was deemed necessary to maintain adequate safety margins in the event of a large angle-of-attack excursion. An example of the response with high α is shown later in Fig. 59.

g. Glide Slope Sensitivity — The conventional glide slope sensitivity displayed on the ADI and HSI of ± 0.7 deg was not sufficient for the -7.5 deg glide path approaches. Although an optimum was not determined, a display sensitivity of ± 1.5 deg was acceptable to both pilots. It was felt that the sensitivity should be reduced as the vehicle gets in close in order to maintain a compatible low-frequency response with the director.

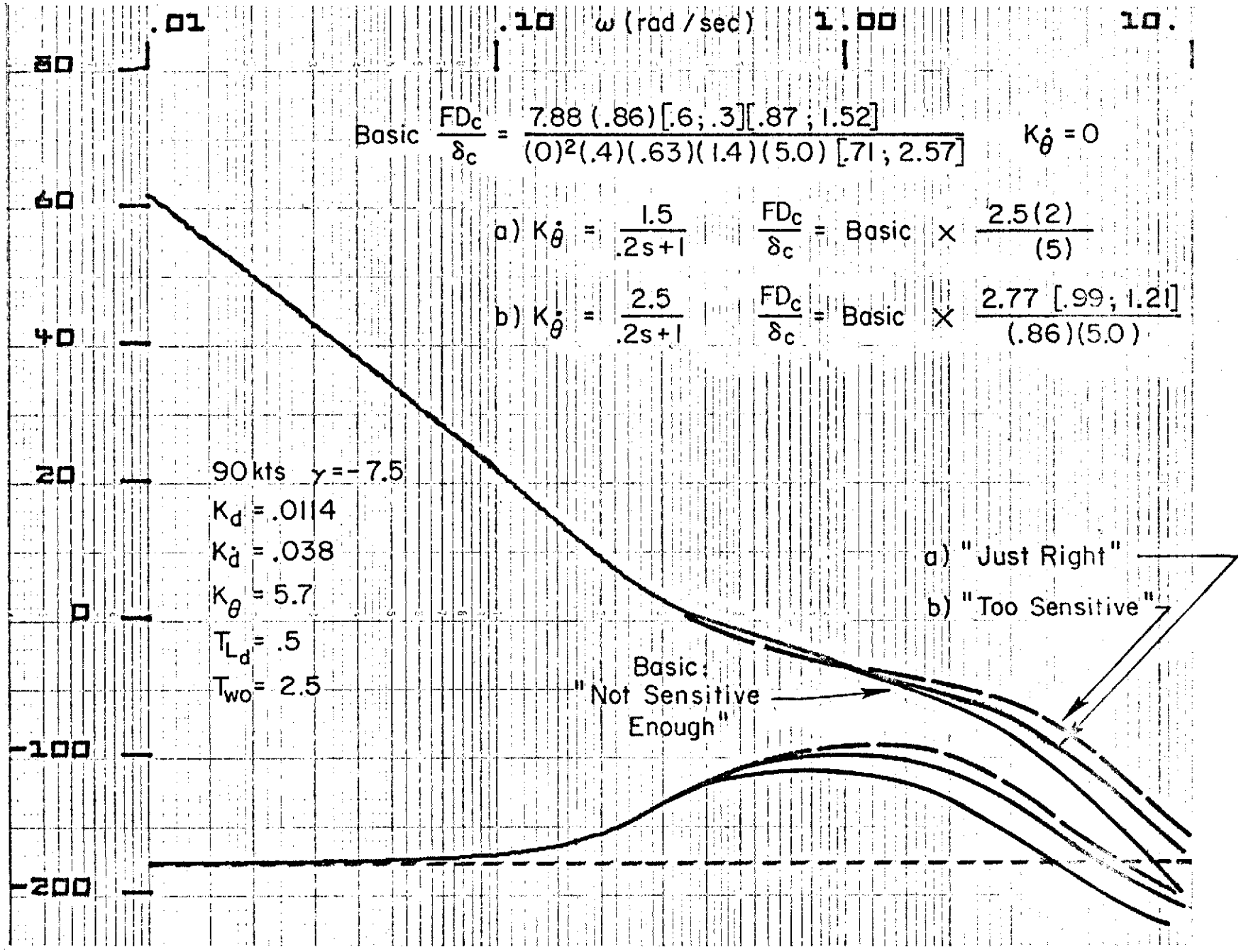

Figure 56. Effect of Pitch Rate Feedback on Pilot Opinion

h. Elevator SAS — In the attitude system, an elevator trim follow-up was required to center the SAS authority. Although the ±7 deg authority of the SAS actuator is adequate for the nominal curved path approach, any significant pilot abuses of off-nominal glide slope conditions resulted in saturation of the RCAH system and subsequent pitch attitude control problems.

2. Longitudinal Flight Director Performance

Longitudinal flight director performance was evaluated based on glide slope capture characteristics and subsequent glide slope tracking errors in wind and wind shear. Limits of performance and safety margins were checked by considerations of speed excursions below 60 kt and angle-of-attack excursions.

An example of a no-turbulence, no-wind, curved path approach is shown in Fig. 57. Starting from the top of this figure the glide slope error trace shows a well-damped glide slope capture. Subsequent glide slope tracking occurs with essentially zero error. Altitude is shown decreasing linearly from 2000 ft to 0 during the run.

Airspeed and angle of attack are displayed on channel three. The speed control system is seen to decelerate the aircraft without overshoots or stand-offs and subsequently holds the commanded speed within 2 or 3 kt. After conversion to backside, the airspeed error signal is passed through a ±10 kt limiter to the column director. While the basic purpose of the feedback is to minimize speed excursions below 60 kt due to disturbance inputs, it is also used for commanded speed changes (below 81 kt). This results in a 3-degree step pitch-up (Channel 4) during the transition to 60 kt and is responsible for an increase in angle of attack from 5 to 8 deg (Channel 3). Pilot commentary indicated that angles of attack near 8 deg leave too little margin for off-nominal conditions. This problem may be resolved by lagging the speed command input to the column director so that it occurs at a lower rate than the aircraft deceleration. An alternate solution is to set the speed feedback limiter so that only negative speed errors (pitch down command) are passed to the column flight director.

The pitch attitude (Channel 4) exhibits an initial pitch over (as per the trim schedule in Fig. 4b) as the aircraft slows to 90 kt and glide slope

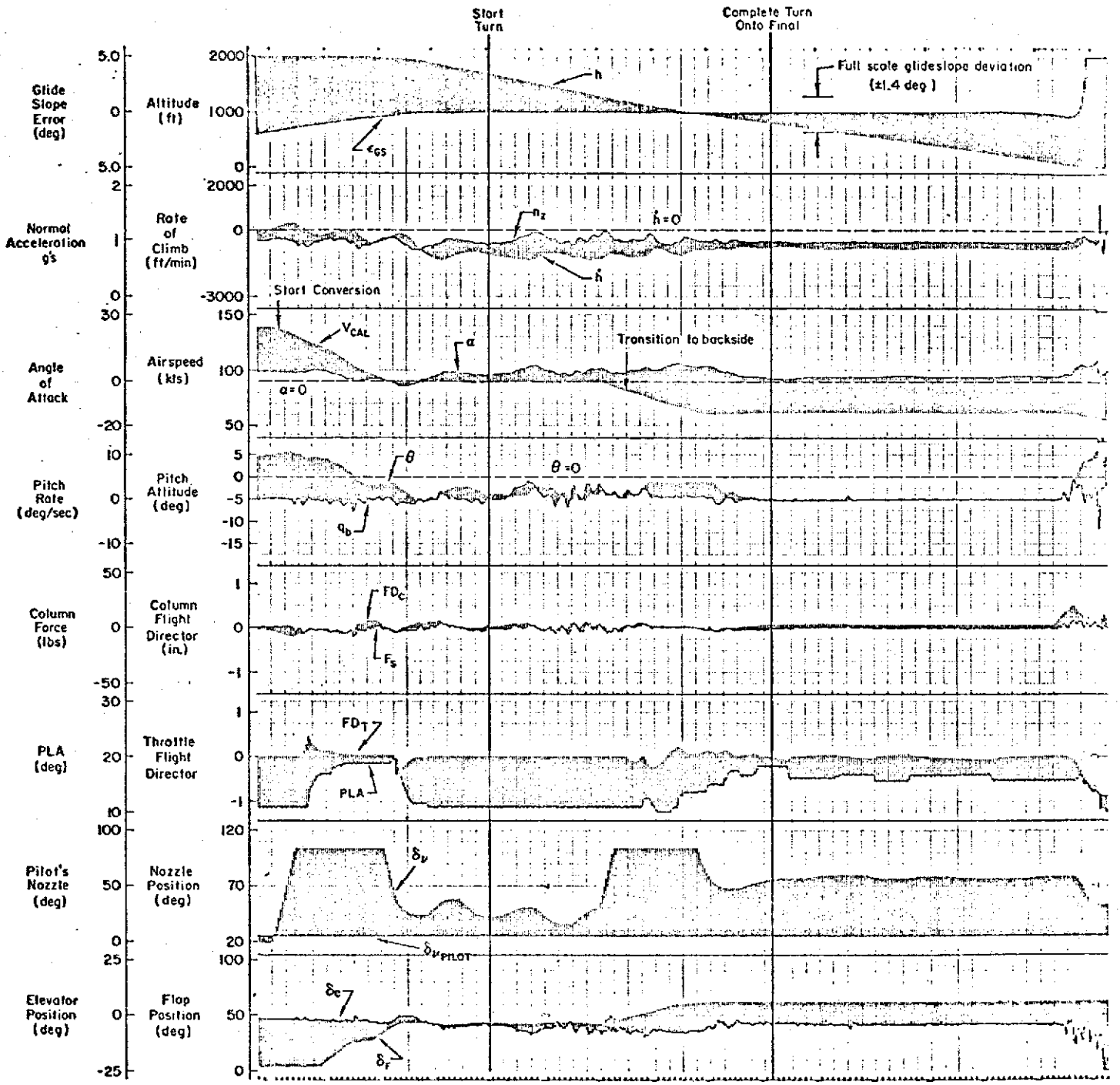

Figure 57. Curved Decelerating Approach with Zero Winds or Turbulence

intercept occurs. As the speed passes through 81 kt, glide path control is transferred to the throttle director. The column director becomes a constant attitude-hold plus speed-error command.

The throttle director (Channel 6) activity is limited to two discrete commands (at 130 kt during transition and at glide slope capture) above the backside transition speed of 81 kt. Below 81 kt, the throttle is seen to become the primary (high-frequency) controller and attitude the secondary (low-frequency) control.

Nozzle (Channel 7) is full forward during deceleration maneuvers, indicating an inherent performance limit of the airplane.

Figure 58 illustrates the effect of a 20 kts east wind (headwind on final). Comparison with the no-wind case reveals that:

- The initial rate of descent (Channel 2) is increased and final rate of descent is decreased as the aircraft is turned into the wind.
- The pitch attitude is lower during the downwind segment (decreased from −4 deg for zero wind to −7.5 deg) as a consequence of the required increase in sink rate to maintain glide slope.
- The angle of attack is lower than the no-wind case during final approach into the wind (0 deg compared to 2 deg).
- Increased power (94 percent) is required while tracking the glide slope with a headwind.

Reversing the wind direction so that the aircraft is in a tailwind on final is shown in Fig. 59 and was found to be the most critical case from the standpoint of angle-of-attack margin. While a tailwind on final is not a common event, it does occur in practice, usually right after the surface winds have shifted enough to change the landing direction but the winds aloft (above a few hundred feet) are still unchanged.

Several salient conclusions from Fig. 59 are summarized as follows:

- The pitch attitude (Channel 4) is initially higher than the no-wind case (−2.5 deg compared to −4 deg) as a result of the decreased rate of descent while tracking the glide slope in a headwind. (Recall that the control technique is frontside or $h \rightarrow \theta$ above 81 kt.) This has little effect on angle of attack because of a lower trim nozzle in the headwind case.

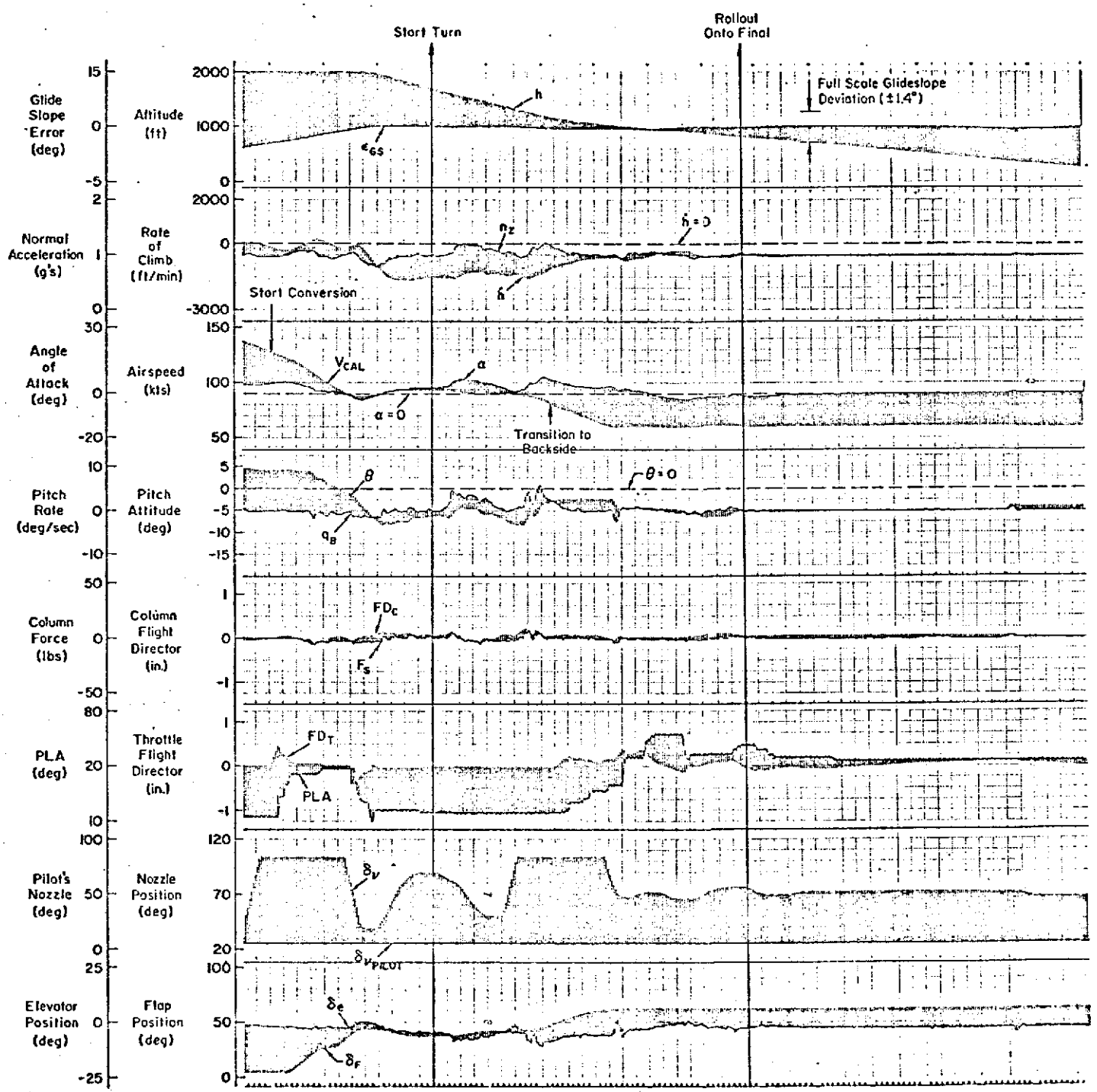

Figure 58. Curved Decelerating Approach with a 20 kt Wind From the East

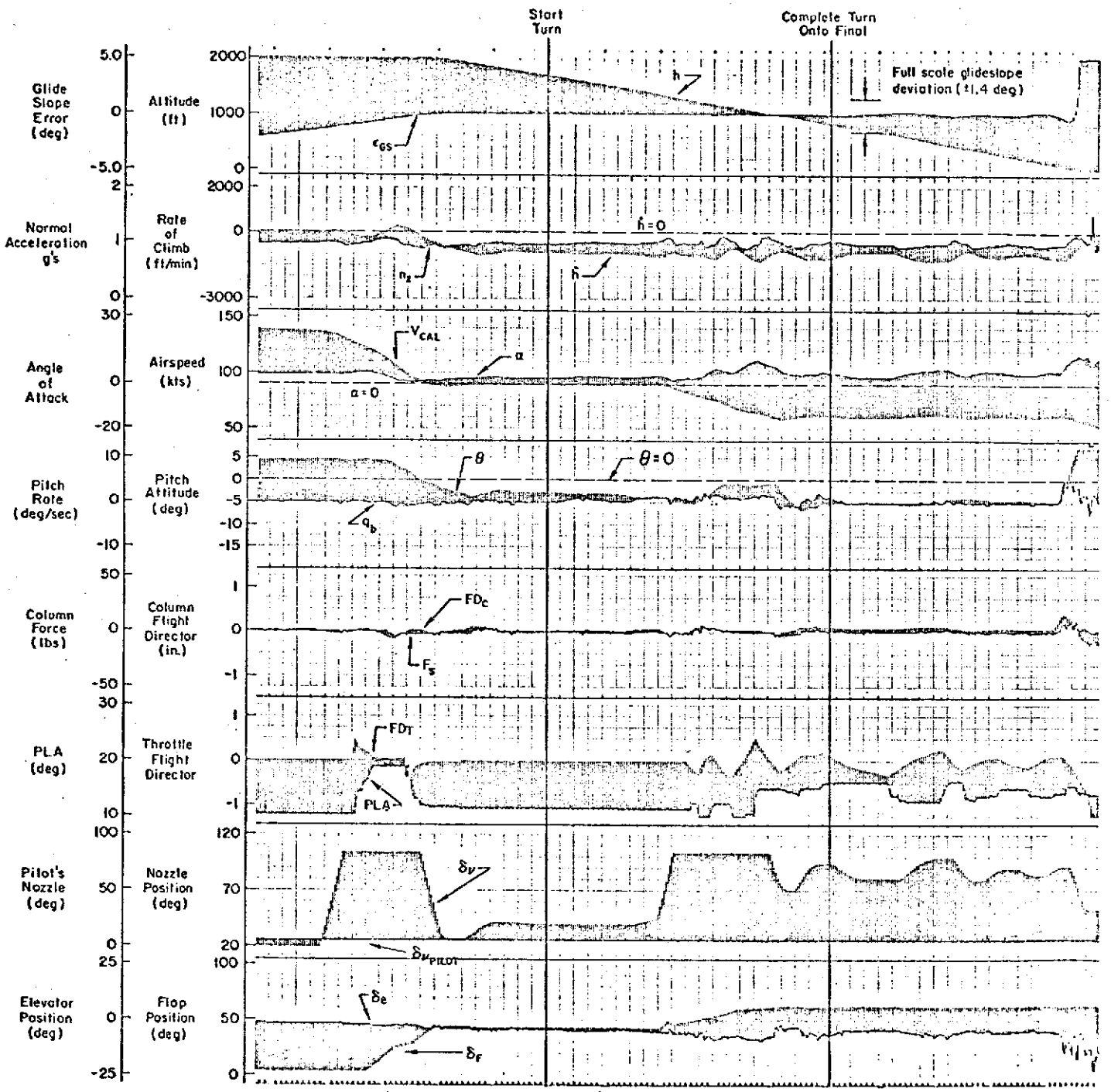

Figure 59. Curved Decelerating Approach with a 20 kt Wind From the West

- The angle of attack (Channel 3) is greater than the no-wind case during the downwind final approach segment (5-6 deg compared to 2 deg).

- A peak angle of attack of 11 deg occurs during the deceleration to 60 kt as a consequence of the previously discussed pitch-up signal that accompanies a reduced speed command input.

- A significant increase in commanded power occurs on the throttle flight director (Channel 6) as the angle of attack increases beyond 8 deg. As previously discussed, this is due to the angle-of-attack protection circuit in the throttle flight director.

This wind condition points out the need for eliminating the pitch-up command that occurs when a lower speed is selected at speeds below 81 kt. Additionally, the oscillatory throttle flight director response at high angles of attack points out the requirement for an improved design on the angle-of-attack protection circuit.

3. Piloted Evaluation of Longitudinal Flight Director

A summary of pilot commentary relative to the longitudinal flight director is given below.

- "The pitch bar is well behaved and easy to keep centered with the elevator."

- "It is necessary to keep the throttle director centered or I can get off in speed."

- "The response to abuses in throttle looked good. All I had to do was center the needles and it came right back."

- "Angle of attack went above 10 deg but the throttle director commanded the proper action."

While no specific ratings were given for the flight director per se, the overall opinions expressed during the debriefing were quite favorable. Primary criticisms were centered about the angle-of-attack excursions above 10 deg in a tailwind.

D. LATERAL FLIGHT DIRECTOR

As discussed in Section IV, two competing lateral flight directors evolved from the design effort (FD A and FD B). Simulation results for each director are discussed in this section.

The trajectory used in the evaluations is given in Fig. 60 and consists of a downwind leg, a 180 deg curved localizer segment, and a variable final approach course length. The outer marker and middle marker were located just before WP 2 and WP 3 to warn the pilot of the impending transition between straight and curved course segments of the approaches.

A block diagram of the computer mechanization is given in Fig. 61 Switches 1 through 7 were implemented to allow a rapid changeover from FD A to FD B and to evaluate the effect of removing or adding certain feedbacks and feedforwards. The feedforward bank angle command, Φ_{cc} in Fig. 61 is governed by the following logic:

$$\Phi_{cc} = \begin{cases} 0 & T_1 - \Delta t_1 > 0 \\ -\tan^{-1}\dfrac{V_{GS}^2}{Rg} & (T_2 - \Delta t_2) > 0 \;\; ; \;\; (T_1 - \Delta t_1) \leq 0 \\ 0 & T_2 - \Delta t_2 \leq 0 \end{cases}$$

$$T_1 = -\frac{X_{WP2} - X}{V_{GS}} \quad ; \quad \text{between WP 1 and WP 2}$$

$$T_2 = R\,\frac{\psi - \frac{\pi}{2}}{V_{GS}} \quad ; \quad \text{between WP 2 and WP 3}$$

where Δt_1 and Δt_2 define the lead time, prior to reaching WP 2 and WP 3, at which the bank angle command is initiated and removed. T_1 and T_2 represent simple time-to-go calculations. The above logic is especially tailored to the flight path in Fig. 60 and will require generalization for implementation into the STOLAND computer.

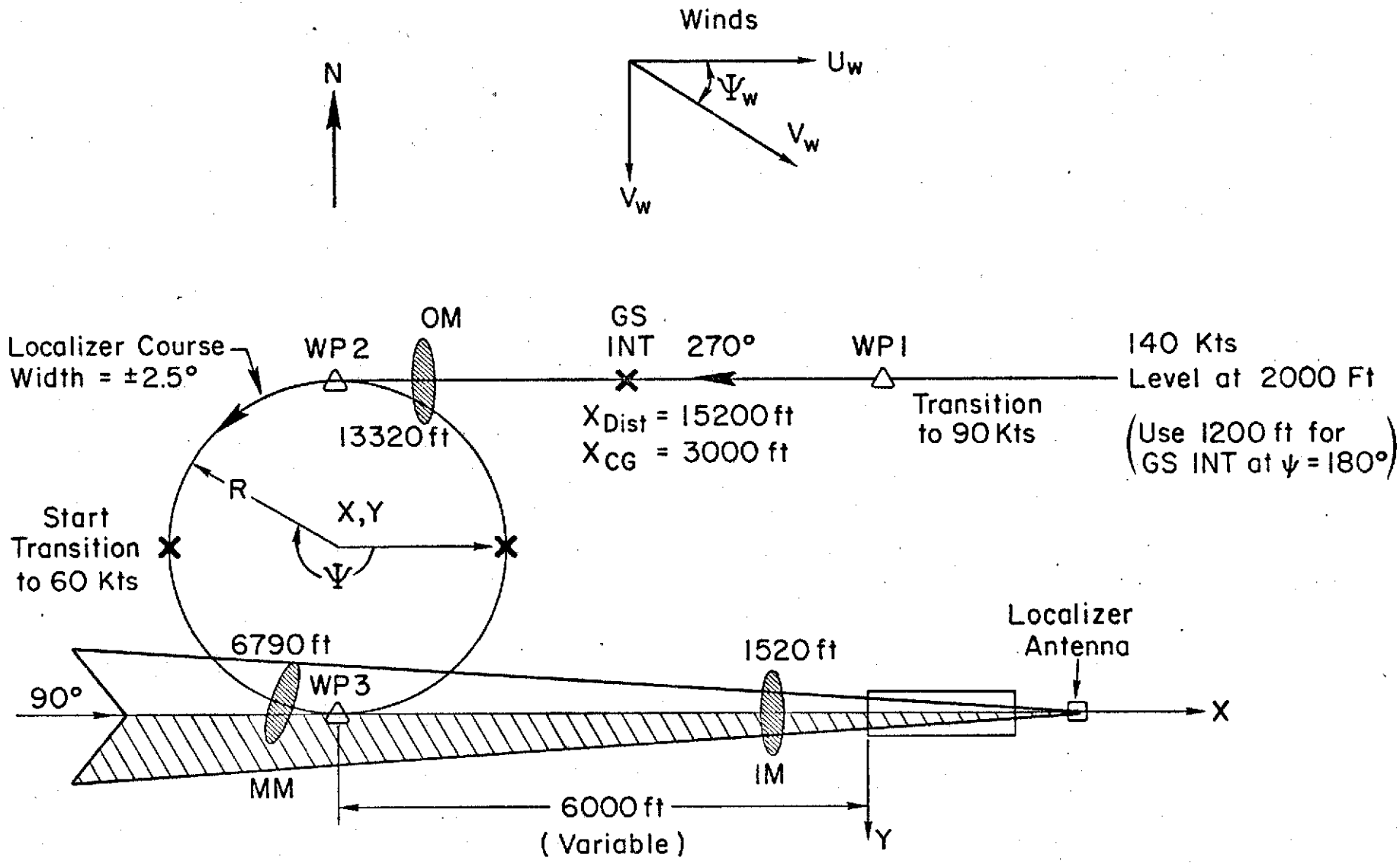

Figure 60. Course Geometry for FSAA Simulator Study

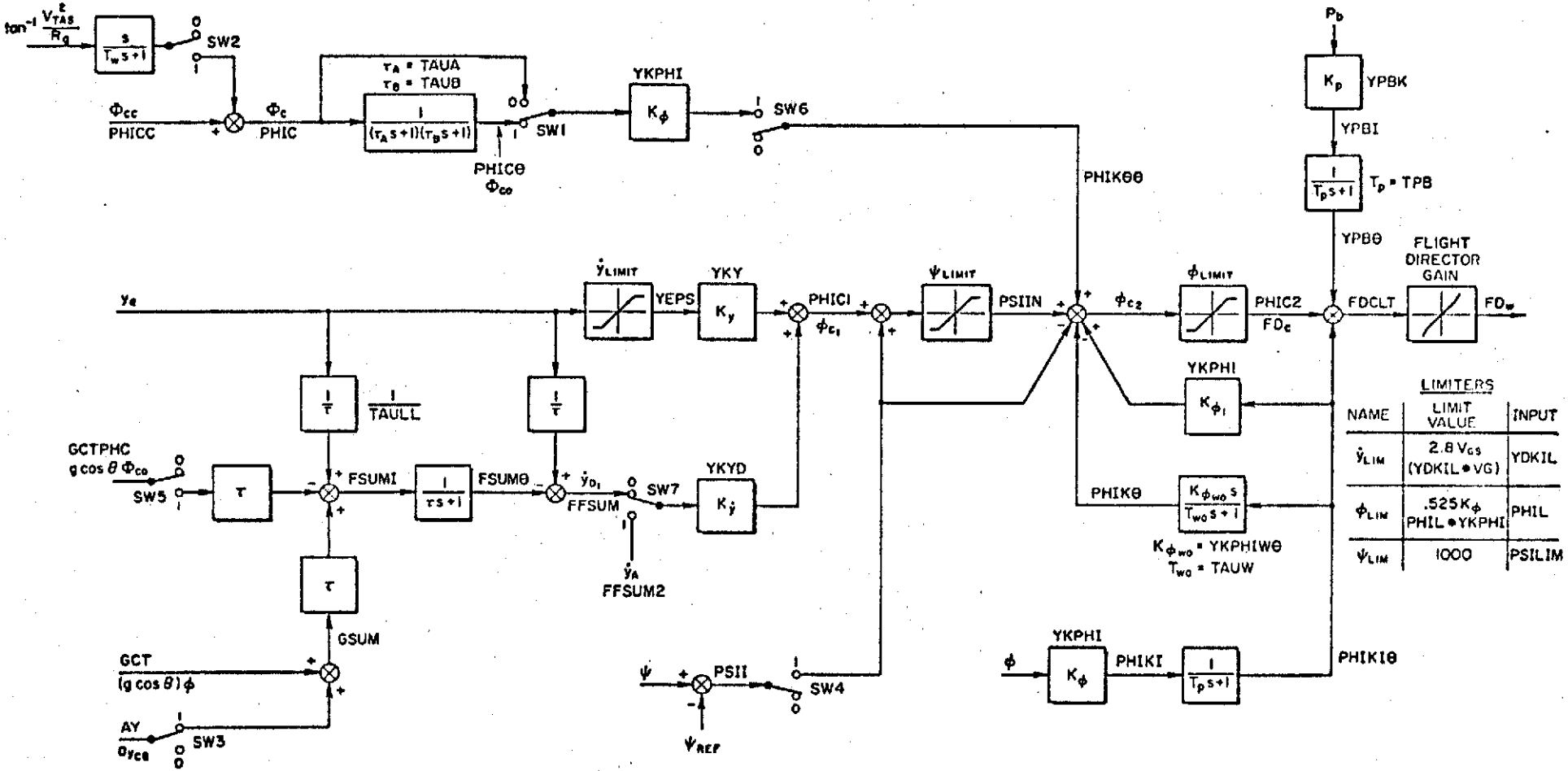

Figure 61. Lateral Flight Director Computer Mechanization

The curved approach segment was intercepted at an indicated airspeed of 90 kt on the -7.5 deg glide slope and a transition to 60 kt was initiated as the aircraft heading passed through 180 deg. This results in a curved, decelerating, descending flight path during the final 90 deg of the curved approach. While the capability of varying the turn radius existed, all evaluations were accomplished with a 2000 ft turn radius to check the system near the limits of performance.

The cockpit instrumentation consisted of the conventional complement of instruments found in current transport-type aircraft. This resulted in a noticeable lack of status information during curved course tracking. Additional display requirements to upgrade the status information to an acceptable level involve a modified horizontal situation indicator (HSI) and/or a moving map display. The conventional HSI has a fixed course datum resulting in incorrect orientation between the course bar and reference aircraft during curved path tracking. A comparison between the conventional HSI and the required modification is given in Fig. 62.

The STOLAND system has both the modified HSI and a moving map display and therefore should result in improved pilot opinion regarding status information.

1. Design Aspects of Simulation

Several of the flight director parameters were optimized on the simulator. A brief discussion of the factors involved in the optimization process is given below for FD A and FD B. Each of the parameters discussed are shown in Fig. 61.

a. Feedforward Shaping Filters (Effect of τ_A and τ_B)

The purpose of the feedforward shaping filter is to eliminate step-like command bar motions in response to the step Φ_c that occurs Δt sec before course intercept. It was originally thought that the command bar motions should occur at a rate below the pilot's tracking frequency. This would allow the pilot to keep the command bar centered at all times. As it turned out, the shaping required to achieve this result gives an erroneous Φ_{co} at path mode frequencies

Note: Course reference bug and course deviation indicator are always parallel.

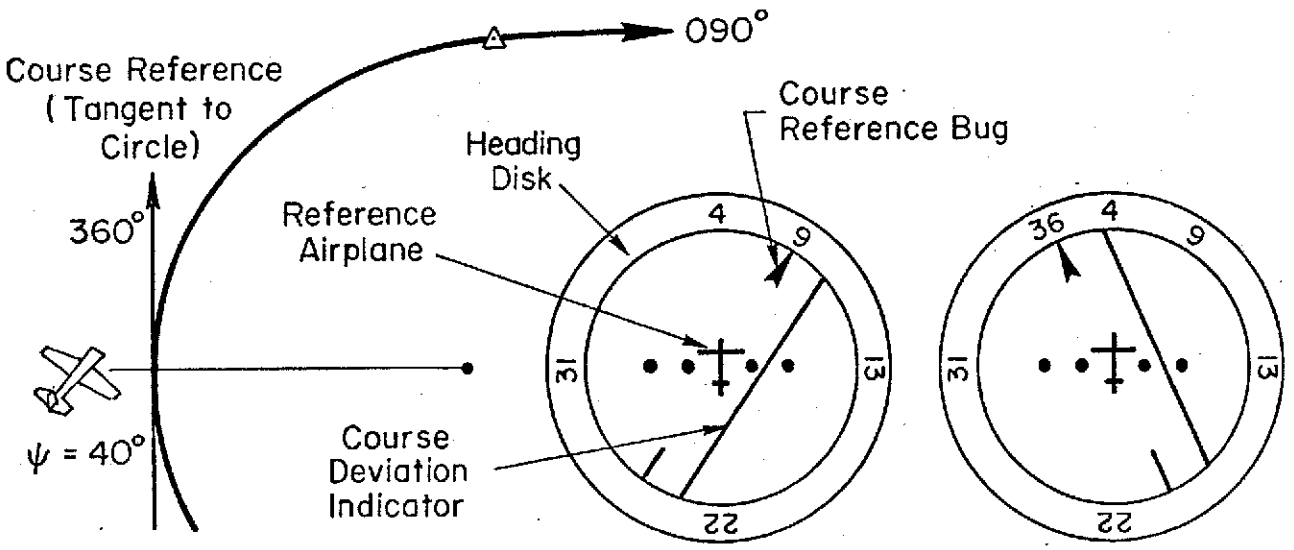

a) CONVENTIONAL HSI

- Incorrect presentation
- Course reference bug fixed with respect to heading disk
- Angle between reference airplane and desired course is incorrect. (shows aircraft is flying away from course)
- Course reference bug set manually

b) MODIFIED HSI

- Correct presentation
- Course reference bug rotates with respect to heading disk
- Shows correct intercept angle between reference airplane and desired circular course
- Course reference bug driven by servo

Figure 62. Required Modification to HSI for Curved Path Status Information

resulting in a standoff in crosstrack deviation. In addition, the pilots did not object to a discrete flight director command as it tended to serve as status information with regards to a change in course geometry. The central factor in pilot opinion was his ability to recenter the bar without overshoots or unduly large control inputs. Setting $\tau_A = \tau_B = 0$ was found to be undesirable because it was difficult to tell how much δ_w was required to get the command bar off the limit, and because of the very abrupt nature of the command. As a final compromise, the lag time constants were set to unity ($\tau_A = \tau_B = 1.0$). This resulted in relatively smooth command bar motions and did not affect the course tracking accuracy, i.e., the requirements for face validity and path mode consistency were both satisfied.

b. Feedforward Initiation Time Increment (Effect of Δt_1 and Δt_2)

As discussed at some length in Section IV, the feedforward command must be initiated prior to curved/straight course transition. Variations of Δt_1 and Δt_2 showed that the transition characteristics are quite sensitive to these parameters. The curved to straight transition (Δt_2) exhibited the greatest sensitivity because the aircraft would be turned on to the straight localizer at the wrong heading as Δt_2 was varied away from its "optimum value." The ensuing bank angle reversals resulted in considerably degraded pilot opinion. Once Δt_2 was set at the "proper value" (3 sec), the straight localizer intercept was very smooth. The optimum value for $\Delta t_{1,2}$ is very insensitive to variations in aircraft speed, course radius, and winds. This results in a desirable system simplification in that $\Delta t_{1,2}$ can be set to a constant without compromise in system performance throughout the flight envelope.

c. Bank Angle Limits

Pilot commentary was unanimous in that a bank angle limit of 30 deg was quite acceptable at speeds near 90 kt. There were some reservations about using this large a bank angle at speeds near 60 kt. Some consideration was given to varying the bank angle limit with speed. However, operational considerations indicate that large bank angle commands are very unlikely at low speeds because:

- The required bank angle varies directly with speed.
- The aircraft is not normally slowed to 60 kt until it is turning toward the final approach course and is in a headwind condition.

Finally, if a strong wind existed, the crew would not use low approach speeds because of the associated turbulence and wind shears.

d. Crosstrack Limiter

The primary purpose of this limiter is to preclude the possibility of large rapid bank angle commands which would occur if the aircraft were significantly offset from course due to a large disturbance or pilot inattention. The limiter is set as a function of ground speed so as to achieve a 20 deg reintercept angle as follows:

$$\left|\dot{y}_{lim}\right| = \frac{K_{\dot{y}}}{K_y}\dot{y} = \frac{K_{\dot{y}}}{K_y} V_{GS} \sin 20^o$$

Note that initial course intercepts are made in the Heading Mode or tracking on a previous NAVAID and that the localizer tracking does not begin until:

$$\left|y_\epsilon + \frac{K_{\dot{y}}}{K_y}\dot{y}_\epsilon\right| < 100 \text{ ft}$$

It follows that the $\dot{y}$ limiter will have no effect on the initial course intercept characteristics.

2. Lateral Flight Director Performance

System performance checks were accomplished using the flight path described in Fig. 60. Disturbance regulation was checked using 25 kts winds from all four quadrants, wind shear, and intentional pilot abuses. As expected, the most critical disturbance was an east wind (tailwind at curved path intercept).

A summary of performance data and pilot commentary is given in the following paragraphs for FD A and FD B.

a. Flight Director A Performance

Time histories for a curved approach in no wind and with a 25 kt tailwind at curved path intercept are shown in Fig. 63 and 64, respectively. The following observations apply.

- Crosstrack errors are less than 1/10 full-scale localizer or 70 ft in both cases.
- The aircraft is driven to the bank angle limit in the 25 kt tailwind case.
- Deceleration on the path has no effect on curved path tracking errors with or without wind.
- Transition from curved to straight course is smooth and without significant heading overshoots. (This also holds true for north and south winds.)

Crosstrack errors were found to be sensitive to the accuracy of the feedforward bank angle command signal. An error of 0.015 rad was found to result in a standoff of about 100 ft. This is discussed in Section IV-C-4.

The maximum bank angle limit acceptable to the pilots was 30 deg. This sets a fundamental performance limit on the minimum achievable turn radius for a given ground speed as shown in Fig. 65. This result holds true for FD A and FD B.

b. Flight Director B Performance

As discussed in Section IV, the washed-out bank angle director, in its simplest form, will exhibit considerable course overshoots at curved course intercept for turn radii less than 4000 ft. This is caused by the lack of a bank angle command just prior to the tangent point which would allow blending into the curved course. In order to evaluate the worst case, a 25 kt tailwind was imposed at the intercept point of the 2000 ft radius turn with the results in Fig. 66, which shows that:

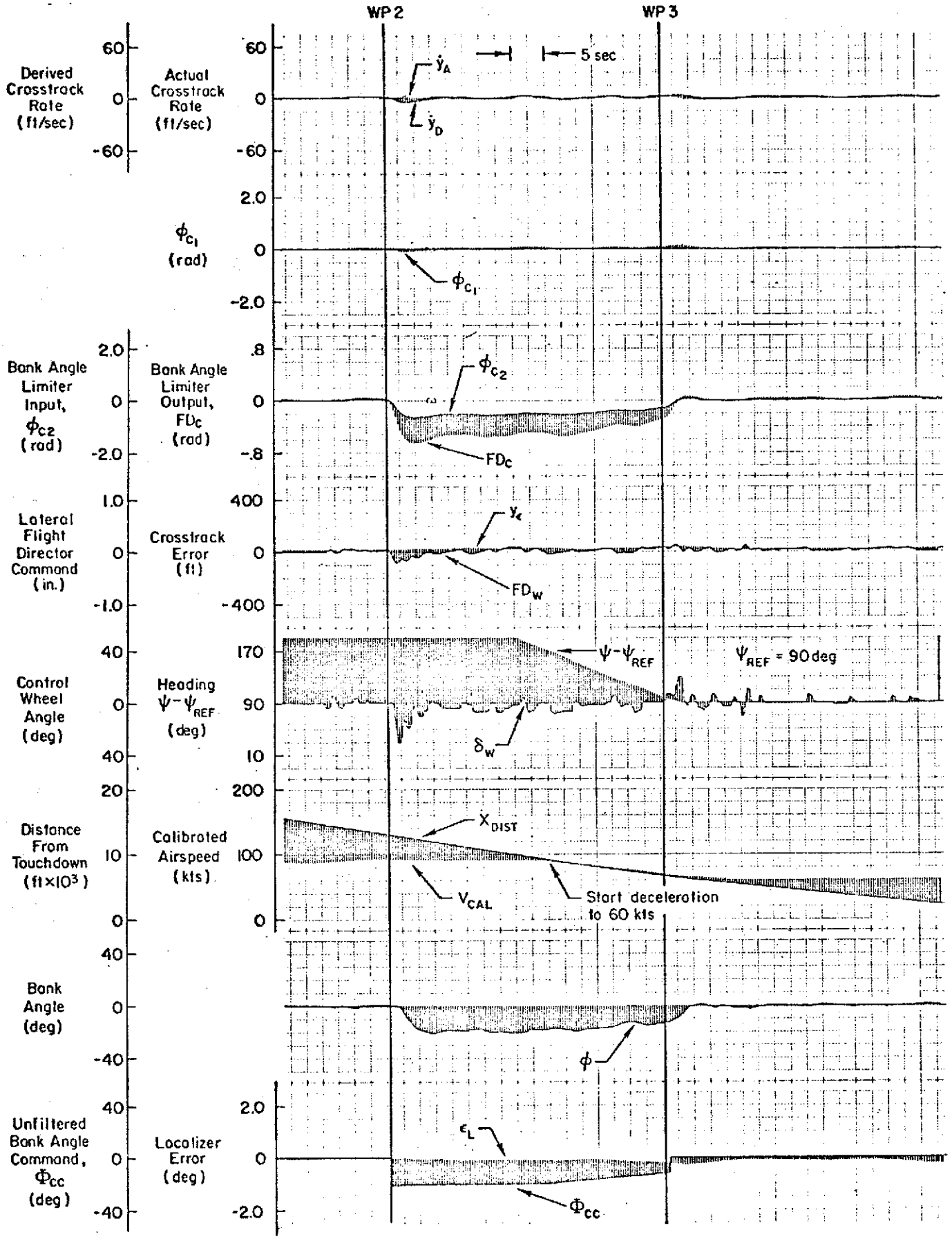

Figure 63. Curved Path Tracking With FD A; No Wind; R_c = 2000 ft

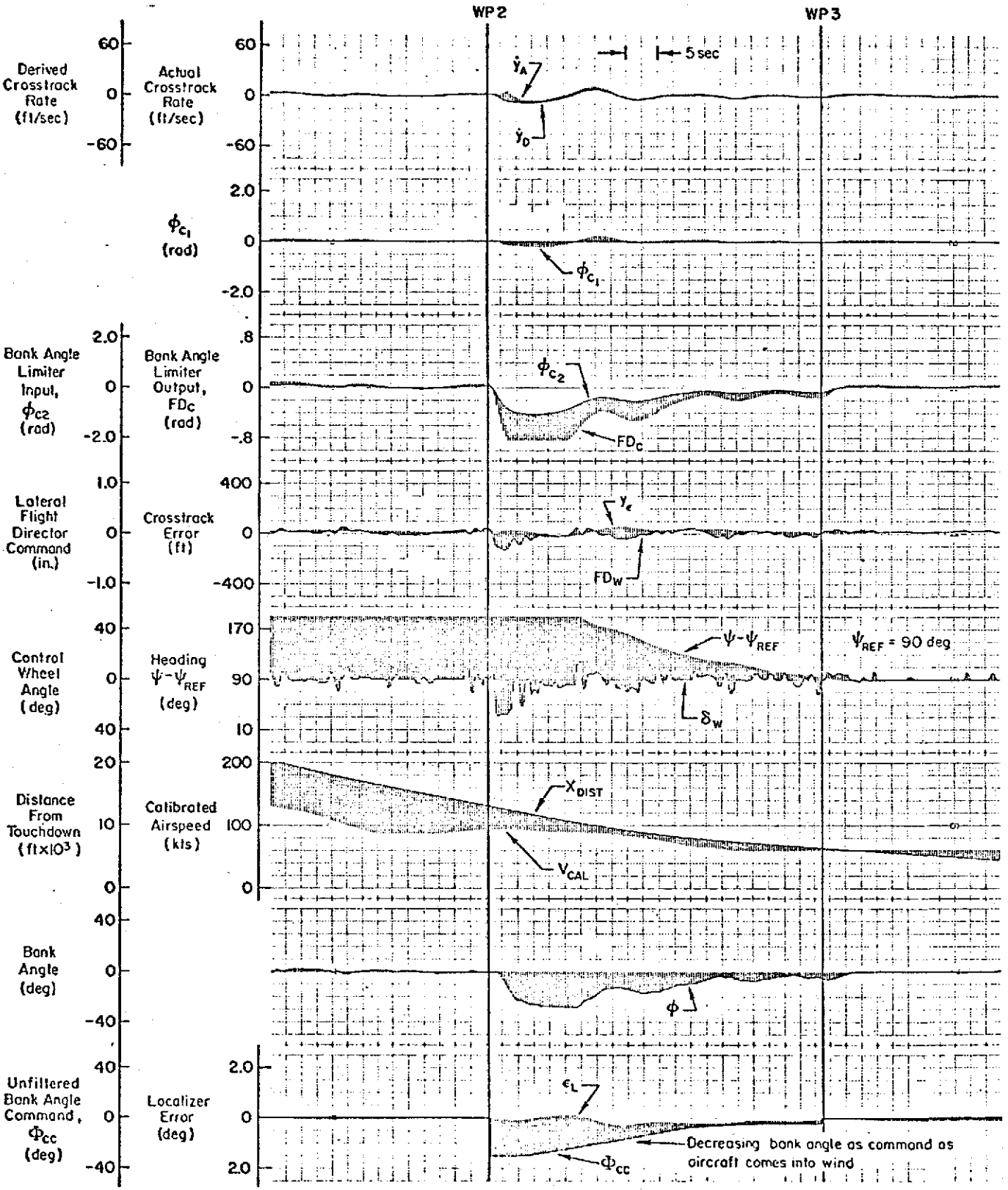

Figure 64. Curved Path Tracking With FD A; −20 kt East Wind; R_c = 2000 ft

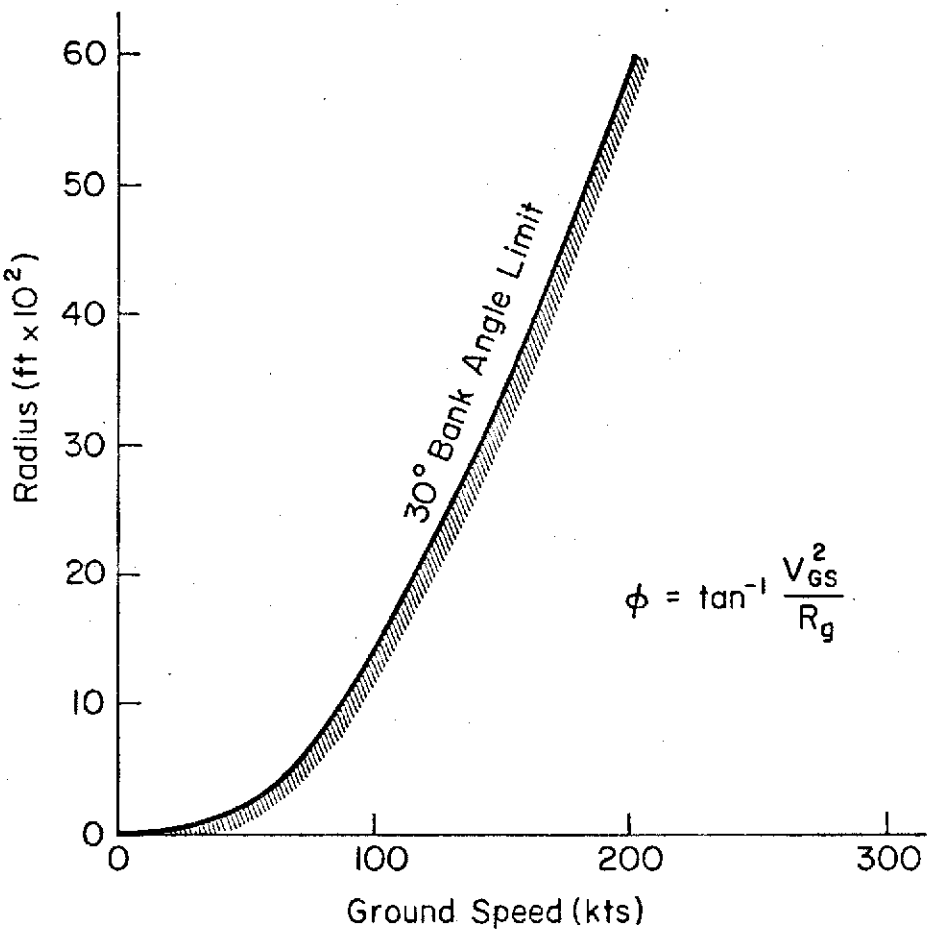

Figure 65. Effect of Bank Angle Limit on Curved Course Tracking

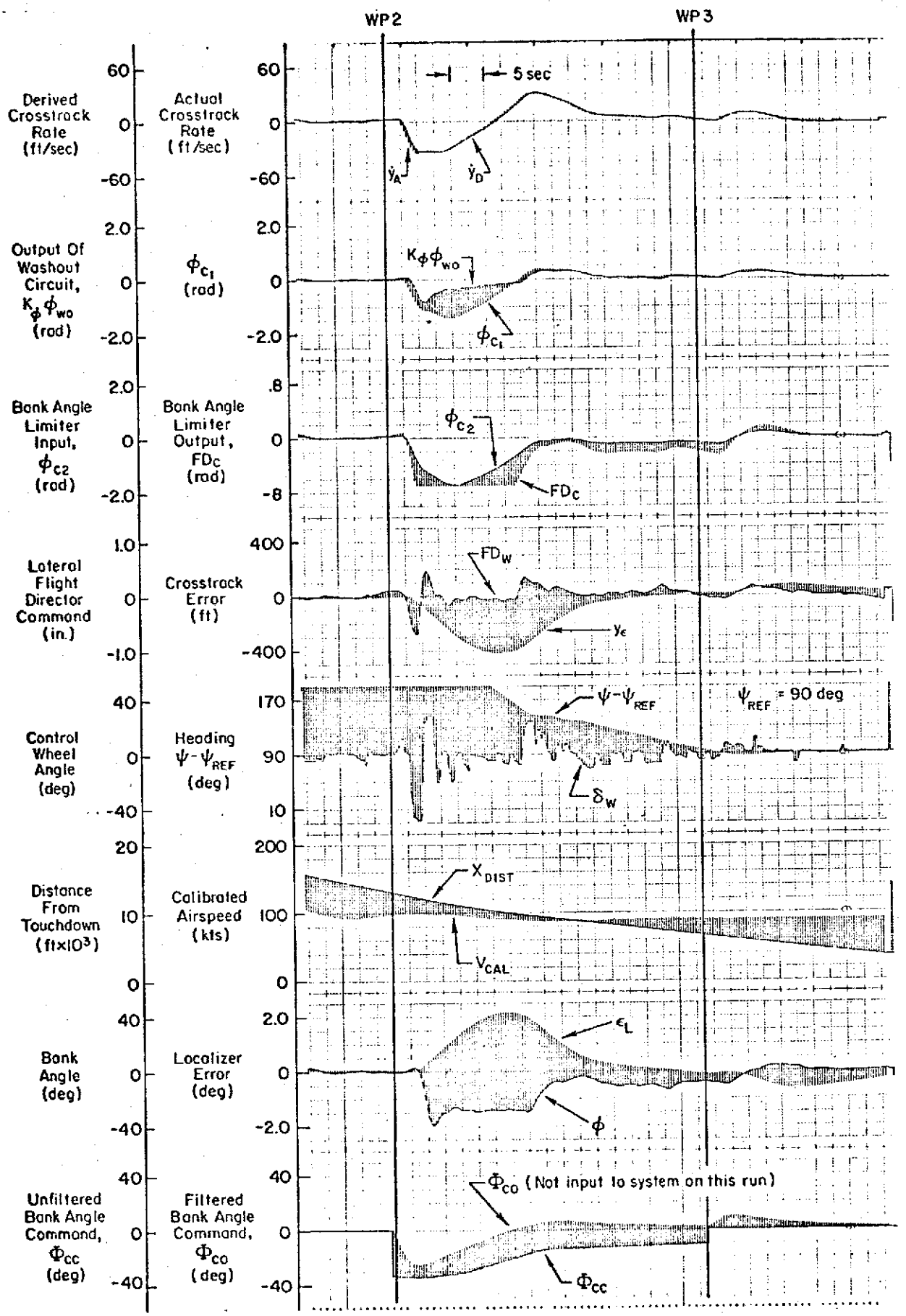

Figure 66. Curved Path Tracking with FD B Without Washed-Out Feedforward; 25 kt East Wind; R_C = 2000 ft

- As predicted in Section IV, the initial course overshoot is about 400 ft. Repeat runs indicated that this varied from 400 ft to 600 ft.

- The aircraft goes to and remains on the bank angle limit until the derived crosstrack rate error signal, $\dot{y}_D$, becomes positive.

- Return to course is smooth and without overshoots.

Addition of a simplified feedforward consisting of a washed-out step bank angle command allows the aircraft to start rolling into the turn just before curved path intercept with the results shown in Fig. 67. (The simplified feedforward is shown in Fig. 53.) As expected, this eliminates the overshoot problems and the tracking characteristics are very similar to FD A. For turn radii greater than 4000 ft, good performance is obtainable without the need for the feedforward command.

3. Pilot Commentary on Lateral System

Due to time limitations and pilot availability, pilot commentary was not obtained for Flight Director B. Pilot comments on Flight Director A are summarized below.

Pilot A

- "No problem with lateral director, easy to fly, keeps me on course."

- "Looks pretty close to something we can put on the airplane."

- "Workload is not unreasonable. I have time to scan the status information."

- "I don't want to give a rating because I don't think that is the intent of this evaluation. The purpose is to design a director that will work on the airplane and I think we are pretty close."

- "I overshot WP 2 (curved course intercept) on purpose. The recovery was good."

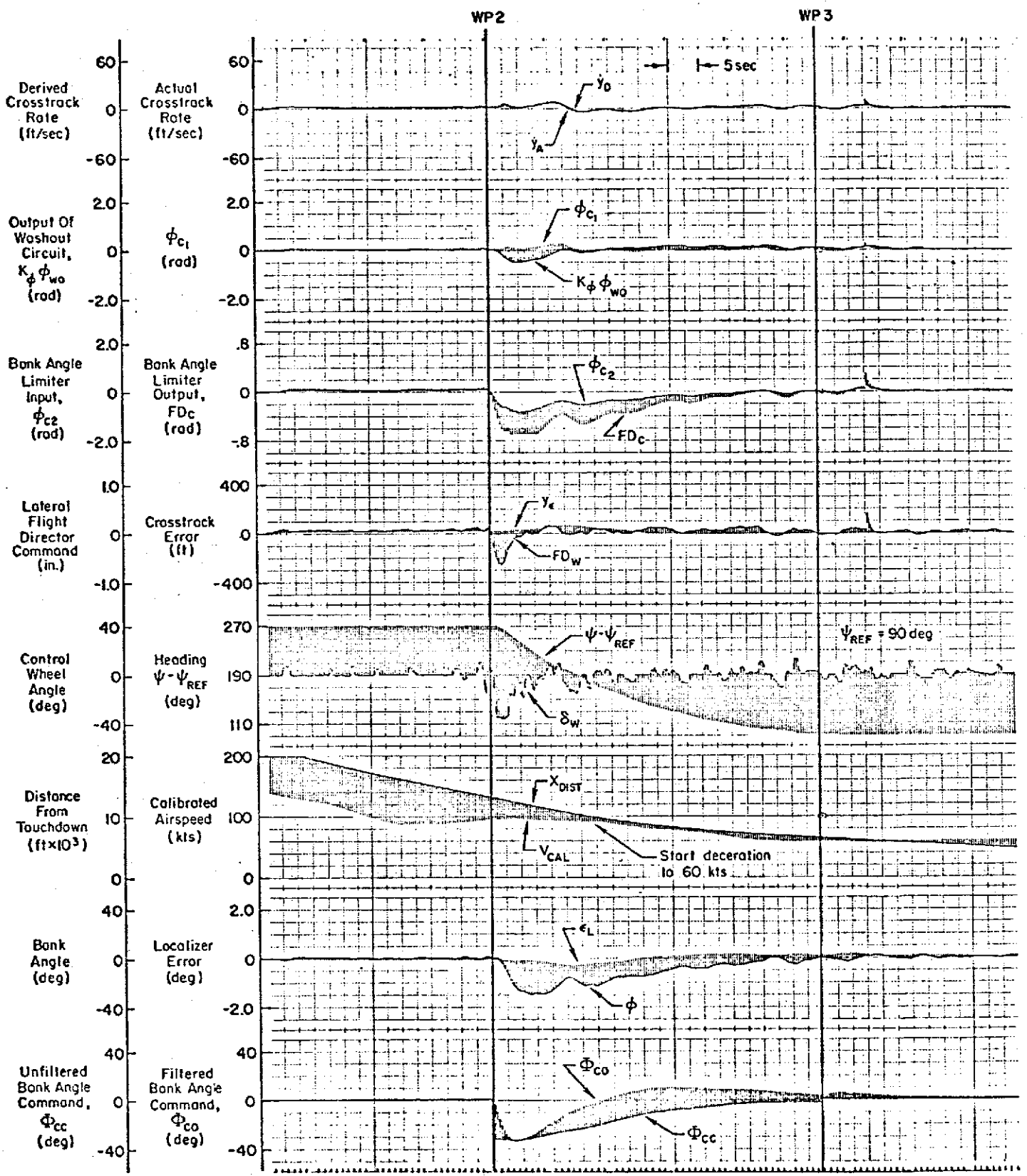

Figure 67. Curved Path Tracking with FD B with Washed-Out Feedforward; 25 kt East Wind; R_c = 2000 ft

Pilot B

- "Keeping the flight director centered requires my full attention. I have very little time to scan the status information [during curved course tracking]."
- "For conventional use the flight director is a POR of 1-1/2. While turning it is a 3. This degradation in rating is due to the constantly changing bank angle required to stay on course (due to winds and deceleration from 90 kt to 60 kt."
- "I feel we need additional status information such as a moving map display [during curved course tracking]."

E. COMPOSITE EVALUATION

This evaluation was one part of a simulation program designed to formulate preliminary STOL certification criteria. Every effort was made to simulate an operational environment including an FAA air traffic controller who gave the pilot delay vectors, clearances, etc. The pilot commentary and ratings are given in unabridged form on the following three pages.

In most cases, the flight-director/configuration-management system resulted in significant improvements in performance as shown by Table 7 of rms localizer and glide slope deviations at the 200 ft decision height point below.

TABLE 7

RMS ERRORS AT DECISION HEIGHT WITH AND WITHOUT THE FLIGHT-DIRECTOR/CONFIGURATION-MANAGEMENT SYSTEM

PILOT	BASIC AWJSRA		WITH FLIGHT DIRECTOR AND CONFIGURATION MANAGEMENT	
	σ_{LOC}	σ_{GS}	σ_{LOC}	σ_{GS}
C	0.76°	0.28°	0.27°	0.28°
D	0.46°	0.39°	0.08°	0.13°

GENERAL PILOT EVALUATION

Pilot FAA Date 8-16-73 Runs

Task ATC exercise with flight director (6 deg glide slope) 5000 ft radius turn

Comments: Programmed flight path was flyable with turbulence and winds; however, pilot's workload increased very much with vectoring, decelerating and communications. On several occasions the workload reached unacceptable level, i.e., two successive vectors combined with deceleration. Resetting of a speed bug necessitated breaking the instrument scan in the middle of a turn.

The configuration of this A/C appears laterally unstable and without the use of the flight director heading command bar; and in turbulence, I was unable to come smartly to the desired heading.

Once on localizer and glide slope it was relatively easy task to fly the command bars. The 5,000 ft turn was gentle and flyable under all wind conditions, and was almost as if flying a straight path.

It is foreseeable that a holding pattern would be equally difficult with single pilot/no-FD guidance in the holding pattern.

Pilot Ratings (where applicable):

a. Straight and level — 3

b. Vectors and slowdown — 6-6.5

c. Turn/glide slope — 3

d. Final (straight) — 2.5

e. D.H. to T. D. — 3

Conditions: Turbulence 4.5, winds
Single pilot operation
Radar vectors
Excessive communications

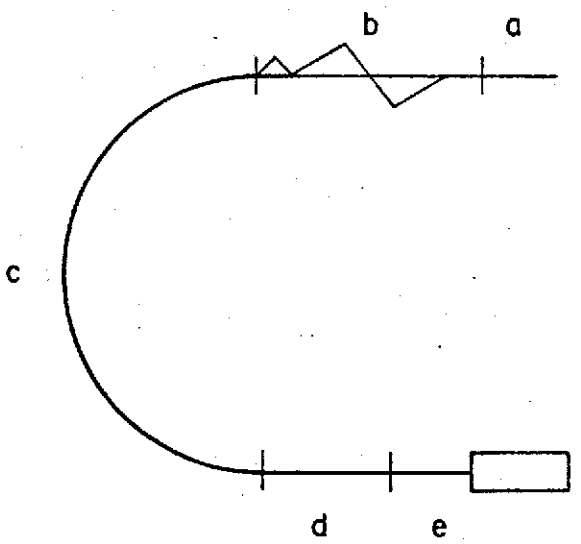

GENERAL PILOT EVALUATION

Pilot FAA Date _____ Runs _____

Task Curved ATC Flight Paths 7.5 deg glide slope (5000 ft radius turn)

Comments: Pilot performance was improved on this set of runs and workload was decreased considerably. The ATC vectors were not as large as on the 6 deg glide slope runs and this resulted in a better initial alignment and eased the pilot's task. The 7.5 deg glide slope did not seem to make much difference and was not noticeable, except on the initial glide slope intercept, where the command bar initially required 10 deg plus pitch over followed by a level-off command. The F/D is considered a must to achieve satisfactory performance to fly the curved approach. One approach was flown on "raw data" and power command was disregarded. This approach was flown IFR and a successful landing was achieved. However, flight path/glide slope/airspeed and power applications must be rated 8+. More practice and better presentation would improve this figure.

Pilot Ratings (where applicable):

a. Straight and level — 3

b. Vectors — 5

c. Turn and glide slope — 3+

d. Straight and glide slope — 2.5

e. Final — 3

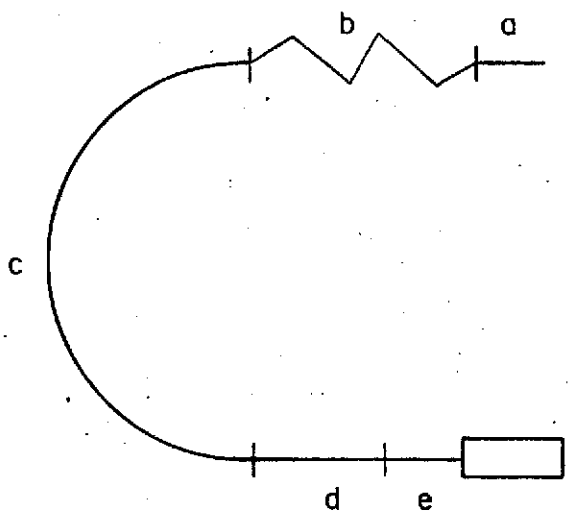

GENERAL PILOT EVALUATION

Pilot FAA Date _____ Runs _____

Task Curvilinear ATC Flight Path 2500 ft R, 7.5 deg glide slope

Comments: This flight path was acceptable and did not present any difficulty. The initial LOC intercept commanded a considerable bank angle initially. This bank together with the initial glide slope intercept pitch over might have been unacceptable from the passenger standpoint. Some anticipation or lead on both the LOC and glide slope is necessary to decrease the initial steer attitude. However, once established in the turn and on the glide slope, the task was relatively easy. The turn on's to the final were accurate and no further maneuvering was required for final alignment. One run was done with the most adverse wind condition (tail wind in the turn, effectively steepening the turn) and this presented no difficulty and the F/D was able to compensate fully for this.

Pilot Ratings (where applicable):

a. Initial tracking was in turbulence and was slightly compounded by the necessity for immediate slowdown — 3

b. Initial ILS and glide slope intercept requiring considerable amount of roll and pitch application — 4

c. LOC and glide slope maintenance throughout the turn — 2+

d. Final straightaway — 2

e. Final straightaway after D.H. — good alignment, no maneuvering necessary — 2

Recommendations: Provide anticipation warning lights: blue 5 sec before LOC intercept, amber 5 sec before glide slope intercept. (This was done on the evaluations but not on the FAA program)

SECTION VI

SUMMARY

The basic objectives of the program were to develop flight director displays and a stability augmentation system for the Augmentor Wing Jet STOL Research Aircraft (AWJSRA). A fundamental mission requirement was to allow manual tracking of a curved ILS beam including the capability for deceleration on the glide slope. A summary of the system which evolved from the resulting design-analysis effort consists of:

- Development of a configuration management system involving a flap-nozzle interconnect with both of these controls automatically driven by the airspeed sensor output.
- A longitudinal flight director consisting of a pitch command bar, and a throttle command bug.
- Two competing lateral flight director system which allow tracking of curved paths.
- A rate command attitude hold pitch SAS.

The resulting system was deemed very desirable by the pilots in that workload was reduced to an acceptable level and minimal compensation was required to obtain the desired performance.

REFERENCES

1. Johnson, Walter A., Samuel J. Craig, and Irving L. Ashkenas, Analysis and Moving-Base Simulation of Transition Configuration Management Aspects of a Powered Lift STOL Aircraft, Systems Technology, Inc., TR-1015-2, August 1973.

2. Klein, Richard H., Lee G. Hofmann, and Duane T. McRuer, Analytical Design and Simulation Evaluation of an Approach Flight Director System for the Augmentor Wing Jet STOL Research Aircraft, Systems Technology, Inc., TR-1015-1, April 1973.

3. McRuer, Duane, Irving Ashkenas, and Dunstan Graham, Aircraft Dynamics and Automatic Control, Princeton University Press, 1973.

4. Ashkenas, I. L, and S. J. Craig, "Multiloop Piloting Aspects of Longitudinal Approach Path Control," presented at the 8th Congress of ICAS, Amsterdam, August 28-September 2, 1972, ICAS Paper No. 72-46.

5. Weir, D. H., R. H. Klein, and D. T. McRuer, Principles for the Design of Advanced Flight Director Systems Based on the Theory of Manual Control Displays, NASA CR-1748, March 1971.

6. Klein, R. H., Longitudinal Flight Director Design for C-8M STOL Aircraft, Systems Technology, Inc., WP-1015-6, December 1971.

7. McRuer, Duane, and David H. Weir, "Theory of Manual Vehicular Control," Ergonomics, Vol. 12, No. 4, July 1969, pp. 599-633.

8. McRuer, Duane, "The Development of Pilot-in-the-Loop Analysis," J. of Aircraft, Vol. 10, No. 9, September 1973, pp. 515-524.

9. Weir, D. H., and R. H. Klein, "Measurement and Analysis of Pilot Scanning Behavior during Simulated Instrument Approaches," presented at the AIAA Guidance, Control and Flight Mechanics Conference, Santa Barbara, Calif., August 17-19, 1970, AIAA Paper No. 70-999.

10. Klein, Richard H., AWJSRA Flight Director Simulation Program, Systems Technology, Inc., WP-1015-8, March 1972.

11. Klein, Richard H., Initial Simulation Plan for C-8M Flight Director Evaluation, Systems Technology, Inc., WP-1015-7, December 1971.

12. Weir, David H., Compilation and Analysis of Flight Control System Command Inputs, AFFDL-TR-65-119, January 1966.

13. Clement, Warren F., Curved and Straight Course Equalization for Lateral Approach Control, Systems Technology, Inc., WP-1015-10, October 1972.

14. Cleveland, William B., Richard F. Vomaske, S. R. M. Sinclair, Augmentor Wing Jet STOL Research Aircraft Digital Simulation Model, NASA TM X-62,149, April 1972.

APPENDIX A

LONGITUDINAL STABILITY AUGMENTATION SYSTEMS

RATE-COMMAND/ATTITUDE-HOLD SAS

The purpose of a rate-command/attitude-hold system is to provide attitude regulation and improved attitude command response. The attitude hold feature provides improved attitude stability and hence improved attitude regulation in the presence of turbulence and/or deterministic winds. The rate command feature provides an attitude response to commands that has desirable K/s-like dynamics, i.e., provides a steady pitch rate proportional to column position. This reduces the need for any pilot compensation, reduces the pilot's effective time delay and remnant (unwanted control action), and permits a wide range of pilot gain that produces good dynamic characteristics. Both of these features reduce the pilot's workload and lead to superior control.

In this appendix we present an extension of the Sperry rate-command/attitude-hold (RCAH) system that essentially replaces the aircraft's attitude response with a selectable transfer function. Evaluation of this system was accomplished by NASA and is therefore not included in this report. This RCAH, shown in Fig. A-1a, uses an efficient combination of feedbacks and feedforwards to produce lead equalization for attitude regulation as well as the rate command itself. A further benefit is washout of the pitch rate feedback that is present when making steady-state turning maneuvers. We shall first develop the equivalent equalization for level flight and then consider the effects of steady-state turning maneuvers.

The RCAH (Fig. A-1a) can be reinterpreted as an equivalent single-loop feedback system (Fig. A-1b) by considering the equation for θ_e, which from Fig. A-1a is:

$$\theta_e = (\theta_c - \theta) - (q - q_c)\left[\frac{(K_q/K_\theta)s}{s + 1/\tau_1}\right] \qquad (A\text{-}1)$$

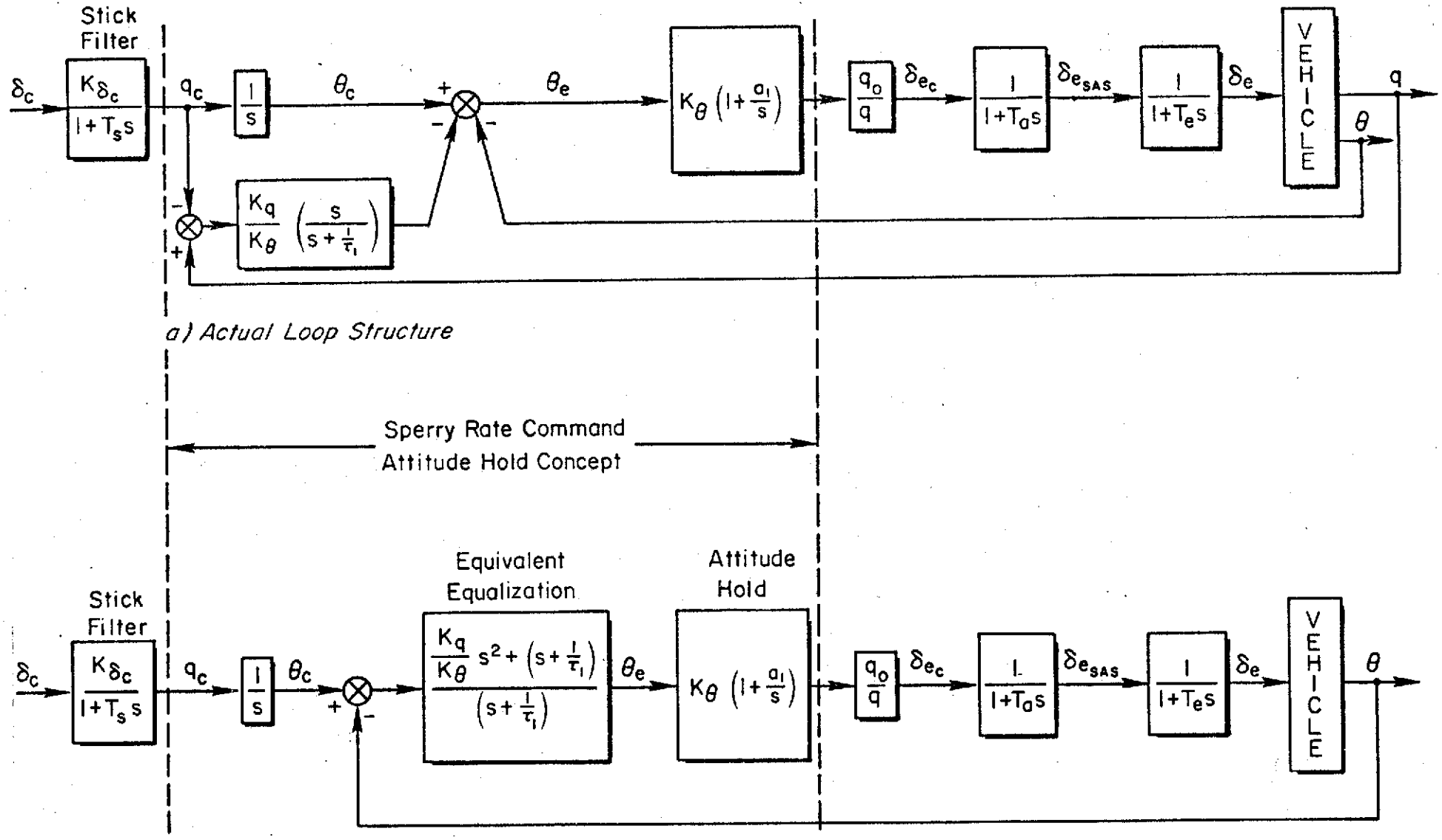

Figure A-1. Rate Command Attitude Hold SAS Concept

Factoring out $(\theta_c - \theta)$ yields:

$$\theta_e = (\theta_c - \theta)\left[1 + \frac{(K_q/K_\theta)s^2}{s + 1/\tau_1}\right] \qquad (A\text{-}2)$$

or the equivalent equalization becomes:

$$\theta_e = (\theta_c - \theta)\left[\frac{(K_q/K_\theta)s^2 + (s + 1/\tau_1)}{s + 1/\tau_1}\right] \qquad (A\text{-}3)$$

Figure A-1b shows the resulting equivalent single-loop system. The "equivalent equalization" capabilities for the RCAH consists of a second-order lead and first-order lag. Consequently, at high frequencies, i.e., above the short period, it is a lead which can be used to compensate for the second-order roll-off of the short-period mode in the θ/δ_e response. The lag can be used to cancel the zero at $1/T_{\theta_2}$, while the second order is put at the short period, thus creating, above the phugoid, a K/s slope. In addition, the phase characteristics of the "equivalent equalization" are such that it has leading phase at all frequencies for any combination of $1/\tau_1$ and K_q/K_θ as can be seen from the expression for the phase:

$$\angle = \tan^{-1}\left[\frac{\tau_1\omega}{1 - \omega^2(\tau_1 K_q/K_\theta)}\right] - \tan^{-1}\ \tau_1\omega \qquad (A\text{-}4)$$

The first term has the same numerator but a smaller denominator compared to the second term. An example phase value is for $\tau_1 = 1$, $K_q/K_\theta = 0.25$ at a frequency of 2 rad/sec which yields:

$$\angle = 90^\circ - 63.5^\circ = 26.5^\circ$$

In steady-state turns the sensed pitch rate, q, no longer equals the derivative of pitch angle. This can be seen from the following equation:

$$q = \frac{1}{\cos \varphi} (\dot{\theta} - r \sin \varphi) \qquad \text{(A-5)}$$

where

$$r \doteq \text{CONST in a steady turn}$$

Since the body axis yaw rate, r, is nearly constant in a steady-state turn, it will not be passed through the washout circuit. Thus, the rate washout in the RCAH SAS yields the desired lead compensation independent of turn rate.

Attitude Loop Transfer Function

For $1/\tau_1 = 1$ and $K_q/K_\theta = 0.25$, the equivalent equalization is:

$$\frac{(1 + s/2)^2}{1 + s}$$

which produces a slight attenuation at 1.0 rad/sec and behaves as a lead above 2 rad/sec. This equivalent equalization, along with:

$$a_1 = 0.2$$

$$K_\theta = 6.$$

$$T_a = T_e = 0.05 \text{ sec}$$

produces the open-loop transfer functions for the 60 kt glide slope and the 140 kt cruise case in Fig. A-2a. These cases have the following cross-over frequencies and phase margins.

	60 kt	140 kt
ω_c (rad/sec)	2.6	2.5
φ_m (deg)	50	80

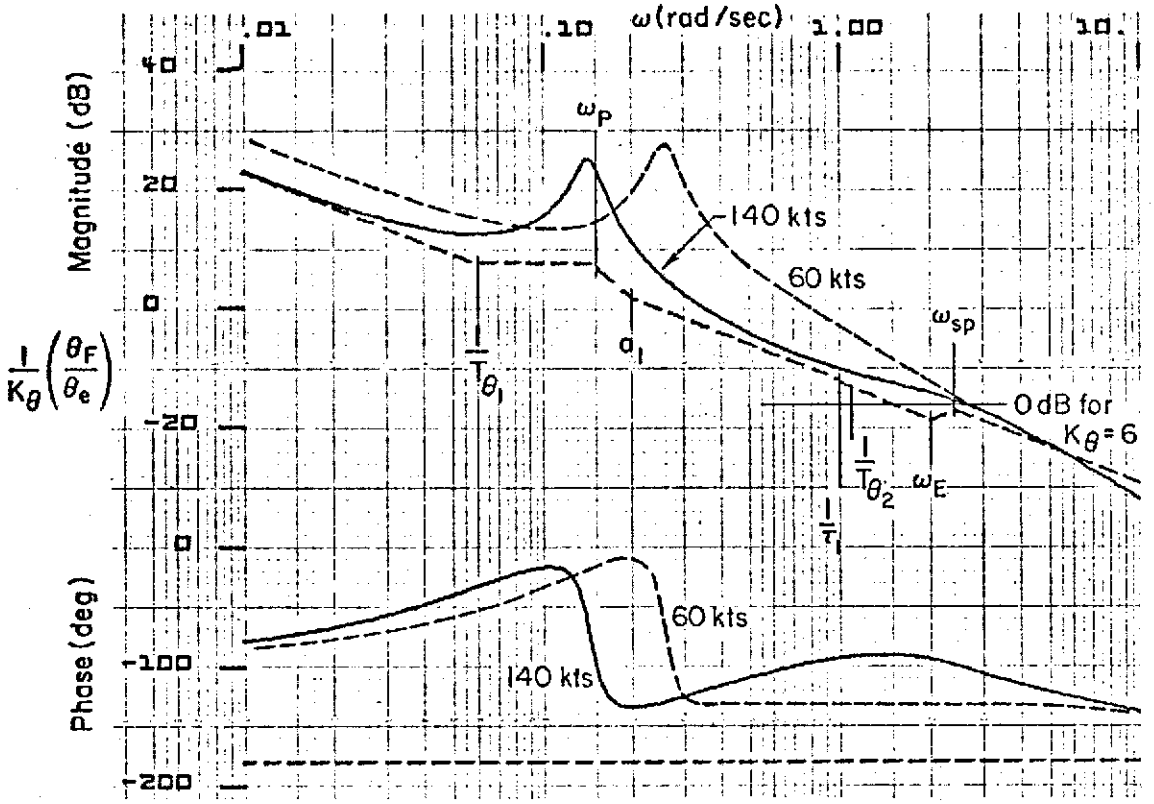

a) Open Loop Transfer Function

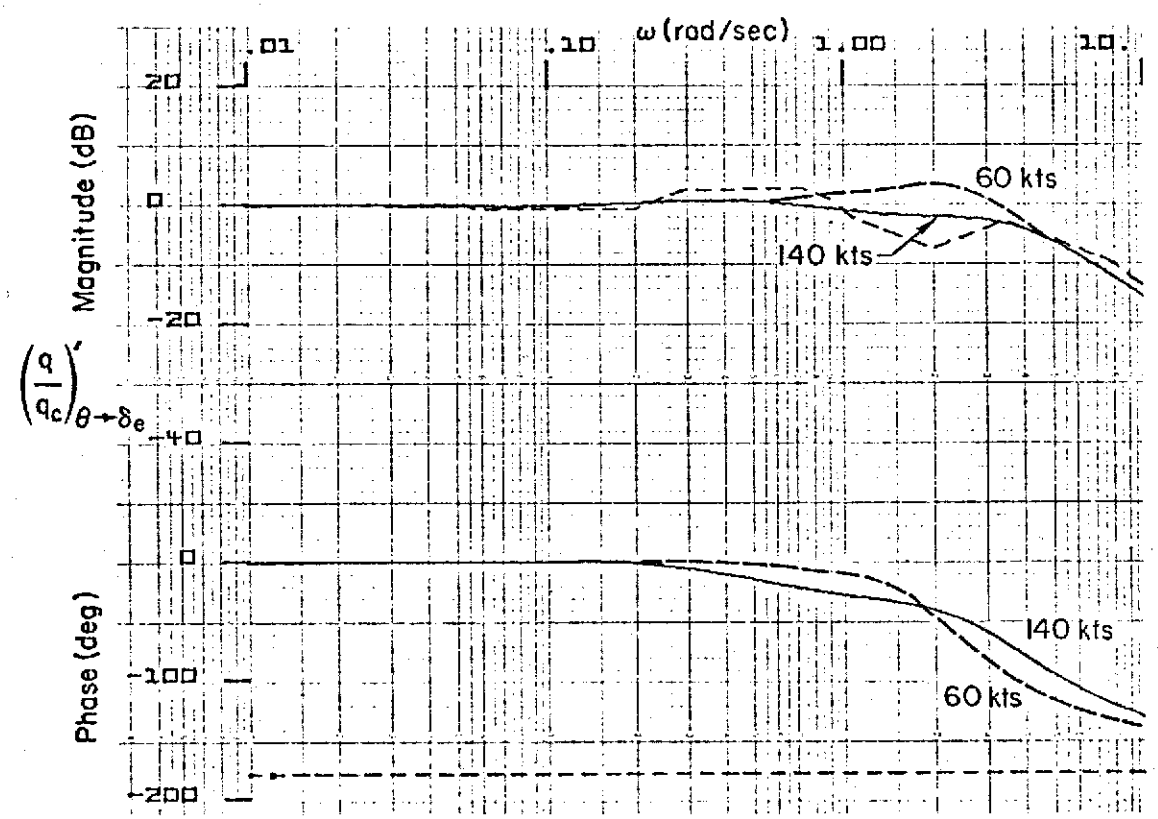

b) Closed Loop Transfer Function

Figure A-2. Attitude Responses, 60 and 140 kt Cruise

The closed-loop pitch-rate-to-rate-command (q/q_c) frequency response characteristics are shown in Fig. A-2. The 60 kt glide slope case has a 3 dB peak at the closed-loop short period, indicative of slightly lower damping at lower speeds.

SAS-On Transient Response

Figure A-3 shows the response to a 4 deg/sec step stick command for 2.5 sec to produce a desired 10 deg attitude pitch up. For the 60 kt glide slope case the SAS actuator stays within the 30 deg/sec rate limit but briefly exceeds the −7 deg position limit. As time approaches 20 sec, the SAS elevator position will approach −7 deg (elevator trim for 10 deg pitch is 7°). This suggests that a follow-up trim system is necessary so that the SAS is not required to hold large steady-state pitch angle changes. As would be expected, the elevator requirements are less at higher speeds.

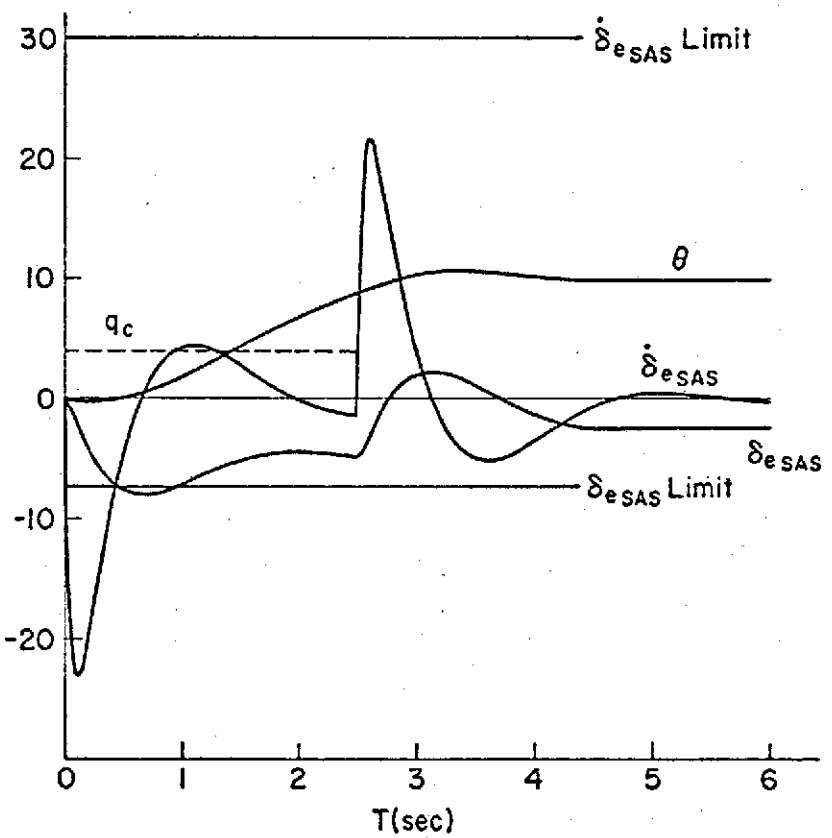

Figure A-3. Transient Response to Step q_c for 2.5 sec with RCAH SAS On (60 kt, Glide Slope)

RMS Response to Gusts

Table A-1 shows the rms gust responses of the vehicle at 60 and 140 kt when using the RCAH SAS. A 0.5 rad/sec gust break frequency was assumed. The results are presented both normalized (σ_{w_g} = 1 ft/sec) and at 3σ values (for σ_{w_g} = 5 ft/sec). The latter was selected as an indication of values that would be exceeded less than 0.27% of the time (if the gusts are assumed to have a Gaussian distribution). The 3σ results in Table A-1 can be used to find the rms gust strength that would just limit the SAS. These rms values are 9.4 ft/sec (at 60 kt) and 41.6 ft/sec (at 140 kt). To hit the rate limit for 3σ = 30 deg/sec the rms w_g would have to be 13.3 ft/sec (at 60 kt) and 47 ft/sec (at 140 kt). Attitude excursions are very small, while the climb rate excursions (600-800 fpm) are controlled. The peak accelerations are about 1/3 g for the cruise case. Thus, this RCAH should not be troubled by random vertical gusts.

TABLE A-1

SAS-ON RMS RESPONSE TO VERTICAL GUSTS

$$\Phi_{w_g} = \left| \frac{A}{s + .5} \right|^2_{s=j\omega}$$

RESPONSE	NORMALIZED (σ_{w_g} = 1 ft/sec)		3 σ VALUE (σ_{w_g} = 5 ft/sec)	
	Glide Slope (60 kt)	Cruise (140 kt)	Glide Slope (60 kt)	Cruise (140 kt)
θ (deg)	0.042	0.049	0.63	0.735
δ_{SAS} (deg)	0.248	0.056	3.72	0.84
$\dot{\delta}_{SAS}$ (deg/sec)	0.752	0.22	11.3	3.2
$\dot{h}$ (ft/sec)	0.78	0.87	11.7	13.2
a_z (ft/sec^2)	0.39	0.66	5.85	9.9

Mechanization

Figure A-4 shows the mechanization to achieve this rate-command/attitude-hold system. Table A-2 summarizes the design parameter values.

The dotted line represents the elevator follow-up required for changes in the trim pitch attitude to avoid SAS limiting. This integrator represents a trim motor and it is suggested to set $K_a = 0.2$ and then set K_{THETI} to zero. Thus, the trim motor would provide the steady-state attitude holding. Note that $K_{DC} = 0$ in this diagram, thus making the system fly-by-wire. In the subsequent simulation program K_{DC} was set at 3.33 deg/in.

TABLE A-2. DESIGN RCAH PARAMETER VALUES

RATE COMMAND ATTITUDE HOLD (Fig. A-1)	DESIGN VALUES	DIAGRAM LABELS
K_q/K_θ	0.25	K_{QB}/K_{THETI}
$1/\tau_1$	1.	W_{W_O}
a_1	0.2	K_{THETI}
T_A	0.05	$T_{E_{SAS}}$
T_e	0.05	T_E
T_s	0.2	T_{COL}
1.	1.	K_{THETA}
	0.	K_{DC}
	1.	K_{qc}
	75.	K_{COL}
	1.	K_I
K_θ	-6.	K_L

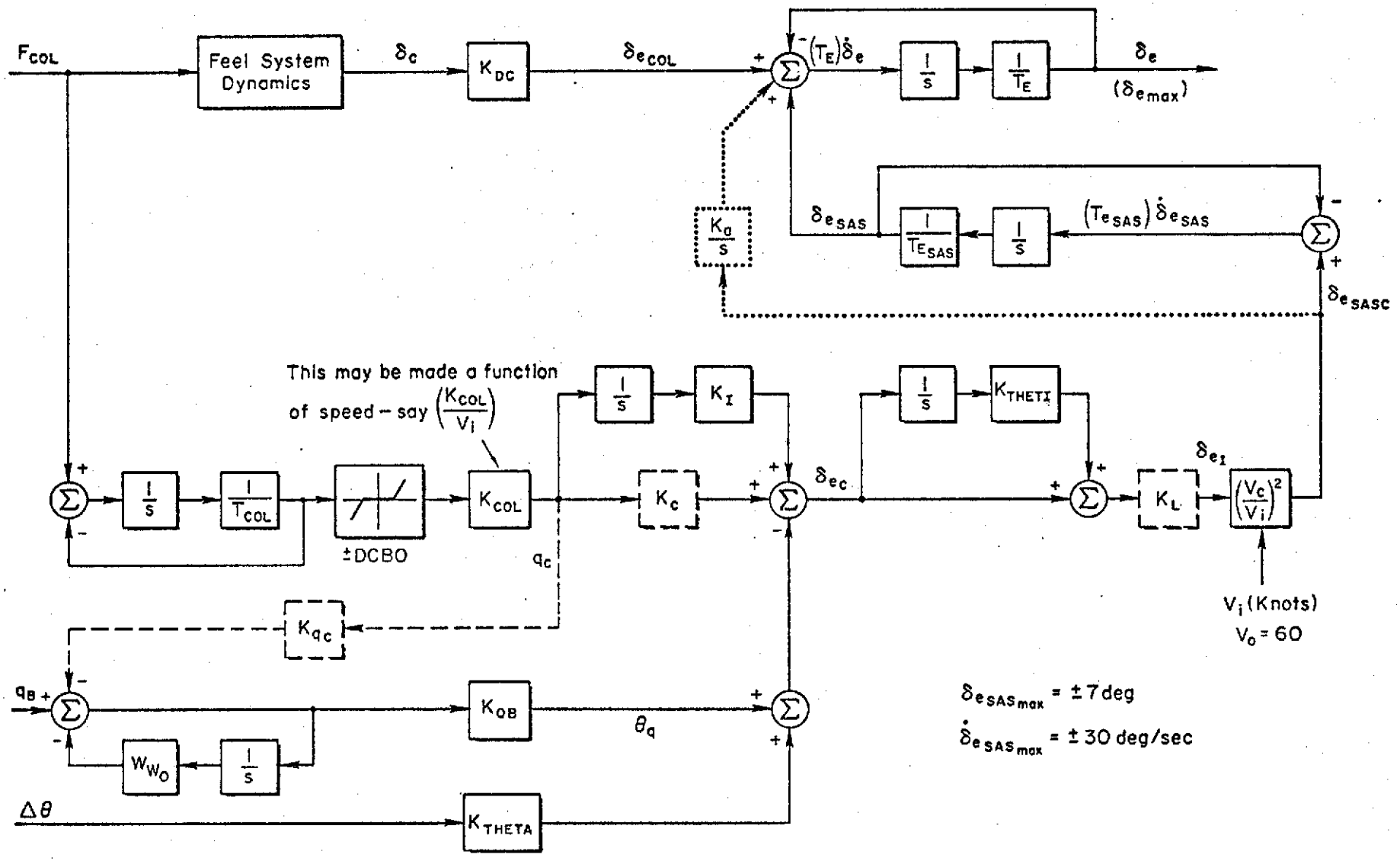

Figure A-4. Pitch Rate Command/Attitude Hold System

APPENDIX B

SIMPLIFIED DIGITAL SIMULATION

As shown in Table 5 an essential part of the lateral flight director design procedure involved consideration of time response properties. Because of the important effect of system nonlinearities (bank angle limit), and the need to check curved path tracking, simple transfer function time responses were not adequate. Numerical integration of a simplified set of equations of motion was therefore required. This was accomplished with the STI generalized equations of motion routine which includes standard subroutines for input-output, numerical integration, and plotting. The program accepts the desired equations of motion in the form $\dot{X} = AX$ in addition to the usual logic and equations of constraint. A block diagram of the flight director system, as programmed, is given in Fig. B 1.

The vehicle equations of motion are given below along with a sketch illustrating the coordinate system and wind convention.

a. Vehicle Equations

$$\dot{\Phi} = p$$

$$\dot{p} = L_{\delta_W}\delta_W - \frac{1}{T_R} p$$

$$\dot{\psi} = \frac{g \sin \Phi}{V_{TAS}}$$

$$\dot{X} = V_{TAS} \cos \psi + V_{WX} + V_{SX}t$$

$$\dot{Y} = V_{TAS} \sin \psi + V_{WY} + V_{SY}t$$

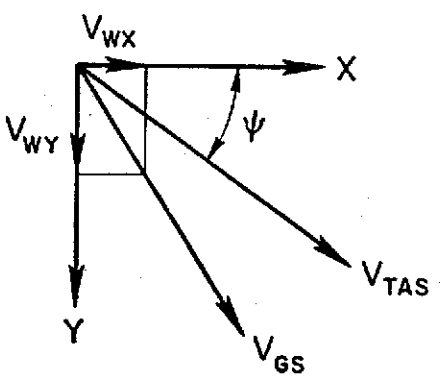

b. Washout Circuit

$$\Phi_{WO} = K_{\Phi}\Phi \frac{s}{\left(s + \frac{1}{T_{WO}}\right)}$$

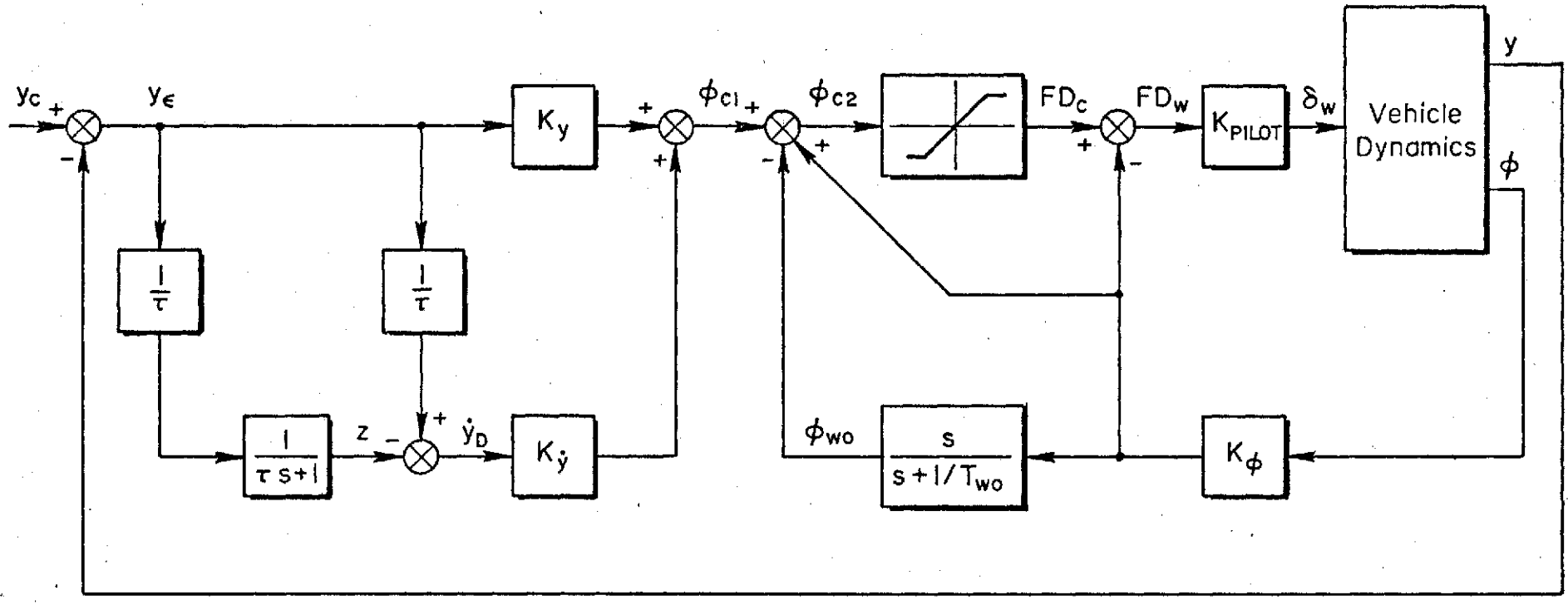

Figure B-1. Block Diagram of Simulated Lateral System

c. Derived Beam Rate

$$\dot{z} = \frac{1}{\tau^2} y_\epsilon - \frac{1}{\tau} Z$$

$$\dot{y}_D = \frac{1}{\tau} y_\epsilon - z$$

d. Control Law

$$\varphi_{c_1} = K_y y_\epsilon + K_{\dot{y}} \dot{y}_D$$

where

$$y_\epsilon = y_c - y \quad ; \quad \text{straight path}$$

$$y_\epsilon = \sqrt{X^2 + Y^2} - R_c \quad ; \quad \text{circular path}$$

$$\delta_w = K_{PILOT} FD_w$$

APPENDIX C

FEEDFORWARD GUIDANCE COMMANDS FOR LATERAL FLIGHT DIRECTOR A

In essence, the guidance and control requirements for command following and disturbance regulation in the lateral flight director are satisfied via the outer loop (crosstrack deviation). Other requirements, such as stability and damping, necessitate the use of inner loops which tend to complicate matters when following curved paths or regulating against wind and wind shear. In these situations the steady-state inner-loop feedbacks are not nominally zero, resulting in standoffs with the crosstrack error signal, y_ϵ. Consider the generalized lateral flight director block diagram in Fig. C-1.

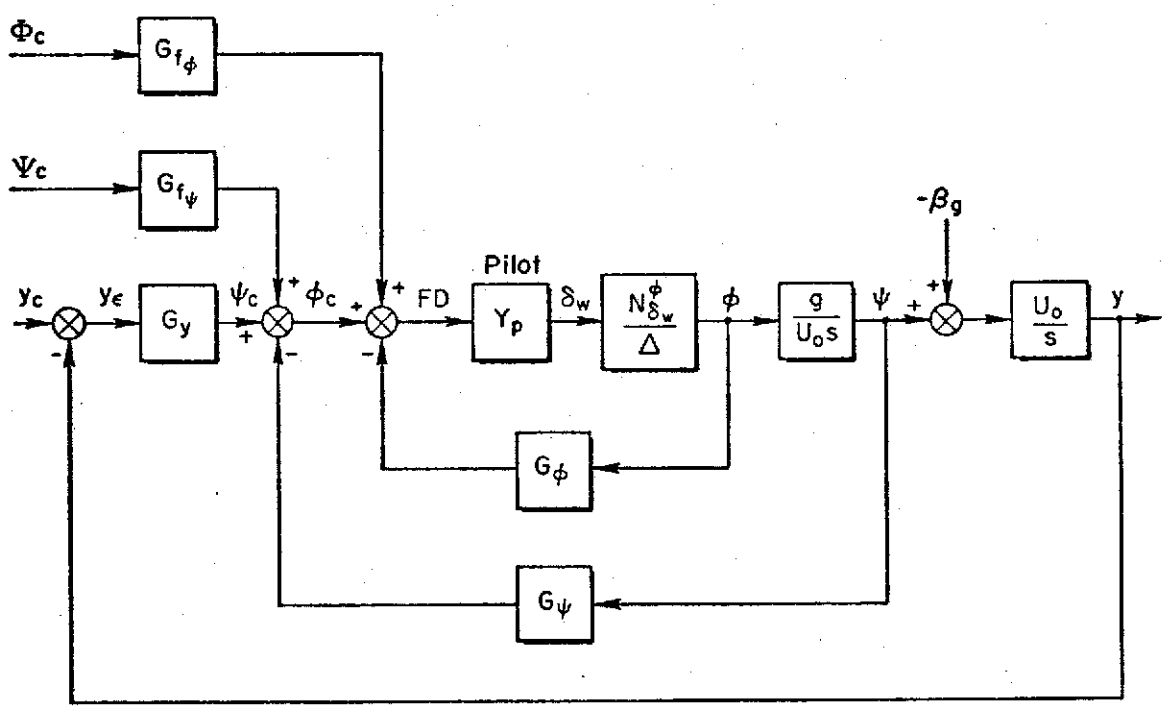

Figure C-1. Generalized Block Diagram for Lateral Flight Director

If the pilot keeps the flight director centered (FD = 0), the control law which is automatically satisfied becomes:

$$FD = -G_{\varphi}\varphi - G_{\psi}\psi + G_{y}y_{\epsilon} + G_{f_{\varphi}}\Phi_{c} + G_{f_{\psi}}\Psi_{c} \qquad (C\text{-}1)$$

where Φ_c and Ψ_c are the feedforward guidance command variables to be later defined. In the absence of feedforward guidance commands, the crosstrack deviation may be written as:

$$y_{\epsilon} = \frac{1}{G_y}\left(G_{\varphi}\varphi + G_{\psi}\psi\right) \qquad (C\text{-}2)$$

Note that the desired result is always to make $y_\epsilon = 0$ and that this will only occur if the bank angle, φ, and heading, ψ, are nominally equal to zero when tracking the desired course. This, of course, is only true for straight paths in the absence of crosswind and crosswind shear. Several ways of getting around this problem exist. One possibility is to wash out φ and ψ via the feedback transfer functions, G_φ and G_ψ. This technique is discussed in Section IV-C-5. A second possibility is to add a parallel integrator to G_y. This is impractical for reasons discussed in Section IV-B-2a. Finally, we can develop feedforward guidance commands for each of the feedback variables resulting in the following control law (see Eq. C-1):

$$FD = G_{\varphi}(\Phi_c - \varphi) + G_{\psi}(\Psi_c - \psi) + G_{y}y_{\epsilon} \qquad (C\text{-}3)$$

where $G_{f_\varphi} = G_\varphi$ and $G_{f_\psi} = G_\psi$. The complexity of the command signals will depend on the shape of the desired course and the nature of the wind disturbance.

Clearly, it is desirable to select inner-loop feedbacks which minimize the complexity of the corresponding feedforward commands. Because of the rapidly changing heading during a turn and the sensitivity of the required heading to crosswinds, it is not practical to use this variable for path damping on a curved path. The same argument holds true for the lateral course angle, λ, discussed in Ref. 10. For this reason, crosstrack rate, $\dot{y}$, has been selected to provide the primary path damping. Note that $\dot{y}$ is nominally zero for all paths and wind conditions and therefore does not require a feedforward command signal.

The bank angle feedforward guidance command is based on nulling the crosstrack acceleration, $\ddot{R}$, for a given turn radius, R_c. These are related as follows:

$$\ddot{R} = \frac{V_{GS}^2}{R_c} - g \tan \varphi \qquad (C\text{-}4)$$

It follows that the command bank angle should be:

$$\Phi_c = \tan^{-1} \frac{V_{GS}^2}{R_c g} \qquad (C\text{-}5)$$

The flight director Eq. C-3 now becomes:

$$FD = G_\varphi \left(\tan^{-1} \frac{V_{GS}^2}{R_c g} - \varphi \right) + G_y y_\epsilon = 0 \qquad (C\text{-}6)$$

Elimination of standoffs in y_ϵ depend upon the following considerations:

1. R_c must be the exact turn radius consistent with the error signal, y_ϵ.
2. Accurate measurement of ground speed is necessary.
3. Accurate measurement of bank angle is required.

The first of these should not present a problem. The sensitivity of standoff errors to errors in measured ground speed and bank angle is discussed in Section IV-C-4.

The bank angle command defined by Eq. C-5 only accounts for wind in the sense that ground speed changes in a turn. The bank angle command for zero steady-state error in the presence of wind and wind shear has been derived in Ref. 13 and is given as:

$$\Phi_c = \tan^{-1} \frac{V_{GS}^2}{R_c g} - \frac{1}{g} \frac{dv_g}{dt} \qquad (C\text{-}7)$$

where v_g is the component of wind perpendicular to the airspeed vector. Expanding this into inertially fixed X and Y coordinates yields:

$$\Phi_c = \tan^{-1} \frac{V_{GS}^2}{R_c g} - \frac{1}{g}[\dot{V}_{WY} \cos \psi - \dot{V}_{WX} \sin \psi - V_{WY} \sin \psi\dot{\psi} - V_{WX} \cos \psi\dot{\psi}] \quad (C\text{-}8)$$

A sketch of the geometry defining the wind coordinates is given below.

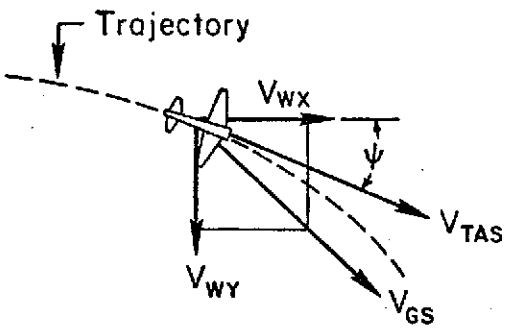

This form of bank angle command is somewhat impractical due to the requirement for continuous measurement of wind and wind shear. Furthermore, simulator results for curved path tracking in the presence of wind and wind shear indicated that crosstrack errors were negligible using the simplified Φ_c in Eq. C-5.

APPENDIX D

LONGITUDINAL CHARACTERISTICS OF AUGMENTOR WING JET STOL RESEARCH AIRCRAFT

Table D-1 presents the longitudinal unprimed dimensional stability derivatives for 4 flight conditions. These derivatives were obtained on the simulator by perturbing each of the independent variables about the trim points. They are therefore representative of the aero model in Ref. 14.

The transfer functions corresponding to the derivatives in Table D-1 are presented in Table D-2.

The transfer functions in Table D-3 represent the vehicle characteristics with the rate command attitude hold SAS described in Appendix A.

Finally, the transfer functions for the vehicle with rate command attitude hold and speed SAS (see Fig. 1) are given in Table D-4. It should be noted that these transfer functions do not reflect the effect of the flap-nozzle interconnect discussed in Section II.

TABLE D-1. SAS OFF LONGITUDINAL DIMENSIONAL DERIVATIVES
(BODY FIXED BODY AXES)

DERIVATIVE	UNITS	FC1	FC2	FC3	FC4
V_{TAS} γ	kt deg	60 −7 1/2	90 −7 1/2	90 0	140 0
α_{TRIM}	deg	.151	4.1	1.34	4.5
$\delta\nu_{TRIM}$	deg	82.5	83.1	55.3	6.0
δ_T	deg	21.0	13.0	20.6	11.8
δ_f	deg	65	34.0	34.0	5.6
X_u	1/sec	−.0236	−.0572	−.0604	−.0227
Z_u	1/sec	−.260	−.232	−.229	−.281
M_u	1/(ft/sec)	.00081	−.00049	−.00135	−.000775
$Z_{\dot{w}}$		−.0126	−.0111	−.0108	−.0105
$M_{\dot{w}}$	1/ft	−.00346	−.00314	−.00298	−.00296
X_w	1/sec	.127	.164	.114	.142
Z_w	1/sec	−.567	−.707	−.767	−1.03
M_w	1/(ft/sec)	−.00514	−.0108	−.0129	−.0159
M_q	1/sec	−.925	−1.46	−1.42	−2.25
X_{δ_e}	$(ft/sec^2)/rad$	.126	.772	.251	2.07
Z_{δ_e}	$(ft/sec^2)/rad$	−4.8	−10.75	−10.8	−25.8
M_{δ_e}	$1/sec^2$	−1.3	−3.04	−2.98	−7.35
X_{δ_T}	$(ft/sec^2)/deg$	−.0492	−.1904	.2070	.52
Z_{δ_T}	$(ft/sec^2)/deg$	−.584	−1.136	−.4746	.00902
M_{δ_T}	$(rad/sec^2)/deg$	.00070	.0030	.00498	.00786
X_{δ_ν}	$(ft/sec^2)/deg$	−.1094	−.0675	−.0889	−.0038
Z_{δ_ν}	$(ft/sec^2)/deg$	−.0142	−.00819	−.0617	−.031
M_{δ_ν}	$(ft/sec^2)/deg$	−.00174	−.00108	−.00098	.000202

TABLE D-2. SAS OFF TRANSFER FUNCTIONS

MOTION	UNIT	SYMBOL	60 kt γ_I = −7.5 deg	90 kt γ_I = −7.5 deg	90 kt γ_I = 0	140 kt γ_I = 0
Denominator	–	Δ	1.01[.90,1.01][.04,.23]	1.01[.808,1.62][.233,.164]	1.01[.756,1.74][.193,.141]	1.01[.122,.139][.808,2.44]
Speed to elevator	(ft/sec)/rad	$N^u_{\delta_e}$	.13(.89)[−.04,13.91]	.78(41.4)[.46,1.41]	.254(3.04)(2.66)(33.8)	2.09(66.5)[.344,1.29]
Vertical velocity to elevator	(ft/sec)/rad	$N^w_{\delta_e}$	−4.8(28.33)[.11,.28]	−10.75(44.32)[.194,.22]	−10.8(43.3)[.14,.213]	−25.8(69.4)[.089,.191]
Attitude to elevator	rad/rad	$N^\theta_{\delta_e}$	−1.30(.097)(.47)	−3.04(.60)(.126)	−2.96(.677)(.101)	−7.35(.931)(.065)
Rate of climb to elevator	(ft/sec)/rad	$N^{\dot{h}}_{\delta_e}$	4.74(4.35)(−3.34)(−.03)	10.69(6.05)(−4.56)(.052)	10.8(6.26)(−4.79)(.0254)	25.9(9.23)(−6.95)(.013)
Speed to throttle	(ft/sec)/in.	$N^u_{\delta_T}$	−.025(1.77)[.70,1.11]	−.193(.78)[.907,17.6]	.209(−.48)[.76,1.79]	.525(−.088)[.77,2.46]
Vertical velocity to throttle	(ft/sec)/in.	$N^w_{\delta_T}$	−.29(.83)[−.08,.14]	−1.136(.187)(−.179)(1.07)	−.475(−.357)[.295,.581]	.009(191.6)[−.514,.203]
Attitude to throttle	rad/in.	$N^\theta_{\delta_T}$	.0014(−.013)(1.25)	.0066(2.19)(.043)	.0064(1.45)(.128)	.008[.935,.55]
Rate of climb to throttle	(ft/sec)/in.	$N^{\dot{h}}_{\delta_T}$	.29(.058)[.84,.74]	1.15(.037)].704,1.38]	.479(.074)[.543,1.82]	.032(.192)[.524,8.75]
Speed to nozzle	(ft/sec)deg	$N^u_{\delta_\nu}$	−.11(−.20)[.94,1.08]	−.068(−.107)[.78,1.65]	−.09(.0018)[.768,1.74]	−.0038(.67)[.99,2.96]
Vertical velocity to nozzle	(ft/sec)/deg	$N^w_{\delta_\nu}$	−.014(11.4)[−.069,.31]	−.0082(19.7)[∓.188,.22]	−.062(3.71)[−.53,.141]	−.031(.698)(.348)(−.343)
Attitude to nozzle	–	$N^\theta_{\delta_\nu}$	−.0017[.83,.40]	−.00106[.768,.459]	−.00081[∓.073,.48]	.0003(2.37)(.019)
Rate of climb to nozzle	(ft/sec)/deg	$N^{\dot{h}}_{\delta_\nu}$	.028(.14)(−1.81)(2.17)	.0122(3.40)(−2.84)(.23)	.0596(.40)(1.71)(−.57)	.031(−.0071)[.64,2.29]

TABLE D-3

TRANSFER FUNCTIONS WITH RATE COMMAND ATTITUDE HOLD SAS ON

MOTION	UNIT	SYMBOL	60 kt γ_I = -7.5 deg	90 kt γ_I = -7.5 deg	90 kt γ_I = 0	140 kt γ_I = 0
Denominator	-	Δ	.203(0)(.117)(.439(1.52) × (5.)[.589,2.30]	.202(0)(.149)(.49)(1.41) × (5.)[.71,2.56]	.202(0)(.118)(.545) × (1.32)(5.)[.69,2.66]	.202(0)(.085)(.674)(1.07) × (5.)[.823,3.13]
Attitude to column	deg/in.	$N^{\theta}_{\delta_e}$	.866(.097)(.474)(12.2) × [.925,1.76]	2.02(.126)(.6)(7.93) × [.871,1.52]	1.98(.101)(.679)(7.93) × [.87,1.52]	4.89(.065)(.932)(6.45) × [.841,1.26]
Rate of climb to column	(ft/sec)/in.	$N^{\dot{h}}_{\delta_e}$			-.126(.025)(-4.72)(6.33) × (7.92)[.87,1.52]	-.301(.013)(6.45)(-6.69) × (9.51)[.84,1.26]
Glide slope rate to column	(ft/sec)/in.	$N^{\dot{d}}_{\delta_e}$	-5.58(-.076)(-3.23)(4.27) × (12.2)[.925,1.76]	-.125(.025)(-4.44)(6.08) × (7.92)[.871,1.52]		
Speed to column	(ft/sec)/in.	$N^{u}_{\delta_e}$	-.0015(.895)(12.2) × [.925,1.76][-.04,13.9]	-.0091(7.92)(41.4) × [.462,1.41][.871,1.52]	-.0029(2.66)(3.04)(7.92) × (33.8)[.871,1.52]	-.024(.645)(66.5) × [.841,1.26][.344,1.29]
Rate of climb to throttle	(ft/sec)/in.	$N^{\dot{h}}_{\delta_T}$			.096(0)(.135)(1.34)(5.) × [.622,2.92]	.0064(0)(.5)[.964,.807] × [.623,9.69]
Glide slope rate to climb	(ft/sec)/in.	$N^{\dot{d}}_{\delta_T}$	.117(0)(.0019)(1.51)(5.) × [.577,2.36]	.224(0)(.0015)(1.47)(5.) × [.67,2.62]		

TABLE D-4. TRANSFER FUNCTIONS WITH RATE COMMAND
ALTITUDE HOLD AND SPEED SAS ON

MOTION	SYMBOL	60 kt γ = −7.5 deg	90 kt γ = −7.5 deg
Denominator	Δ	.203(0)(.566)(1.53)(5.) × [.61,.818][.585,2.3]	.202(0)(.631)(1.39)(5.) × [.736,.69][.712,2.57]
Attitude to column	$N^{\theta}_{\delta_c}$	.865(.594)(12.2)[.589,.829] × [.924,1.76]	.202(.733)(7.93)[.72,.69] × [.87,1.52]
Rate of climb to column	$N^{\dot{h}}_{\delta_c}$		
Glide slope rate to column	$N^{\dot{d}}_{\delta_c}$	−.056(−3.23)(4.26)(12.2) × [.618,.761][.925,1.76]	−.125(−4.44)(6.08)(7.92) × [.772,.664][.871,1.52]
Speed to column	$N^{u}_{\delta_c}$	.0015(.895)(1.)(12.2) × [.925,1.76][−.04,13.9]	.0091(1.)(7.92)(41.4) × [.462,1.41][.871,1.52]
Rate of climb to throttle	$N^{\dot{h}}_{\delta_T}$		
Glide slope rate to throttle	$N^{\dot{d}}_{\delta_T}$	.117(0)(1.52)(5.)[.632,.79] × [.574,2.36]	.224(0)(1.45)(5.)[.77,.644] × [.673,2.62]

APPENDIX E

LATERAL CHARACTERISTICS OF THE AUGMENTOR WING JET STOL RESEARCH AIRCRAFT

The lateral flight director design was based on the existing NASA stability augmentation given in Ref. 14. A block diagram of the lateral SAS is given in Fig. E-1. Perturbation derivatives were obtained for four flight conditions on the FSAA simulation and are presented in Table E-1. These derivatives were obtained with the lateral SAS turned on and therefore represent the augmented airplane.

The transfer functions for a lateral wheel input to the augmented airplane are given in Table E-2.

The dutch roll frequency and the spiral mode were checked with simulator time response characteristics at 60 kts and 140 kts. These are compared in Table E-3.

In all cases the dutch roll mode and complex roll numerator zero are nearly equal indicating negligible dutch roll response to wheel inputs. The augmented lateral airplane is therefore well represented as:

$$\frac{\varphi}{\delta_w} = \frac{L'_{\delta_w}}{(s + \frac{1}{T_s})(s + \frac{1}{T_R})} \qquad \text{(E-1)}$$

Variations in each of the parameters in Eq. E-1 with airspeed is quite small as shown in Fig. E-2.

The spiral mode is stabilized as the SAS switches are turned on below 100 kts (Fig. E-1) and in all cases is at frequencies well below the flight director/pilot crossover frequencies (near 1 rad/sec).

For the purpose of lateral flight director design the aircraft lateral characteristics were considered constant with speed as follows:

$$\frac{\varphi}{\delta_w} = \frac{.6}{s(s + 1.6)} \qquad \text{(E-2)}$$

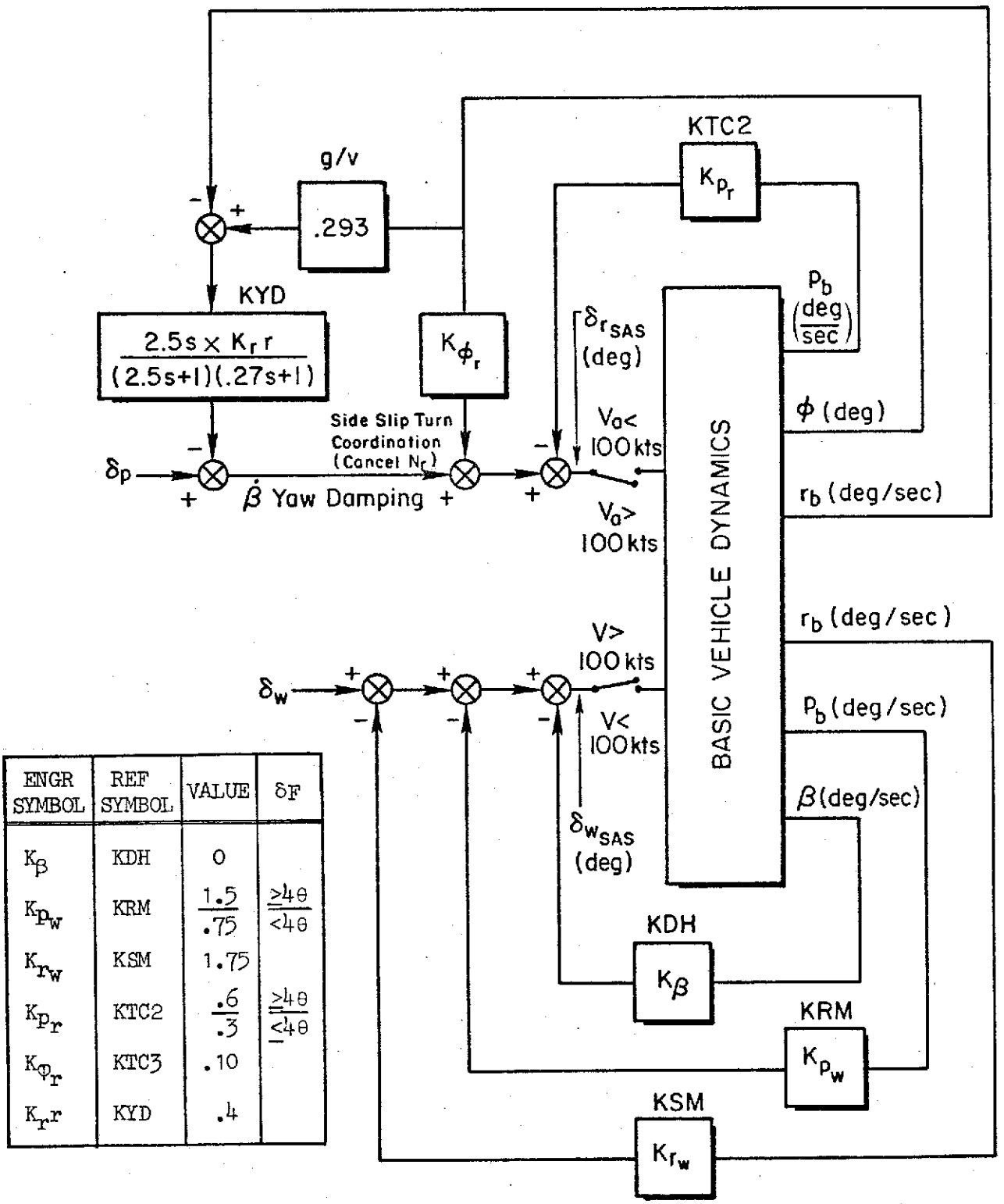

ENGR SYMBOL	REF SYMBOL	VALUE	δF
K_β	KDH	0	
K_{p_w}	KRM	$\frac{1.5}{.75}$	$\frac{\geq 4\theta}{<4\theta}$
K_{r_w}	KSM	1.75	
K_{p_r}	KTC2	$\frac{.6}{.3}$	$\frac{\geq 4\theta}{<4\theta}$
K_{ϕ_r}	KTC3	.10	
$K_r r$	KYD	.4	

Figure E-1. Lateral-Directional SAS for Augmentor Wing Jet STOL Research Aircraft (From Ref. 14)

TABLE E-1. SAS ON LATERAL DERIVATIVES BODY AXES

		FC1	FC2	FC3	FC4
V_{TAS}	kts	60	90	90	140
γ	deg	-7.5	-7.5	0	0
α_{trim}	deg	.151	4.1	1.34	4.5
$\delta_{\nu trim}$	deg	82.5	83.1	55.3	6.0
δ_T	deg	21.0	13.0	20.6	11.8
δ_F	deg	65	34	34	5.6
Y_v	1/sec	-.096	-.142	-.132	-.310
Y_{δ_w}	$(ft/sec^2)/rad$	-2.165	-4.011	-4.25	-3.675
Y_{δ_p}	$(ft/sec^2)/rad$	-.603	-1.357	-1.357	-3.28
L_β	$1/sec^2$	.000018	-.096	-.0309	-.207
L_p	1/sec	-1.58	-1.822	-1.908	-1.49
L_r	1/sec	-.026	-.307	-.392	.954
L_{δ_w}	$1/sec^2$	.711	.937	.979	.594
L_{δ_p}	$(rad/sec^2)/in.$	-.03	-.067	-.067	-.163
N_β	$1/sec^2$	.415	.802	.796	1.570
N_p	1/sec	.240	.219	.279	.242
N_r	1/sec	-.238	-.333	-.338	-.405
N_{δ_w}	$1/sec^2$	-.013	.026	.0167	.030
N_{δ_p}	$1/sec^2$	.072	.162	.162	.392

AIRCRAFT CONSTANTS

A = 1116.9 ft
S = 865.0 ft^2
b = 78.7 ft
W = 400,000 lbs

I_{xx} = 287200 slug-ft^2
I_{zz} = 416700 slug-ft^2
I_{xz} = 27910 slug-ft^2

TABLE E-2. SAS ON LATERAL TRANSFER FUNCTIONS

MOTION	SYMBOL	FC1	FC2	FC3	FC4
Denominator	Δ	(.046)(1.56)[.23,.65]	(.052)(1.79)[.26,.91]	(.04)(1.85)[.27,.91]	(-.086)(1.53)[.27,1.28]
Bank angle to wheel	$N_{\delta_w}^{\phi}$	.71[.233,.665]	.94[.24,.93]	.99[.25,.92]	.61[.30,1.29]
Yaw rate to wheel	$N_{\delta_w}^{r}$	.035(4.31)[-.087,.79]	.089(2.77)[-.014,.80]	.083(3.66)[-.064,.74]	.07(2.40)[.15,.87]
Sideslip to wheel	$N_{\delta_w}^{\beta}$	-.021(.499)(-1.12)(3.97)	-.026(-.58)[.89,2.00]	-.028(-.42)[.98,2.45]	-.016(-.35)[.68,2.67]
Lateral acceleration to wheel	$N_{\delta_w}^{a_y}$	-2.17(.263)(1.72)[-.116,.736]	-4.01(.39)(1.74)[.025,.77]	-4.25(.45)(1.82[-.008,.70]	-3.68[-.15,.61][.82,1.22]
Lateral course angle to wheel	$N_{\delta_w}^{\lambda}$	-.022(-2.58)(4.12)[.211,.641]	-.027(-2.05)(3.77)[.25,.88]	-.028(-2.05)(3.83)[.28,.87]	-.016(-2.0)(2.99)[.36,1.17]

TABLE E-3

COMPARISON OF SIMULATOR TIME RESPONSE
WITH TRANSFER FUNCTIONS

	140 kt SIMULATOR	TRANSFER FUNCTION	60 kt SIMULATOR	TRANSFER FUNCTION
T_s(sec)	−.068	−.086	0	.046
ω_d(rad/sec)	1.25	1.28	.6	.65

The value of L'_{δ_w} used in Eq. E-2 was based on earlier estimates and is slightly below the average value in Fig. E-2. Since this will only affect the estimated pilot gain for a given crossover frequency, it has no effect on the analyses in Section IV.

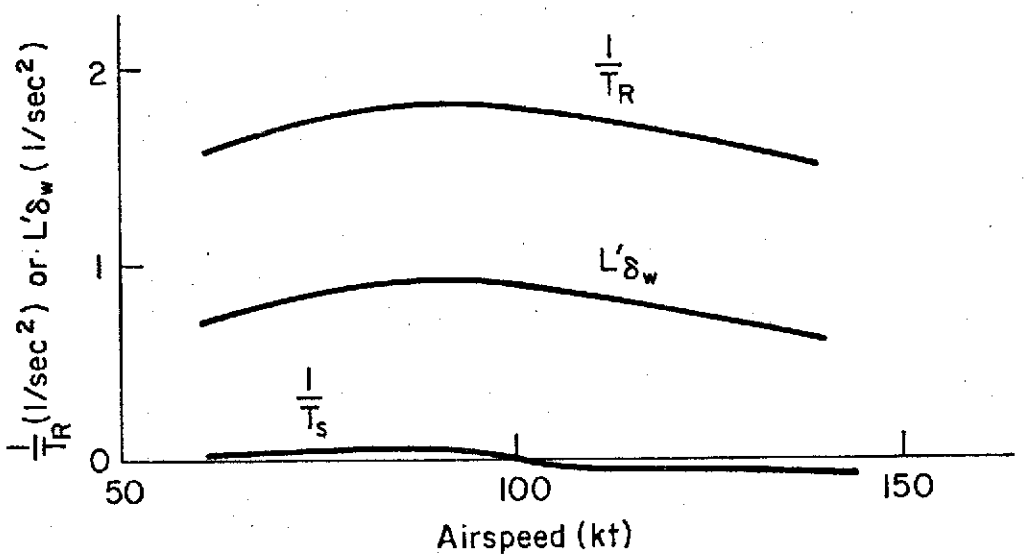

Figure E-2. Variation of Lateral Modes and Control Effectiveness with Speed